Bonded Porous Revetments - Effect of porosity on wave-induced loads and hydraulic performance – An Experimental Study –

Von der
Fakultät Architektur, Bauingenieurwesen und Umweltwissenschaften
der Technischen Universität Carolo-Wilhelmina
zu Braunschweig

zur Erlangung des Grades eines
Doktoringenieurs (Dr.-Ing.)
genehmigte

Dissertation

von
Sven Liebisch
geboren am 24.05.1978
aus Hannover

Eingereicht am: 15. April 2015
Disputation am: 19. Juni 2015

Berichterstatter: Prof. Hocine Oumeraci
Prof. Holger Schüttrumpf
Prof. Andreas Kortenhaus

2015

Vorwort

Die Idee dieser Arbeit ist bei einer Exkursion zum Großen Wellenkanal (GWK) am Forschungszentrum Küste (FZK) in Hannover entstanden, die ich als Lehrstuhlassistent mit Studenten der Vertiefungsrichtung „Hydromechanik und Küsteningenieurwesen“ durchgeführt habe. Zu dieser Zeit wurde im GWK ein offenporiges, polyurethangebundenes Deckwerk hinsichtlich der Wirksamkeit und Widerstandsfähigkeit bei Wellenbelastung untersucht.

Ich möchte mich daher zunächst bei der Deutschen Forschungsgemeinschaft (DFG) bedanken, die mir mit dem entgegengebrachten Vertrauen und der finanziellen Unterstützung die Möglichkeit gegeben hat, meine Forschungsidee umzusetzen.

Ich möchte insbesondere die Mühen meines Doktorvaters Prof. Dr.-Ing. Oumeraci hervorheben, der mich bereits als sein Lehrstuhlassistent ermuntert hat, dieses Forschungsprojekt zu beantragen. Weiterhin danke ich für die vielen Stunden, die er dafür verwendet hat, Zwischenberichte und die spätere Dissertation selbst kritisch zu lesen, Hilfestellungen zu geben und Probleme zu diskutieren. Ohne seine Unterstützung und die des Leichtweiß-Instituts für Wasserbau wären auch meine Besuche von internationalen Konferenzen nicht möglich gewesen.

Ich möchte mich aber natürlich auch bei all meinen Kollegen in der Abteilung „Hydromechanik und Küsteningenieurwesen“ des Leichtweiß-Instituts bedanken für die vielen Jahre mit freundlichem Miteinander, interessanten fachlichen Diskussionen und tollen Momenten im Institut selbst, aber auch abseits des Arbeitsalltags. Diese Zeit war wirklich schön mit euch und ich habe so viel von euch gelernt, sowohl fachlich als auch menschlich.

Zu allerletzt aber möchte ich mich bei meiner Lebensgefährtin Hanne Holtz bedanken, die mich in dieser Zeit immer unterstützt hat und an meiner Seite stand, obwohl das sicherlich oftmals alles andere als leicht war. Danke dafür, dass es Dich gibt, dass Du mir immer wieder die Kraft gegeben hast, die aufgetretenen schwierigen Momente durchzustehen und zu meistern und dass du mir immer den Rücken freigehalten hast.

Braunschweig, 2015 Sven Liebisch

Abstract

Porous revetments made of crushed stones durably bonded by polyurethane or by any other type of binding material are increasingly used for coastal protection. Such revetments have several advantages as compared to conventional revetments. The crucial effect of the revetment porosity on the wave loading and the response of the structure has been illustrated by Liebisch et al. (2012). Though the revetment porosity may substantially be reduced over design life time (e.g. marine growth, sediment deposition), the porosity is not yet explicitly and adequately considered in the current design practice. Therefore, the primary objective of this study is to improve the knowledge related to the effect of the porosity of a porous bonded revetment for different slope steepnesses on the hydrodynamic processes on and beneath the revetment. To achieve the aforementioned objectives, extensive scale model tests have been conducted.

The current knowledge is reviewed and analysed to identify the knowledge gaps related to the processes in front of, on and beneath the revetment, particularly considering the laboratory study by Oumeraci et al. (2010b) and the completed numerical PhD-studies of Foyer (2013) and Alcérreca Huerta (2014). Preliminary scale model tests with a simplified model set-up, in which the slope steepness, roughness and porosity of the revetment can easily be varied, are conducted to study the relative importance of the effect of these three revetment parameters on the aforementioned processes. The results of these tests are primarily used to develop a more realistic model set-up and to determine an optimized programme for the main tests which represent the major base of the PhD-study. A systematic analysis of the following processes involved in the interaction of irregular waves and the porous revetment and its soil foundation is performed (a) processes in front of and on the revetment such as wave reflection, wave set-up and wave run-up/run-down, (b) wave-induced pressures on the revetment including wave breaking, wave load classification, peak pressure and its location on the revetment, (c) processes beneath the revetment such as the damping of wave-induced pressures in the revetment, the pore pressure in the sand core beneath the revetment, the internal mean water level and the stability of the sand core.

Overall, the results have revealed for the first time the relative importance of the effect of the revetment porosity and slope steepness on all the aforementioned processes involved in the interaction of irregular waves with a bonded porous revetment, thus providing an improved understanding of both effects. More specifically, it was shown for the first time that an increasing porosity leads to a larger effect of the incident wave height on the reflection coefficient. With increasing wave heights the highly porous revetment behaves increasingly like an impermeable revetment. A larger porosity also leads to lower values of both relative wave run-up and run-down with a more significant effect of the porosity on wave run-up. The spatial development of the internal mean water level in the sand core beneath bonded porous revetments, which is decisive for the structure stability, was investigated systematically for irregular waves for the first time, showing that for the flatter slope 1:6 the internal wave set-up η_{int} near the shoreline of the sand core is less affected by the swash processes than for the steeper slope 1:3. As in the main tests only two porosities (n = 20% & n = 45%) and two slope steepnesses (1:3 & 1:6) were considered, the validity of the obtained formulae is cautiously limited to the tested or similar conditions.

Kurzfassung

Poröse Deckwerke aus gebrochenem, mittels Polyurethankleber oder anderen Bindemitteln verklebtem Kies finden immer häufiger Anwendung im Küstenschutz, da sie einige Vorteile gegenüber herkömmlichen Deckwerken haben. Der erhebliche Einfluss der Porosität auf die Wellenbelastung und die Reaktion des Deckwerks wurde bereits in Liebisch et al. (2012) veranschaulicht. Obwohl die Porosität eines Deckwerks im Laufe der Zeit durch z.B. das Einwachsen mariner Organismen erheblich reduziert werden kann, ist diese bisher nicht explizit und ausreichend in der derzeitigen Bemessungspraxis berücksichtigt. Daher besteht das Hauptziel dieser Arbeit darin, den Wissensstand bezüglich der Auswirkungen der Porosität auf die hydrodynamischen Prozesse auf und unterhalb offenporiger, gebundener Deckwerke bei unterschiedlichen Böschungsneigungen zu verbessern. Um dieses Ziel zu erreichen, wurden umfangreiche kleinmaßstäbliche Modellversuche durchgeführt.

Der Wissensstand wurde zunächst analysiert, um Wissenslücken hinsichtlich der Prozesse vor, auf und unterhalb dieser Deckwerke herauszuarbeiten. Dabei wurden insbesondere die bereits vorhandenen Studien von Oumeraci et al. (2010b) (Laborstudie) und die abgeschlossenen Doktorarbeiten von Foyer (2013) und Alcérreca Huerta (2014) (beide numerisch) berücksichtigt. Anschließend wurden bei kleinmaßstäblichen Modellversuche mit vereinfachtem Modellaufbau die Parameter Böschungsneigung, Rauheit und Porosität des Deckwerks variiert, um die relative Bedeutung dieser drei Parameter auf die vorher genannten Prozesse zu untersuchen. Die Ergebnisse dieser Vorversuche wurden genutzt, einen realistischeren Modellaufbau zu entwickeln und das Testprogramm für die Hauptversuche zu optimieren, welche das Fundament dieser Dissertation darstellen. Die Prozesse bei Wechselwirkung von unregelmäßigem Seegang mit dem porösen Deckwerk und seinem Unterbau wurden systematisch analysiert: (a) Prozesse vor und auf dem Deckwerk (Reflexion, Brandungsstau, Wellenauf- und -ablauf); (b) welleninduzierte Druckbelastung auf dem Deckwerk unter Einbeziehung von Wellenbrechen, einer Klassifizierung der Wellenbelastung, der Maximaldrücke und deren Lage auf dem Deckwerk; (c) Prozesse unterhalb des Deckwerks einschließlich der Dämpfung der welleninduzierten Drücke durch das Deckwerk, des Porenwasserdruckabbaus im Sandkern, des internen, mittleren Wasserspiegels (IMWL) und der Stabilität des Sandkerns.

Insgesamt haben die Ergebnisse zum ersten Mal die relative Bedeutung von Deckwerksporosität und -neigung gezeigt und zu einem verbesserten Verständnis ihres Einflusses auf alle vorher genannten Prozesse geführt. Im Einzelnen wurde erstmalig gezeigt, dass eine erhöhte Porosität zu einem größeren Einfluss der einlaufenden Wellenhöhe auf den Reflexionskoeffizienten führt. Mit ansteigender Wellenhöhe verhält sich das hochporöse Deckwerk zunehmend wie eine undurchlässige Struktur. Eine höhere Porosität führt außerdem zu reduzierten Wellenauf- und -ablaufhöhen, mit größerem Einfluss auf den Wellenauflauf. Die räumliche Verteilung des mittleren Wasserspiegels im Sand, die einen entscheidenden Einfluss auf die Bauwerksstabilität hat, wurde erstmalig systematisch für unregelmäßigen Seegang untersucht. Dabei hat sich gezeigt, dass der interne Brandungsstau η_{int} nahe der Uferlinie bei flacherer Böschungsneigung (1:6) weniger von Auf-und Ablaufprozessen auf dem Deckwerk beeinflusst wird als bei steilerer Böschung (1:3). Da in den Hauptversuchen nur zwei Porositäten und zwei Böschungsneigungen untersucht wurden, ist die Gültigkeit der gewonnenen empirischen Formeln auf die hier gewählten oder vergleichbare Testbedingungen beschränkt.

Contents

List of Figures

List of Tables

List of Notations

Parameter	Dimension	Description
A,B,C,D	-	empirical coefficients
a,b,c,d		empirical coefficients
a_{grad}, $b_{grad,}$ c_{grad}	-	empirical coefficients for the description of the relative uplift pressure difference in the sand core
a_{imp}, $b_{imp,}$ c_{imp}	-	empirical coefficients for the description of the impact pressure component
a_{IMWL}, b_{IMWL}	-	empirical coefficients for the description of the development of the IMWL
$a_{loc,up}$, $b_{loc,up}$	-	empirical coefficients for the description of z_{pmax}, upper envelope
$a_{loc,low}$, $b_{loc,low}$	-	empirical coefficients for the description of z_{pmax}, lower envelope
a_{refl}, b_{refl}	-	empirical coefficients for the reflection behaviour
a_{rd}, b_{rd}	-	empirical coefficients for the wave run-down behaviour
a_{ru}, b_{ru}	-	empirical correlation coefficients for the wave run-up behaviour
A_{Sand}	-	empirical coefficient for the description of the pressure reduction in the sand
a_{stat}, b_{stat}, c_{stat}	-	empirical coefficients for the description of the quasi-static pressure component
a_{su}, b_{su}	-	empirical coefficients for the wave set-up behaviour
c	m/s	local wave celerity
c_0	m/s	deep water wave celerity
c_1	-	Empirical coefficient for the description of wave run-up (Schüttrumpf (2001))
c_{1*}	-	Empirical coefficient for the description of wave run-up (Schüttrumpf (2001))
$c_{corr,B}$	-	correction factor for the differences in coefficient B
C_d	-	dissipation coefficient
c_{IMWL}, d_{IMWL}	-	empirical coefficients for description of development of IMWL
C_m	-	virtual mass coefficient
C_r	-	reflection coefficient
c_{ve}	m²/s	consolidation coefficient
c_s	N/m²	cohesion
d	m	grain diameter
d_{10}	mm	grain diameter at 10% passing
d_{15}	mm	grain diameter at 15% passing
d_{50}	mm	grain diameter at 50% passing
d_{60}	mm	grain diameter at 60% passing
d_c	m	thickness of cover layer
D_p		Damping performance of the revetment
d_f	m	thickness of filter layer

d_{rev}	m	thickness of revetment
E_i	m	incident wave energy
E_r	m	reflected wave energy
g	m/s²	acceleration of gravity
h	m	water depth
h_b	m	water depth at breaking point
H	m	wave height
H_0	m	deep water wave height
H_b	m	wave height at breaking point
H_i	m	incident wave height
H_m	m	mean wave height
H_{m0}	m	spectral wave height (zeroth moment)
H_r	m	reflected wave height
H_{rms}	m	root mean square wave height
H_S	m	significant wave height
I	-	hydraulic gradient
k	-	angular wave number
K	N/m²	elastic compression modulus
k_f	m/s	hydraulic conductivity coefficient
K_s	-	shoaling factor
L	m	wave length
L_0	m	deep water wave length
n	-	porosity
p_0	Pa	initial pressure in layer 2
p_a	Pa	atmospheric pressure
p_i	Pa	pore pressure in layer i
p_{imp}	Pa	impact pressure component
p_{imax}	Pa	peak pressure in layer i
p_{istat}	Pa	quasi-static pressure component in layer i
p_{max}	Pa	peak pressure
$\overline{p}_{max}$	Pa	relative peak pressure
p_{stat}	Pa	quasi-static pressure component
r^2	-	coefficient of determination
R_c	m	freeboard
R_d	m	wave run-down height
$R_{d2\%}$	m	wave run-down height exceeded by 2% of the run-down events
$R_{d2\%,EMWL}$	m	$R_{d2\%}$ referred to EMWL

Re_i	-	Reynolds-number
R_u	m	wave run-up height
$R_{u2\%}$	m	wave run-up height exceeded by 2% of the run-up events
$R_{u2\%,EMWL}$	m	$R_{u2\%}$ referred to EMWL
S_{up}	-	stability factor
$\tan\alpha$	-	slope steepness
t	s	time
T	s	wave period
T_m	s	mean wave period
$T_{m-1,0}$	s	spectral wave period from zeroth an minus first moment
T_p	s	peak period
u	Pa	pore pressure
u_{0*}	Pa	initial pore pressure on the sand core at time t
u_t	Pa	pore pressure in depth z' at time t
u_{t*}	Pa	transient pore pressure in depth z' at time t
u_r	Pa	residual pore pressure in depth z' at time t
v_r	m/s	horizontal flow velocity
x	m	horizontal distance parallel to SWL
x_{local}	m	distance between PT in the sand and SWL and sand intersection
x'	m	distance parallel to the revetment
x'_{max}	m	distance parallel to the revetment between SWL and location of peak pressure
z	m	vertical distance normal to SWL
z_2	m	characteristic length for pore pressure damping (de Groot et al. (2006))
z'	m	depth in the sand normal to the revetment
z_{pmax}	m	vertical distance between SWL and location of peak pressure
$\bar{z}_{pmax}$	m	relative vertical distance between SWL and location of peak pressure
α	-	slope angle
β	m^2/N	elastic compressibility of pore water
γ_b	-	reduction coefficient for a berm
γ_f	-	reduction coefficient for roughness of the slope
γ_w	N/m^3	unit weight of water
γ_θ	-	reduction coefficient for oblique wave attack
Δu_{rel}	-	relative uplift pressure difference in the sand core
η_{int}	m	internal wave set-up
η_s	m	wave set-up
$\eta_{s,int}$	m	wave set-up at interface of revetment and substructure
κ	-	breaking index

ν	m²/s	kinematic viscosity
ξ	-	surf similarity parameter
ξ_b	-	surf similarity parameter at incipient point of breaking
$\xi_{m-1,0}$	-	surf similarity parameter regarding H_{m0} and $T_{m-1,0}$
ξ_m	-	surf similarity parameter regarding H_m and T_m
ξ_{mod}	-	modified surf similarity parameter of Foyer (2013)
ξ_p	-	surf similarity parameter regarding H_S and T_p
ξ_{S0}	-	surf similarity parameter regarding H_S and L_0
ξ_0	-	surf similarity parameter regarding H_0 and L_0
ξ_{0p}	-	surf similarity parameter regarding H_0 and T_p
ρ	kg/m³	fluid density
ρ_c	kg/m³	density of the revetment cover layer
ρ_f	kg/m³	density of the revetment filter layer
ρ_r	kg/m³	density of the revetment
ρ'_s	kg/m³	bulk density of the submerged soil
ρ_w	kg/m³	water density
σ	-	standard deviation
σ	N/m²	total stress
σ'	N/m²	effective stress
σ'_{diff}	-	coefficient of standard variation
τ	N/m²	shear strength

CEM	Coastal Engineering Manual
EMWL	external mean water level
FFT	Fast Fourier Transformation
FZK	Forschungszentrum Küste (Coastal research centre)
GWK	Großer Wellenkanal (Large Wave Flume)
IMWL	internal mean water level
IPPB	interlocked pattern placed block
JONSWAP	Joint North Sea Wave Project
LWI	Leichtweiß-Institute for hydraulic engineering and water resources
MWL	mean water level
PBA	polyurethane bonded aggregate
PT	pressure transducer
PU	polyurethane
RUG	run-up gauge
SPM	Shore Protection Manual
SWL	still water level
WG	wave gauge

1 Introduction

Since the first constructions thousands of years ago to protect the coast, people have increasingly learned from previous failures, so that nowadays diverse concepts and protective structures against the threats from the sea are available. Due to climate change impacts (e.g. sea-level rise and increasing storminess) and the still increasing anthropogenic pressure on coastal zones (e.g. urbanisation and infrastructures) coastal protection will become more important in the coming years and decades, thus requiring new concepts and technologies to cope sustainably with the increased threats.

Among the diverse types of coastal structures, revetments are the most commonly used to protect shores, embankments and dike slopes against sea waves and currents. One of the most recent innovative structures of this type is the polyurethane bonded aggregate (PBA) revetment (Oumeraci et al. (2010b), Oumeraci et al. (2010a)) which has been introduced in 2004 for the protection of the island "Hamburger Hallig" as a new type of highly porous revetment made of crushed stones which are durably and elastically bonded by polyurethane (PU). PBA-revetments, like any other similar porous revetments bonded with other types of bonding agents, have several advantages as compared to conventional revetments. Some of these advantages may be summarized as follows (Oumeraci et al. (2010b)): (i) as compared to smooth impermeable revetments less wave reflection, less wave run-up and thus lower required height of the defence structure, (ii) as compared to other un-bonded stone and block revetments, smaller required stone sizes and smaller revetment thicknesses to resist the design wave load due to the high porosity combined with the durable elastic bonding, (iii) ecologically compatible with the marine environment as shown by field and laboratory studies (e.g. Lock (2008)).

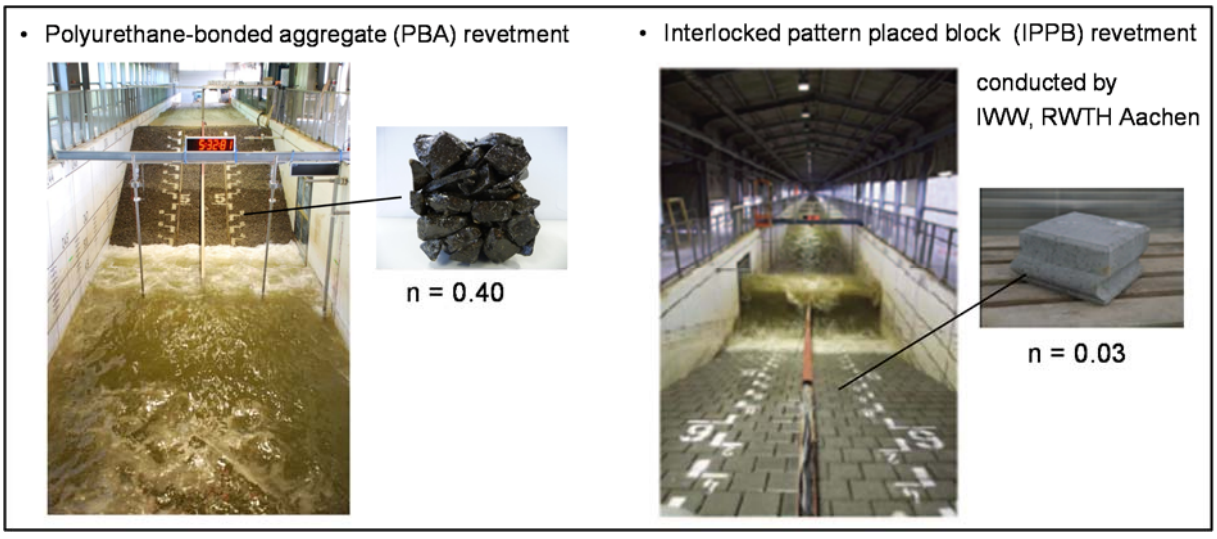

Fig. 1.1: Photos of different revetments under wave attack in the GWK, Hanover, Germany: a) PBA-revetment (Oumeraci et al. (2010b)), b) IPPB revetment (Gier et al. (2012)).

Despite all these advantages, the knowledge of the physical processes associated with the hydraulic performance, the wave loading and the response of the bonded porous revetment and its foundation was very limited still up to the end of the last decade. Therefore, systematic large-

scale model tests in the Large Wave Flume (GWK) of the Coastal Research Centre (FZK), a joint institution of Universities Braunschweig and Hanover, were conducted in 2009 using highly porous (n = 40%) PBA-revetments (Oumeraci et al. (2010b)). Later in 2010 and 2011, an almost impermeable (n = 3%) interlocked placed pattern block (IPPB) revetment was also tested in GWK (Gier et al. (2012)). The comparison of the results of these two studies with revetments of significantly different porosities (see Fig. 1.1) by Liebisch et al. (2012) has illustrated the crucial effect of the revetment porosity on the wave loading and the hydraulic performance of the structure and its foundation. Though the porosity of porous revetment may substantially be reduced over design life time (e.g. marine growth, sediment deposition), the porosity is not yet explicitly and adequately considered in the current design practice (e.g. EAK (2002), EurOtop (2007), CIRIA/CUR/CETMEF (2007)). This is mainly due to the lack of sufficient knowledge related to the effect of the revetment porosity on the wave loading and further processes on and beneath porous revetments. Therefore, it is crucial to improve the understanding of the hydrodynamic processes on and beneath porous bonded revetments, including the effect of revetment porosity, and based on this improved understanding to develop more physically-based and more generic design formulae. For this purpose, two PhD-studies, essentially based on numerical simulations using the results of the GWK-tests by Oumeraci et al. (2010b), were conducted (Foyer (2013) and Alcérreca Huerta (2014)). Despite the substantial advance and results which have been achieved in the comprehensive large scale model study in GWK and the two comprehensive numerical PhD-studies, some of the limitations are worth to mention:

- Only one revetment porosity was considered in the GWK-tests and in the numerical simulations, so that the effect of the porosity on the aforementioned processes is still not well understood. Moreover, the relative importance of the effect of the porosity as compared to that of the revetment roughness and that of the slope steepness is still unknown.
- Only regular wave tests could be performed in the numerical studies, so that direct comparisons to the irregular wave tests is not yet possible
- The duration of the numerical tests was very limited, so that the development of the processes in the sand core beneath the revetment (e.g. internal wave set-up) could not be completely obtained.

1.1 Objectives

Based on the aforementioned considerations and motivations, the primary objective of this study is to improve the knowledge related to the effect of the porosity for different slope steepnesses of a bonded revetment on the hydrodynamic processes on and beneath the revetment, including:

(i) wave reflection, wave run-up and run-down,
(ii) wave loads on and beneath the revetment,
(iii) wave-induced pore pressure in the sand core beneath the revetment and
(iv) wave set-up and the development of the internal mean water level in the sand core.

Moreover, the relative importance of the revetment porosity and slope steepness will also be investigated. Formulae which account explicitly for the revetment porosity on each of the aforementioned processes will also be developed.

1.2 Methodology

To achieve the aforementioned objectives, more systematic and extensive scale model tests need to be conducted in a smaller wave flume than GWK due to the considerable amount of time and costs for large scale tests. The entire study includes the following four phases which will be specified more precisely in the concluding section of chapter 2, based on the implications of the results of the analysis of the current knowledge obtained from that chapter:

- Phase 1: Review and analysis of current knowledge with the objective of identifying the knowledge gaps and the most relevant approaches to be used in this research
- Phase 2: Preliminary scale model tests using a very simplified revetment model allowing an easier variation of revetment porosity and roughness as well as slope steepness with a focus on regular waves
- Phase 3: Optimization of the model set-up and programme for the main tests based on the results of Phase 2
- Phase 4: Main scale model tests using a more realistic bonded revetment model with a focus on irregular waves

Based on the results of chapter 2, both objectives and methodology are specified more precisely in section 2.4.

2 State of the Art Review

In this chapter the current knowledge of the processes and the available formulae which are relevant for the interaction of waves with bonded porous revetments are reviewed and analysed. As illustrated in Fig. 2.1, this includes the processes in front of and on the revetment, the wave-induced pressure on the revetment and the hydro-geotechnical processes in the sand core beneath the revetment.

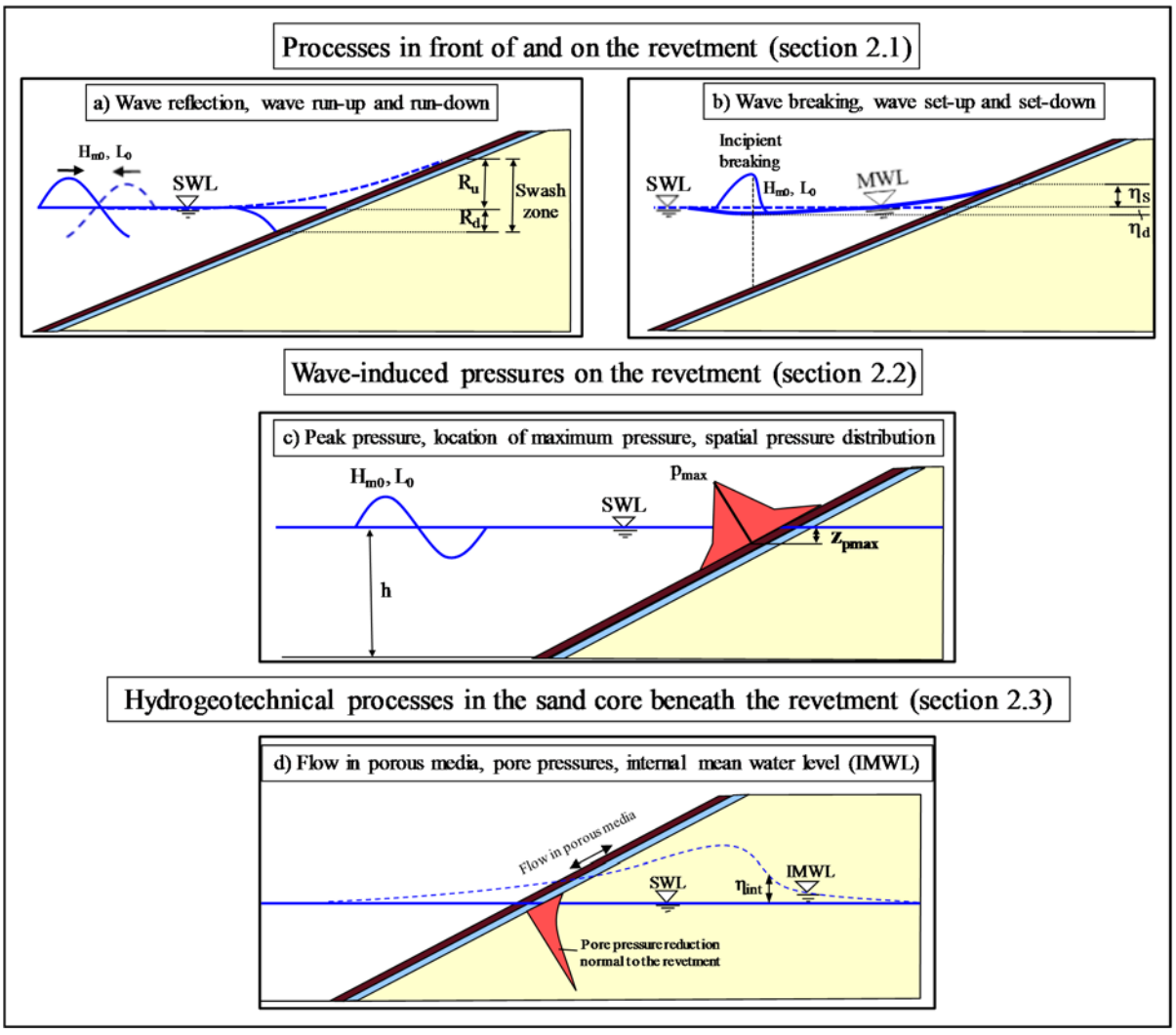

Fig. 2.1: Processes involved in the wave-structure-subsoil interaction relevant for bonded porous revetments

In section 2.1 the processes taking place in front of and on the revetment, including the available prediction formulae, are addressed. The processes which are considered are wave breaking, wave reflection, wave-run up and run-down as well as wave set-up and set-down (see Fig. 2.1 a and b).

Section 2.2 is dedicated to the wave-induced pressures on the revetment with a focus on the peak pressure p_{max} as well as its location z_{pmax} (impact point) and the spatial pressure

distribution related to p_{max} on the revetment (see Fig. 2.1 c). This also includes a classification of the wave loading into impact and non-impact loads and the resulting implications.

Section 2.3 focusses on the hydrogeotechnical processes in the sand core (Fig. 2.1 d), which include the wave-induced pore pressure development and the damping in the sand core, the development of the internal mean water level (IMWL) as well as a brief description of basic soil mechanics relevant to soil liquefaction. The processes within the bonded porous revetment are not among the objectives of this thesis due to the difficulties of direct measurements within the revetment. Nevertheless, the review also includes a brief description of the Forchheimer flow, which is typical in porous media, because this is important for a better understanding of energy dissipation and pressure damping through the porous revetment.

Based on the identified knowledge gaps, the implications for this study are drawn at the end of each section. In section 2.4 the key results are summarized and the objectives and methodology for this study are specified more precisely based on the implications of these results.

2.1 Processes in front of and on the revetment

In this section, the most relevant hydrodynamic processes in front of and at the revetment such as wave breaking, wave reflection as well as those on the revetment such as wave run-up, wave run-down and wave set-up, including the available prediction formulae are reviewed and analysed. Wave reflection, but very often also wave breaking and energy dissipation, takes place at the revetment and are thus related to the energy balance within the wave-structure interaction. Moreover, both wave breaking and wave reflection strongly depend on wave conditions (water depth h, wave period T, wave height H) and revetment characteristics (slope steepness, porosity and roughness) and may significantly affect the wave loads, wave run-up/run-down and wave set-up. The latter is particularly important as it affects all other processes on and beneath the revetment.

2.1.1 Wave breaking

Waves propagating into shallower water get steeper due to shoaling. When a critical wave steepness is reached, the waves become instable and break. The horizontal particle velocity at the wave crest becomes equal or larger than the wave celerity, so that the water particles move faster than the wave crest.

The location of incipient wave breaking is called breaking point with the related breaker height H_b and the breaking depth h_b. Wave breaking represents the most important mechanism for wave energy dissipation and is associated with the highest wave loads on structures. A part of the incident wave energy is dissipated and the wave height decreases significantly after breaking. For waves breaking on the revetment, the highest wave loads occur in the impact area located in the swash zone and strongly depend on the breaker type.

The initiation of breaking process was subject of several studies to describe wave breaking through a breaker index, which is very often described as a relation of breaker height H_b and breaking depth h_b (e.g. McCowan (1894), Goda (2010)). Other approaches use a critical wave steepness especially to explain wave breaking in deep water independent from water depth (e.g. Miche (1944), Battjes & Janssen (1978)).

Different breaker types can develop which determine the temporal and spatial development of energy dissipation. The breaker type is therefore crucial for the wave loading and all other processes involved in wave-structure-interaction. Iversen (1952) was the first who defined three different breaker types, which can be distinguished by the amount and the development of dissipated energy as compared to the amount of reflected energy (see Fig. 2.2).

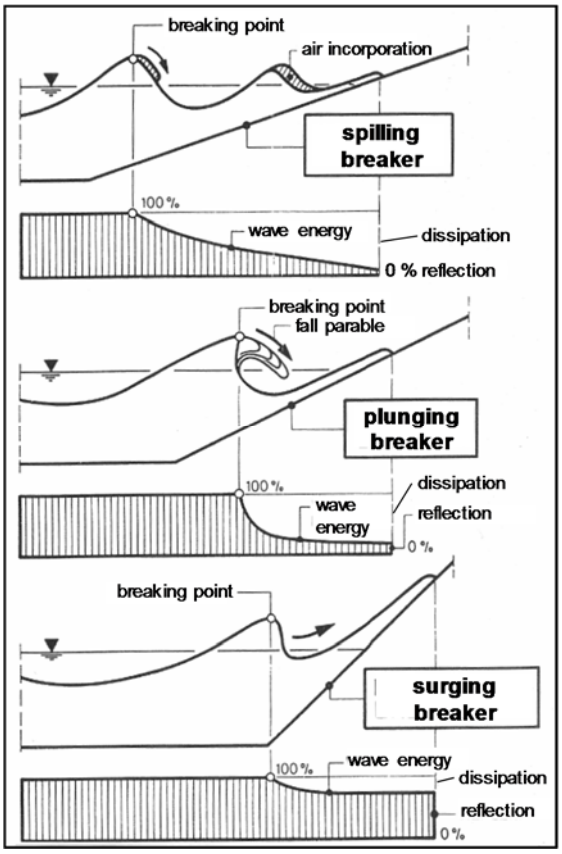

Fig. 2.2: Breaker types with dissipated and reflected energy amount (EAK (2002))

Spilling breakers mostly develop over relatively flat slopes. Wave energy is dissipated over a long distance (several wave lengths). The wave height decreases progressively after breaking. The amount of reflected wave energy is smaller than that of the dissipated energy.

Plunging breakers occur on slopes with a moderate slope steepness. During the curling process, the wave crest plunges resulting in an entrapped air pocket. The energy dissipation is released abruptly over a very small distance (fraction of the wave length) inducing a violent impact. The wave height decreases rapidly and only small reformed waves remain. Only a small amount of energy is reflected.

Surging breakers occur on very steep beach slopes and are characterised by the highest reflected energy and the lowest energy dissipation, thus leading to a larger wave run-up as compared to other breaker types. Therefore, incident waves are strongly affected by the reflected wave, so a curling of the wave crest is unlikely.

Collapsing breaker was defined later by Galvin (1968) as a transition zone between plunging and surging breakers, which is also now considered in several design guidelines (e.g. USACE (2002) and EurOtop (2007)).

A decisive parameter to classify the breaker types on sloping bottom or structures is the surf similarity parameter ξ, which is also called Irribarren-number. This parameter combines wave characteristics (wave steepness H/L) with characteristics of the structure (slope steepness $\tan\alpha$) and represents therefore a key parameter to describe all processes associated with wave breaking such as wave reflection, wave run-up/down and wave set-up. Different surf similarity parameters have been proposed in previous studies depending on the wave height used (in deep water or locally). Using deep water wave height H_0, Bruun & Günbak (1977) defined the offshore surf similarity parameter ξ_0 as follows:

$$\xi_0 = \frac{\tan\alpha}{\sqrt{H_0 / L_0}} \tag{2.1}$$

Based on the local wave height at incipient breaking (breaker height H_b), a further surf similarity parameter ξ_b was also defined by Bruun & Günbak (1977):

$$\xi_b = \frac{\tan\alpha}{\sqrt{H_b / L_0}} \tag{2.2}$$

As shown by eq. (2.1) and eq. (2.2) different definitions of the surf similarity parameter might result in different ranges of ξ for which the breaker types may occur (see Tab. 2.1). This needs to be carefully considered, particularly when comparing results based on different definitions of the surf similarity parameters.

Tab. 2.1: Breaker type classification (Bruun & Günbak (1977))

Breaker type	ξ_0	ξ_b
Spilling breaker	< 0.5	< 0.4
Plunging breaker	0.5-3.3	0.4-2.0
Surging breaker	> 3.3	> 2.0

For irregular wave tests with a PBA-revetment in GWK, Oumeraci et al. (2010b) used the surf similarity parameter $\xi_{m-1,0}$, which is based on the characteristic wave period $T_{m-1,0}$ and the wave height H_{m0}.

Based on numerical investigations using regular waves, Foyer (2013) and Alcérreca Huerta (2014) also proposed a classification of breaker types based on the surf similarity parameter ξ_0. This classification is shown in Tab. 2.2 with a comparison with regular wave tests in GWK.

Tab. 2.2: Breaker type classification for bonded porous revetments for regular waves

		Spilling	Plunging	Collapsing	Surging
GWK-tests (Oumeraci et al. (2010b))	ξ_0	-	<2.2	2.2-4.5	>4.5
Numerical study (Foyer (2013))	ξ_0	<1.0	1.0-2.4	2.4-5.2	>5.2
Numerical Study (Alcérreca Huerta (2014))	ξ_0	-	0.6-2.4	2.4-3.4	>3.4

The ranges of the different breaker types for regular waves as shown in Tab. 2.2 cannot be transferred directly to irregular wave tests due to the different wave-wave interaction of the incident and downrushing waves. Especially the effect of a changing porosity on the breaking behaviour and the ranges of different loading cases was not investigated in the test series shown in Tab. 2.2.

Wave breaking is the most crucial mechanism for energy dissipation. Its effect on other processes strongly depends on the breaker type which is described by the surf similarity parameter ξ. As the latter is defined differently depending on the applied wave parameters, caution is recommended when comparing results based on different definitions of ξ.

As large database from numerical and experimental studies is available for regular waves, more focus must be put to extend the database for irregular waves on bonded porous revetments. To ensure comparability with the irregular wave tests in GWK by Oumeraci et al. (2010b) used for the analysis of the different processes associated with wave breaking, surf similarity parameter $\xi_{m-1,0}$ will also be adopted in this study.

The effect of a changing porosity on the breaking behaviour on bonded porous revetments is not yet investigated and thus represents a knowledge gap.

2.1.2 Wave reflection

The energy of a wave interacting with a structure is generally composed of reflected, dissipated and transmitted wave energy. Depending on the structure and incident wave parameters the relative amount of these energy components may greatly differ, thus leading to a large variation of the reflection behaviour for different types of structures and for different structure parameters such as slope steepness, porosity and roughness. Smooth impermeable vertical and sloping structures are much more reflective than rough and porous structures due to larger energy dissipation at and inside the latter. The reflected energy is described by the reflection coefficient which is defined as the ratio of the square root of reflected wave energy to incident wave energy or more practically as the ratio of reflected wave height H_r to incident wave height H_i:

$$C_r = \frac{H_r}{H_i} = \sqrt{\frac{E_r}{E_i}} \tag{2.3}$$

Wave reflection is particularly important because the incident and reflected waves interact to build a complex wave field at and in front of the structure. This might for instance lead to an enhanced erosion of the sea bed in front of the structure which might increase the effect on other processes such as wave loads, wave run-up and wave overtopping.

Miche (1951) was the first to establish a reflection theory showing that a part of the energy of an incident wave which exceeds the critical wave steepness is dissipated on a smooth, impermeable slope while the remaining energy is reflected. Miche's theoretical approach was extended in Battjes (1974) by introducing the surf similarity parameter to describe the wave reflection coefficient. Afterwards, several prediction formulae for wave reflection C_r based on the surf similarity parameter emerged (see Tab. 2.3). A comparative analysis of the prediction formulae for C_r was performed by Oumeraci & Muttray (2001) showing that these formulae have a coefficient of variation of 10 to 140%. Amongst the existing models, the formula by Seelig & Ahrens (1981) was found to be the most widely used and also associated with the lowest uncertainties:

$$C_r = \frac{A \cdot \xi_0^2}{B + \xi_0^2} \tag{2.4}$$

where empirical parameters A and B depend on the permeability, the roughness, the geometry and the water depth in front of the structure.

Tab. 2.3: Design formulae for the reflection coefficient (Muttray et al. (2006))

Author	Breaker index ξ	Reflection formula C_r	Mean error[1]	Standard deviation abs.	Standard deviation rel.
Battjes (1974)[2]	$\frac{\tan\alpha}{\sqrt{H/L_0}}$	$0.1\xi^2$	2.34	0.59	138%
Gimenez-Curto (1979)	$\frac{\tan\alpha}{\sqrt{H/L_0}}$	$\frac{1}{2} - \frac{\exp(-0.125\xi)}{2}$	0.67	0.16	37%
Seelig & Ahrens (1981)	$\frac{\tan\alpha}{\sqrt{H/L_0}}$	$\frac{0.6\xi^2}{6.6+\xi^2}$	1.20	0.12	28%
Buerger et al. (1988)	$\frac{\tan\alpha}{\sqrt{H/L}}$	$\frac{0.6\xi^2}{12+\xi^2}$	1.09	0.10	24%
Postmar (1989)	$\frac{\tan\alpha}{\sqrt{H/L_0}}$	$0.125\xi^{0.73}$	1.23	0.14	33%
van der Meer (1992)[3]	$\frac{\tan^{0.62}\alpha}{(H/L_0)^{0.46}}$	$0.07(P^{-0.08}+\xi)$	1.23	0.16	37%
Hughes & Fowler (1995)	$\sqrt{\frac{h}{gT^2\tan\alpha}}$	$\frac{1}{1+7.1\xi^{0.8}}$	0.94	0.06	14%
Davidson et al. (1996)[4]	$\frac{\tan\alpha}{\sqrt{H/L_0}}$	$0.298\ln\xi + f(D,P,h,\alpha,H,L_0)$	0.88	0.09	20%
Zanuttigh & van der Meer (2006)	$\frac{\tan\alpha}{\sqrt{H/L_0}}$	$\tanh(0.12\xi^{0.87})$	1.32	0.15	35%
This study	–	Equation 7	0.99	0.02	5%

[1] Mean error $= \frac{1}{n}\sum_{i=1}^{n}\frac{C_{r,calculated}}{C_{r,measured}}$

[2] Not applicable for rubble mound structures

[3] Includes besides breaker index wave transmission D/H, permeability P, roughness of slope ($\sqrt{D/L_0}\cot\alpha$) and relative water depth at the toe h/L_0 (with rock diameter D)

[4] Permeability coefficient $P = 0.4$ for multi layered rubble mound structures

[5] Uses wave period $T_{m-1,0}$ ($= m_{-1}/m_0$) instead of peak wave period

The last equation in Tab. 2.3 by Zanuttigh & Van der Meer (1988) was derived from a large data set (more than 6000 data points) related to several types of structures:

$$C_r = \tanh\left(a \cdot \xi_0^b\right) \tag{2.5}$$

Eq. (2.5) has the advantage that C_r tends against 1.0 for very large surf similarity parameters. This behaviour is physically more justified for structures without any wave energy transmission (like revetments) than in other equations for structures where a part of the incident wave energy is transmitted. For instance in eq. (2.4), such a behaviour is only possible if coefficient A is set to 1.0.

The reflection behaviour of a bonded porous PBA-revetment was investigated for the first time by Oumeraci et al. (2010b). The results of the large scale model tests (PBA-revetment) are given in Fig. 2.3, together with those of a smooth impermeable slope and a porous two layer rock armour revetment for comparison.

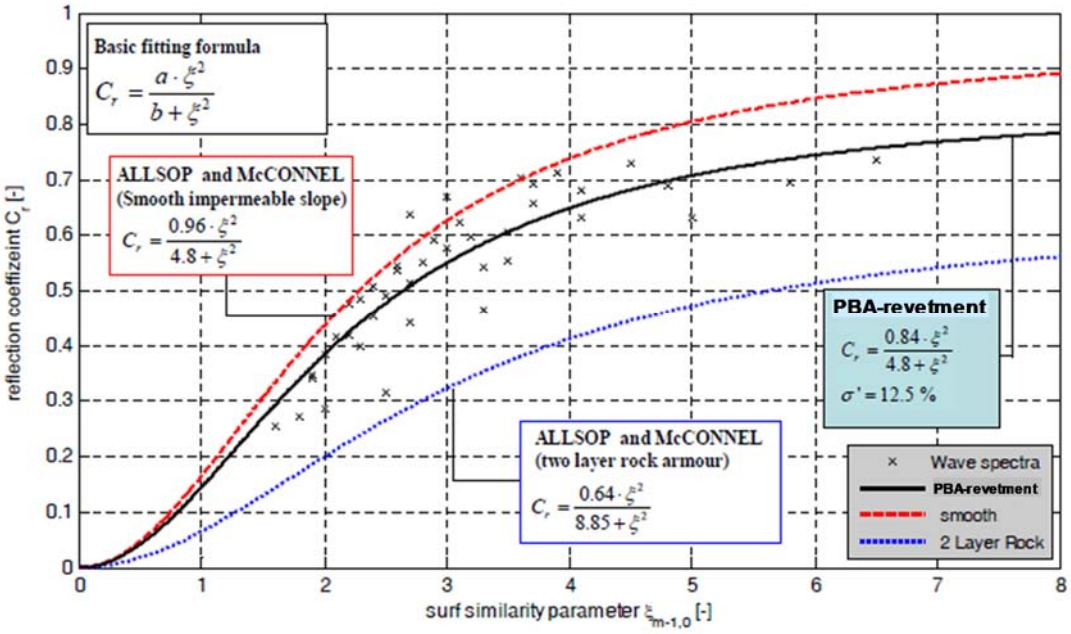

Fig. 2.3: Reflection coefficient C_r for different surf similarity parameters $\xi_{m-1,0}$ (Oumeraci et al. (2010b))

It is obvious in Fig. 2.3 that the reflection coefficient for PBA-revetments is smaller than for impermeable smooth slopes. In contrast, the reflection on a two layer rock armour revetment is still much smaller. Based on the model of Seelig & Ahrens (1981) the following equation was obtained for the investigated PBA-revetment:

$$C_r = \frac{0.84 \cdot \xi_{m-1,0}^2}{4.8 + \xi_{m-1,0}^2} \tag{2.6}$$

with $\xi_{m-1,0}$ based on eq. (4.5)

The large scattering of the data, which was much more decisive for irregular wave tests than for regular wave tests, was found to be mainly due to the effect of the wave period which was

found much more important than it is considered by the surf similarity parameter $\xi_{m-1,0}$. This scattering was also observed in previous studies with porous structures and was also visible in the different databases of Zanuttigh & Van der Meer (1988). For future research Oumeraci et al. (2010b) recommended to develop another parameter which better accounts for the wave period $T_{m-1,0}$.

In the numerical investigations of Foyer (2013) on PBA-revetments, the following prediction formulae was developed for regular waves:

$$C_r = \frac{\xi_{mod}^2}{6.74 + \xi_{mod}^2} \tag{2.7}$$

Eq. (2.7) is based on a modified model of Seelig & Ahrens (1981) by setting the empirical coefficient A to 1.0 in order to better fulfil the condition that C_r should tend to 1.0 for large surf similarity parameters and by using the following modified surf similarity parameter to consider the effect of revetment thicknesses d_{rev} on wave breaking and thus on the related reflection behaviour:

$$\xi_{mod} = \frac{\tan\alpha}{\sqrt{\frac{H_m}{L_0} \cdot \left(1 + \frac{d_{rev}}{H_m}\right)}} \tag{2.8}$$

Alcérreca Huerta (2014) also investigated numerically the effect of revetment thickness d_{rev} of PBA-revetments for regular waves. No correlation could be found using the modified surf similarity parameter ξ_{mod}, and therefore ξ_0 was used instead. Moreover, he used the model proposed by Zanuttigh & Van der Meer (1988) for the analysis of the numerical data. The results showed that the revetment thickness of a PBA-revetment has only a slight effect on the reflection coefficient. For very small and very large surf similarity parameters the effect even becomes negligible.

Both numerical studies, Foyer (2013) and Alcérreca Huerta (2014), could not confirm the findings of Oumeraci et al. (2010b) of an additional effect of the wave period resulting in a large scattering of the data, which might be due to the consideration of only regular waves in the numerical studies. For regular wave tests this phenomenon was also smaller in Oumeraci et al. (2010b). Consequently, more research on the aforementioned additional effect of the wave period is necessary for irregular waves.

Wave reflection strongly affects the wave field in front of and directly over the revetment, and thus all other processes such as wave loading, wave run-up/down and wave set-up. Consequently, it is crucial to accurately predict the reflected wave energy, which depends directly on the wave energy dissipated by the reflective structure which again depends on the breaker type. The surf similarity parameter ξ determines the breaker type and has therefore been applied in most studies to describe wave reflection. The application of a modified surf similarity parameters such as eq. (2.8) from Foyer (2013) was already tested in Alcérreca Huerta (2014) and no correlation was found. Consequently, it is not applied in this study.

Among the diverse models available to predict wave reflection Cr as a function of ξ, the model of Seelig & Ahrens (1981) and the model of Zanuttigh & Van der Meer (1988) appear to be the most promising for this study.

The effect of porosity interacting with different slope steepnesses on the reflection performance of bonded porous revetments has not yet been investigated and represents a knowledge gap.

Though the wave period is already included in surf similarity parameter ξ, its additional effect on wave reflection C_r still needs further investigations. This additional effect might explain the large scatter of C_r plotted against ξ which was observed in all studies with porous structures.

2.1.3 Wave run-up and run-down

Wave run-up and run-down provide the total water excursion over the slope over a wave cycle and define the swash zone which represents the most important area of interaction between waves and revetment, particularly for wave loads (see Fig. 2.1a). The wave run up height R_u is commonly defined as the maximum elevation from still water level (SWL) to the point to which the water surface rises on the revetment. It therefore describes the upper boundary for the swash processes and is an important parameter to determine the required crest height of the structure. The wave run-down height R_d describes the lowest point that is reached by the down rushing water on the slope. Like R_u, R_d is also commonly related to SWL (Fig. 2.1a). It represents the lower boundary for the swash processes and is thus important to define the required minimum downward extent of the revetment. The wave run-down may significantly affect the breaking behaviour and the run-up process of the following incident waves. For irregular waves, both wave run-up and run down may vary significantly. Characteristic values $R_{u2\%}$ and $R_{d2\%}$ which are exceeded by 2% of the incident waves are commonly used for design purposes (e.g. EurOtop (2007)).

Several research studies have been performed in the past, showing that wave run-up (and thus also wave run-down) on smooth impermeable slopes generally depends on the incident wave height and the surf similarity parameter. For porous and rough revetments, where the energy dissipation mainly takes place not only on but also within the revetment, most of the studies available are focussed on rip-rap or similar types of revetment. More recently, the case of porous bonded revetments such as PBA-revetments was also addressed comprehensively. Among all these investigations, only the most relevant for this study are considered in the following.

a) Wave run-up

The first formulae to predict wave run-up height R_u was proposed by Hunt (1959) for regular waves breaking on a smooth impermeable slope. Re-written by Battjes (1974) in terms of surf

similarity ξ in eq. (2.9), Hunt's formula still represents the basis for most of the available prediction formulae for wave run-up:

$$\frac{R_u}{H} = \xi \quad \text{for } 0.1 < \xi < 2.3 \tag{2.9}$$

In further studies, this linear relation and its range of validity were modified and adapted to account for further different types of revetment and structure parameters.

Based on the comparative results of scale model tests with regular waves on smooth slopes between 1:1.5 and 1:3, comparatively to rubble mound breakwater slopes which are plotted using the relation $R_u/H = \xi$ in eq. (2.9), Bruun & Günbak (1977) were the first to show the fundamental difference of the relative wave run up R_u/H for the two different types of revetments (Fig. 2.4) . This also illustrates the effect of a porous and rough slope on the relative wave run-up. For smooth impermeable slopes, higher R_u/H-values are obtained, especially around $\xi = 2 - 4$ where the difference becomes highest. For larger ξ-values ($\xi > 6$), the difference has the tendency to get negligibly small.

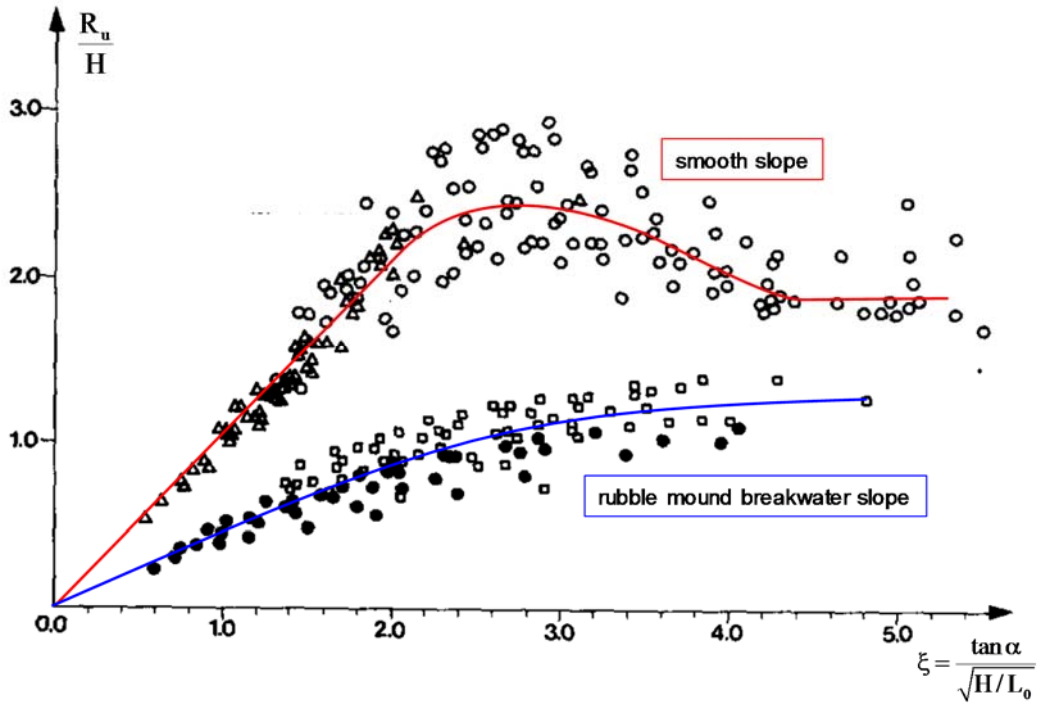

Fig. 2.4: Wave run-up on smooth and rubble mound breakwater slopes for irregular waves (modified from Bruun & Günbak (1977))

Based on several data sets from available and own experiments with irregular waves on wave run-up on smooth slopes and on different types of rough and porous slopes, Van der Meer & Stam (1992) confirmed and extended the results of the fundamental analysis in Fig. 2.4 for surf similarity parameters up to $\xi_p = 10$. The results showed that:

(i) a linear relationship of relative wave run up $R_{u2\%}/Hs$ and surf similarity parameters ξ_p exists only for $\xi_p < 2.0$:

For smooth, impermeable slopes: $$\frac{R_{u2\%}}{H_S} = 1.5 \cdot \xi_p \quad (2.10)$$

For rough and porous slopes: $$\frac{R_{u2\%}}{H_S} = 0.83 \cdot \xi_p \quad (2.11)$$

(ii) the largest difference between $R_{u2\%}/H_S$-values on the two basic types of slopes occurs for ξ_p = 2-4

(iii) the effect of porosity and roughness becomes negligible for very large surf similarity parameters $\xi_p > 6$

The results of Van der Meer & Stam (1992) showed the connection between wave run-up and the energy dissipation on the revetment. Dependent on the surf similarity parameter and the associated breaker types, a different amount of wave energy is dissipated during breaking process on the different investigated revetments. The difference is largest for strong breaking waves (ξ_p = 2-4). For large $\xi_p > 6$ the effect of the structure porosity becomes negligibly small.

Schüttrumpf (2001) performed model tests also with irregular waves on smooth impermeable slopes with steepnesses of 1:3, 1:4 and 1:6. Using the hyperbolic tangent model in eq. (2.12), clearly resulted in a better fit for the experimental data of the relative wave run-up as a function of surf similarity parameter ξ_{S0} based on the significant wave height H_S and deep water wave length L_0. The approach especially describes the transition from collapsing to surging breaker more appropriate.

$$\frac{R_u}{H_S} = c_1 \cdot \tanh(c_1^* \cdot \xi_{S0}) \quad (2.12)$$

with c_1 = 3.0 and c_1* = 0.65 for the tested conditions.

Looking for an alternative parameter instead of the surf similarity parameter to describe nearshore coastal processes on beaches and coastal structures Hughes (2004b) introduced the wave flux parameter. This approach is based on the radiation stress theory of Longuet-Higgins & Stewart (1964). Hughes (2004b) established an empirical equation for the estimation of the wave momentum flux parameter and used it in Hughes (2004a) for the estimation of wave run-up on smooth, impermeable slopes for regular and irregular waves. The developed equation overestimated the relative run-up for steep slopes and long waves significantly.

Madsen & Fuhrman (2007) disagreed with the conclusions of Hughes (2004a) that the surf similarity parameter is not a good choice as the governing parameter for the wave run-up. In their study of the wave run-up of long waves they used Carrier and Greenspan's shallow water theory which is based on the surf similarity parameter ξ and the relative water depth H/h to derive prediction formulae for the wave run-up. A comparison of the analytic solution with experimental dataset resulted in a relatively good agreement only for collapsing and surging breakers but not for plunging breakers.

In Tab. 2.4 an overview is given of most of the mentioned wave run-up formulae from previous studies together with a short description. It becomes obvious that most of the studies used the surf similarity parameter for the derived model.

Tab. 2.4: Summary of selected wave run-up formulae from previous studies

Author	Formula	Considerations
Hunt (1959)	$\frac{R_u}{H_0} = C \cdot \xi_0$ with $1.49 < C < 1.87$	Empirical approach for **regular waves** and uniform gentle slope. **Extend** by Battjes & Roos (1974) **for irregular waves** and C=1.6
Losada & Giménez-Curto (1981)	$\frac{R_u}{H_0} = A_U \cdot \left(1 - \exp\left(B_U \cdot \xi\right)\right)$	Based on a dimensionless analysis and experimental databases for rough permeable slopes under **regular waves**
Foyer (2013)	$\frac{R_u}{H_m} = \frac{\xi_m{}^2 + 14.6 \cdot \xi_m}{\xi^2 + 6.23^2} + \bar{\eta}$	Wave run-up related to MWL, without consideration of the wave set-up. Based on numerical modelling of PBA-revetments; **regular waves**
Alcérreca Huerta (2014)	$\left(\frac{R_u - \bar{\eta}_{S,RUG}}{H_0}\right)_{UE} = A \cdot (\xi_0 - A) \cdot \exp\left[-\frac{(\xi_0 - A)^2}{4A}\right] + \left(\frac{Ru - \bar{\eta}_{S,RUG}}{H_0}\right)_{UE}$	Wave run-up related to MWL, without consideration of the wave set-up. Based on numerical modelling of PBA-revetments; **regular waves** Upper envelopes: A = 0.55 for d_{rev} = 0.15 m A = 0.77 for d_{rev} = 0.25 m A = 0.97 for d_{rev} = 0.35 m
Ahrens & Heisnbaugh (1988)	$\frac{R_u}{H_{m0}} = \frac{A \cdot \xi}{1 + B \cdot \xi}$	Developed for **irregular waves** on rip-rap revetments
Van der Meer & Janssen (1995)	$\frac{R_{u2\%}}{H_S} = 1.5 \cdot \gamma_h \cdot \gamma_f \cdot \gamma_\beta \cdot \xi_{eq}$	Inclusion of correction factors for the effect of shallow water, slope roughness and oblique wave attack; **irregular waves**
Schüttrumpf (2001)	$\frac{R_{u2\%}}{H_S} = 3.0 \cdot \tanh\left(0.65 \cdot \xi_{S0}\right)$	Based on scale model tests with a smooth, impermeable slope; **irregular waves**
Hughes (2004)	$\frac{R_{u2\%}}{h} = 1.75 \cdot \left(1 - \exp\left[-1.3 \cdot \cot\alpha\right]\right) \cdot \left(\frac{M_F}{\rho g h^2}\right)$ $\frac{R_{u2\%}}{h} = 4.4 \cdot \left(\tan\alpha\right)^{0.7} \cdot \left(\frac{M_F}{\rho g h^2}\right)^{1/2}$	Based on the momentum flux parameter (M_F) instead of surf similarity parameter ξ_0; **irregular waves**
Madsen & Fuhrman (2008)	$\frac{R_{u2\%}}{H_{m0}} = \left(\frac{1.6}{2}\right) \cdot 2\pi^{3/4} \cdot \left(\frac{H_{m0}}{2h_0}\right)^{-1/4} \cdot \xi^{-1/2}$	Analytical approach based on linear and nonlinear shallow water equations for periodic long waves; **irregular waves**
Oumeraci et al. (2010b)	$\frac{R_{u2\%}}{H_{m0}} = \min\left[\begin{array}{l} 0.54 \cdot \left(1.65 \cdot \xi_{m-1,0}\right) \\ 0.78 \cdot \left(4 - \frac{1.5}{\sqrt{\xi_{m-1,0}}}\right) \end{array}\right]$	Based on GWK-tests with PBA-revetments; **irregular waves**

The current design practice is based on conducted investigations and the empirical approaches show a large dependency on the surf similarity parameter. The two most important guidelines are cited in the following:

(i) The Coastal Engineering Manual (CEM) (USACE (2002)) represents the technical advices for the American region. Herein an overview for the newest and most used investigations can be found. The CEM recommends to use eq. (2.13) which is divided into two parts with a separation point at a surf similarity parameter of 2.5. Eq. (2.13) is based on deep water parameters and irregular waves.

$$\frac{R_{u2\%}}{H_S} = \begin{cases} 1.6 \cdot \xi_{op} & for\ 0 < \xi_{op} \le 2.5 \\ -0.2 \cdot \xi_{op} & for\ \xi_{op} > 2.5 \end{cases} \tag{2.13}$$

(ii) The European wave overtopping handbook EurOtop (2007) is mainly based on the approach of TAW (2004), which is also a split function depending on surf similarity parameter $\xi_{m-1,0}$ (see eq. (2.14)). It contains reduction coefficients to consider the effects of a berm (γ_b) and oblique wave attack (γ_θ). The reduction coefficient γ_f to consider roughness effects also contains the effect of porosity of the structure

$$\frac{R_{u2\%}}{H_{m0}} = \min \begin{pmatrix} 1.65 \cdot \gamma_b \cdot \gamma_f \cdot \gamma_\theta \cdot \xi_{m-1,0} \\ \gamma_f \cdot \gamma_\theta \cdot \left(4.0 - \frac{1.5}{\sqrt{\xi_{m-1,0}}} \right) \end{pmatrix} \tag{2.14}$$

Generelly, the current design practice does not distinguish between the effect of porosity and roughness and the effect of porosity is included in the reduction coefficient for the roughness, because both parameters are connected inseperably with each other on revetments.

Based on the approach of EurOtop (2007) in eq. (2.14) by using a reduction coefficient γ_f to account for both porosity and roughness of PBA-revetments on the wave run-up, the results of the large-scale tests with irregular waves by Oumeraci et al. (2010b) are given in Fig. 2.5. The comparison with the relative wave run-up on the smooth impermeable slope ($\gamma_f = 1$) clearly illustrates the significant effect of the porous and rough slope on the wave run-up.

In the numerical study using regular waves on PBA-revetments by Foyer (2013), the wave run-up and run-down heights were analysed for the first time as related to the mean water level (MWL) instead of the commonly used approach using SWL as a reference level. In the latter approach the wave set-up η_S is implicitly included in the wave run-up R_u and run-down R_d, while it is removed and considered separately in Foyer (2013) due to the significantly different time scale (see eq (2.15)). The following equation for wave run-up and run-down heights describes two curves which are symmetric around MWL and the coefficients a and b depend on revetment thickness. This is also shown in Fig. 2.6:

$$\frac{R_u}{H_m} = -\frac{R_d}{H_m} = \frac{\xi_m^2 + b \cdot \xi_m}{\xi_m^2 + a^2} + \eta_S \tag{2.15}$$

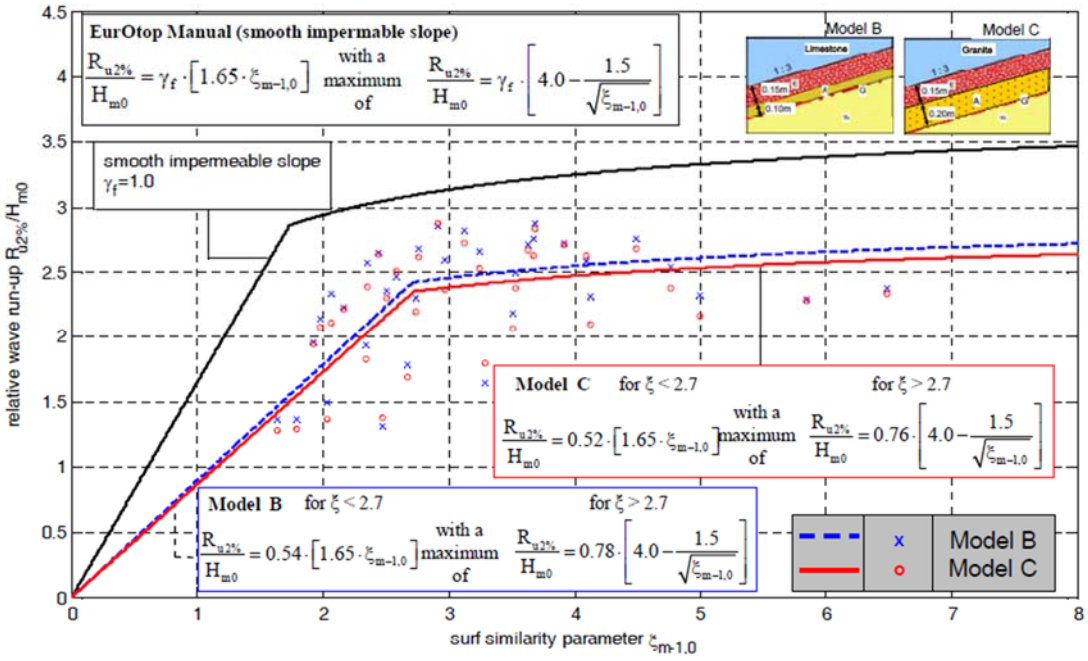

Fig. 2.5: Wave run-up height $R_{u2\%}$ for irregular waves (Oumeraci et al. (2010b))

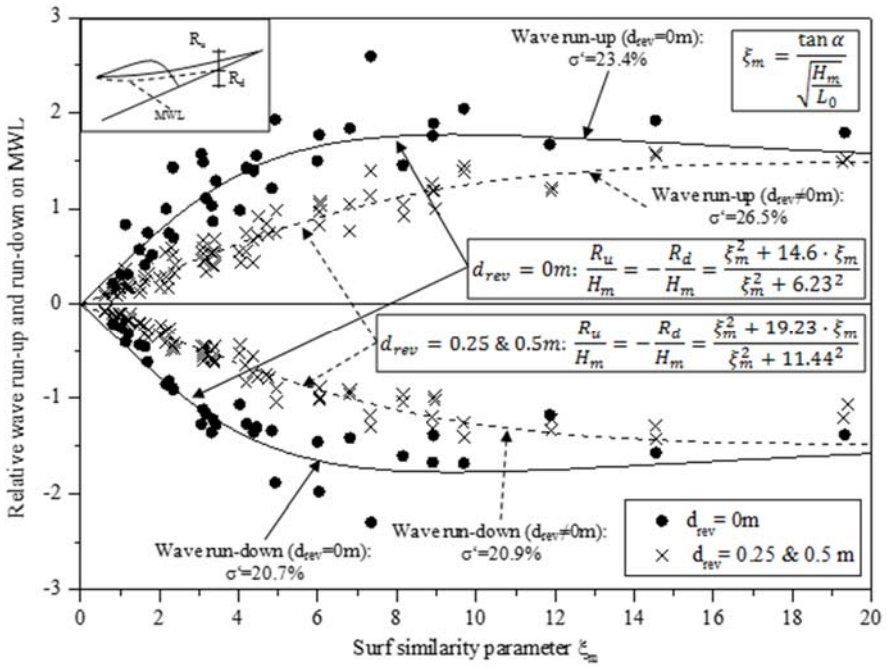

Fig. 2.6: Fitted curves for the wave run-up and run-down height related to MWL with and without revetment (Foyer (2013))

Alcérreca Huerta (2014) also applied in his numerical study with regular waves on PBA-revetments the same approach using MWL instead of SWL as a reference level for wave run-up and run-down. Moreover a basic distinction was made between impact and a non-impact component. The maximum run-up and run-down heights were obtained for surf similarity parameters between 2.0 and 4.0 and the resulting plunging and collapsing breakers (see Fig.

2.7). Instead of fitting functions for the numerical data, only upper envelopes were proposed due to the large scattering of the data (conservative approach for design).

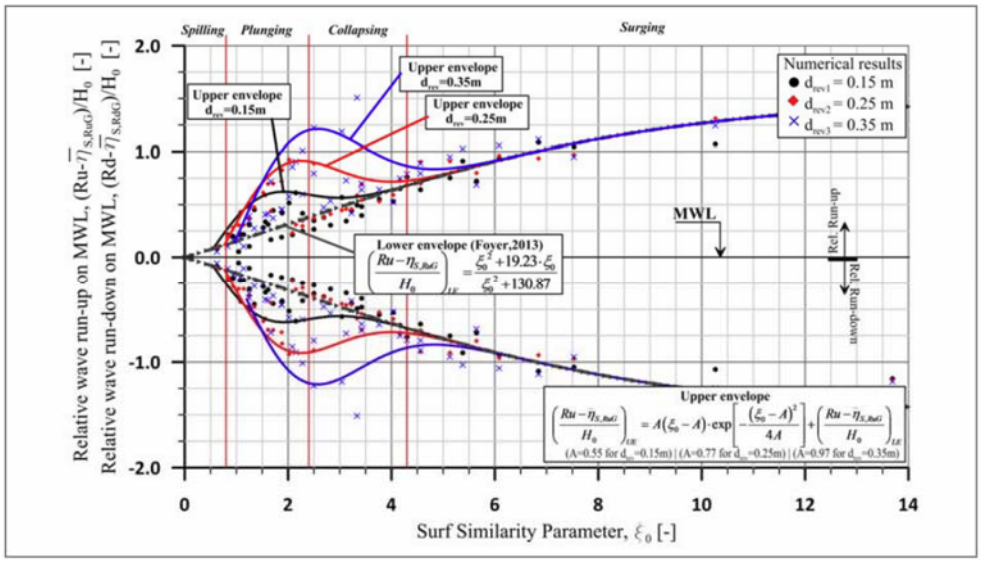

Fig. 2.7: Fitted curves for the wave run-up and run-down height related to MWL for different revetment thicknesses (Alcérreca Huerta (2014))

b) Wave run-down

In comparison to the large amount of studies on the wave run-up, the number of studies on wave run-down is very limited.

Bruun & Günbak (1977) also studied the wave run-down in their test series on breakwater slopes. The regular wave model tests were performed on smooth slopes with an angle between 1:1.5 and 1:3. In the tests the wave run-down provided positive values for $\xi < 2.2$ (plunging breakers) which means that run-down values did not fall under the still water level. The derived eq. (2.16) only showed a good fit for the obtained values for $\xi < 3.5$:

$$\frac{R_d}{H} = (1 - 0.45 \cdot \xi) \cdot \xi \tag{2.16}$$

Losada et al. (1981) studied the wave run-down too and also determined an exponential approach. This is shown in eq. (2.17).

$$\frac{R_d}{H} = A \cdot (1 - e^{B \cdot \xi}) \tag{2.17}$$

In addition to the data sets of Van der Meer & Stam (1992), Van der Meer (1993) also proposed a design formula for the wave run-down. A reduction of the data scatter was achieved by the consideration of slope steepness and the introduction of factor n to consider the effect of permeability through the pores in the equation (eq. (2.18)). These results showed clearly that there is an effect of a porous structure on wave run-down.

$$\frac{R_{d2\%}}{H_S} = -2.1 \cdot \sqrt{\tan\alpha} + 1.2 \cdot n^{0.15} - 1.5 \cdot e^{-60 \cdot s_{om}} \tag{2.18}$$

$$\text{with: } s_{om} = 2 \cdot \pi \cdot \frac{H_S}{g \cdot T_m^2}$$

Using a tangent hyperbolic model to fit the data for the relative wave run-down height Schüttrumpf (2001) proposed the following equation for irregular waves on smooth impermeable slopes:

$$\frac{R_{d2\%}}{H_S} = 0.7 + 0.7 \cdot \tanh(\xi_{SO} - 2.1) \tag{2.19}$$

For regular wave tests Schüttrumpf (2001) also obtained values above SWL for $\xi < 2.2$ (spilling and plunging breakers) which could not be fit by the tangent hyperbolic function in eq. (2.19).

An overview of the formulae found for wave run-down in previous studies together with a short description can be found in Tab. 2.5. According to wave run-up, also for the wave run-down most of the studies used the surf similarity parameter for the derived model.

Tab. 2.5: Summary of selected wave run-down formulae from previous studies

Author	Formula	Considerations
Battjes & Roos (1974)	$R_d = R_u \cdot (1 - 0.4 \cdot \xi_0)$	Empirical approach for **regular waves** and uniform smooth impermeable slope
Losada & Giménez-Curto (1981)	$\frac{R_u}{H_0} = A_U \cdot (1 - \exp(B_U \cdot \xi))$	Based on a dimensionless analysis and experimental databases for rough permeable slopes under **regular waves**
Foyer (2013)	$\frac{R_d}{H_m} = \frac{\xi_m^{\,2} + 14.6 \cdot \xi_m}{\xi^2 + 6.23^2} + \bar{\eta}$	Wave run-down related to MWL. Based on numerical modelling of PBA-revetments; **regular waves**
Alcérreca Huerta (2014)	$\left(\frac{R_d - \bar{\eta}_{S,RUG}}{H_0}\right)_{UE} = -A \cdot (\xi_0 - A) \cdot \exp\left[-\frac{(\xi_0 - A)^2}{4A}\right] + \left(\frac{Ru - \bar{\eta}_{S,RUG}}{H_0}\right)_{UE}$	Wave run-down related to MWL. Based on numerical modelling of PBA-revetments; **regular waves** Upper envelopes: A = 0.55 for d_{rev} = 0.15 m A = 0.77 for d_{rev} = 0.25 m A = 0.97 for d_{rev} = 0.35 m
Van der Meer (1988)	$\frac{R_{d2\%}}{H_S} = -2.1 \cdot \sqrt{\tan\alpha} + 12 \cdot P^{0.15} - 1.5 \cdot \exp(-60 s_{om})$	Developed for **irregular waves** on rock slopes; consideration of the notional permeability P
Pilarczyk (1987)	$\frac{R_{d2\%}}{H_S} = \begin{cases} -0.8 \cdot \xi_0 - 0.5 & \text{for } 0 < \xi_0 < 2.5 \\ -2.5 & \text{for } \xi_0 > 2.5 \end{cases}$	Maximum wave run-down for **irregular waves** on impermeable and rip-rap slopes
Schüttrumpf (2001)	$\frac{R_{d2\%}}{H_S} = -0.7 \cdot [1 + \tanh(\xi_{S0} - 2.1)]$	Based on scale model tests with a smooth, impermeable slope; **irregular waves**
Oumeraci et al. (2010b)	$\frac{R_{d2\%}}{H_{m0}} = \max\begin{bmatrix} -0.42 \cdot \xi_{m-1,0} + 0.17 \\ -2.25 \end{bmatrix}$	Based on GWK-tests with PBA-revetments; **irregular waves**

In the current design practice the following equations can be found for the determination of the wave run-down:

(i) The CEM (USACE (2002)) recommends to use eq. (2.20) which is, according to the wave run-up model (eq. (2.20)), divided into two parts with a separation point. Surprisingly, this separation point at $\xi_{op} = 4.0$ differs from the one found for wave run-up. Eq. (2.20) is also based on deep water parameters and irregular waves and was developed for an impermeable revetment.

$$\frac{R_{d\,2\%}}{H_S} = \begin{cases} -0.33 \cdot \xi_{op} & for\ 0 < \xi_{op} \le 4 \\ -1.5 & for\ \xi_{op} > 4 \end{cases} \tag{2.20}$$

(ii) The „Rock Manual“ by CIRIA/CUR/CETMEF (2007) also gives a design formula for wave run-down on porous riprap revetment which is based on Thompson und Shuttler (1977):

$$\frac{R_{d1\%}}{H_S} = -0.34 \cdot \xi_p + 0.17 \tag{2.21}$$

In the context of the large-scale tests of Oumeraci et al. (2010b), the wave run-down height on PBA-revetment was also analysed. The results in Fig. 2.8 show that the wave run-down height is not significantly affected by the porous structure in comparison to an impermeable and smooth revetment.

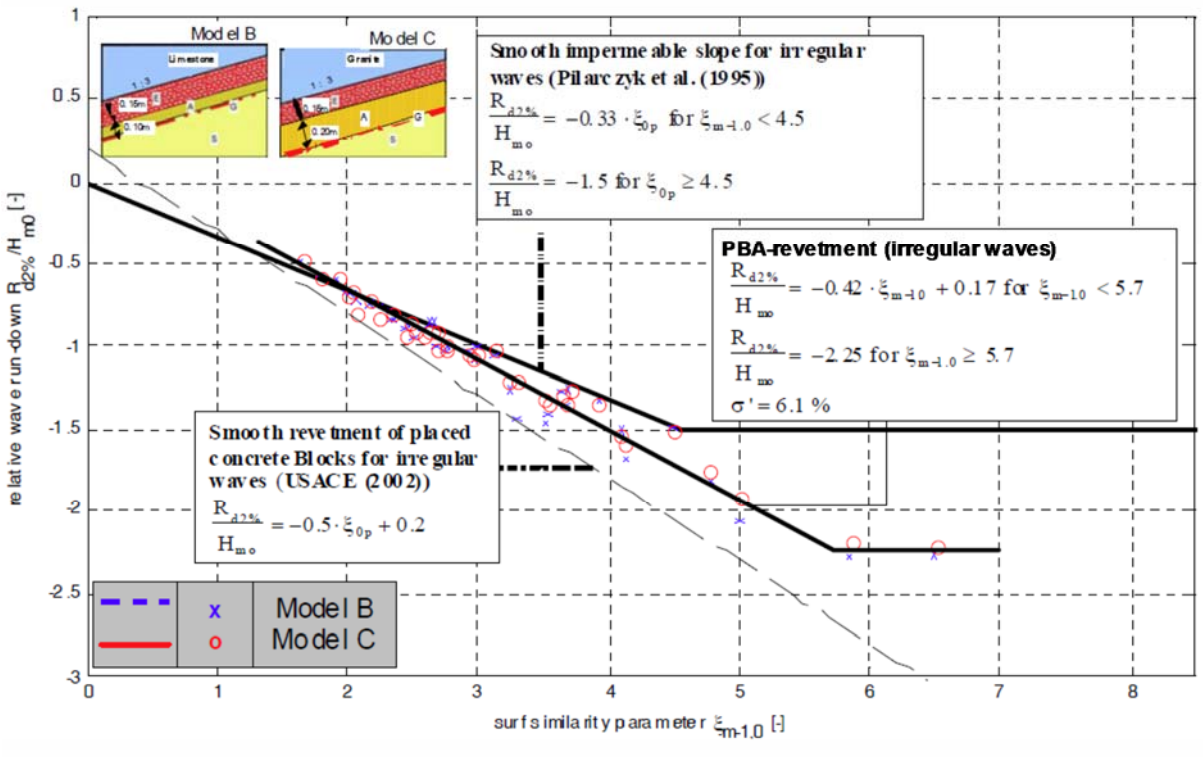

Fig. 2.8: Wave run-down height $R_{d2\%}$ for irregular waves (Oumeraci et al. (2010b))

The results for the wave run-down of the numerical study using regular waves on PBA-revetments by Foyer (2013) were already shown in Fig. 2.6 together with the wave run-up related to MWL. The fitting curve was found to be symmetric wave run-up and run-down depending on the revetment thickness.

A similar approach by Alcérreca Huerta (2014) (see Fig. 2.7) with the application of upper envelopes also showed symmetry between wave run-up and run-down related to MWL. This also includes the maximum wave run-down heights in the range of plunging and collapsing breakers (see Fig. 2.7).

A significant amount of studies related to wave run-up on revetments are available as compared to those on wave run-down. Most of them were focussed on smooth and impermeable slopes, showing that the parameter governing wave run-up/run-down is the surf similarity parameter. The studies for rough and permeable revetments are generally restricted to specific types of structures, showing that the highest effect of roughness and porosity as compared to smooth impermeable slopes occurs for surf similarity parameter $\xi = 2\text{-}4$ (plunging-collapsing breakers). More research is necessary, which is based on more systematic irregular wave tests with different revetment porosities and covering the full range of surf similarity parameters (plunging to surging breakers).

No study could be found which addresses the effect of the porosity and roughness on wave run-up/run-down separately and more systematically. It was already shown that roughness and porosity both decrease wave run-up. Thus, systematic research is necessary to investigate the effect of porosity and roughness separately.

The effect of porosity interacting with different slope steepnesses on the reflection performance of bonded porous revetments has not yet been investigated.

More recent studies related to porous bonded revetments have shown the advantage of relating wave run-up and wave run-down to the mean water level (MWL) instead of the common approach using SWL as a reference level due to the significantly different time scale. It is therefore recommended to apply this method in the current study.

Most of the derived models including the design practice recommend the application of split functions for the determination of the wave run-up and run-down. Among the diverse models available to predict wave run-up and run-down as a function of ξ, the model of Schüttrumpf (2001) appear to be the most promising for this study, because the tanh-model especially describes the transition from collapsing to surging breaker more appropriately.

2.1.4 Wave set-up

Wave set-down and wave set-up are generated in the process of wave shoaling and breaking, respectively; i.e. shoaling causes the water level to decrease up to the breaking point where the set-down reaches its maximum value. The water level then increases toward the shore as a result of wave energy dissipation. The final result is a mean water level (MWL) instead of SWL in

the absence of wave action. As the effect of wave set-up is directly linked to the loading area on the revetment and therefore affects all the processes on and beneath the revetment only the wave set-up is addressed in this section. For regular waves, the MWL is constant over time while it varies continuously for irregular waves, also including a dynamic component that oscillates with the wave group period.

Longuet-Higgins & Stewart (1964) were the first to describe the relation between the wave momentum flux based on the radiation stress concept and the wave set-up process.

Based on the radiation stress concept and a wave breaking model, the following equation for the variation of the set-up η_S of irregular waves over distance x was proposed by Goda (1975) which was successfully validated by laboratory tests and field measurements:

$$\frac{d\eta_S}{dx} = -\frac{1}{(\eta_S + h)} \frac{d}{dx} \cdot \left[\frac{1}{8} \cdot H_{rms}^2 \left(\frac{1}{2} + \frac{2kh}{\sinh 2kh} \right) \right] \tag{2.22}$$

In Kim (2010) an overview of the empirical and theoretical approaches for wave setup is given by Dean & Walton (2010). For the breaking of monochromatic waves in shallow water the following equation for wave setup η_S:

$$\eta_S = -\frac{\kappa H_b}{16} + \frac{3\kappa^2 / 8}{(1 + 3\kappa^2 / 8)} (h_b - h) \tag{2.23}$$

The breaking index $\kappa = H_b/h_b$ is determined related to the beach slope (e.g. based on Dally et al. (1985)). Moreover, a summary of several field studies on permeable and impermeable beach slopes, showing that both static and dynamic components of the wave set-up must be considered as both affect the MWL in the surf zone. The static component is directly caused by the waves as described by the theory of radiation stress the dynamic component is caused by infragravity waves as described by the theory of surf beat (Lo (1988)) . The dominant role of the slope steepness and the wave steepness for the wave set-up is also shown. However, permeability and porosity of the beach slope is not taken into account in the formulae (Dean & Walton (2010)).

Battjes (1972) was one of the first to perform laboratory tests with irregular waves showing that the variation of the width of the energy spectrum hardly affects the wave set-up. However, the measured wave set-up significantly differs from the theoretically predicted values.

A much better agreement of the predicted wave set-up based on nonlinear wave theories with the data of a comprehensive laboratory study was obtained by Stive & Wind (1982).

The CEM (USACE (2002)) provides general guidance to determine wave set-up for both regular and irregular waves. For the wave set-up induced by regular waves at the still water shoreline the following equation is given:

$$\eta_S = \eta_b + \left[1 \Big/ \left(1 + \frac{8 \cdot h_b^2}{3 \cdot H_b^2} \right) \right] \cdot h_b \tag{2.24}$$

Ludwigs & Oumeraci (2011) further analysed the data of Oumeraci et al. (2010b) for regular waves in order to determine wave set-up on porous bonded revetments. Applying the wave length instead of the wave height as commonly used in several previous studies to make the wave set-up dimensionless, a better correlation between relative wave set-up η_S/L_0 and surf similarity parameter ξ_m was obtained in Fig. 2.9 also showing the significant effect of the slope steepness on the wave set-up in the numerical investigations of Foyer (2013).

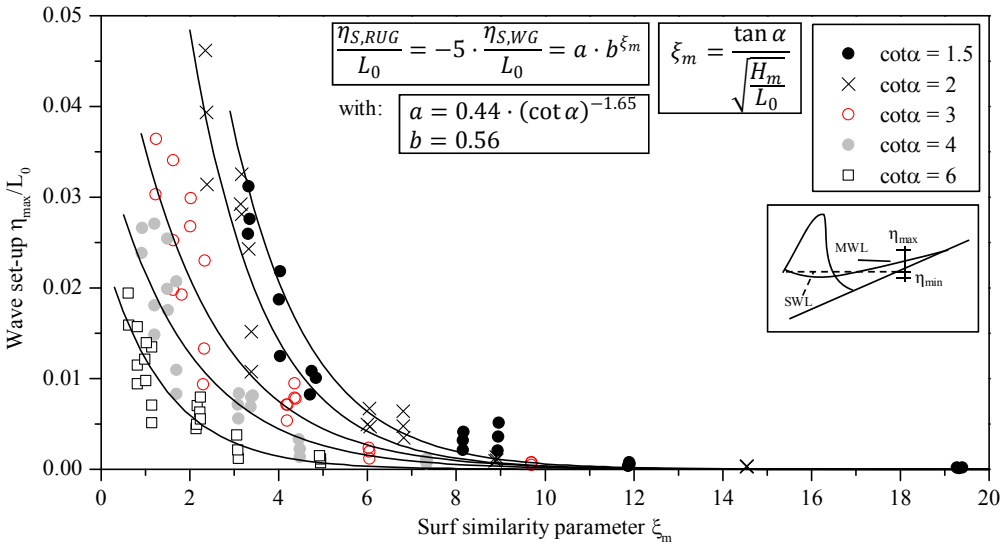

Fig. 2.9: Relative wave set-up as a function of surf similarity parameter for regular waves on slopes with different steepnesses (Foyer (2013))

The significant effect of slope steepness on relative wave set-up η_S/L_0 in Foyer (2013) is confirmed by the numerical study with regular waves by Alcérreca Huerta (2014), using a slightly different model to fit the numerical data (see Fig. 2.10), but achieved a similar result.

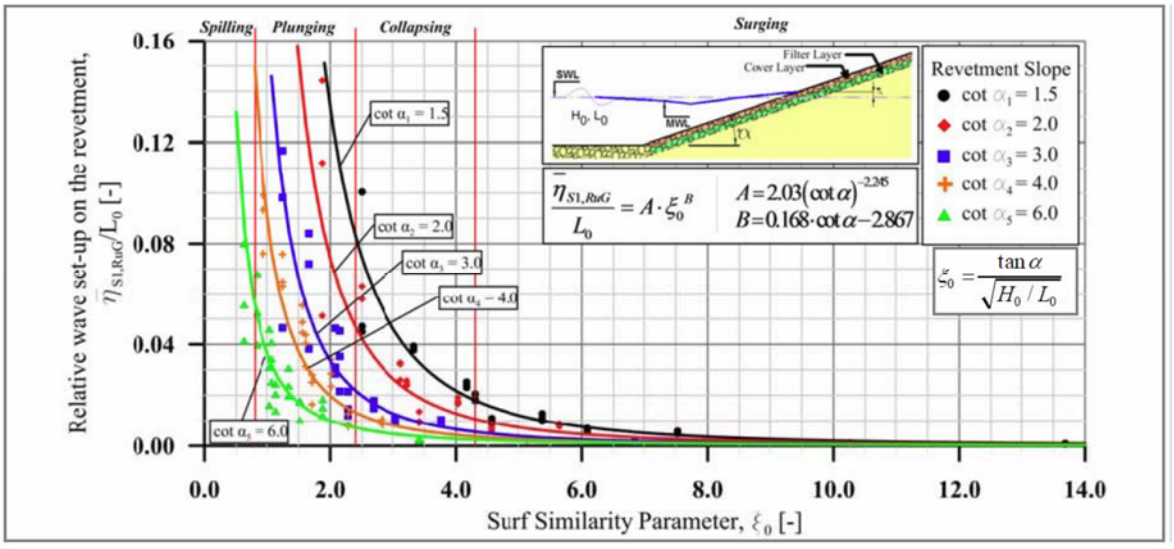

Fig. 2.10: Relative wave set-up as a function of surf similarity parameter for regular waves on slopes with different steepnesses (Alcérreca Huerta (2014))

Moreover, it was also shown that the effect of slope steepness on the wave set-up was much more important than the effect of the revetment-filter thickness

Alcérreca Huerta (2014) also determined the internal wave set-up at the interface of revetment and sand core ($\eta_{S,int}$) as a function of the wave set-up on the revetment η_S, showing that the wave set-up directly at the bottom of the revetment on the sand core is 21% larger than on the revetment:

$$\eta_{S,\text{int}} = 1.21 \cdot \eta_S \tag{2.25}$$

Defined as the external mean water level (EMWL) resulting from wave action, the wave set-up on porous revetment is directly related to the development of the internal mean water level (IMWL) in the sand core (see section 2.3), thus affecting not only all other processes on the revetment, but also those beneath the revetment and in the sand core. As particularly and clearly shown by the results of the comprehensive numerical studies by Foyer (2013) and Alcérreca Huerta (2014) for regular waves, the consideration of the effect of wave set-up on all other processes and beneath the revetment is crucial. However, a confirmation for these findings for irregular wave tests is still missing.

Moreover, the results from both studies have also clearly shown that the wave length is more appropriate than the commonly used wave height to define the relative wave set-up and that the effect of the slope steepness on the wave set-up on the revetment is dominant as compared to that of the revetment-filter thickness. Consequently, this approach appears to be also promising for this study and has to be verified within irregular wave tests.

The effect of a changing porosity on wave set-up was not yet addressed in previous studies and has to be determined for both regular and irregular waves.

2.2 Wave-induced pressures on the revetment

The processes described in the previous section are in close relation to the wave-induced pressure on the revetment. Especially the wave breaking and breaker types (see section 2.1.1) significantly affect the energy dissipation on the structure and thus the wave-induced pressures. Wave reflection (section 2.1.2) and wave run-up and run-down (section 2.1.3), which indirectly affect wave-induced pressure through the wave breaking process, are also affected by the breaker types. Therefore, a classification in quasi-static and impact loads (Fig. 2.11) is commonly used in the analysis of the wave-induced pressure on the revetment.

In many studies this dynamic pressure was in the focus of the investigations (e.g. Witte (1988), van Vledder (2001)). Davidse (2009) and Ludwigs (2009) give a very good overview over previous investigations concerning this issue.

a) Wave load classification

The time history of both quasi-static and impact load are schematically shown in Fig. 2.11.

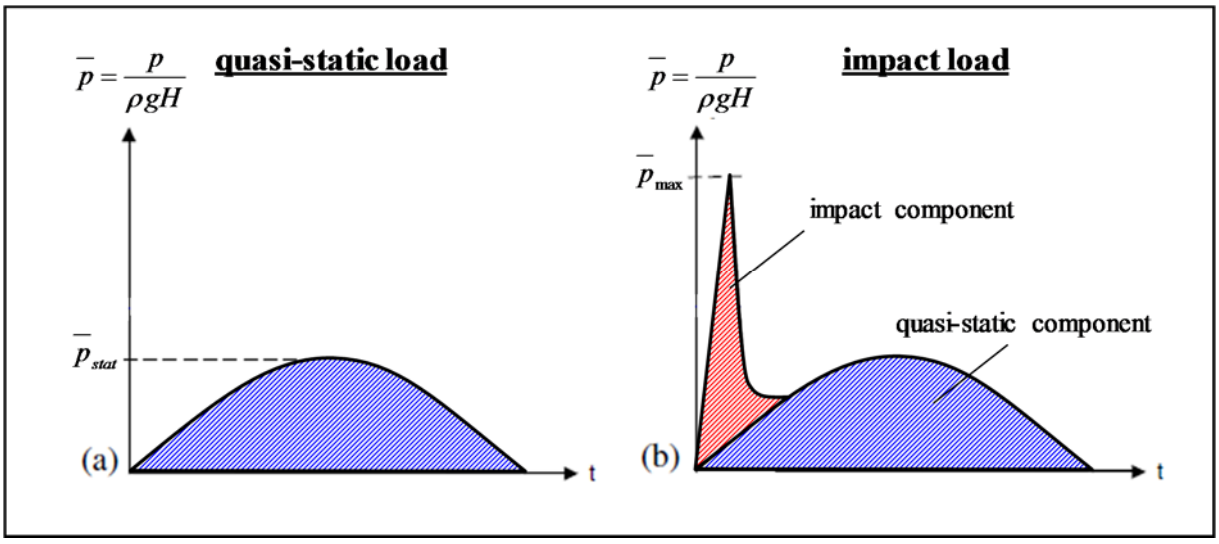

Fig. 2.11: Schematic pressure history of a) a quasi-static load and b) an impact load

The classification of the wave loads is mainly based on the breaker type, which is described by surf similarity parameter ξ for sloping structures (see Tab. 2.2). Quasi-static wave loads on sloping structures are generally induced by surging breakers with a cyclic variation according to the wave motion. Only a single pressure peak occurs in the pressure signal ($p_{stat} = p_{max}$) (see Fig. 2.11a). The impact load Fig. 2.11b) is generally induced by stronger plunging or collapsing breakers. It is composed of two components: an impact component with a very high peak pressure and a very short duration (ca. 0.1 to 0.001 s) and quasi-static component similar to the quasi-static wave load in Fig. 2.11a. Between these two different wave loads a transition zone can be observed.

Based on large-scale tests in GWK, a wave load classification was proposed by Oumeraci et al. (2010b), including impact load ($\xi_{m-1,0}$ = 1.6-2.5), non-impact load ($\xi_{m-1,0}$ > 2.9) and a transition zone ($\xi_{m-1,0}$ = 1.6-2.5).

b) Magnitude of peak pressure on the revetment

One of the first experiments at prototype scale to investigate wave-induced pressures were conducted by Stive (1984) in the Delta Flume. An impermeable asphaltic revetment with a slope steepness of 1:3 and a 1:4 concrete stone pavement with regularly placed stones were tested. The following relations for the peak pressure as a function of wave height H were proposed:

Asphaltic revetment (1:3): $$p_{max} = 2.7 \cdot \rho \cdot g \cdot H \quad (2.26)$$

Concrete stone pavement (1:4): $$p_{max} = 2.3 \cdot \rho \cdot g \cdot H \quad (2.27)$$

Moreover, it was found that the peak pressure also depends on the wave steepness. With decreasing wave steepness, a larger thickness of the water layer from the previous wave on the slope was observed which damps the impact of the next breaking wave.

Zhong (1985) conducted model tests in a scale of 1:10 together with large-scale tests on an asphaltic revetment with regular waves on a slope 1:4. Peak pressure p_{max} was found to follow a log-normal-distribution. The normalised impact pressure reaches a maximum value for "wave steepness" $H/(gT^2) = 0.0045$. The effect of slope steepness on the impact pressure was further tested for regular waves by Führböter & Sparboom (1988) on a concrete revetment with slopes 1:4 and 1:6. The following relations for the peak pressures were obtained:

Slope steepness 1:4 $$p_{\max} = 6.0 \cdot \rho \cdot g \cdot H \tag{2.28}$$

Slope steepness 1:6 $$p_{\max} = 4.0 \cdot \rho \cdot g \cdot H \tag{2.29}$$

Klein Breteler et al. (2000) investigated the influence of ageing of block revetments. In case of block revetments ageing means the washing in of silt and sand through the gaps between the stones leading to a reduction of permeability in the cover and filter layer. Klein Breteler et al. (2000) conducted large-scale tests in the Deltaflume in Delft with revetments made of rough natural stone and rectangular concrete blocks. It was concluded from their experiments that damages on block revetment which was exposed to ageing processes occur at the same or even larger wave heights compared to non-aged block revetments. That means that ageing effects with a connected decreasing porosity did not increase the probability of a failure of the revetment.

The crucial effect of aeration and scaling on wave impact pressures was investigated among others (e.g. Popov & Ryabykh (1969), Chanson & Lee (1997)) and Bullock et al. (2001)). The peak pressures were found to decrease with the aeration level. Bullock et al. (2001) found out that in seawater the entrained air bubbles are much smaller than in freshwater. Based on their field measurements the crucial importance of air content for scale effects was also shown for seawater.

The first large-scale model study related to wave-induced pressures on and beneath bonded porous revetments was performed in GWK by Oumeraci et al. (2010b) with regular and irregular waves. The following equations were obtained for the relative impact pressure peak induced by irregular waves:

On the revetment: $$\frac{p_{\max}}{\rho \cdot g \cdot H_{m0}} = -4 \cdot \xi_{m-1,0} + 12.5 \quad \text{for} \quad 1.6 < \xi_{m-1,0} < 2.5 \tag{2.30}$$

Just beneath the revetment: $$\frac{p_{2\max}}{\rho \cdot g \cdot H_{m0}} = 0.6 \cdot \left(-4 \cdot \xi_{m-1,0} + 12.5\right) \quad \text{for} \quad 1.6 < \xi_{m-1,0} < 2.5 \tag{2.31}$$

Eq. (2.30) and (2.31) show the peak of impact pressure on the revetment is decreased by a factor of 0.6 as compared to that just beneath the revetment. In contrast, the transmission of the quasi-static pressure through the revetment was not significantly affected.

A similar large-scale test series was conducted by Gier et al. (2012) with a IPPB-revetment, which was further analysed by Alcérreca Huerta & Oumeraci (2012) and compared to Oumeraci et al. (2010b) by Liebisch et al. (2012). The low porous IPPB-revetment showed significantly

higher peak pressures compared to the PBA revetment (for the same wave conditions) thus implying that lower peak pressures occur rather on porous revetments than on impermeable revetments.

Alcérreca Huerta (2014) investigated the effect of revetment thickness of bonded porous revetments on the wave-induced pressure and developed a model for the upper envelope of the numerical data for regular waves which includes two distinct pressure components:

$$\frac{p_{1\max}}{\rho g H_0} = A \cdot \xi_0 \cdot \exp\left(-\frac{\xi_0^2}{B}\right) + 2\frac{\xi_0^2 + 6.7 \cdot \xi_0}{\xi_0^2 + 38.5} \tag{2.32}$$

As shown in Fig. 2.12 for three revetment thicknesses, the first component describes the impact pressure, which becomes negligible for surging breakers and only occurs for plunging and collapsing breakers. The second component describes the quasi-static pressure which is present for all breaker types.

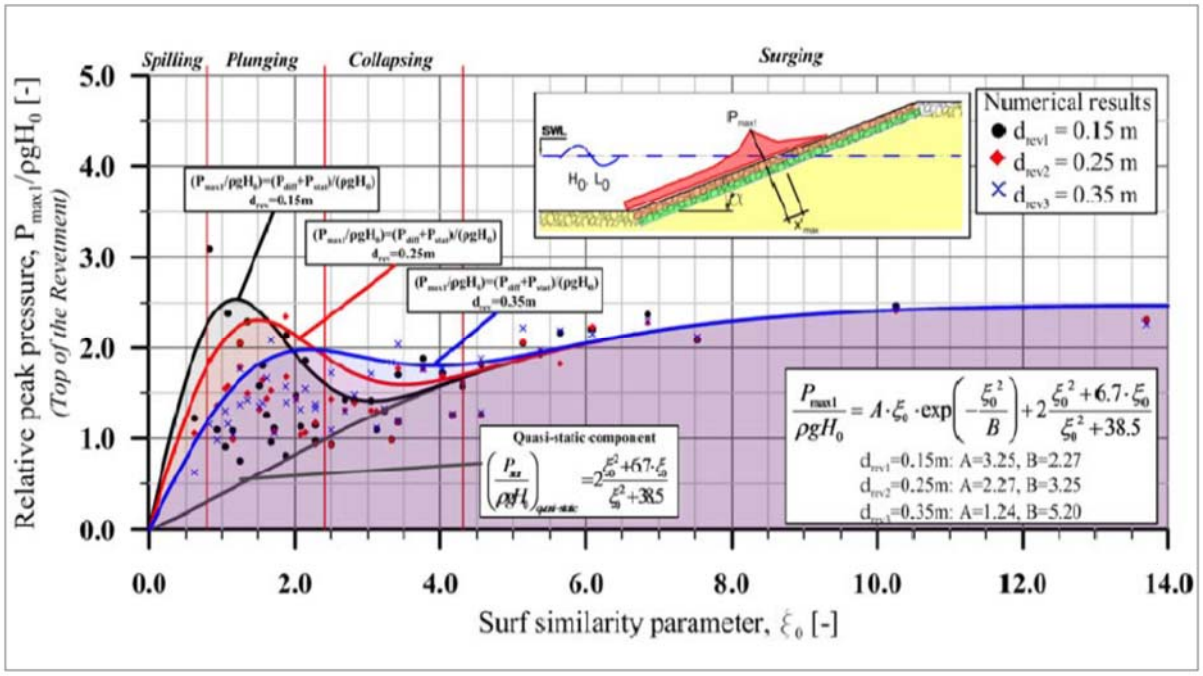

Fig. 2.12: Relative peak pressure on the revetment for different revetment thicknesses and applied model for an upper envelope for regular waves (Alcérreca Huerta (2014))

The quasi-static component is not affected by the revetment thickness. In contrast, the effect of the latter on the impact component, though not fully clear due to the limited amount and large scatter of the data, seems to strongly depend on surf similarity parameter ξ_0 and even basically differs for $\xi_0 < 2.4$ and $\xi_0 > 2.4$.

c) Location of the peak pressure on the revetment

Besides the magnitude of the peak pressure, its location on the revetment is also important. In earlier studies (e.g. Stive (1984)) a location at H/2 beneath the still water level was suggested.

In more recent studies the location of peak pressure z_{pmax} was found to be strongly related to surf similarity parameter ξ.

Schüttrumpf (2001) used a model with hyperbolic tangent to fit the data of the location of peak pressure in his experiments on smooth slopes. He derived the following equation for both, regular and irregular waves.

$$\frac{z_{p\max}}{H_s} = 0.8 + 0.6 \cdot \tanh(\xi_{S0} - 2.1) \tag{2.33}$$

In the context of the validation of the software GOLFKLAP®, Klein Breteler (2007) developed a formula for the location of the peak pressure dependent on the surf similarity parameter. But Klein Breteler (2007) used a straight line up to a maximum value at $\xi \approx 4.45$ for his equation.

$$\frac{z_{p\max}}{H_s} = \min\begin{Bmatrix} 0,45\xi_{S0} - 0,3 \\ 1,7 \end{Bmatrix} \text{ für } 1 \le \xi_{S0} < 6 \tag{2.34}$$

Oumeraci et al. (2010b) adopted the model of Klein Breteler (2007) on PBA-revetments to develop the following two equations for the location of the peak pressure:

$$\frac{z_{p\max}}{H_{m0}} = 0.7 \cdot \xi_{m-1,0} - 0.6 \quad \text{for } \xi_{m-1,0} < 3.2 \tag{2.35}$$

$$\frac{z_{p\max}}{H_{m0}} = 0.2 \cdot \xi_{m-1,0} + 1.0 \quad \text{for } \xi_{m-1,0} > 3.2 \tag{2.36}$$

In his numerical simulations with regular waves, Alcérreca Huerta (2014) also investigated the location of the peak pressure on PBA-revetments. Due to the large scattering of the numerical data for three revetment thicknesses an upper and lower envelope were developed, based on the eq. (2.12) by Schüttrumpf (2001) which was modified in order to fulfil the condition that for $\xi_0 = 0$ and $z_{pmax}/H_0 = 0$:

Upper envelope:
$$\frac{z_{p\max}}{H_0} = -1.34 \cdot \tanh\left(0.07\xi_0^{1.58}\right) \tag{2.37}$$

Lower envelope:
$$\frac{z_{p\max}}{H_0} = -1.64 \cdot \tanh\left(1.04\xi_0^{1.59}\right) \tag{2.38}$$

The results of Alcérreca Huerta (2014) (Fig. 2.13) showed no correlation to the different tested revetment thicknesses.

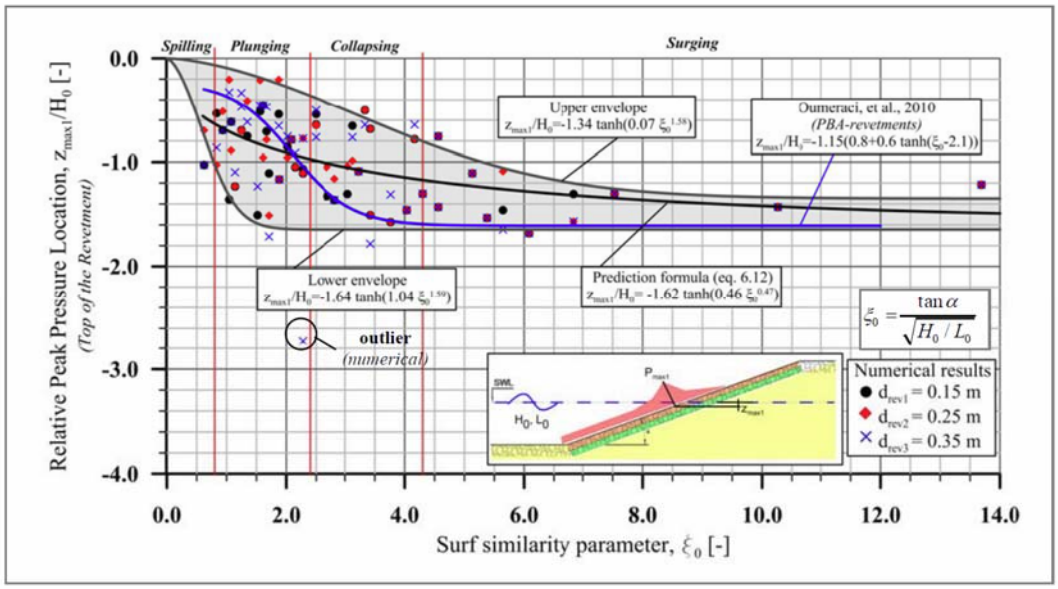

Fig. 2.13: Relative location of peak pressure on the revetment as a function of surf similarity parameter and applied model for an upper and lower envelope for regular waves (Alcérreca Huerta (2014))

d) Pressure distribution on the revetment

In addition to the magnitude and location of the peak pressure, the pressure distribution on the revetment is required to obtain the total wave loading of the structure.

Popov & Ryabykh (1969) belong to the first who documented the spatial pressure distribution. In their study, the peak pressure was always located under the still water level.

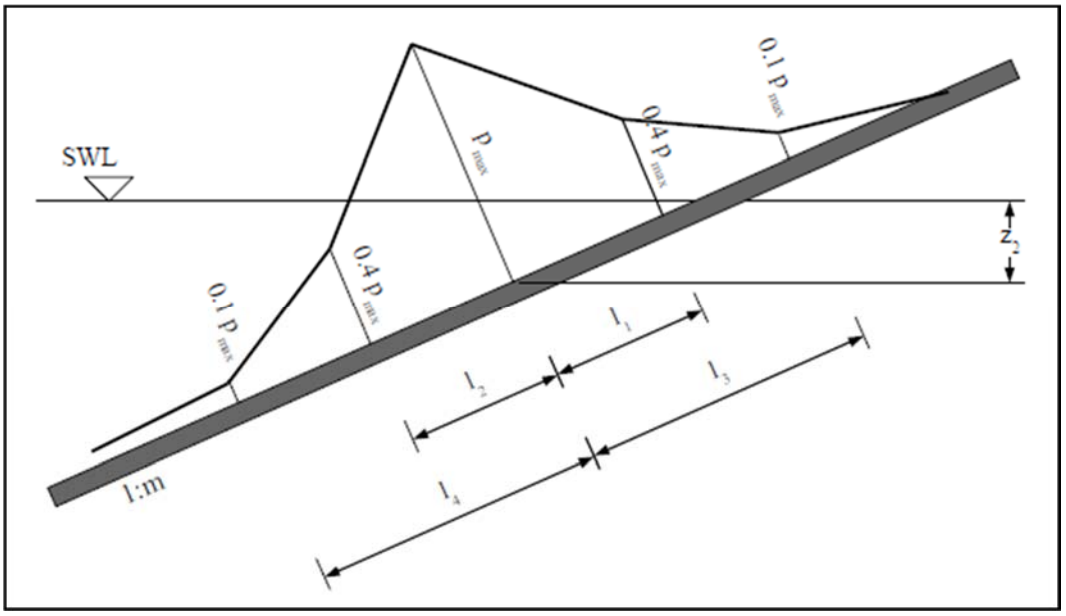

Fig. 2.14: Spatial distribution of wave-induced pressure on an impermeable asphaltic revetment (Lattermann (2006))

In scale model tests with regular waves on impermeable asphaltic revetments, Lattermann (2006) determined the spatial distribution of the wave-induced pressure due to breaking waves

as shown in Fig. 2.14. Formulae to determine the peak pressure as well as distances l_1-l_4 are also provided in Lattermann (2006).

Similar to Lattermann (2006) but using the pressure related to peak pressure p/p_{max} and distances related to its location z_{pmax} (z'/z'_{pmax}), Oumeraci et al. (2010b) also described the spatial pressure distribution on and just beneath a PBA-revetment based on a linear interpolation between characteristic points along the revetment slope (x'-axis). For impact-loads five points were chosen and three points for non-impact loads. Design formulae were established for the particular points of the spatial pressure distribution and their distance to the location of peak pressure on the x'-axis.

Alcérreca Huerta & Oumeraci (2012) used a continuous empirical equation for to describe the spatial pressure distribution on a low porous IPPB-revetment in relation to the peak pressure on the revetment. Due to the limited data sets from GWK-tests, this approach was successfully applied only for impact loads.

$$\frac{p}{p_{max}} = \frac{A - B \cdot \left(x'/x'_{max} \right)}{1 + C \cdot \left(x'/x'_{max} \right) + D \cdot \left(x'/x'_{max} \right)^2} \tag{2.39}$$

with A, B, C, D = empirical coefficients

Using more extensive numerical data sets for regular waves, it was shown for the first time by Alcérreca Huerta (2014) that the pressure distribution for both impact and non-impact loads can be described by a single equation (eq. (2.39)). Moreover, Alcérreca Huerta (2014) identified a second pressure peak in the spatial pressure distribution for both loading cases above the location of the main peak pressure.

Wave-induced pressure on the revetment basically differ depending on the prevailing loading case. Therefore, a distinction must be made between two basic loading cases: impact and non-impact loads which are relatively well-described by surf similarity parameter ξ.

To describe the total wave load on the revetment, three load characteristics are necessarily required: the peak pressure p_{max} (because it is decisive for the design), its location with respect to SWL and the spatial pressure distribution on the revetment.

Among the structural parameters affecting the wave load on the revetment, the slope steepness and the porosity of the revetment appear to be the most relevant parameters. Though the former is already included in surf similarity parameter ξ to distinguish between the different loading cases, indications on possible additional effects on the aforementioned load characteristics can hardly be found in the literature. Further research is necessary to investigate these additional effects of slope steepness of bonded porous revetments which particularly focus on irregular wave tests. As the numerical simulations of Foyer (2013) and Alcérreca Huerta (2014) provide a large database for regular wave tests, the investigations should be extended to systematic irregular wave tests. Moreover, no study is available which provides explicitly quantitative indications on further effects of the porosity or on the combined effects of both porosity and slope steepness on the wave loads.

The wave-induced pressures are mostly described by split functions based on the wave height or the surf similarity parameter depending on the two basic loading cases. The fully new approach proposed by Alcérreca Huerta (2014) using a model for the upper envelope of the numerical data for regular waves which includes two distinct pressure components might also be promising for this study to cope with large data scatter for plunging breakers. For the spatial pressure distribution on the revetment a continuous model was successfully applied by Alcérreca Huerta (2014). Among the diverse (mostly linear) models available to predict the location of peak pressure z_{pmax} as a function of ξ, the tanh-model of Schüttrumpf (2001) would be most promising, if no z_{pmax}-values above SWL are obtained.

2.3 Pressure damping through and beneath porous revetments

As shown in the previous sections, revetment porosity is an important structure parameter as it contributes among others to reduce wave reflection and wave run-up. Apart from that, it causes the flow to propagate through the revetment and the underlying sand core, thus causing the pressure induced on the revetment to be transmitted and energy to be dissipated through the porous layers which both decrease with depth inside and beneath the revetment. The processes associated with the pressure damping through the different layers and particularly those inside the sand core are important for the stability of the revetment.

In this section, an attempt is therefore made to briefly review the current knowledge, together with some basics, which are most relevant for the processes involved in the damping of wave-induced pressure through porous revetments and the underlying sand core. First, some basics related to the Darcy-Forchheimer flow in porous media (section 2.3.1) and to stability analysis against soil liquefaction (section 2.3.2) are given. Both are relevant for porous revetments. Then a brief review of the studies directly related to the damping of wave-induced pressure through porous revetments and inside the sand core beneath the revetment is made, including the possible failure mechanisms (section 2.3.3).

2.3.1 Flow in porous revetment

The water resulting from the breaking waves on the porous revetment flows rapidly through the pores of the revetment and then much slower through the underlying sand core, resulting in a different flow behaviour, energy dissipation and pressure damping inside the two different porous media. In the sand core the flow is assumed to be laminar and steady, so that Darcy's law is valid: $i = k \cdot v_f$. It is a linear equation describing the proportionality between hydraulic gradient i and filter velocity v_f (fictive or Darcy's flow velocity), where proportionality factor k describes the hydraulic permeability which has the same dimensions as filter velocity v_f (m/s) and depends on the properties of the porous medium and the pore fluid. For coarser soil material such as gravel and the commonly used aggregates in PBA-revetment, v_f becomes higher so that the flow may not remain laminar (dominated by viscous forces), but turbulent (dominated by inertial forces). In the latter case, the validity of Darcy's law becomes questionable. Therefore,

Darcy's law was extended by Forchheimer by adding a non-linear term to consider the inertial forces associated with turbulent flow, leading to the so-called Darcy-Forchheimer equation:

$$i = a \cdot v_f + b \cdot |v_f| \cdot v_f \tag{2.40}$$

where a and b are the Forchheimer coefficients in [s/m] and [s²/m²], respectively.

Several formulae are available to determine a and b, showing that coefficient b mainly depends on the properties of the porous media such as porosity n and grain size d while coefficient a like k in the Darcy law also depends on the viscosity of the pore fluid. Some of the most relevant formulae for a and b are given in Tab. 2.6.

Tab. 2.6: Equations for the determination of coefficients a und b

Author	Coefficient a	Coefficient b	Considerations
Ergun (1952)	$\alpha_f \frac{(1-n)^2}{n^3} \frac{\nu}{gd^2}$	$\beta_f \frac{1-n}{n^3} \frac{1}{gd}$	$\alpha_f = 150$ and $\beta_f = 1.75$
Engelund (1953)	$\alpha_f \frac{(1-n)^3}{n^2} \frac{\nu}{gd^2}$	$\beta_f \frac{1-n}{n^3} \frac{1}{gd}$	$\alpha_f = 780$ and $\beta_f = 1.8\text{-}3.6$
Ward (1964)	$\alpha_f \frac{\nu}{gd^2}$	$\beta_f \frac{1}{gd}$	$\alpha_f = 360$ and $\beta_f = 10.44$
Koenders (1985)	$\alpha_f \frac{(1-n)^2}{n^3} \frac{\nu}{gd_{15}^2}$	$\beta_f \frac{1}{n^5} \frac{1}{gd_{15}}$	$\alpha_f = 290$ (confidence levels 95%: 250-330), $\beta_f = 1.4$
Den Adel (1987)	$\alpha_f \frac{(1-n)^2}{n^3} \frac{\nu}{gd_{15}^2}$	$\beta_f \frac{1}{n^2} \frac{1}{gd_{15}}$	$\alpha_f = 160$ (confidence levels 95%: 75-350), $\beta_f = 2.2$ (confidence levels 95%: 0.9-5.3)
Shih (1990)	$\alpha_f \frac{(1-n)^2}{n^3} \frac{\nu}{gd_{15}^2}$	$\beta_f \frac{1-n}{n^3} \frac{1}{gd_{15}}$	$\alpha_f = 1684+3.12\text{x}10^{-3}(g/\upsilon^2)^{2/3}\ (d_{15})^2$ $\beta_f = 1.72+1.57\ \exp[-5.1\ \text{x}\ 12\text{x}10^{-3}(g/\upsilon^2)^{1/3}\ (d_{15})]$ For wide grade material replace d_{15} by: $d_* = d_{15}\ (d_{15}/d_{50})^{-1.11}\ (d_{50}/d_{85})^{0.52}$

The first linear term in eq. (2.40) represents the contribution of laminar flow as described by Darcy's law while the second non-linear term is the contribution of the turbulent flow. However, both terms describe steady flow. To also account for unsteady flow, a time-dependent term was introduced in the Darcy-Forchheimer equation by Polubarinova-Kochina in 1952 as follows:

$$i = a \cdot v_f + b \cdot |v_f| \cdot v_f + c \cdot \frac{\partial v_f}{\partial t} \tag{2.41}$$

For the determination of coefficient c [s²/m], several formulae are available, from which the two most relevant are given below:

$$c = \frac{1 + C_m \frac{1-n}{n}}{g} \tag{2.42}$$

$$c = \frac{1 + C_m \frac{1-n}{n}}{n \cdot g} \tag{2.43}$$

where C_m is a virtual mass coefficient and n the porosity.

The determination of coefficient c is based on a virtual mass concept in which the virtual mass is the inertia added to a system. The virtual mass derives from the accelerating body that also has to accelerate the surrounding. If eq. (2.42) or eq. (2.43) is more appropriate is not yet clear. If the same assumption regarding the cross-section of the flow are made for C_m like for the fictional velocity v_f (cross-section includes both pores and grains), eq. (2.42) would be used (Burcharth & Andersen (1995)).

Based on extensive tests for oscillatory flow through different porous media (n > 38%) in a water tunnel, van Gent (1993) determined the relative contribution of the three terms in eq. (2.41) to hydraulic gradient i, and thus of the relative importance of corresponding coefficients a, b and c. The results show that for a similar tested crushed stone material (n = 40%) to that in the GWK-tests of Oumeraci et al. (2010b), the second non-linear term with Forchheimer coefficient b provides the largest contribution over the entire flow cycle, while the contribution of the third term c is only noticeable over a very short time near the zero-crossings in the signal of hydraulic gradient i, but still smaller than the contribution of the first linear term with Forchheimer coefficient a outside the zero-crossing area (see example in Fig. 2.15).

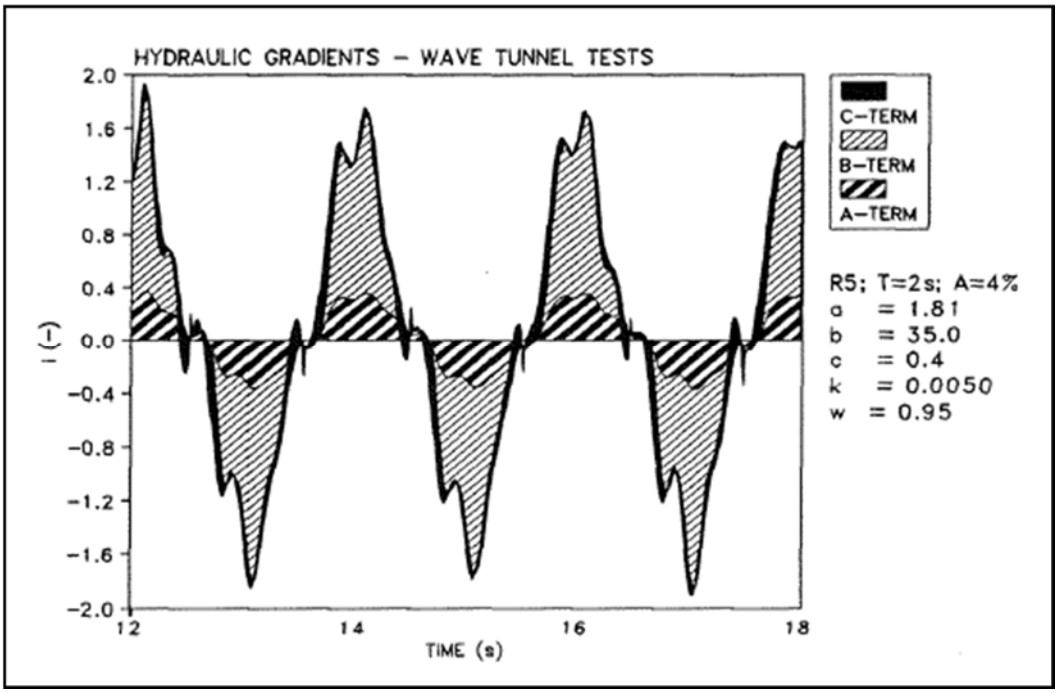

Fig. 2.15: Relative contribution of coefficients a, b and c for the extended Darcy-Forchheimer equation (van Gent (1993))

Revetment porosity is an important structure parameter for the prevailing regime of the flow through the revetment. It thus significantly affects the energy dissipation and pressure reduction inside and beneath the revetment. For the wave-induced flow conditions as well as for the properties of the granular material of the revetment and the underlying soil which are relevant for this study, the following implications can be drawn:

The flow in the porous revetment is predominantly turbulent and the second non-linear term with coefficient b in eq. (2.41) provides the largest contribution over the entire flow cycle. In the sand core beneath the revetment the situation is different with a predominantly laminar flow, leading to pressure gradients at the interface revetment and the sand core.

For the stability of the entire structure, it is important to investigate the pressure gradient over time in the experiments and the effect of a changing porosity and slope steepness on the pressure gradient.

2.3.2 Stability of the sand core and failure mechanisms

In general soil consists of a particular grain structure and pores, which can be partially or fully filled with water. When a saturated soil is loaded, the load is carried by the grain structure and the pore water. The pore (water) pressure is reduced over time, as long as drainage is not hindered. The total stress (σ) consists of pore pressure u and effective stress σ' (average stress between soil grains) according to the following relationship:

$$\sigma' = \sigma - u \tag{2.44}$$

The degree of saturation provides the response on a partially saturated soil. In partially saturated soils the total stress is increasing together with both effective stress and pore pressure when a drainage of the soil is not possible. When the total stress is still increasing in a fully saturated soil, pore pressure is also still increasing but without the effective stress. Whereas for a fully saturated soil under drained conditions the effective stress increases but not the pore pressure. This is shown in Fig. 2.16 of a partially saturated soil under drained and undrained conditions.

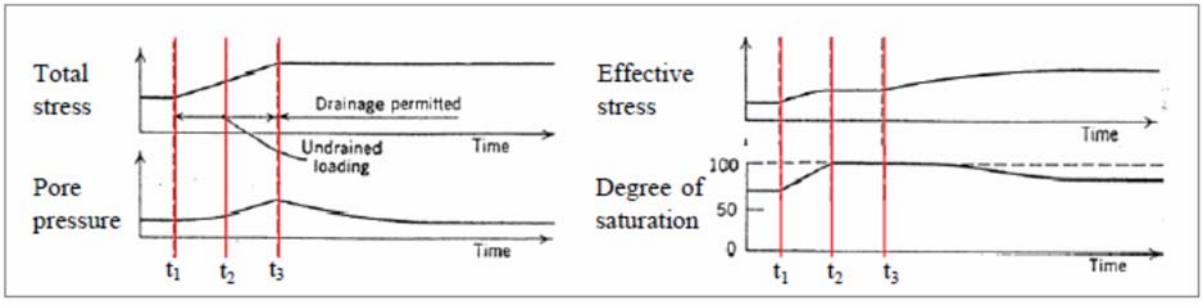

Fig. 2.16: Behaviour of pore pressure, soil effective and total stresses in partially saturated soils (Lambe & Whitman (1969))

The effect of pore pressure on the deformation behaviour and the stability of a soil is indirect via a change in the effective stress which directly affects the shear strength. The grain structure fails when the inner stress condition changes so significantly that the soil breaks (brittle failure behaviour) or starts to flow (ductile behaviour). Soil liquefaction occurs, if the pore pressure in the soil reaches the value of the total stress and the effective stress tends to zero. The relationship between effective strength σ' and shear strength τ is described by the limit condition of Coulomb:

$$\tau = c_s + \sigma' \cdot \tan\varphi \tag{2.45}$$

where c_s is the cohesion and φ the friction angle of the soil material.

For non-cohesive materials such as the sand core beneath a bonded porous revetment with (c_S=0) an increase of pore pressure u up to u = σ' may cause a shear strength τ approaching zero. The soil then behaves like a viscous fluid resulting in large soil deformations. On slopes, the liquefied soil may be transported downwards the slope.

For the sand core beneath PBA-revetments, Oumeraci et al. (2010b) identified two types of soil liquefaction beneath the revetment: Transient (or instantaneous) liquefaction and residual liquefaction. The mechanism of transient liquefaction is well-illustrated in Fig. 2.17 by Alcérreca Huerta & Oumeraci (2014) based on a modified figure from Oumeraci et al. (2010b) by adding the infiltration and exfiltration processes from de Groot et al. (2006).

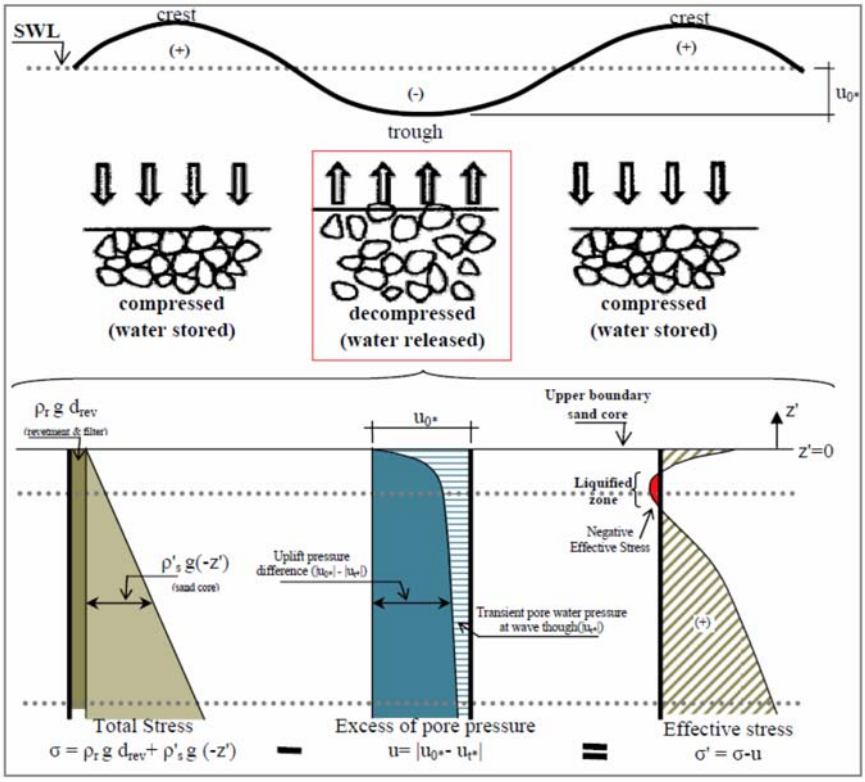

Fig. 2.17: Transient liquefaction due to cyclic wave loading and physical process description (Alcérreca Huerta (2014)) modified from Oumeraci et al. (2010b)

Transient liquefaction might occur under cyclic wave loading during the passage of a wave trough where the excess pore pressure in the soil beneath the revetment gets „negative“. An upwards directed pressure difference (u_{0*}-u_t) between the top of the sand core (initial pressure u_{0*}) and a sand layer at a deeper location (pore pressure u_t) is induced. In this case, the pressure gradient at depth z’ normal to the slope beneath the top of the sand core can reach the value of effective stress σ’ and the soil gets in suspension and behaves like a fluid, thus resulting in an instantaneous liquefaction.

Residual liquefaction in the soil occurs when the residual pressure u_r gradually increases due to plastic deformation of the soil skeleton and exceeds the value of total stress and the effective stress tends to zero. Usually both residual and transient pore pressure occur together during wave attack. The transient pore pressure u_{t*} and the residual pore pressure u_r are superimposed. Oumeraci et al. (2010b) used the following equation in a stability analysis for the identification of liquefaction failures:

$$\sigma' = \left(\rho_r g d_{rev} + \rho'_s g z'\right) - \left[u_{0*} - \left(u_{t*} + u_r\right)\right] \leq 0 \qquad (2.46)$$

with:

ρ_r	=	density of revetment material	[kg/m³]
ρ'_s	=	bulk density of submerged soil	[kg/m³]
d_{rev}	=	thickness of the revetment	[m]
z’	=	depth beneath the top of the sand core (normal to the slope)	[m]
u_{0*}	=	initial pore pressure at the top of sand core (z’=0) at time t	[N/m²]
u_{t*}	=	transient pore pressure in depth z’ at time t	[N/m²]
u_r	=	residual pore pressure in depth z’ at time t	[N/m²]

2.3.3 Studies on wave-induced pressure beneath porous revetments

As compared for instance to the studies on the hydrodynamic processes on the revetment such as wave loads and wave-run up, only very few studies were performed on wave-induced pore pressures in the soil beneath revetments.

Kudella & Oumeraci (2006) performed large-scale experiments to investigate the pore pressure development in the sand foundation of caisson breakwaters. They found out that the compaction density of the soil under the caisson breakwater greatly affects the residual pore pressure development. Furthermore, the drainage conditions of the soil are crucial. For regular waves and very long drainage lengths the residual pore pressures may lead to total liquefaction. This represents the difference to sloped bonded porous revetments with an easier drainage. Here liquefaction is predominantly caused by transient pore pressures.

Different processes of partial and total soil liquefaction with the relevant parameters and conditions are comprehensively described in de Groot et al. (2006). It was outlined that pore pressure is fluctuating with the wave-load leading to an excess of pore pressure under the wave

trough. Consequently, liquefaction may also most likely be induced under a wave trough. For revetments maximum excess pore pressure is connected to wave run-down process. It was stated in de Groot et al. (2006) that residual pore pressure may lead to partial liquefaction, but the ability of drainage and release of the excess of pore through the interface of revetment and soil leads to a higher resistance against the generation of large excess pore pressures. According to de Groot et al. (2006), the pore pressure damping in a linear elastic, homogeneous soil can be described by the following equation:

$$\left(\frac{p}{p_0}\right) = \exp\left(\frac{z'}{z_2}\right) \tag{2.47}$$

In this equation z_2 describes the characteristic length for pore pressure amplitude damping due to elastic storage. The parameter z_2 is described by:

$$z_2 = \sqrt{c_{ve}\frac{T}{\pi}} \tag{2.48}$$

with:
$$c_{ve} = \frac{k_f}{\gamma_w(\alpha + n\beta)} \approx \frac{k_f}{\gamma_w n\beta}$$

de Groot et al. (2006) states that in a depth of $3z_2$, the initial pore pressure is completely damped and hardly any pore pressure fluctuation occurs. However, de Groot et al. (2006) only reviewed the stability of the porous seabed against liquefaction and the application of eqs. (2.47) and (2.48) for the stability analysis of the subsoil for PBA-revetments against liquefaction during irregular wave attack has to be verified.

In the large-scale tests of Oumeraci et al. (2010b) the wave-induced pore pressures in different depths of the sand core beneath a PBA-revetment were investigated. Both transient and residual pore pressures were considered, but the former were found to be determinant for the stability of the sand core under cyclic wave loading. Residual pressure was relatively much smaller, und was therefore not taken into account in the stability analysis. The pore pressure damping in the different layers was related to the initial pressure at the interface between revetment and sand core and the damping rate was found to significantly depend on the initial pressure. Unexpectedly, no impact pressure was recorded in the sand core where all the pressure are rather quasi-static, irrespective of the type of wave load taking place on the revetment. The developed formulae for the pore pressure damping show that all pressure are almost completely damped at a depth of less one meter in the sand core beneath the revetment. No difference was found in pressure reduction in the sand for the different locations of initial pressure.

During the experiments failure of the PBA-revetment occurred and a stability analysis of the sand core beneath the revetment was performed, showing that the failure was due to transient soil liquefaction of the upper sand layers. As illustrated in Fig. 2.18, the collapse of the revetment occurred between wave 74 and wave 75 and was induced by the progressive increase of “negative” pore pressure in the upper layer of the sand core.

Barends (1993), Losada et al. (1998) and Hall & Foster (1990) proposed different approaches to describe the internal wave set-up. Barends (1993) suggested the water storage capacity of the porous structure during wave attack as the dominant mechanism. Losada et al. (1998) suggested an internal wave breaking while the rising water level in front of the structure was suggested by Hall & Foster (1990). Therefore, Foyer (2013) further analysed the pore pressures recorded in the sand core beneath PBA-revetments in Oumeraci et al. (2010b) to investigate the development of the internal mean water level (IMWL). Foyer (2013) found out that the IMWL is directly related to the external mean water level (EMWL) and that this relation depends on the breaker type. A prediction formula for the spatial distribution of the relative internal set-up was developed (see Fig. 2.19). It was underlined that this approach was tentative and not fully physically based so that more research is necessary to understand the processes. The results of the analysis, also show that no build-up of residual pore pressure under PBA-revetment occurred, thus confirming the finding of Oumeraci et al. (2010b).

Alcérreca Huerta (2014) conducted an extensive numerical study of the pore pressure distribution beneath PBA-revetments for regular waves. Based on the results, the approach of de Groot et al. (2006) was recommended for the prediction of pore pressure development in the sand core. Furthermore, the parameter study showed that soil parameters such as permeability are rather important to describe pore pressure development and that the surf similarity parameter should not be used for this purpose. Alcérreca Huerta (2014) also conducted a stability analysis against soil liquefaction beneath PBA-revetments with different revetment thicknesses which was validated with the data of Oumeraci et al. (2010b). He explained the failure of the PBA-revetment which occurred in the GWK-tests (see Fig. 2.18) with the accumulation of small liquefied zones in the sand core into a larger liquefied area leading to the collapse of the revetment.

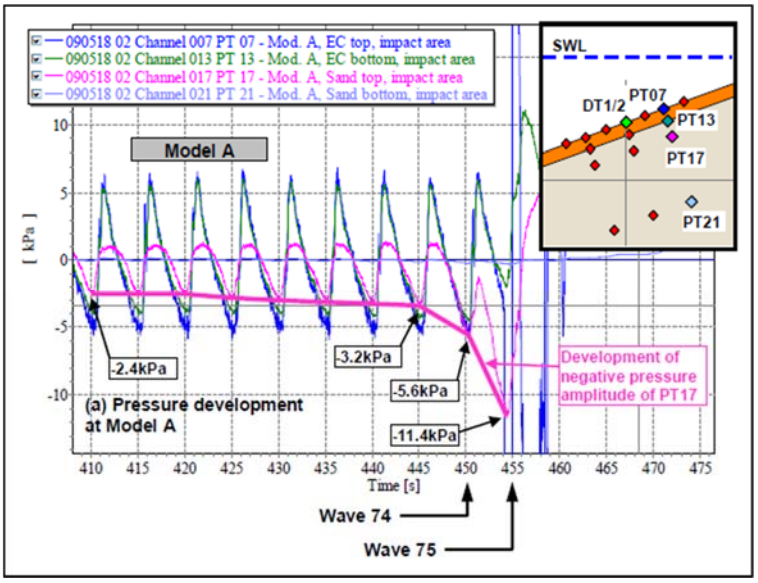

Fig. 2.18: Pore pressure development in the substructure of the PBA-revetment model at the moment of failure (Oumeraci et al. (2010b))

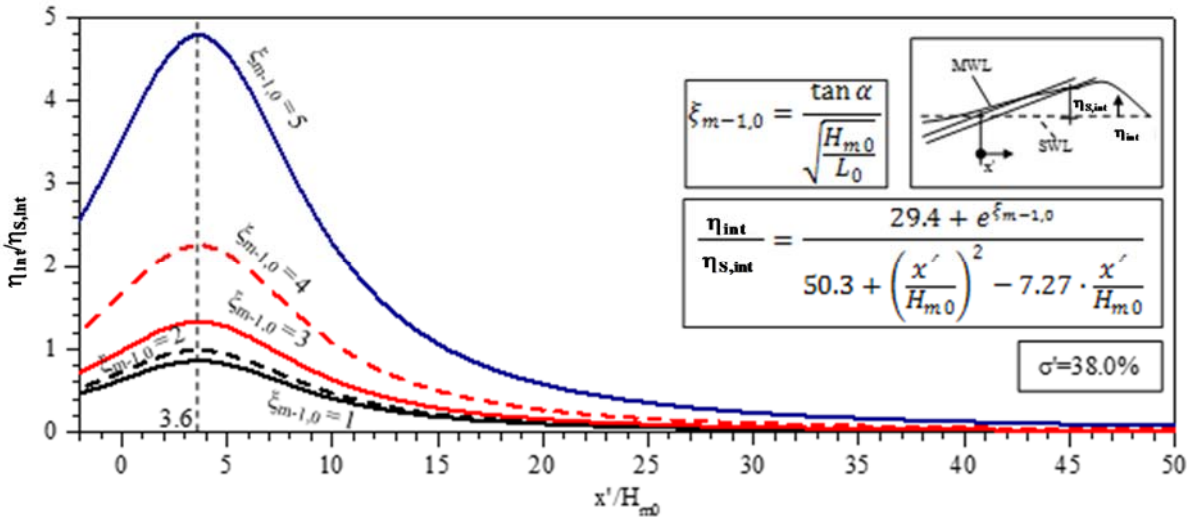

Fig. 2.19: Relation between internal mean water level in the sand core η_{int} and the mean water level directly at the bottom of the revetment $\eta_{S,int}$ for different surf similarity parameters (Foyer (2013))

The failure of the PBA-revetment in the experiments of Oumeraci et al. (2010b) showed the crucial relevance of the analysis of pore pressure in the sand core beneath bonded porous revetments. However, the transient and the residual pore pressure have been investigated mostly for porous seabeds and not for the sand core underneath revetments. For the sand core beneath PBA-revetments, Oumeraci et al. (2010b) identified two types of soil liquefaction beneath the revetment: transient (or instantaneous) liquefaction and residual liquefaction.

As the cyclic wave loading was found to be affected by a porous revetment (see section 2.2) it is assumed that also the pore pressure development underneath the revetment is directly connected to changes in the processes on the revetment. Consequently, further systematic research is necessary to investigate the effect of the porosity and slope steepness on the wave-induced pressures in the sand core underneath bonded porous revetments.

The approach of de Groot et al. (2006) was successfully applied by Alcérreca Huerta (2014) for the description of the pore pressure development in the sand core under bonded porous revetments subject to regular waves. An application of this model for irregular waves has to be verified.

Furthermore, a stability analysis against soil liquefaction beneath bonded porous revetments with different thicknesses was conducted for regular waves by Alcérreca Huerta (2014). This approach is very promising for a systematic application on revetments with different porosities and slope steepnesses in order to identify the effect of both parameters on the stability of the sand core under irregular wave attack.

Foyer (2013) found out that the IMWL is highly dependent on the EMWL. The relation between IMWL and EMWL at the revetment depends on the breaker type. No build-up of residual pore pressure was found by Foyer (2013) under the bonded porous revetment. However, the long-term investigations of the development of the IMWL was only conducted for one specific revetment.

In the numerical investigations of Foyer (2013) and Alcérreca Huerta (2014) no investigation of the long-term development was possible due to hardware restrictions. An extension of the experimental data is necessary to describe the development of IMWL under irregular waves as a function of the revetment porosity and slope steepness.

2.4 Specification of objectives and methodology

In this chapter, the current knowledge related to the processes in front of, on and beneath revetments, which are relevant for bonded porous revetments under wave attack was reviewed and analysed. The main implications drawn from the results of this chapter may be summarized as follows:

- ***For wave reflection,*** only two types of models were found to be appropriate among the several formulae available: eq. (2.4) as the most widely used model with the lowest uncertainties, and eq. (2.5) which was successfully used to fit 6000 data from a data base for different types of structures. The results of the application of both models to porous bonded revetments by Oumeraci et al. (2010b) (eq. (2.4)) und by Alcérreca Huerta (2014) (eq. (2.5)) showed that both models are promising for this study.
- ***For wave set-up and wave run-up/run-down,*** it was shown that both increasing revetment porosity and roughness result in a decrease of the wave run-up/run-down while no study could be found about the effect of porosity and roughness on wave set-up. The swash processes are also obviously affected by the storage capacity and the saturation of the revetment. The time scale of wave run-up/run-down (seconds) and that of wave set-up (hours) are quite different and the latter was shown to strongly affect all processes on and beneath the revetment. Moreover, wave set-up is also crucial for the development of the internal mean water level (IMWL) in the sand core beneath the revetment. Therefore, it is physically more appropriate to consider wave set-up and wave run-up/run-down separately; i.e. instead of the common approach using SWL as a reference water level for wave run-up/run-down, the external mean water level (EMWL) should be used. The latter approach was successfully applied only for regular waves and need thus to be verified for irregular waves. For this purpose, a focus on irregular wave tests would be required to further investigate the effect of the porosity and slope steepness on wave set-up and wave run-up/run-down.
- ***For wave loads on and beneath the revetment,*** it is often assumed that porous revetments are associated with lower peak pressures than impermeable revetments. In contrast to impact pressures, quasi-static pressures are not affected by the thickness of porous revetments. For regular waves, only slight differences were found in the non-dimensional spatial distribution of the pressure on the revetment for impact and non-impact loads. However, the effect of the porosity for different slope steepnesses on the location of the peak pressure on the revetment and the related spatial pressure distribution as well as on the related pressure through the different porous layers of the revetment and the sand core are still unknown.

- ***For wave-induced pressure in the sand core and stability analysis,*** the previous studies, especially the numerical study by Alcérreca Huerta (2014), have shown that the most promising and simplest approach for the prediction of pore pressure distribution in the sand core beneath a bonded porous revetment are the formulae by de Groot et al. (2006), which were initially proposed for the development of wave-induced pressure in a porous seabed without any protective cover. Moreover, it was shown that for the stability analysis of porous bonded revetments, not only transient pore pressure is important, but also residual pore pressure induced by the internal mean water level (IMWL), which is strongly related to EMWL (i.e. to the wave set-up) and that this relation is governed by the surf similarity parameter, i.e. by the breaker type (Foyer (2013)). Since the above mentioned numerical study was performed only for regular waves without any variation of the revetment porosity, laboratory tests focusing on irregular wave tests and the effect of the porosity for different slope steepnesses on the pore pressure in the sand core beneath the revetment would be required.

2.4.1 Specification of objectives

The analysis of the current knowledge in this chapter confirms the primary objective of this study as briefly formulated in section 1.1, which consists in the improvement of the knowledge related to the effect of the porosity for different slope steepnesses of a bonded revetment on the hydrodynamic processes on and beneath the revetment. Based on the aforementioned implications from the results of this chapter, an improved understanding is particularly required regarding the effect of the revetment porosity for different slope steepnesses on the following processes by focusing on irregular waves:

(i) Processes in front of and on the revetment, including wave reflection, wave set-up and wave run-up/run-down
(ii) Wave-induced pressures on the revetment, including wave breaking and wave load classification, peak pressure, its location and the spatial pressure distribution on the revetment
(iii) Processes in the sand core beneath the revetment, including wave damping through the revetment, damping of the transient pore pressure in the sand core beneath the revetment, development of the internal mean water level (IMWL) as well as their effect on the stability of the sand core beneath the revetment

Moreover, the relative importance of the effect of the revetment porosity and roughness and that of the slope steepness should also be first investigated before starting with more detailed experimental investigations and with the development of formulae which account explicitly for the effect of the revetment porosity on these processes. This must be considered in the specification of the work phases of the methodology described below.

2.4.2 Specification of methodology

To achieve these objectives, the methodology as illustrated in Fig. 2.20 is proposed which includes the four work phases already mentioned in section 1.2 and specified more precisely below:

Phase 1: Review and analysis of current knowledge. The main objective of this phase as reported in this chapter was to identify the knowledge gaps related to (a) the processes in front of and on the revetment such as wave breaking, wave reflection, wave run-up/run-down, wave set (EMWL) (b) wave loads on and beneath the revetment, including peak pressure as well as its location and the spatial pressure distribution on the revetment and (c) wave-induced pore pressures in the sand core beneath the revetment, including the development of the internal mean water level (IMWL) in the sand core and their importance for the stability analysis. In this respect, the laboratory study by Oumeraci et al. (2010b) and the completed numerical PhD-studies of Foyer (2013) and Alcérreca Huerta (2014) were particularly considered, as they comprehensively address diverse processes directly related to porous bonded revetments. As a final result of phase 1, both objectives and methodology for this PhD-study are specified more precisely.

Phase 2: Preliminary scale model tests. To study the effect of the revetment porosity on the aforementioned processes and its relative importance as compared to the effect of the slope steepness and roughness, a variation of a very large number of structural parameters would be required which might be practically not feasible in a usual scale model set-up using common "realistic" revetment models. Therefore, a simplified model set-up in which the slope angle, roughness and porosity can be easily and quickly varied would be required for preliminary scale model tests. In order to determine the relative importance of the effects of these parameters on the aforementioned processes, a large number of systematic tests with a focus on regular waves are necessary. The obtained results, though primarily used for phase 3 as described below, are expected to substantially contribute to an improved understanding of the effect of the revetment porosity (including the variation of both slope steepness and roughness) on the processes in front of, on and beneath the revetment.

Phase 3: Optimization of the model set-up and programme for the main tests. The results from the preliminary tests in phase 2, together with those from the GWK-tests by Oumeraci et al. (2010b) as well as with the findings from the completed PhD-studies of Foyer (2013) and Alcérreca Huerta (2014) are used to develop an optimized and more realistic model set-up and to determine an optimized programme for the main tests in phase 4 both in terms of efficiency and practical feasibility within the frame of the allocated time and resources. The optimisation also includes for instance the determination of (a) the most appropriate solution to reproduce different porosities of a bounded revetment and (b) the most adequate locations of the limited available number of measuring devices for this study and further technical constraints and boundary conditions.

Phase 4: Main scale model tests. This phase which particularly focusses on irregular waves represents the major work phase of the PhD-study. It includes the performance of the main tests using the experimental set-up with a more realistic model set-up and with the optimized

locations of the measuring devices as determined in the previous phase as well as the analysis of the results in order to obtain a better understanding of the effect of the revetment porosity and slope steepness. Therefore, a systematic analysis of the following processes is performed with a focus on irregular waves (a) processes in front of and on the revetment (wave reflection, wave set-up and wave run-up/run-down), (b) wave-induced pressures on the revetment (wave breaking and wave load classification, peak pressure, its location and the spatial pressure distribution on the revetment), (c) processes beneath the revetment (damping of wave-induced pressures in the revetment, pore pressure in the sand core beneath the revetment, internal mean water level, stability of the sand core).

Chapters 2-7 corresponding to the aforementioned work phases are indicated in Fig. 2.20. In the concluding chapter 8, the key results are summarized, including their limitations and the implications for future research.

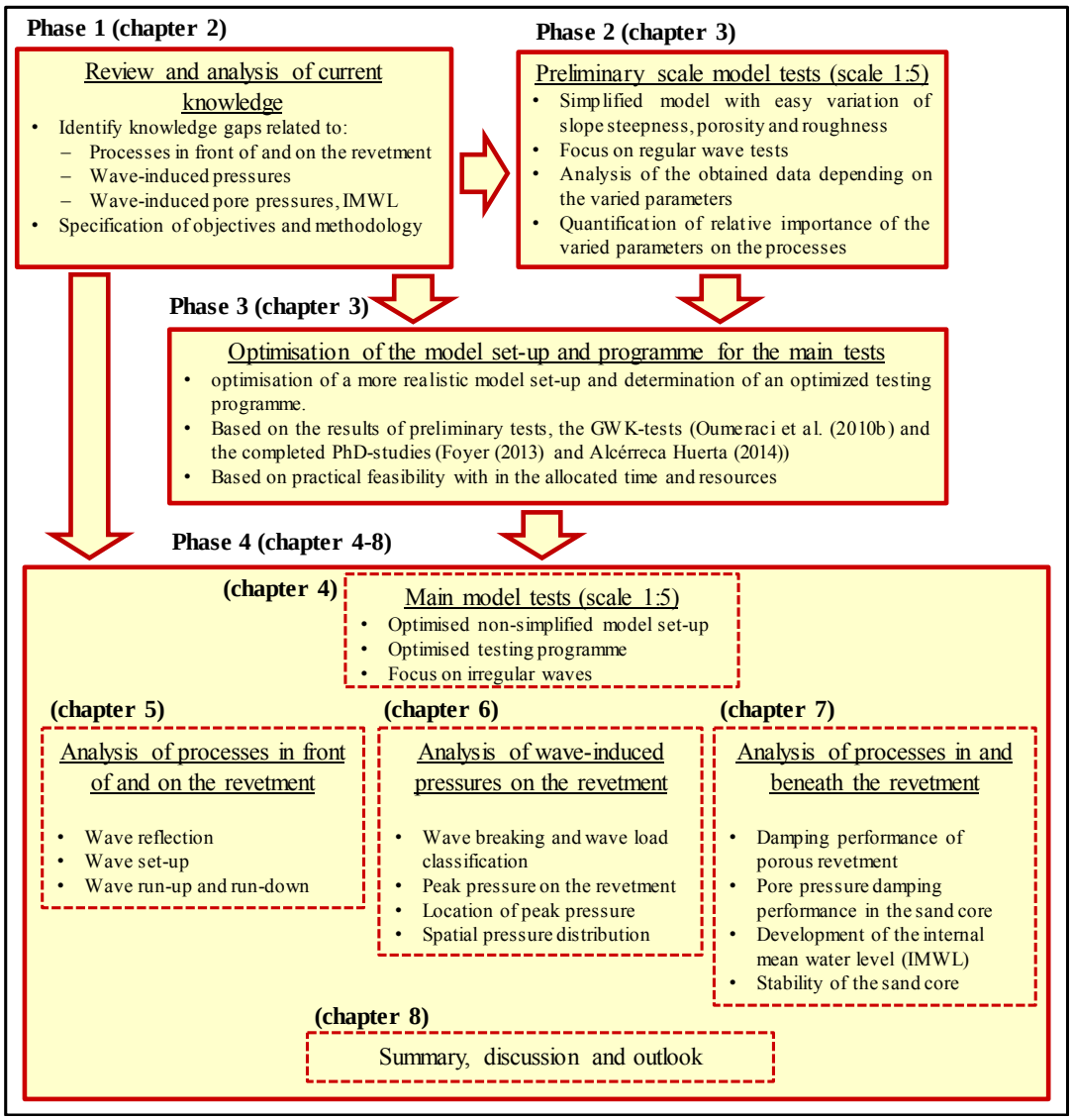

Fig. 2.20: Specified methodology and work phases of the PhD-study

3 Preliminary model tests

This chapter describes briefly phases 2 and 3 of the methodology specified in Fig. 2.20, which includes the performance of preliminary hydraulic model tests with a simplified revetment and model set-up to easily vary the slope angle, roughness and porosity of the revetment and to quantify the effects of these parameters on the wave-loading. Even though roughness and porosity are inextricably linked with each other in bonded porous revetments, these two parameters are considered separately in the preliminary tests to achieve a better process understanding.

The results of the preliminary tests together with the results of a parallel conducted numerical study of Alcérreca Huerta & Oumeraci (2013), of the GWK-tests by Oumeraci et al. (2010b) and of a previous numerical study of Foyer (2013) are used to optimise the model set-up and the testing programme for the main tests with a more realistic revetment model.

The model set-up and the programme of the preliminary tests are briefly described in section 3.1. In section 3.2 only selected results of the analysed model tests are addresses which contribute most to optimise the model set-up and the programme for the main tests. The implications for this purpose are drawn in section 3.3.

The detailed description of the preliminary tests and their analyses with all obtained results are reported in Liebisch et al. (2013b).

3.1 Model set-up and test programme

Based on the given restrictions in terms of the dimensions of the LWI wave flume and the possible range of wave parameters, a model scale of 1:5 related to the larger model tested in GWK (Oumeraci et al. (2010b)) is selected. A similar model set-up to that of the GWK-tests is important to ensure comparability and to assess possible scale effects.

In the preliminary model tests slope steepnesses of 1:3 and 1:6 are selected which are associated with significantly different effects on the wave loading of the revetment, but still within the range of common slope steepness values used in coastal protection practice. A slope steepness of 1:4 obviously represents a transition between such different effects, especially with regards to the propability of the breaking waves impacting on a water free revetment surface due to the timing of the wave run-down (e.g. Führböter (1991)). Consequently, these two slope steepnesses are chosen for the model tests because, a slope of 1:3 is commonly used for highly porous revetments and the flatter slope of 1:6 is typical for the seaside slope of sea dikes.

To fulfil the requirement of a fast and easy variation of slope steepness, roughness and porosity of the in the preliminary tests, a revetment model is developed which uses relatively thin metal sheets (d = 1.5 mm) as a cover layer instead of the bonded porous cover layer. Overall, one impermeable sheet (p0) and two different perforated metal sheets with a porosity of n = 23% (p1) and n = 48% (p2) are used. The roughnesses variation is achieved by the fixation of roughness elements made of wood (L/W/D = 0.10/0.06/0.04 m) on the revetment. The elements

are arranged in two layouts on the metal sheets in order to obtain two significantly different roughnesses described by a covering index CI, which is defined as the surface covered by the roughness elements as related to the total surface (see eq. (3.1) and Fig. 3.1):

$$CI = \frac{\text{surface covered by roughness elements}}{\text{total surface}} \tag{3.1}$$

Fig. 3.1 illustrates the two different layouts for the arrangement of the roughness elements.

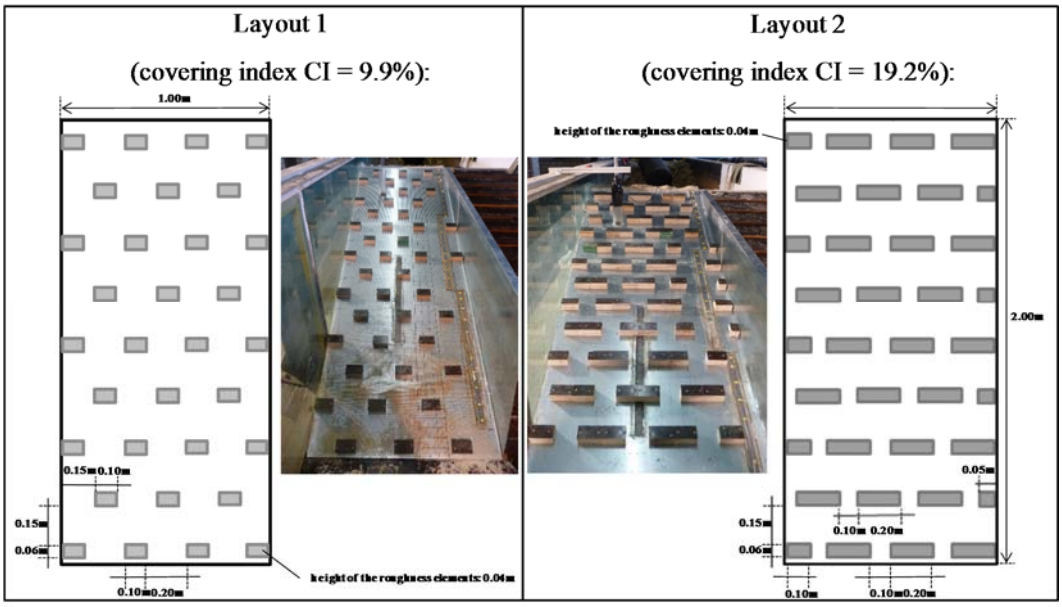

Fig. 3.1: Layouts of roughness elements on the slope, left: covering index 9.9%, right covering index 19.2%

The combined variation of porosity (p0, p1 & p2) and roughness (r0, r1 & r2) result in 9 model configurations as defined in Tab. 3.1.

Tab. 3.1: Configurations investigated in the preliminary scale model tests (phase 2)

Configuration	Porosity 0 n = 0%	Porosity 1 n = 23%	Porosity 2 n = 48%	Roughness 0 smooth	Roughness 1 Layout 1	Roughness 2 Layout 2
p0r0	X			X		
p0r1	X				X	
p0r2	X					X
p1r0		X		X		
p1r1		X			X	
p1r2		X				X
p2r0			X	X		
p2r1			X		X	
p2r2			X			X

The revetment model was constructed in front of a brick wall with a height of 1.10 m (see Fig. 3.3). Sand with a mean grain size d_{50}=0.14 mm is used for the sand core. This results in a scale factor of 1:2.43 related to the grain size used in the large-scale tests of Oumeraci et al. (2010b). In fact, a downscaling with a factor of 1:5 would result in a cohesive material. A filter layer is placed on the sandy substructure with a geotextile in between to prevent a wash out of the sand material. The filter material in the large-scale tests of Oumeraci et al. (2010b) was

made of crushed limestone 20/40 mm. Scaled in 1:5 it would result in a grain size of 4/8 mm which might result from the occurrence of possible laminar flow in the filter layer. To prevent such effects the filter grain size is chosen to 8/16 mm resulting in a distortion factor of 2.0. The metal sheets are placed on top of the filter material.

Altogether, a total of nine revetment configurations are tested for both slope steepnesses. This systematic procedure allows to quantify the effect of structure parameters on the hydrodynamic processes on and beneath the revetment. Each of the 9 revetment configurations is subject to the same wave conditions. This includes 14 tests with regular waves (16-150 waves/test, depending on the wave period), 5 tests with wave spectra (600 waves/test) and 3 tests with solitary waves. Wave heights are chosen between 0.08 m and 0.25 m with wave periods from 1.0 s up to 6.0 s. Consequently, a wide range of surf similarity parameters ξ_m between 0.93 and 7.21 (1:3) resp. between 0.62 and 3.61 (1:6) results to cover the full range of wave loading conditions from impact load to pulsating wave load conditions. In total, 210 model tests are performed in phase 2. The test programme for each of the 9 revetment configurations is summarized in Tab. 3.2.

Tab. 3.2: Test programme for each of the 9 revetment configurations (R = regular waves, S = wave spectra)

		wave height H_m resp. H_{m0}				
		0.08	0.12	0.16	0.20	0.25
solitary waves			X	X	X	
wave period T_m resp. $T_{m-1,0}$	1.0		S	R	R	
	1.5		R	R		R
	2.0			R		
	2.5	R	R	S	S	
	3.0			R		R
	4.0		S		R	
	5.0			R	R	
	6.0		R		S	

Based on the wave conditions in Tab. 3.2, pre-calculations are conducted to optimize the model set-up, including the number and location of the necessary measuring devices. The detailed calculations can be found in Liebisch et al. (2013b) and the implications from the results might be described as follows.

From the 23 pressure transducers (PT) which are deployed, 11 are placed on the revetment (layer 1), and 4 PTs are placed in different layers underneath the revetment: at the bottom of the filter layer on the geotextile (layer 2) and in the sand in a depth of 5 cm (layer 3) and 10 cm (layer 4). This results in 4 columns with 4 PTs perpendicular to the slope (also see Fig. 3.3) to measure the wave-induced pressure on the slope and its reduction through the different layers of the revetment. The 11 pressure transducers on the revetment are situated in a water-proof metal box where they are fixed in the cap of the box. During the experiments, the cap is flush-mounted with the revetment cover layer (metal sheet). This construction is required to ensure a fast change of the cover layer without moving the pressure transducers. Furthermore, the wave run-up and run-down are measured by run-up gauges placed on the slope. The development of

the internal water level in the sand core is recorded over time by means of a wave gauge (1:3 revetment) resp. a PT (1:6 revetment) placed in a plastic pipe in the sand (see Fig. 3.3). The water surface elevation is measured at two gauge arrays with 5 wave gauges each. To visualize the test results and to review possible inconsistencies during data analysis, two digital video cameras were deployed. One was placed on top of the wave flume and one laterally.

The water depth is varied from 0.45 m to 0.7 m in order to allow the waves to break within the location where most of the pressure transducers were installed (see Fig. 3.3).

A plan view of the model set-up in the flume is shown exemplarily for the model with the 1:3 slope in Fig. 3.2.

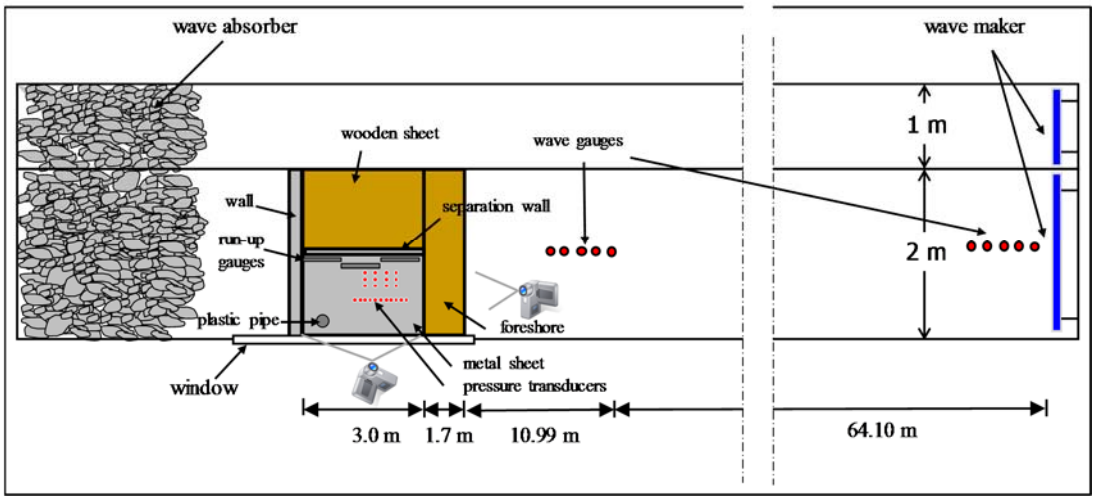

Fig. 3.2: Plan view of the model set-up for the preliminary tests in the 2 m wide wave flume of LWI (exemplarily for slope steepness 1:3)

The detailed model set-up with the deployed measuring devices exemplarily for the 1:6 revetment model is sketched in a side view in Fig. 3.3. The different layers 1-4 and columns A-D of PTs are also illustrated.

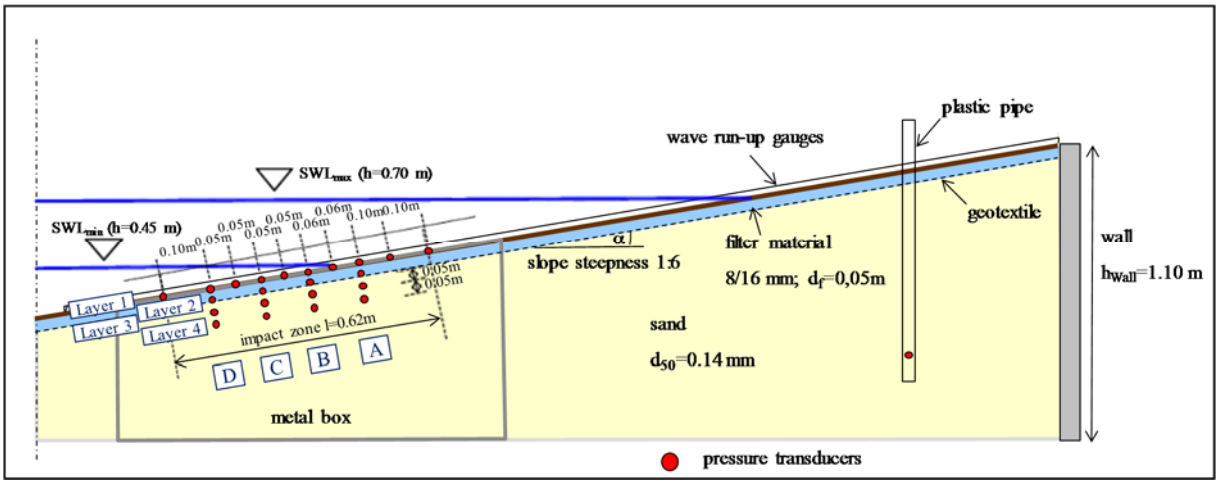

Fig. 3.3: Side view of the model set-up for the preliminary tests in the 2 m wide wave flume of LWI (exemplarily for slope steepness 1:6)

3.2 Results of preliminary tests

Even though a very simplified revetment model was used in the preliminary tests, adequate conclusions can be drawn regarding the processes on and in front of the revetment. Particularly, a proper assessment of the pore pressure damping with increasing depth in the subsoil with proper implications for the optimization of the locations of the pressure transducers in the sand core of the main tests can be obtained. In this section, the most important findings of the preliminary tests are briefly and systematically reported according to the different processes in front of, on and beneath the revetment. The procedures for the acquisition, pre-processing and analysis of the data are described in Liebisch et al. (2013b) and generally comply with the procedures used in the main tests reported in chapter 1 below.

3.2.1 Processes in front of and on the revetment

a) Wave reflection

The analyses of the preliminary tests show that both roughness and porosity have a decreasing effect on the reflection coefficient. Irrespective of the slope steepness, the roughness elements induce more turbulence on the revetments leading to higher energy dissipation. The latter is more significant for larger surf similarity parameters, because the effect of porosity and roughness is more pronounced for surging breakers than for other breaker types such as plunging breakers which are anyway associated with a high energy dissipation even on a smooth and impermeable revetment. The effect of the porosity on the reflection coefficient is much smaller (up to 50%) for both slope steepnesses compared to that of the roughness.

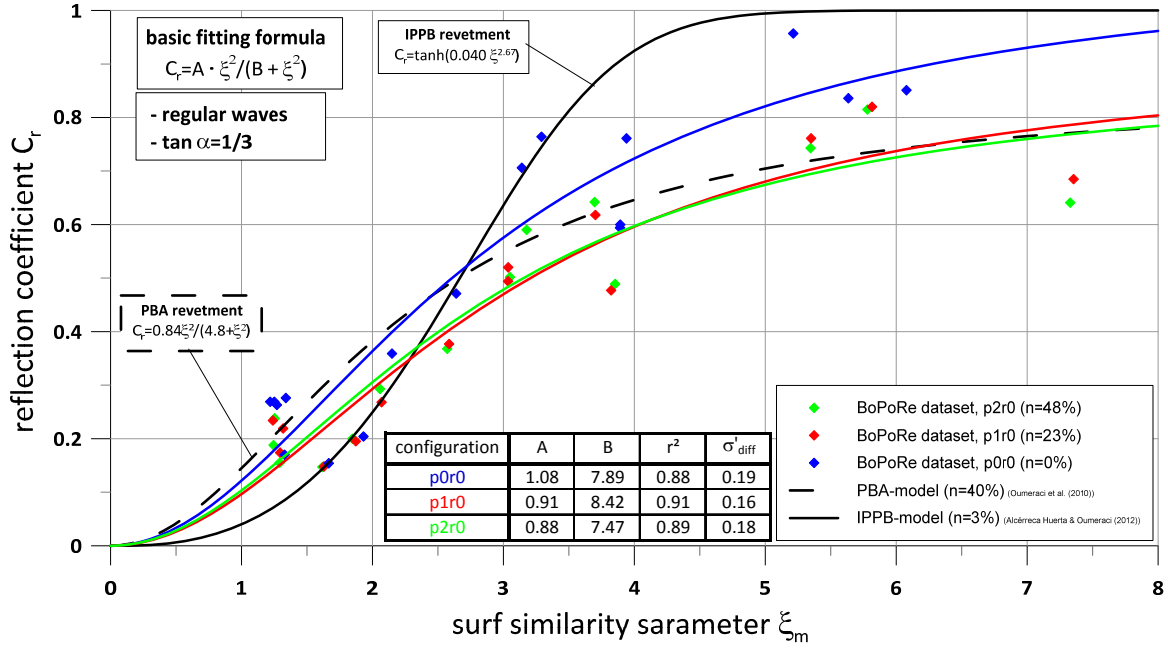

configuration	A	B	r^2	σ'_{diff}
p0r0	1.08	7.89	0.88	0.19
p1r0	0.91	8.42	0.91	0.16
p2r0	0.88	7.47	0.89	0.18

Fig. 3.4: Effect of porosity on the wave reflection coefficient as a function of surf similarity parameter ξ_m for regular waves (slope steepness 1:3)

When porosity increases from n = 0% to n = 23%, a significant decrease (up to 38%) of the reflection coefficient occurs. For a larger porosity n = 48% almost no additional effect is observed ("saturation"). Obviously this is due to the limited capacity of the porous revetment to cope with the infiltration of the uprushing water into the slope (see Fig. 3.4).

Combining both effects, an increasing roughness results in smaller reflection coefficients on a highly porous revetment, but no additional effect can be obtained by further increasing the porosity of a revetment with a high roughness.

The slope steepness also affects the reflection coefficient. The 1:6 revetment provides reflection coefficients which are up to 40 % smaller than those for the 1:3 slope. However, this has to be proven also for large surf similarity parameter (ξ_m > 3.7), which are lacking for the 1:6 revetment.

For all configurations and both slope steepnesses an increase of the reflection coefficient for small surf similarity parameters was observed.

The effect of roughness dominates the effect of porosity on the reflection performance.

It can be assumed that for a given ξ_m there must be a threshold value of the porosity where "saturation" occurs, so that the effect on wave reflection becomes negligible. This statement has to be proven in the main tests by the investigation of at least two revetment configurations with significantly different porosities.

The slope steepness also affects the reflection coefficient. The flatter slope provided smaller reflection coefficients compared to the steep slope. Consequently, it is recommended to investigate two slope steepnesses at minimum with an extension of the data sets for large surf similarity parameter (ξ_m > 3.7).

b) Wave setup

In the preliminary tests the relative wave set-up is found to slightly increase with an increasing roughness. This effect is larger for the 1:6 than for the 1:3 revetment. However, the effect of slope steepness on the relative wave set-up is decisive. For the flatter slope the relative wave set-up is smaller than for the steeper slope. The results of relative wave set-up are comparatively shown for both tested slopes 1:3 and 1:6 in Fig. 3.5, together with the related equations and determination coefficients r^2 obtained.

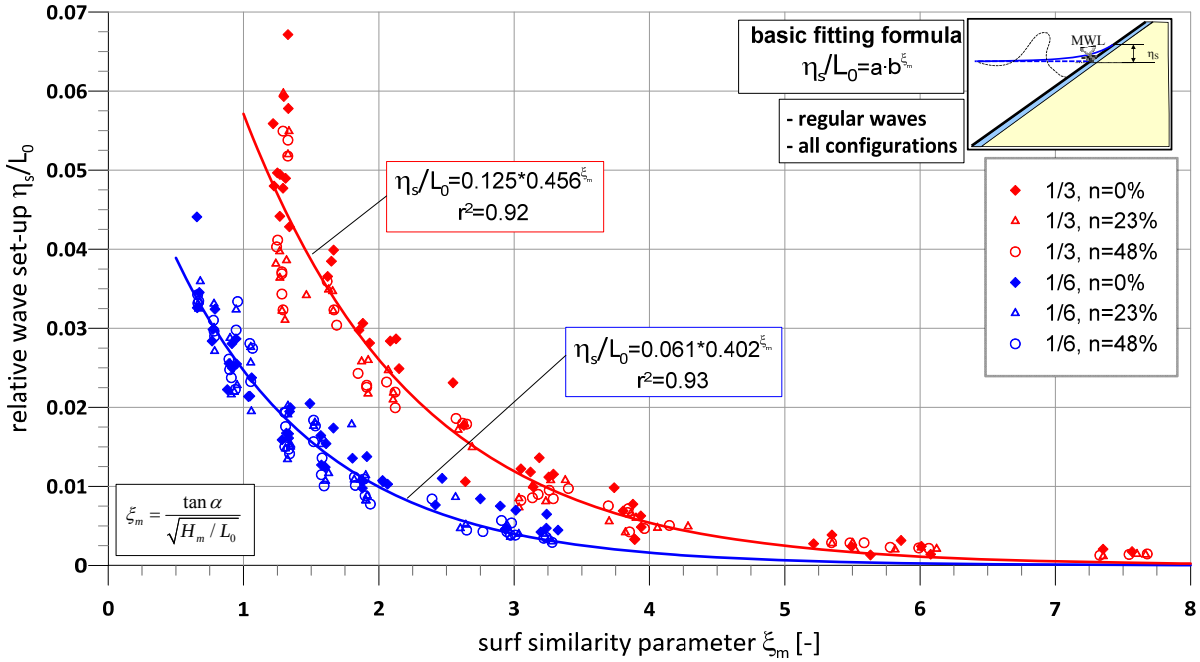

Fig. 3.5: Effect of slope steepness on relative wave set-up as a function of surf similarity parameter ξ_m for regular waves (all configurations)

A larger scattering occurs for the 1:3 revetment and surf similarity parameters smaller than 2. Obviously, for plunging breakers the slope steepness is not the only parameter which strongly affects the wave set-up.

Especially for smaller surf similarity parameters (plunging breakers) more research is necessary as the slope steepness is not the only important structure parameter strongly affecting the wave set-up. For the main experiments, more appropriate measurements of the wave set-up inside the sand core would be required in order to better describe the relation between the external mean water level and the internal mean water level in the sand.

c) Wave run-up and run-down

The wave run-up decreases significantly with increasing porosity, due to the infiltration of the up-running water mass into the porous structure and the associated higher turbulence and energy dissipation. In Fig. 3.6 the time series of wave run-up and run-down on a smooth revetment (r0) are exemplarily shown for the 3 tested porosities n = 0%, 23%, and 48%. The selected test for regular waves with a height of H_m = 0.16 m and a period T_m = 3.0 s in a water depth h = 0.60 m corresponds to non-impact load conditions, thus resulting in larger wave run-up than for impact loads.

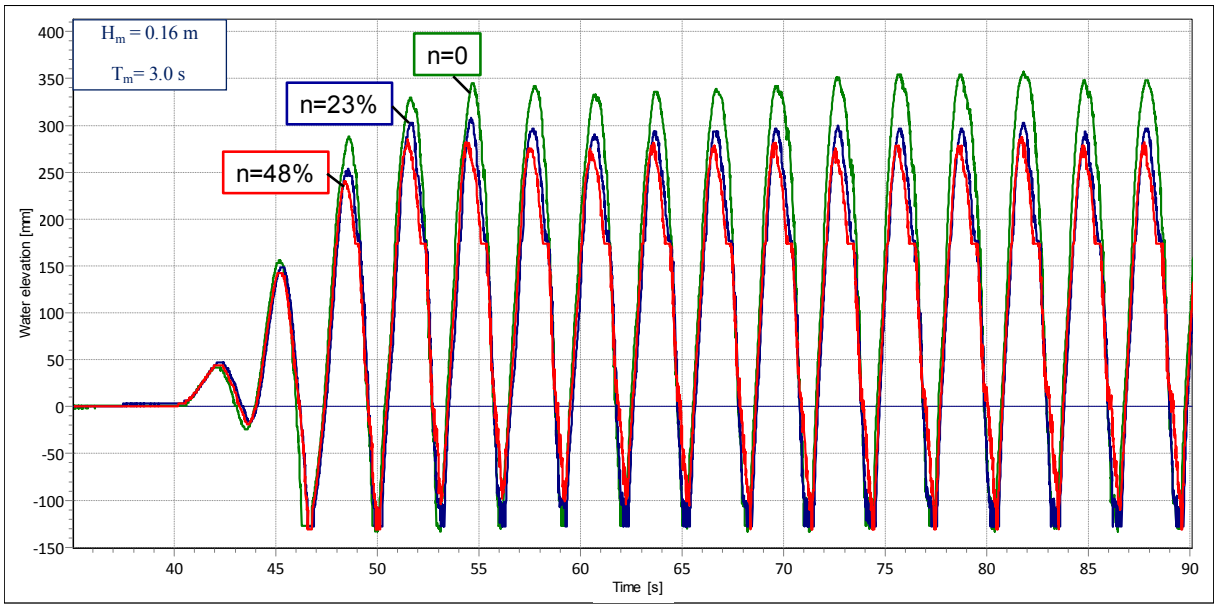

Fig. 3.6: Time series of wave run-up and run-down for smooth revetments with different porosities (regular waves, H_m = 0.16 m, T_m = 3.0 s, h = 0.60 m)

In this example, the wave run-up for the impermeable revetment (n = 0%) is reduced by more than 20% on the highly porous revetment (n = 48%), which corresponds to the findings of Oumeraci et al. (2010b) for a comparison of the results obtained for highly porous PBA-revetment and the run-up formula for smooth impermeable revetments. The effect of the porosity on wave run-down is less distinct and less pronounced. This might be due to the exfiltration processes which are more influenced by the porosity of the soil beneath the revetment than by that on the relatively thin revetment itself. Generally, similar results for the effect of the porosity of the smooth revetment are also obtained for the different roughnesses tested. However, the effect of porosity by varying the roughness is much more complex. For instance, it is not imperative that wave run-up decreases with increasing porosity. This is probably due to the combined effect of turbulence induced by the roughness elements and the infiltration/exfiltration processes which needs to be examined in more detail. For the 1:6 slope the effect of roughness is much more significant due to a larger ration of roughness element height to the water layer thickness on the slope. With the relative wave run-up and run-down as related to the external mean water level (EMWL) the results are confirmed. This method is physically much more appropriate than that related to SWL and a much smaller scattering is obtained.

Both roughness and porosity have a decreasing effect on the wave run-up. This effect is more pronounced for larger surf similarity parameters.

It is physically much more appropriate to analyse wave run-up and run-down related to the external mean water level (EMWL) than related to still water level (SWL).

3.2.2 Wave-induced pressures

An example of a recorded time series of the wave-induced pressure in different layers on and beneath the high porous revetment (p2) is illustrated for column C in Fig. 3.7 for regular waves with a height of 0.25 m and a period of 1.5 s in a water depth of h = 0.50 m which corresponds to impact load conditions.

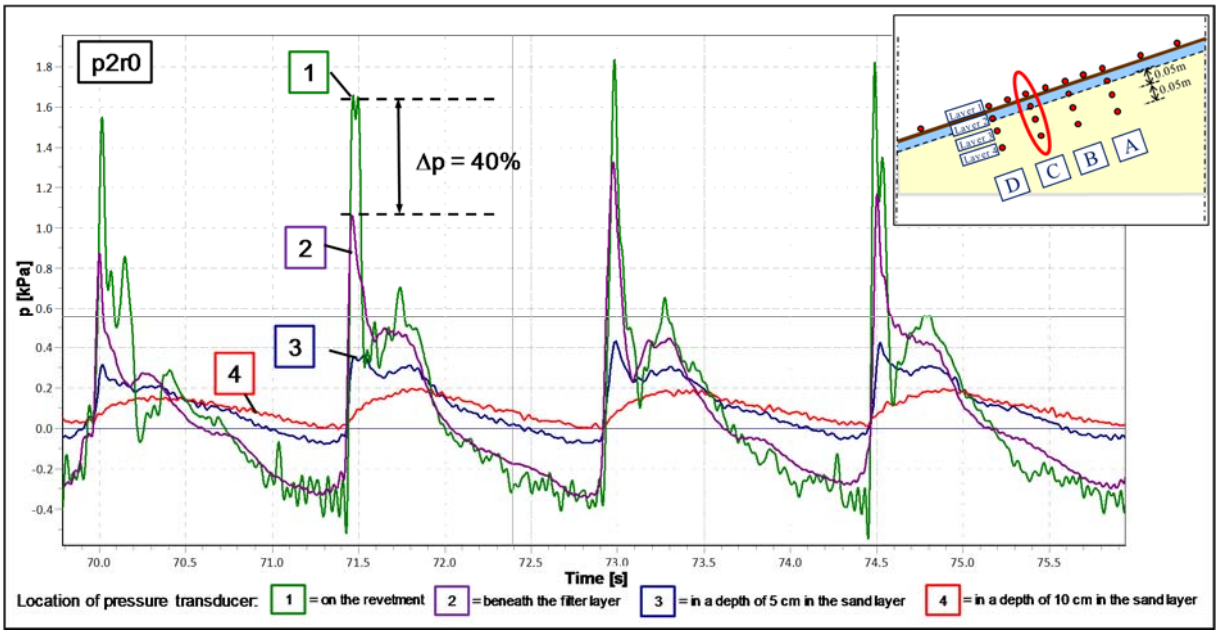

Fig. 3.7: Time series of wave-induced pressures on and beneath a highly porous and smooth revetment (regular waves, H_m = 0.25 m, T_m = 1.5 s, h = 0.50 m)

The reduction of the pressure through the revetment becomes obvious. The pressure peak is damped up to 40% by the porous revetment and the filter layer underneath. In the second sand layer in a depth of 10 cm, only small pressure values are visible so that the impact pressure is damped completely in a depth of 10 cm in the sand. Furthermore, it is also obvious that the quasi-static loads are transferred nearly completely through the cover and the filter layer. The entire porous structure induces almost no damping of the quasi-static loads which typically occur for larger surf similarity parameters.

Both roughness and porosity have a damping effect on the peak pressure for impact loads for both tested slope steepnesses. However, due to the retaining effect of the roughness elements a water layer remains on the revetment which damps the pressure peaks more significantly as compared to the present porosity. The slope steepness also affects the loading of the revetment. For steeper slopes high pressure peaks are less likely than for flatter slopes. Quasi-static loads are not affected by porosity or roughness.

Regarding the location of the peak pressure the direct relation with the wave run-down and the residence time of the associated water layer on the slope is underlined. If a water layer remains longer on the slope the incident waves glide on this water layer and break further upwards the slope. As the effect of roughness on the wave run-down is more distinctive than the effect of porosity, the same also applies for the location of the peak pressure on the slope.

Based on the model of Alcérreca Huerta & Oumeraci (2012) for the spatial pressure distribution to analyse the data, almost no change is found in the spatial pressure distribution with an increasing porosity. Similar to the location of the peak pressure it is found that the wave run-down also affects the spatial pressure distribution leading to a smoother distribution. The spatial pressure distribution for quasi-static loads is affected neither by roughness nor porosity for both tested slopes 1:3 and 1:6. However, it is not possible to "close" the spatial pressure distribution at the toe of the revetment, because no measurements are available at this location.

The peak pressure is affected by both roughness and porosity only for impact loads. The location of peak pressure and the spatial pressure distribution are closely related to the wave run-down and the residence time of the associated water layer on the slope, and thus especially affected by the roughness.

An additional pressure measurement at the toe of the revetment is necessary to "close" the spatial pressure distribution.

3.2.3 Wave-induced pore pressures

A time series of the pore pressure recorded for impact loads in the preliminary tests was already shown in Fig. 3.7. The results confirm the findings of the exponential reduction of the wave-induced pore pressure in the sand in Oumeraci et al. (2010b). However, for many of the preliminary tests especially those related to non-impact loads, the pore pressure distribution in the sand core is not entirely captured as shown at the deepest measuring location (layer 4) in Fig. 3.8, where the amplitude of the pore pressure signal (red line) is not zero, but still relatively high.

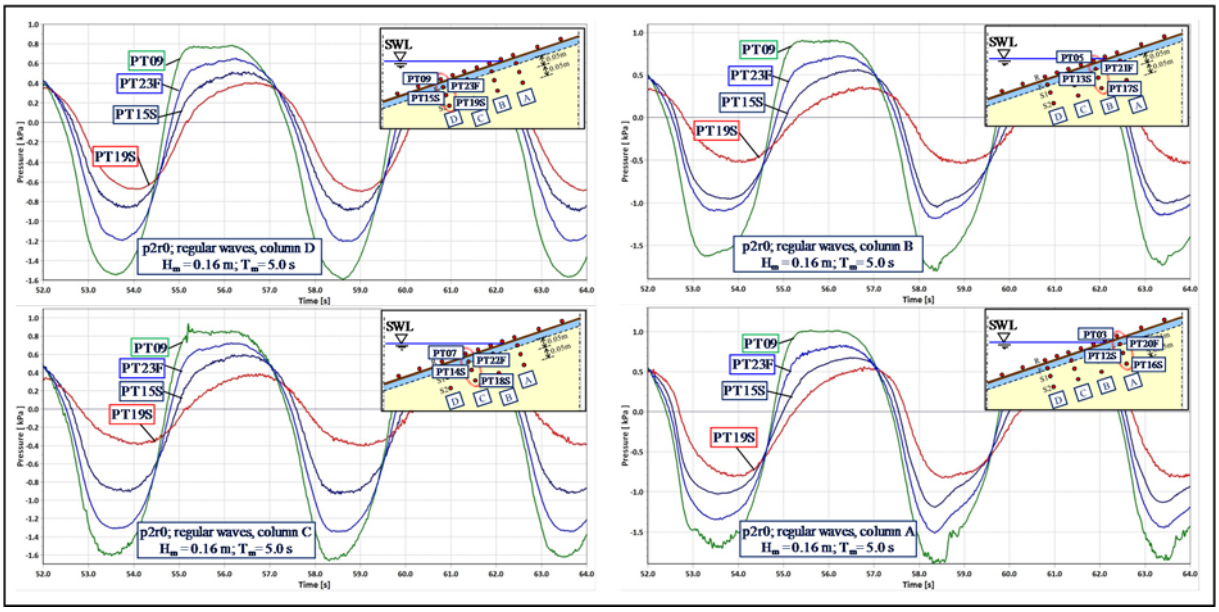

Fig. 3.8: Time series of wave-induced non-impact pressure on a porous and smooth revetment

In the preliminary tests, no effect of the revetment porosity or roughness on the pore pressure development in the sand core was found, but the wave period seems to substantially affect the infiltration depth of wave-induced pore pressures. Like in the GWK-tests by Oumeraci et al. (2010b) and in the numerical study by Alcérreca Huerta & Oumeraci (2013) no difference in pore pressure distribution is obtained for the four columns of PTs.

Pressure signals of the IMWL at a single point in the sand using a plastic pipe with a pressure transducer inside (see Fig. 3.3) could be obtained for the 1:6 revetment model. In case of the 1:3 revetment a piling up of the water occurred in front of the boundary brick wall for some tests and affected the development of the IMWL. Consequently, a comparison with the results obtained by Ludwigs & Oumeraci (2011) is so far not possible due to the missing measurement of the spatial development of IMWL in the sand core.

The wave-induced pore pressures are reduced exponentially in the sand core, but is not completed for many tests especially for non-impact loads at the deepest measuring location (layer 4).

Due to the lack of measurements at different points of the internal mean water level (IMWL) in the sand core, no statements on the spatial distribution and temporal development of the IMWL are so far possible. In the main tests a finer resolution of measuring points for the IMWL in the sand is necessary.

3.3 Summary and implications for the main tests

The different processes in front of, on and beneath the simplified model revetment investigated in the preliminary tests with the purpose of optimising the model set-up and the programme of the main tests. Both are described in detail in Liebisch et al. (2013b). The most important results with respect to the aforementioned purpose have briefly been discussed in this chapter. For this purpose, the results of the GWK tests (Oumeraci et al. (2010b)) and those of the numerical studies of Foyer (2013) and Alcérreca Huerta (2014) were also considered.

In this respect the following implications for the model set-up of the main tests can be drawn:

- The simplified revetment will be replaced by a more realistic bonded porous revetment. Two significantly different porosities need to be investigated. A small porosity in the range 10% is recommended. This is particularly important for identifying a possible threshold value of the porosity where “saturation” occurs and the effect on wave reflection becomes negligible. In advance it has to be tested with small test cubes if it is technically possible to achieve such a low porosity for a revetment.
- The effect of roughness dominated the effect of porosity on the reflection performance. However, roughness and porosity are inextricably linked with each other in bonded porous revetments, so these two parameters have to be considered together in the main tests.

- For the 1:3 revetment a larger distance between the revetment and the rear boundary (brick wall) of the model is required to prevent a piling up of the water in front of the brick wall in the sand.
- Due to the effect of slope steepness on most of the processes on and beneath the revetment, the slopes 1:3 and 1:6 tested in the preliminary study are also the most appropriate to be further considered for the main tests.

For the location of the measuring devices in the main tests, the following implications are drawn:

- A pressure transducer at the toe of the revetment is necessary to "close" the spatial pressure distribution on the revetment.
- A fifth layer of pressure transducers at a deeper location (20 cm) in the sand core is necessary to fully describe the wave-induced pore pressure reduction.
- To capture the spatial development of the IMWL a sufficient amount of pressure transducers in the rear part under the EMWL is needed.
- Due to the limited amount of pressure transducers (PT), the PT-columns may be reduced from four to three to obtain more devices for the spatial development of the IMWL. This is possible because no significant difference in the pore pressure distribution was observed at the four PT-columns.

Regarding the testing programme the following issues have to be regarded:

- For the development of more generic formulae, a substantially improved understanding of the processes on and beneath the revetments is required which can be achieved through a large number of more systematic regular and irregular wave tests. The numerical studies of Foyer (2013) and Alcérreca Huerta (2014) provide a large data set for regular wave tests. Therefore it is necessary to extend the data set with irregular wave tests. Especially for the investigations of the long-term development of IMWL the tests have to be long enough to capture the complete development of IMWL. The latter is especially important for regular wave tests.
- To ensure comparability with the preliminary tests and the large-scale tests of Oumeraci et al. (2010b) selected tests from both studies have to be reproduced in the main tests
- A wider range of surf similarity parameters have to be extended especially for the 1:6 slope regarding surf similarity parameter ξ larger than 3.5.

For the data analysis the following issues have to be remarked:

- It is recommended to use wave run-up and run-down height related to the EMWL in the analyses because it is physically much more appropriate than to SWL.
- The relation of external mean water level and internal mean water level in the sand needs to be determined in the main tests.

A comprehensive description of the planning of the main tests phase with the considerations of practical restrictions in the laboratory can be found in Liebisch et al. (2013a).

4 Experimental set-up and programme for the main model tests

Based on the results of the preliminary tests with the simplified model implications for the main tests were drawn in chapter 3 to develop a more realistic model set-up as well as to optimise the locations of the measuring devices and the test programme (phase 4 in Fig. 2.20). This chapter first give some general remarks on scale effects in section 4.1 and then the optimised model set-up together with the optimised locations of the measuring devices is described (section 4.2). The developed test programme with a focus on irregular wave tests is addressed in section 4.3. The final section 4.4 of this chapter is dedicated to the description of the procedure for the pre-processing and analysis of the data which is applied to generate the results reported in chapters 5, 6 and 7.

The detailed calculations for the determination of the locations for the deployed measuring devices are reported in Liebisch & Oumeraci (2014).

4.1 General remarks on model scale and scale effects

To possibly ensure comparability to the large-scale model tests in GWK of Oumeraci et al. (2010b), the preliminary tests of Liebisch et al. (2013b) and the model in the main tests needs to be designed accordingly. Based on the given restrictions in terms of the dimensions of the LWI wave flume and the possible range of wave parameters, a model scale of 1:5 related to the larger model tested in GWK (Oumeraci et al. (2010b)) is selected.

For scaled model tests a geometric, kinematic and dynamic similitude is necessary to transfer the obtained results into prototype scale. It is hardly possible to achieve a dynamic similitude in small scaled model tests because the characteristic fluid parameters (surface tension, viscosity, compressibility) cannot be scaled and model effects occur, which have to be considered in the interpretation of the results. For physical model tests in coastal engineering the model law of FROUDE is recommended, because the processes are mainly governed by gravity forces. In terms of the processes in front of, on and beneath bonded porous revetments, possible scale effects which might be considered in the analysis of the processes are discussed in the following.

a) Processes in front of and on the revetment

For the scale effects concerning the processes in front of and on the revetment (wave propagation, wave breaking, wave run-up/run-down), Schüttrumpf & Oumeraci (2005) analysed the scale effects in their experiments on wave run-up and overtopping on a smooth, impermeable revetment model in the wave flume of the LWI. More specifically, the influence of surface tension and viscosity on the afore mentioned processes were analysed showing that scale effects can be neglected considering wave propagation and wave breaking for common test conditions in the wave flume of the LWI (for wave-induced pressure due to wave breaking, see section c) below).

As the study of Schüttrumpf & Oumeraci (2005) was focussed on the analysis of wave overtopping processes, it was stated that tests with overtopping Reynolds numbers $Re_q < 10^3$ with $Re_q = 2(R\text{-}R_c)^2/(\nu T)$ have to be interpreted carefully. Since this study is focussed on the analysis of the swash processes on bonded porous revetments, for most of the tests $R_{u2\%} < R_c$ and no wave overtopping occurs. For this case, Schüttrumpf & Oumeraci (2005) recommended tests in large scale, because especially near run-up height R_u small swash velocities on the slope might result in a larger relevance of surface tension and viscosity. As the investigations of Schüttrumpf & Oumeraci (2005) were carried out on a smooth and impermeable revetment, this effect might be increased by the porous structure in this study, due to the flow in the porous structure during the swash processes. The magnitude of the scale effects due to surface tension and viscosity during swash in and on the revetment can hardly be determined. For the reduction of the scale effects due to flow in the porous media see next section b) below. The swash processes on the revetment are additionally affected by the degree of saturation of the porous structure underneath, which again affects the layer thicknesses during run-up/run-down leading to a changing effect of surface tension and viscosity depending on the degree of saturation. With a fully saturated porous revetment, larger water layers on the revetment are more likely resulting in a smaller relevance of scale effects for the swash processes. Overall, the magnitude of possible scale effects for wave run-up/run-down can only be estimated by the comparison of the results obtained in the small-scale tests with those of the GWK-tests.

Due to the much larger time scale of wave set-up, scale effects are unlikely for this process and do not have to be considered in the analysis of the small scale tests.

b) Flow in porous media and scaling of the porous revetment

The flow on and especially in the revetment is affected by surface tension and viscosity (see section a) above). Scaling the grain size of the revetment stones might result in too large viscous forces and possibly in laminar flow in small-scale models. The revetment material in the large-scale tests of Oumeraci et al. (2010b) was made of crushed limestone 20/40 mm. Scaled in 1:5, it would result in a grain size of 4/8 mm, for which the occurrence of laminar flow in the porous layer is more likely. To prevent exaggerated viscous effects in the small scale model according to Jensen et al. (1983), the grain size is chosen to 8/16 mm (also see Liebisch et al. (2013b)) resulting in a distortion factor of 2.0. Using this grain size for the revetment, viscous effects are largely prevented when the grain-size related Reynolds-number $Re_{crit} = vd_{50}/\nu > 5.0$. Even though the Reynolds-number varies over time during the swash processes on the revetment, this requirement is fulfilled most of the time. For a mean grain diameter $d_{50} = 0.011$ m and a kinematic viscosity of $\nu = 10^{-6}$ m²/s, a porous flow velocity of $v = 0.05$ cm/s is necessary to prevent viscous effects.

Nevertheless, the method of Jensen et al. (1983) is only valid for the assumption of a constant hydraulic gradient (steady flow), which is not given for a revetment under wave attack. Consequently, the application of a distortion factor might result in additional scale effects in the analysis of other processes in front of, on and just beneath (pressure damping of the revetment) the porous structure. The magnitude of this potential scale effects cannot be determined at this stage from a direct comparison of the small-scale tests of this study and the GWK-tests.

For a smaller porosity like in the down-scaled GWK-tests (n = 40%), the relevance of viscous effects increases again. Thus, the results are, strictly speaking, valid only for the tested conditions and cannot used directly and without correction for prototype conditions.

c) Wave-induced pressures on the revetment

Similar to the GWK-tests, the full range of relevant wave conditions (breaker types from plunging to surging breakers) and associated loading cases (from impact loads to quasi-static wave loads) is investigated. Scale effects are very likely for plunging breakers and the associated impact loads. The entrapped and compressed air in plunging breakers cannot be scaled by the Froude-law. Its effect is more pronounced in the smaller scale model, thus resulting in a larger damping of the peak pressures for impact loads (e.g. Bullock et al. (2001)), which has to be considered in the analysis. For surging breakers and the associated non-impact loads, scale effects are not expected, because this effect is not relevant.

d) Wave-induced pore pressures in the sand core

In fact, it is not possible to scale the grain size of the sand used in the large-scale tests of Oumeraci et al. (2010b) with a scale of 1:5, because a cohesive material would result. A grain size d_{50}=0.14 mm is used for the sand core resulting in a scale factor of 1:2.43 related to the grain size used in the GWK-tests. The processes in the sand core are dominated by viscous effects which cannot properly be scaled by the FROUDE law, thus resulting in a hardly possible direct comparison of the obtained results with those of the large-scale tests. A qualitative description of the processes in the sand core is nevertheless possible.

4.2 Model set-up and measuring devices

As afore mentioned, the revetment in the main tests needs to be designed accordingly to the large-scale model tests in GWK of Oumeraci et al. (2010b) and the preliminary tests of Liebisch et al. (2013b). For instance, slope steepness 1:3 investigated in both GWK-tests and preliminary tests is also used for the main tests. For the same reason mentioned in chapter 3, slope 1:6, investigated in the preliminary tests, is also used for the main tests.

Moreover, the same crushed stones (8/16 mm) for the filter layer and the same sand material (d_{50} = 0.14 mm) in the underlying sand core as in the preliminary tests (see chapter 3) are used. The main function of the filter layer is to provide an additional weight for the stability against uplift. A geotextile (Terrafix® 609) is located between the sand layer and the crushed stones to ensure stability of the sand against wash out.

As already mentioned in chapter 3, it is practically not feasible to test 9 model configurations for each slope steepness like in Liebisch et al. (2013b). Thus, PBA-samples are manufactured with different grain sizes to firstly test which porosities are possible using polyurethane-glue. It was shown that porosities less than 20% can hardly be achieved (Liebisch & Oumeraci (2014)). Based on a small test series of small scale tests (1:15) in the small wave flume ("Berliner Rinne") of the LWI, a highly porous cover layer with porosity n = 20% could be achieved only through a mixture of grain sizes (50 Vol.-% 4/8 mm, 25 Vol.-% 2/4 mm and

25 Vol.-% 1/2 mm) (Liebisch & Oumeraci (2014)). The two PBA-samples with the highest and lowest porosity of the cover layers (45% and 20%) which are used in the main tests are shown in Tab. 4.1.

Tab. 4.1: PBA-samples with the highest (45%) and lowest (20%) porosity of the cover layers used in the main tests

	PBA-sample	
No.	1	2
picture		
grain size [mm]	8/16	50 Vol.-% 4/8 + 25 Vol.-% 2/4 + 25 Vol.-% 1/2
pore volume [%]	45	20

The mass distributions of the two cover layer materials together with the characteristic grain diameters are reported in Liebisch & Oumeraci (2014). Small changes in surface roughness between the two materials occur, but they are not considered in the analyses, because these differences would also occur in large scale caused by aging processes. The two cover layers are placed on the filter layer. Therefore, the cover layer material is mixed with the 2-component polyurethane agent in small batches outside the flume and modelled batch by batch on the filter layer.

Three configurations (see Tab. 4.2) are used to investigate the effect of porosity and slope steepness on the processes in front of, on and beneath the revetment.

Tab. 4.2: Model configurations in the main tests related to slope steepness and revetment porosity

configuration	slope steepness	Porosity (revetment no.)
c1	1:3	45% (1)
c2	1:3	20% (2)
c3	1:6	45% (1)

The thickness of the cover layer is set to 5 cm for all configurations, because the effect of the revetment thickness on the processes in front of, on and beneath the revetment was already

investigated in Foyer (2013) and because a variation of this parameter in laboratory tests is highly time and cost consuming.

A brick wall is constructed in the flume to border the revetment model on the back side. Draining holes in the brick wall prevent a water level rising in the sand due to a water storage in front of the brick wall. Based on the findings of the preliminary tests for the 1:3 slope a horizontal sand platform between the revetment crest and the brick wall is built (see Fig. 4.1). This is not necessary for the 1:6 slope, because in the preliminary tests no piling up of the water at the brick wall was observed. If the latter is nevertheless observed these tests are excluded from the analysis of the development of the IMWL. Further tests are excluded from the analysis of the IMWL-development if wave overtopping occurs on the 1:3 slope and results in a water layer on the horizontal platform, because the measurements are affected by the infiltrating water. The seaward boundary for all model configurations is realized by a foreshore with a slope steepness of 1:17.

The general model set-up can be seen in Fig. 4.1 and Fig. 4.2.

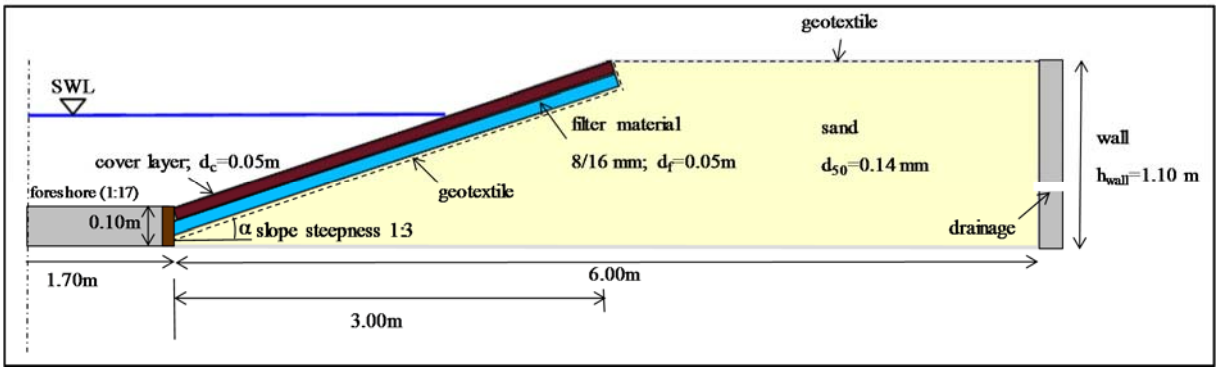

Fig. 4.1: General model set-up for model configuration c1 and c2 with a slope steepness of 1:3

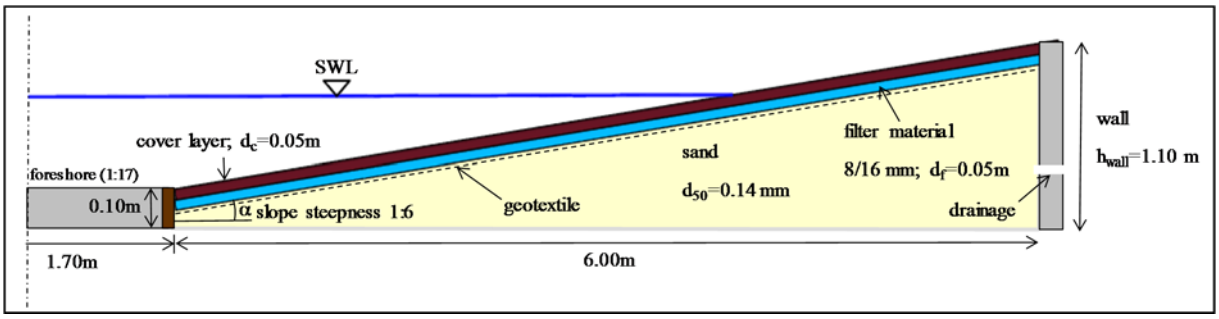

Fig. 4.2: General model set-up for model configuration c3 with a slope steepness of 1:6

Based on the implications of the preliminary tests and the hydraulic boundary conditions, as set in section 4.3, the optimal locations of the measuring devices are determined. The detailed calculations are reported in Liebisch & Oumeraci (2014). 11 pressure transducers (PTs) are used for the wave-induced pressure on the revetment. 10 of them are placed in a water-proofed metal box and one transducer at the toe of the revetment to “close” the spatial pressure distribution on the revetment. The metal boxes were successfully used in the preliminary tests and allow an easy change of the cover layer without relocating the measuring devices. The

distance between the single PTs is set to 5 cm or 6 cm in the inner impact area and 10 cm in the outer zone. Depending on the wave conditions the water level varies between 0.45 m and 0.70 m to ensure that the location of peak pressure is in the inner impact area. For configurations c2 and c3 only 10 PTs are used to measure the wave-induced pressure on the revetment due to a damage of a PT in the tests with configuration c1.

Three PT-columns (A-C) perpendicular to the slope were used to record the pore pressure development in the sand core (see Fig. 4.3). As an important implication from the finding of the preliminary tests (Liebisch et al. (2013a)), a PT-layer 5 is added in a depth of 20 cm in the sand core in order to obtain a complete distribution of the pore pressures normal to the slope in the main tests. The upper PT-layers are located like in the preliminary tests: layer 2 to measure the initial pressure p_0 on top of the sand core, layer 3 in a depth of 5 cm and layer 4 in a depth of 10 cm (layer 4) (see Fig. 4.3).

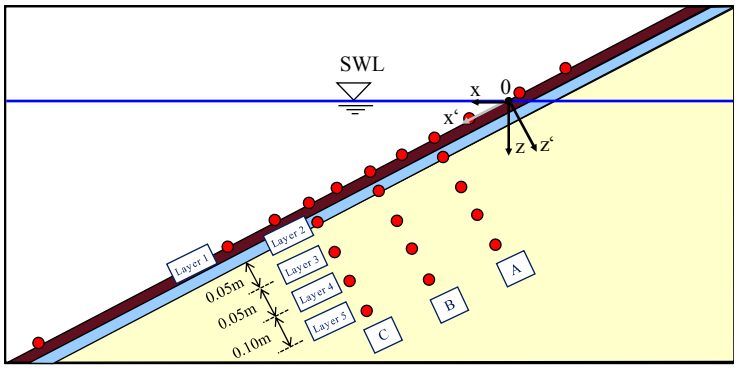

Fig. 4.3: Locations of the PT-layers and PT-columns of the pressure transducers (PTs) on and beneath the revetment

Like in the preliminary tests, the PTs in the sand are installed in a fixation unit (see Fig. 4.4) to avoid possible changes in the planned location of the devices in the sand core, especially during the construction period and the compaction of the sand layer. Furthermore, the PTs are installed next to the metal box to prevent an unintended effect of the box on the measurements. The PTs in layer 2 on the top of the sand layer were fixed on the geotextile between sand and filter material.

The metal box and the fixation unit with the PTs in the sand core are depicted in Fig. 4.4.

To ensure a finer spatial resolution than in the preliminary tests for the measurement of the development of the IMWL, 6 additional PTs are installed in the rear sand core below the external mean water level (EMWL) 20 cm above the flume bottom (Fig. 4.5). In this depth the pressure transducers are not affected by the swash oscillations induced by the waves on the slope.

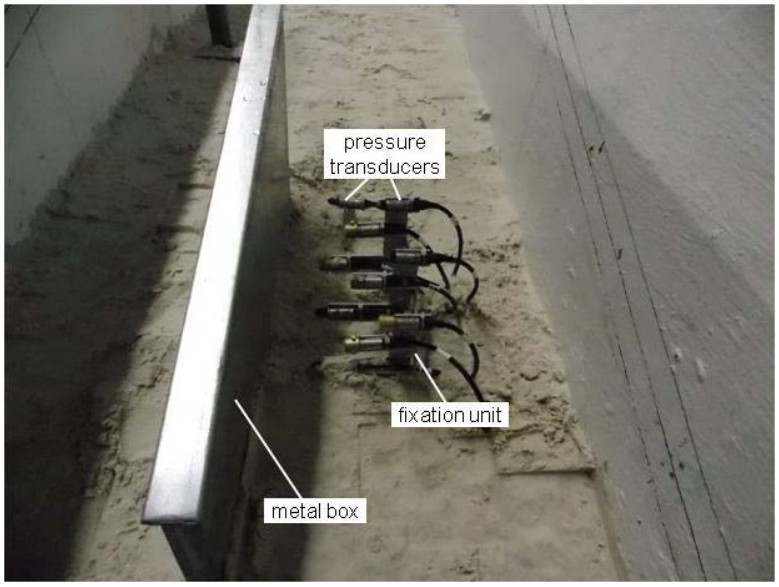

Fig. 4.4: Metal box and fixation unit with pressure transducers during construction period (slope steepness 1:3)

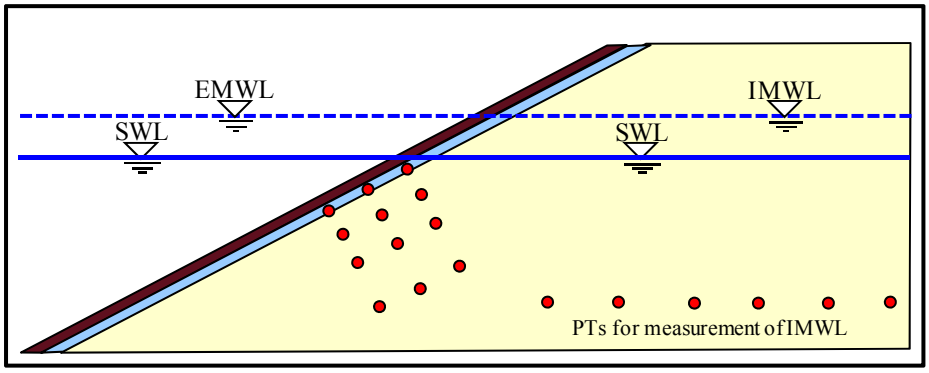

Fig. 4.5: Locations of the pressure transducers (PTs) for the measurement of the internal mean water level (IMWL)

The tests with configuration c1 showed that the locations of the pressure transducers to measure the IMWL in Fig. 4.6 were not suited to also capture the development of the IMWL further away from the shoreline. Therefore, the locations of these PTs were adjusted accordingly for the tests with configurations c2 (Fig. 4.8) and c3 (Fig. 4.9).

The measurement of the wave run-up and run-down on the revetment is realized by run-up-gauges (RUG) placed flush-mounted with the porous cover layer as shown in Fig. 4.7. 3 RUG with a length of 1 m each are used on the 1:3 model (Fig. 4.11) and 5 RUG on the 1:6 slope (Fig. 4.12). The water surface elevation is measured by 10 wave gauges (WG) which are arranged in two wave gauge arrays (Fig. 4.11 and Fig. 4.12). This arrangement is necessary for the reflection analysis using the standard approach of Mansard & Funke (1980). The distances between the wave gauges are dependent on the wave lengths in the test programme. Due to the slightly different testing programmes for the two slopes 1:3 and 1:6 (see section 4.3) also different distances between the single gauges in the wave gauge arrays are obtained (Tab. 4.3 and Tab. 4.4).

Tab. 4.3: Distances between the 5 wave gauges in the two wave gauge arrays (slope steepness 1:3)

wave gauge No.	1	2	3	4	5
distance [m]	0.30	0.45	0.60	1.00	

Tab. 4.4: Distances between the 5 wave gauges in the two wave gauge arrays (slope steepness 1:6)

wave gauge No.	1	2	3	4	5
distance [m]	0.25	0.4	0.55	1.15	

The final model set-up with the exact locations of the measuring devices for configuration c1 with the 1:3 slope are illustrated as a side view in Fig. 4.6 and as a top view in Fig. 4.7.

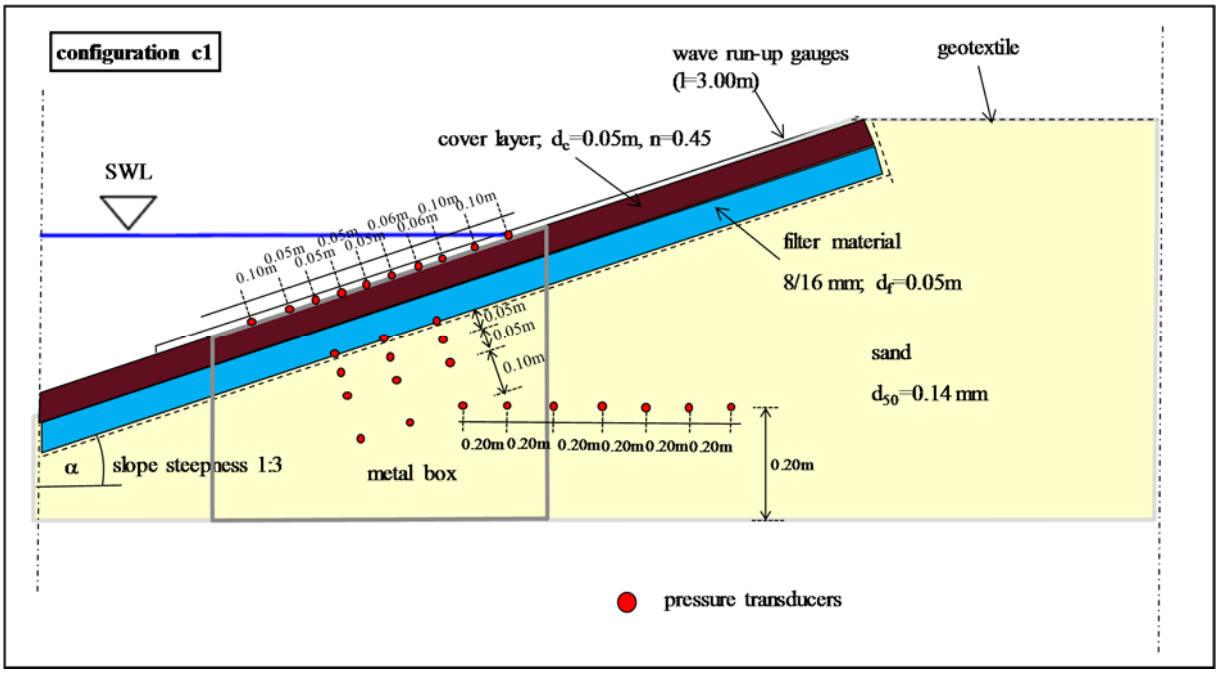

Fig. 4.6: Final model set-up and locations of pressure transducers (PTs) for configuration c1 (slope steepness 1:3, porosity n = 45%)

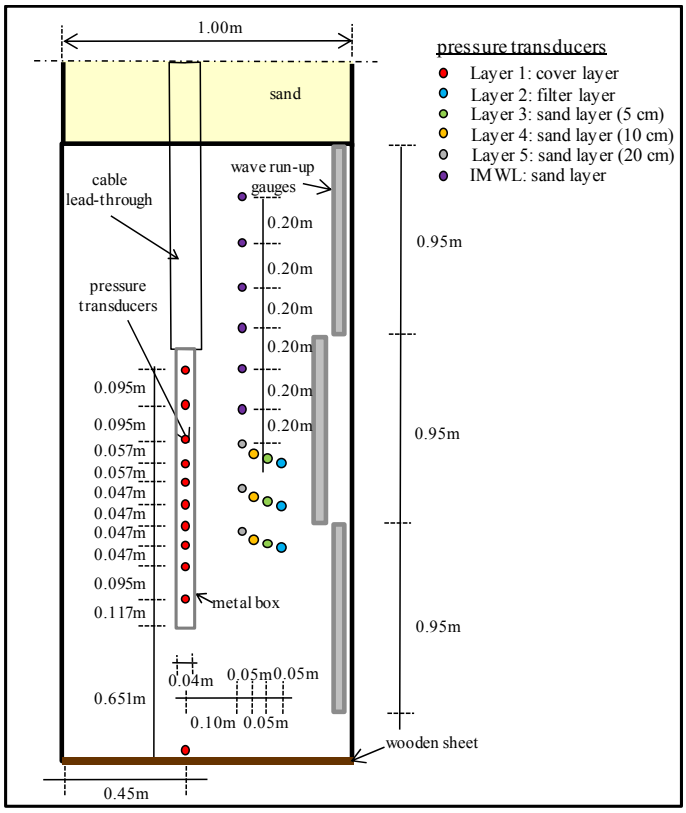

Fig. 4.7: Top view of the final model set-up and locations of pressure transducers (PTs) for configuration c1 (slope steepness 1:3, porosity n = 45%)

The final model set-up for configuration c2 with the adjusted locations of the PTs to measure the IMWL further inside the sand embankment is shown in Fig. 4.8.

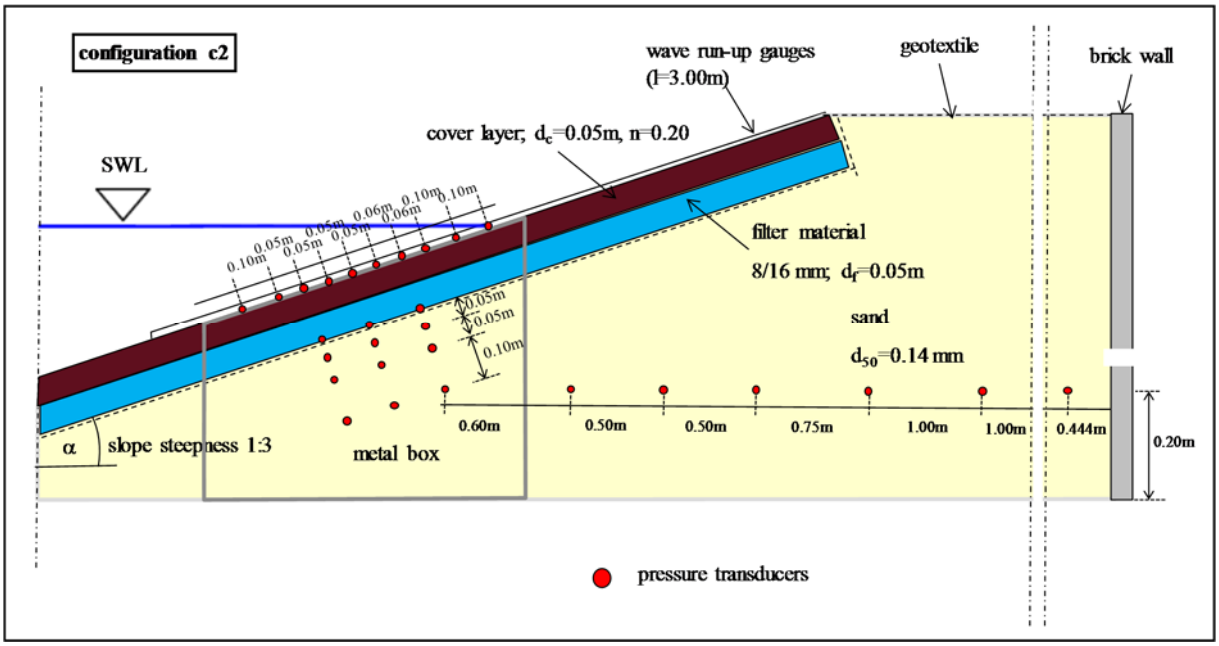

Fig. 4.8: Final model set-up and locations of pressure transducers (PTs) for configuration c2 (slope steepness 1:3, porosity n = 20%)

For configuration c3 with a 1:6 slope the side view is shown in Fig. 4.9.

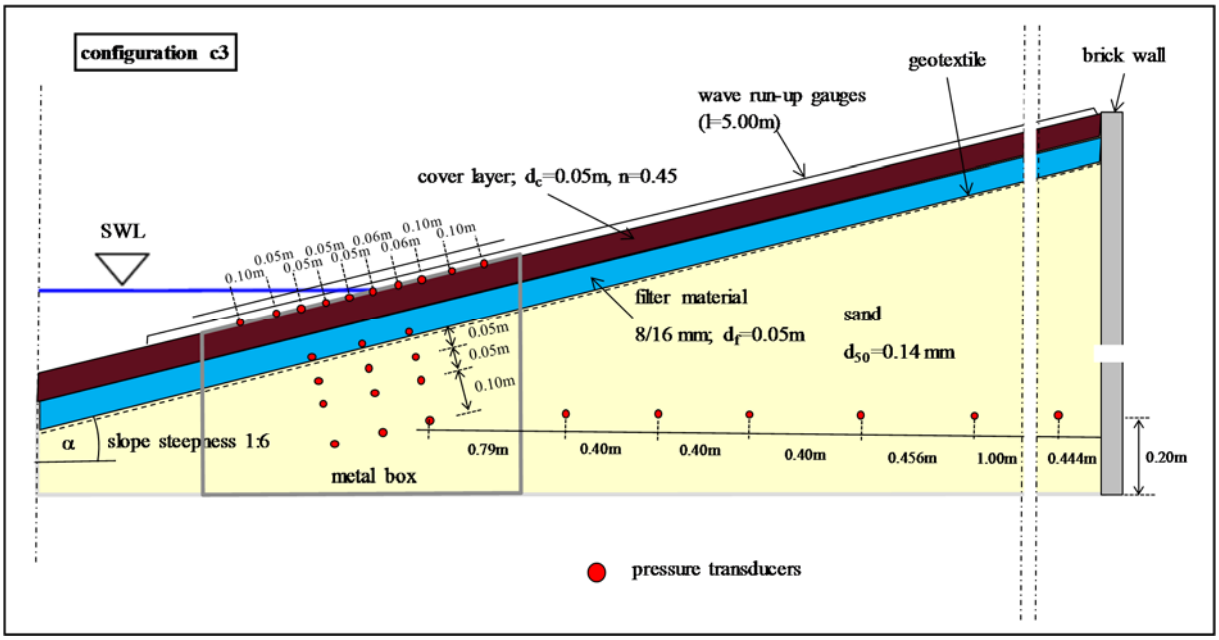

Fig. 4.9: Final model set-up and locations of pressure transducers (PTs) for configuration c3 (slope steepness 1:6, porosity n = 45%)

A photograph of the completed model with the measuring devices and the PBA-revetment is exemplarily shown in Fig. 4.10 for configuration c1.

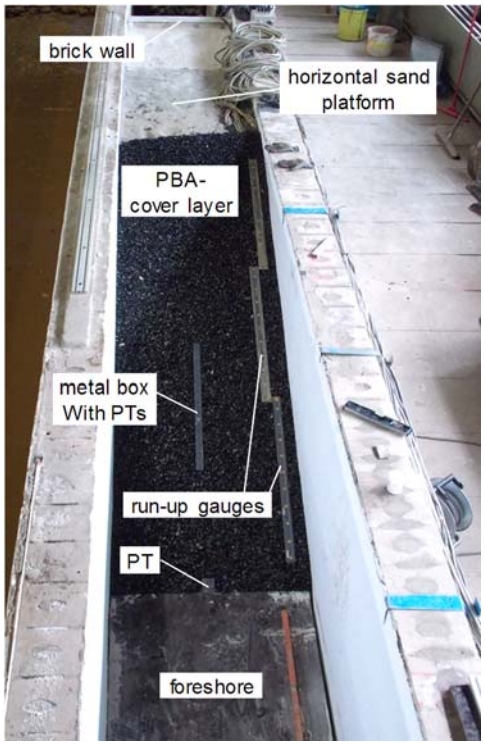

Fig. 4.10: Completed model in the 1m-wide wave flume, exemplarily for model configuration c1

Two digital video cameras at two different locations are deployed to support the analysis of the measured data (e.g. identification of breaker types and inconsistencies with wave and wave run-up signals). An overview of the models in the flume is shown in Fig. 4.11 for the model with the 1:3 slope and in Fig. 4.12 with the 1:6 slope.

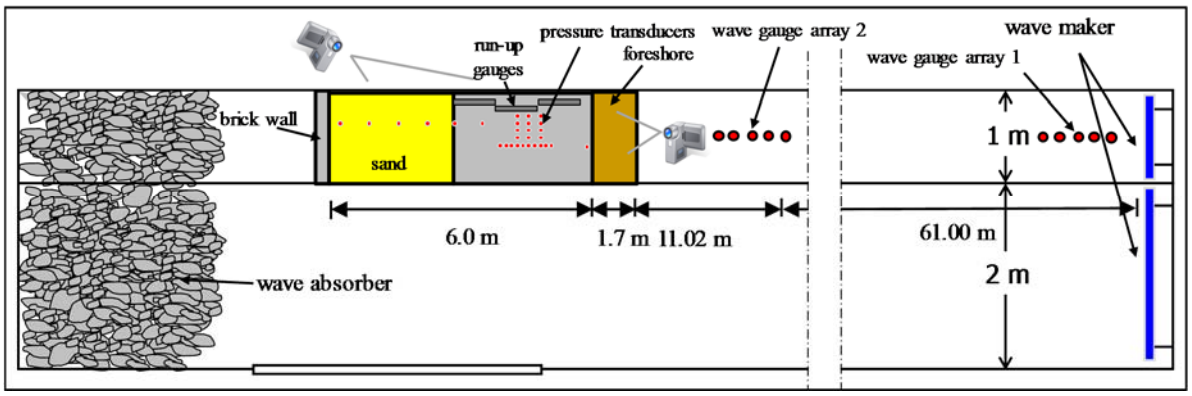

Fig. 4.11: Overview of the model with the 1:3 slope in the 1 m-wide flume

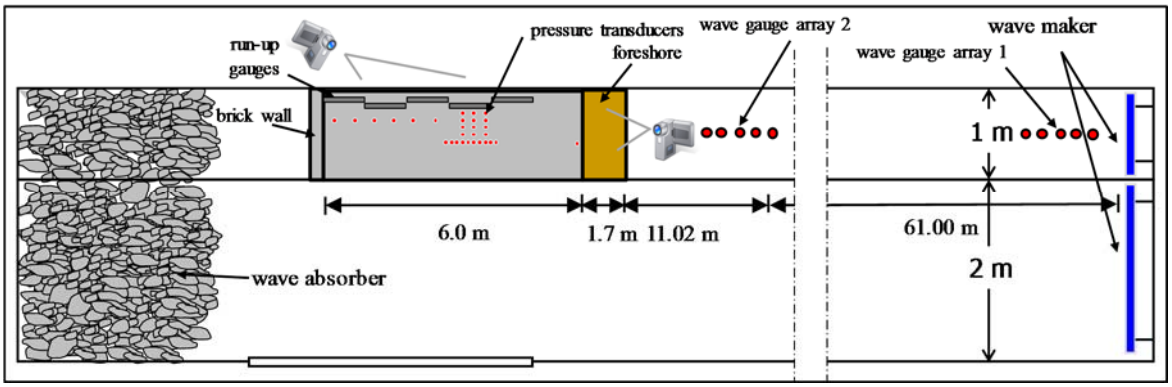

Fig. 4.12: Overview of the model with the 1:6 slope in the 1 m-wide flume

4.3 Test programme

The preliminary tests reported by Liebisch et al. (2013b) provided the primary basis for the development of the programme for the main tests. However, some adjustments were made because on the one hand in the main tests a focus is made on irregular waves and on the other hand tests with wave periods of 1.0 s and 6.0 s performed in the preliminary tests are not repeated in the main tests due to large energy dissipation and water depth limitations.

A wide range of wave conditions is considered. The single test conditions with regular waves (R) and JONSWAP-spectra (S) based on characteristic wave height H_m or H_{m0} and wave period T_m or $T_{m-1,0}$ together with the respective surf similarity parameter ξ_m or ξ_{m0}, can be seen in Tab. 4.5 for the 1:3 revetment and in Tab. 4.6 for a slope steepness of 1:6. Depending on the wave conditions the water level varies between 0.45 m and 0.70 m to ensure that the location of peak pressure is in the inner impact area. The wave parameters given in Tab. 4.5 and Tab. 4.6 are nominal values. In the tests the measured wave heights H_m or H_{m0} in front of the revetment

model are used to determine the deep water wave height to ensure comparability with the GWK-tests. The surf similarity parameters are calculated like in Liebisch et al. (2013b) by:

Regular waves: $$\xi_m = \frac{\tan\alpha}{\sqrt{H_m / L_0}} \quad (4.1)$$

with: $$L_0 = \frac{g \cdot T_m^2}{2 \cdot \pi}$$

Wave spectra: $$\xi_{m0} = \frac{\tan\alpha}{\sqrt{H_{m0} / L_0}} \quad (4.2)$$

with: $$L_0 = \frac{g \cdot T_{m-1,0}^2}{2 \cdot \pi}$$

The irregular wave tests consist of 600 waves in most cases and of 1000 waves for some selected tests to examine the influence of the test duration on the results. Selected tests of the wave spectra programme are repeated to control the repeatability of the tests and the scattering of the data. At least 65 wave spectra tests are conducted for each configuration. Furthermore, for each revetment configuration, 11-18 tests with regular waves (16-150 waves each, depending on the wave period) are performed to allow a comparison with the preliminary tests of Liebisch et al. (2013b) and the numerical simulations of Alcérreca Huerta (2014) which both were focused on regular waves. The entire programme of the main tests with the nominal values of wave height, wave period and surf similarity parameter is given in Tab. 4.5 for the 1:3 slope (configurations c1 and c2) and in Tab. 4.6 for the 1:6 slope (configuration c3). Due to the flatter slope for configuration c3 the wave period of 1.8 s was replaced by a wave period of 5.5 s and the wave height of 0.14 m was replaced by a wave height of 0.04 m to achieve a similar range of surf similarity parameters. The nominal values of the surf similarity parameters ($\xi_{m-1,0}$ = 0.67-8.10) cover the full range of relevant wave conditions (breaker types from plunging to surging breakers) and associated loading cases (from impact loads to quasi-static wave loads).

Tab. 4.5: Test programme for the main tests (slope steepness 1:3)

h=0.55-0.70 m		wave height H_m or H_{m0}						
		0.08	0.10	0.12	0.14	0.16	0.20	0.22
wave period T_m or $T_{m-1,0}$	1.5	S 2.21	S 1.98	R/S 1.80	S 1.67	R/S 1.56	S 1.40	S 1.33
	1.8	S 2.65	S 2.37	S 2.16	S 2.00	S 1.87	S 1.68	R/S 1.60
	2.0	S 2.95	S 2.63	S 2.40	S 2.23	R/S 2.08	S 1.86	S 1.78
	2.5	R/S 3.68	S 3.29	R/S 3.01	S 2.78	S 2.60	R/S 2.33	S 2.22
	3.0	S 4.42	S 3.95	S 3.61	S 3.34	R/S 3.12	S 2.79	S 2.66
	4.0	S 5.89	S 5.27	S 4.81	S 4.45	S 4.17	R/S 3.73	S 3.55
	5.0	S 8.10	S 7.24	S 6.61	S 6.12	R/S 5.73	R/S 5.12	S 4.88

R 1.80	regular waves ξ_m
S 1.67	wave spectra ξ_{m0}
S	repeated test
$\xi_{m0} < 2.5$	Impact load
$2.5 \le \xi_{m0} \le 2.9$	Transition zone
$2.9 \le \xi_{m0}$	Non-Impact load

Tab. 4.6: Test programme for the main tests (slope steepness 1:6)

h=0.45-0.65 m		wave height H_m or H_{m0}						
		0.04	0.08	0.10	0.12	0.16	0.20	0.22
wave period T_m or $T_{m-1,0}$	1.5	S	S	S	R/S	R/S	S	R/S
		1.56	1.10	0.99	0.90	0.78	0.70	0.67
	2.0	S	S	S	S	R/S	R/S	S
		2.08	1.47	1.32	1.20	1.04	0.93	0.89
	2.5	S	S	S	S	R/S	S	S
		2.60	1.84	1.65	1.50	1.30	1.16	1.11
	3.0	S	S	S	R/S	R/S	S	S
		3.12	2.21	1.98	1.80	1.56	1.40	1.33
	4.0	R/S	R/S	S	S	S	S	S
		4.17	2.95	2.63	2.40	2.08	1.86	1.78
	5.0	S	S	S	S	R/S	S	S
		5.21	3.68	3.29	3.01	2.60	2.33	2.22
	5.5	S	S	S	S	S	S	S
		5.73	4.05	3.62	3.31	2.86	2.56	2.44

R	regular waves
1.30	ξ_m
S	wave spectra
1.50	ξ_{m0}
S	repeated test
$\xi_{m0} < 2.5$	Impact load
$2.5 \leq \xi_{m0} \leq 2.9$	Transition zone
$2.9 \leq \xi_{m0}$	Non-Impact load

Transferring the test programme in Tab. 4.5 and Tab. 4.6 to prototype scale (1:1) would results in wave heights H_{m0} between 0.20 m and 1.10 m with wave periods $T_{m-1,0}$ between 3.35 s and 12.30 s.

4.4 Procedure for data pre-processing and data analysis

The acquired raw data must be pre-processed prior to their analyses, including further preparations. The general procedure for data pre-processing, further data preparations and data analyses which has been adopted throughout this study is briefly described in this section to avoid repetitions in the subsequent chapters. More details on this general procedure and other specific procedures are provided accordingly in the corresponding subsequent chapters.

Immediately after each test, all recorded signals are carefully checked regarding abnormal signals or mal-functioning devices.

For all conducted tests time frames are defined for all measuring devices. These time frames are necessary to exclude the ramping-up phase of the wave maker and the time that the waves need to propagate through the flume to reach the model. Furthermore, they include a defined number of waves for irregular waves for data analysis: 600 waves in most cases and 1000 waves for some selected tests. For regular wave tests the set time frames also exclude waves re-reflected by the wave maker. All analyses are conducted for the defined time frames.

The incident and reflected waves are determined by the commonly applied reflection analysis based on Mansard & Funke (1980), which is conducted for both wave gauge arrays deployed in the wave flume (see Fig. 4.11 and Fig. 4.12). However, the incident wave parameters for the loading of the revetment model are determined at wave gauge array 2 and contain the incident wave height (H_m or H_{m0}), the wave period (T_m or $T_{m-1,0}$) as well as the reflection coefficient (C_r), which is analysed in chapter 5.

To maintain comparability with the GWK-tests by Oumeraci et al. (2010b), the numerical tests by Alcérreca Huerta & Oumeraci (2012) and the 1:5 downscaled preliminary tests by Liebisch

et al. (2013b) the measured incident wave heights H_i at wave gauge array 2 are transformed in the deep water wave heights H_0. For the calculation of H_0 the shoaling factor K_s was used:

$$\frac{H_i}{H_0} = K_s = \sqrt{\frac{1}{2n} \cdot \frac{c_0}{c}} \tag{4.3}$$

with:

$$n = 0.5 \cdot \left(1 + \frac{(4\pi h / L)}{\sinh(4\pi h / L)} \right)$$

Nevertheless, in this study the calculated deep water height H_0 is called H_m (regular waves) and H_{m0} (irregular waves). These wave heights are used with wave period T_m (regular waves) and $T_{m-1,0}$ (wave spectra) for the calculation of surf similarity parameter ξ_m and $\xi_{m-1,0}$, respectively:

$$\xi_m = \frac{\tan\alpha}{\sqrt{H_m / L_0}} \tag{4.4}$$

$$\xi_{m-1,0} = \frac{\tan\alpha}{\sqrt{H_{m0} / L_0}} \tag{4.5}$$

Like in Liebisch et al. (2013b) wave run-up/run-down is measured with run-up gauges (RUG) (see section 4.2) consisting of four measuring channels for 25 cm each (see Fig. 4.13). Three RUGs are used on the 1:3 slope and five RUGs on the 1:6 slope. To obtain a time series of the total wave run-up and run-down on the revetment model, the single channels are added together in a new written channel to describe the total wave run-up and run-down. This method is also illustrated in Fig. 4.13 for a regular wave test. Wave run-up and run-down is analysed for the selected time frames.

The RUGs are also used to analyse the wave set-up in the considered time frame of the tests. The wave set-up η_S is determined as the difference between the still water level (SWL) and the external mean water level (EMWL). More details on the procedure are given in chapter 5.

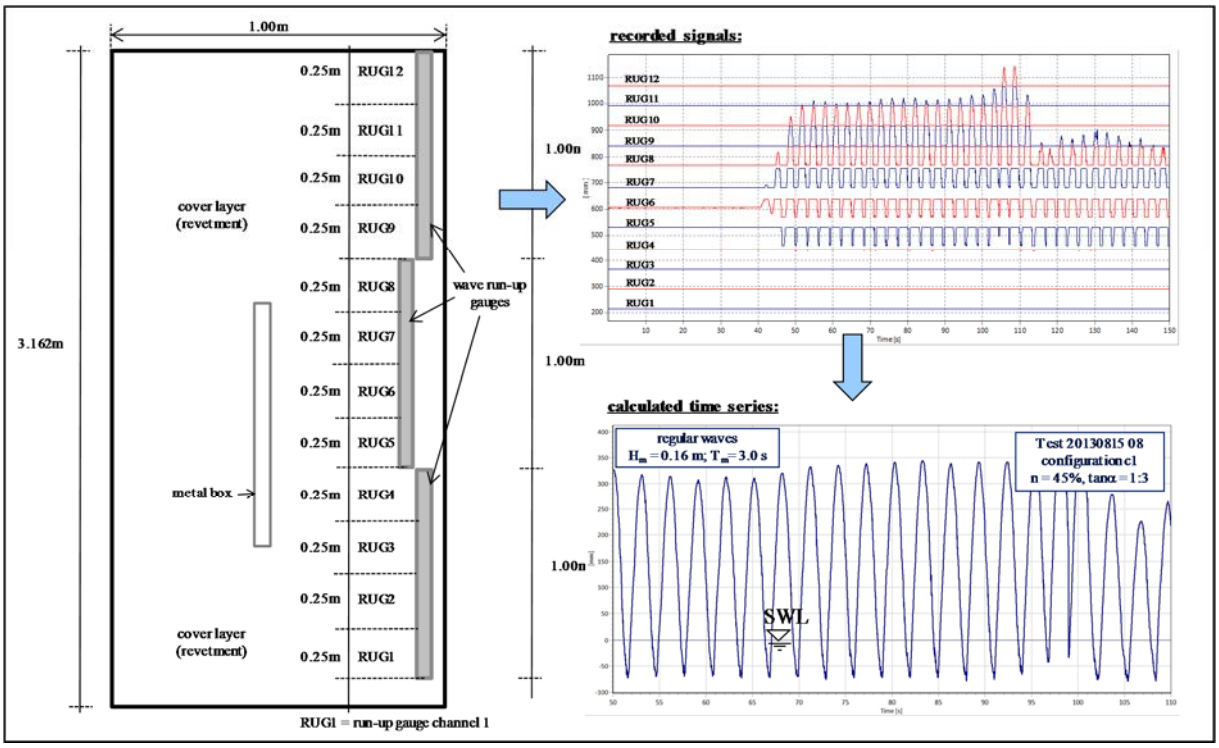

Fig. 4.13: Wave run-up gauges with recorded signals of the measuring channels and calculated time series (exemplarily for slope steepness 1:3)

Prior to the analysis of any recorded pressure signals of the PTs, all measured data independently of their location is pre-processed by filtering the data with a low pass filter of 25 Hz. In PT-column B and C (see section 4.2) the pre-processing of the signals also includes some more correctional filtering due to the large noise recorded at these locations.

For each PT the maximum pressure p_{max} recorded in the considered time frame is determined. Using this procedure the peak pressure on the revetment (PT-layer 1) is determined for every test. The peak pressure on top of the sand core in PT-layer 2 is directly connected with this peak pressures p_{max} PT-layer 1, meaning that for every PT-column A-C the peak pressure in PT-layer 1 is identified and the associated damped pressure is determined in the PT-layer 2. This peak pressure on top of the sand core is defined as the initial pressure p_0 on top of the sand core and all measured pressures p_i in the layers beneath are normalized by p_0 (p_i/p_0) for the analyses of the pore pressure damping in the sand core.

For the pressure transducers in the sand core further pre-processing of the signal is necessary to identify possible residual pore pressure and to separate the residual from the transient pore pressure component. For this purpose the method proposed by Oumeraci & Kudella (2006) and shown in Fig. 4.14 is used. A Fast Fourier Transformation (FFT) is applied on the pressure signal to determine the magnitude and the phase spectra. A low pass filter of 0.03 Hz is then applied using an Inverse Fourier Transformation for all measured signals in the sand core to separate the low frequency residual pore pressure (mean component) from the high frequency transient pore pressure (oscillating component).

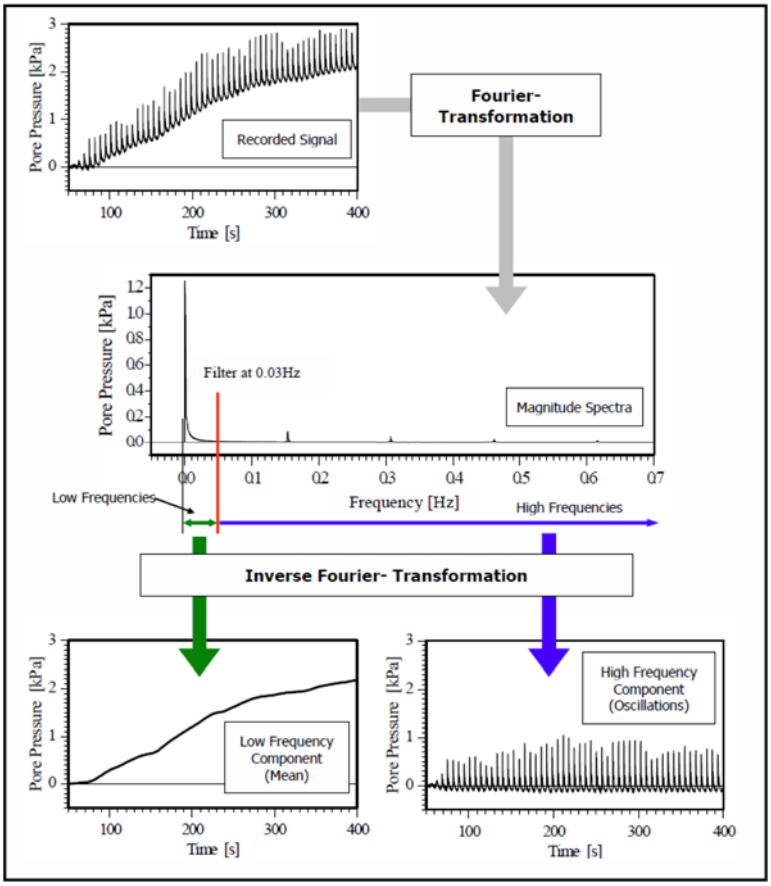

Fig. 4.14: Separation of the recorded signal in mean and oscillating component (Oumeraci et al. (2010b))

For the development of empirical formulae based on regression analysis, the statistical parameters, already used in Liebisch et al. (2013b) are also applied in this study to describe the fitting accuracy for the results of the main tests. Kortenhaus (2003) divided the standard deviation by the measured mean value and obtained the coefficient of variation, which is less dependent on the input values:

$$\sigma'_{diff} = \frac{\sqrt{\frac{1}{n-1}\sum\left(y - f(x)\right)^2}}{\overline{y}} \tag{4.6}$$

In addition to the coefficient of variation the coefficient of determination is given, which is calculated by:

$$r^2 = 1 - \frac{\sum\left(y - f(x)\right)^2}{\sum\left(y - f(x)\right)^2 + \sum\left(\overline{y} - f(x)\right)^2} \tag{4.7}$$

5 Processes in front of and on the revetment

In this chapter the results of the systematic main tests concerning the processes taking place in front of and on the revetment are analysed. The wave reflection is presented in section 5.1. In section 5.2 the wave set-up at the structure is analysed which describes the change of EMWL (wave set-up). The swash processes on the revetment including wave run-up and run-down are addressed in section 5.3 both related to the SWL and the MWL, followed by a summary and the implications of the key results in section 5.4.

All analyses are conducted first for the configurations with the same slope steepness (1:3) and different porosities to investigate the effect of porosity on the considered process. Afterwards, the effect of slope steepness with a constant porosity is considered.

5.1 Wave reflection

One of the most important processes which has to be considered when planning a revetment is the wave reflection, because it can lead to scouring at the toe of the structure or higher loading of the structure due to the interaction of the incident waves and the reflected waves which are in phase at the structure. Knowing the reflection coefficient C_r, the energy dissipation (coefficient C_d) can easily be determined under the assumption of no wave overtopping by:

$$C_d = \sqrt{1 - C_r^2} \tag{5.1}$$

The key results of the preliminary model tests concerning wave reflection were already shown in section 3.2.1a). In section 2.1.1 the most commonly used model proposed by Seelig & Ahrens (1981) was introduced in eq. (2.4), which was also used in Oumeraci et al. (2010b) to fit the GWK-data.

In the following the reflection coefficient is analysed as a function of the surf similarity parameter for all tested revetment configurations tested with irregular waves. The results of the large-scale tests of Oumeraci et al. (2010b) and Alcérreca Huerta & Oumeraci (2012) and the preliminary tests in Liebisch et al. (2013b) are also considered for comparison.

5.1.1 Effect of the revetment porosity

Firstly, the reflection coefficient is investigated for configurations c1 and c2 with a slope steepness 1:3 (also see Tab. 4.2). The porosity changes from n = 45% (configuration c1) to n = 20% (configuration c2). Fig. 5.1 illustrates the effect of porosity on reflection coefficient C_r as a function of surf similarity parameter $\xi_{m-1,0}$ for configurations c1 and c2 tested with wave spectra. The model of Seelig & Ahrens (1981) (eq. (2.4)) is applied on the results and compared to the studies of Oumeraci et al. (2010b), Alcérreca Huerta & Oumeraci (2012) and Allsop (1990).

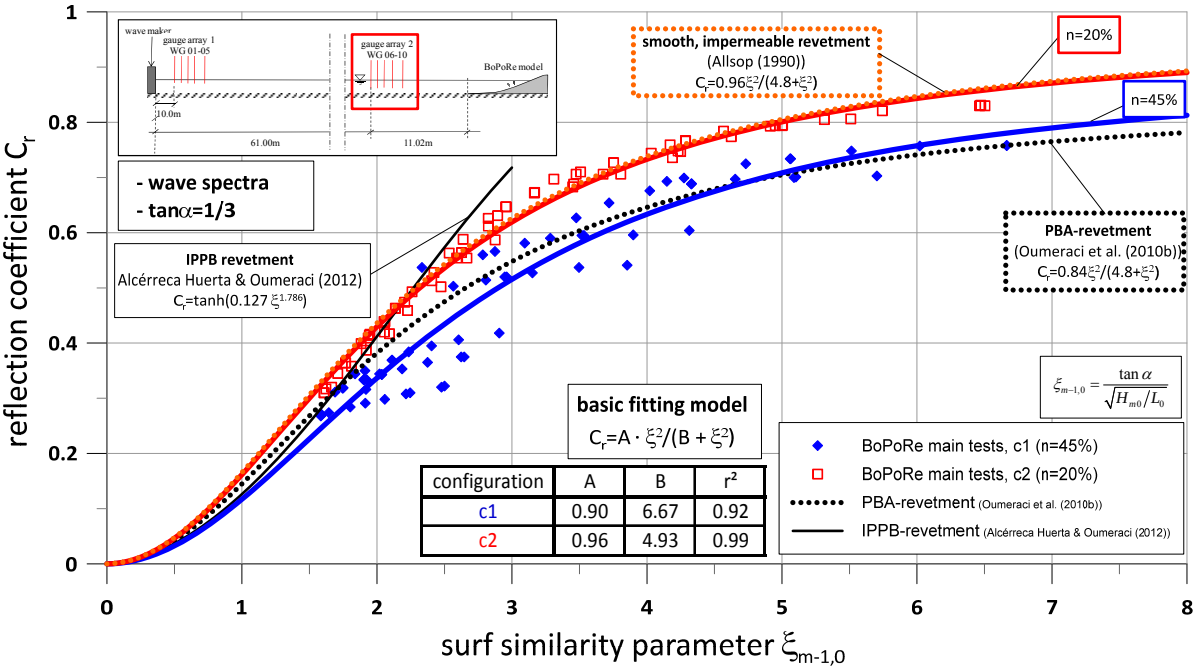

configuration	A	B	r²
c1	0.90	6.67	0.92
c2	0.96	4.93	0.99

Fig. 5.1: Effect of the revetment porosity on reflection coefficient C_r as a function of surf similarity parameter $\xi_{m-1,0}$ for wave spectra (slope steepness 1:3)

Fig. 5.1 shows that the highly porous configuration c1 provides lower reflection coefficients compared to the less porous configuration c2 for almost all surf similarity parameters. As expected, more energy is dissipated by the more porous revetment. Furthermore, the results for configuration c1 show a quite good agreement with the results of the large-scale tests of Oumeraci et al. (2010b) indicated by the dashed line. This was expected because the PBA-revetment tested in GWK had a similar porosity (n = 40%). The porous structure with lower porosity (n=20%) behaves almost like an impermeable revetment as shown in Fig. 5.1 by the comparison of the fitting function for revetment c2 (also see eq. (5.3) and that of Allsop (1990) found for a smooth and impermeable revetment (A = 0.96, B = 4.80). The GWK-tests performed by Gier et al. (2012) with another almost impermeable smooth revetment (IPPB-revetment) were analysed by Alcérreca Huerta & Oumeraci (2012). For the reflection performance the model of Zanuttigh & Van der Meer (1988) was used. This formula also provides a good agreement for the data of c2 up to a surf similarity parameter of 2.5 (see Fig. 5.1). No comparison was possible for $\xi_{m-1,0} > 3$ since the focus of the tests by Gier et al. (2012) was focused on impact loads ($\xi_{m-1,0}$ = 1.5-3).

For both configurations c1 and c2 the model of Seelig & Ahrens (1981) shows a good agreement with coefficients of determination larger than 90 %. The following equations were found:

Configuration c1 (tanα = 1:3; n = 45%): $$C_r = \frac{0.90\cdot\xi_{m-1,0}^2}{6.67+\xi_{m-1,0}^2} \quad (5.2)$$

Configuration c2 (tanα = 1:3; n = 20%): $$C_r = \frac{0.96\cdot\xi_{m-1,0}^2}{4.93+\xi_{m-1,0}^2} \quad (5.3)$$

However, for configuration c1 a larger scattering occurs with a kind of clustering of the data points into distinct groups. This was already observed in Oumeraci et al. (2010b), where it was stated that the effect of wave period is much more important than considered in the surf similarity parameter. It can be seen that for the cover layer with a porosity of 20 % in Fig. 5.1 no clustering occurs and the results are also well described with the model of Seelig & Ahrens (1981).

To examine the data clustering more closely, the results of the reflection coefficient for configuration c1 are subdivided into groups with respect to the wave period $T_{m-1,0}$ and also with respect to the wave height H_{m0}. This is shown in Fig. 5.2 for configuration c1 (n = 45%) with different colours and legends for each group of wave period. For each group the model of Seelig & Ahrens (1981) is applied. The different wave heights are indicated with dashed lines.

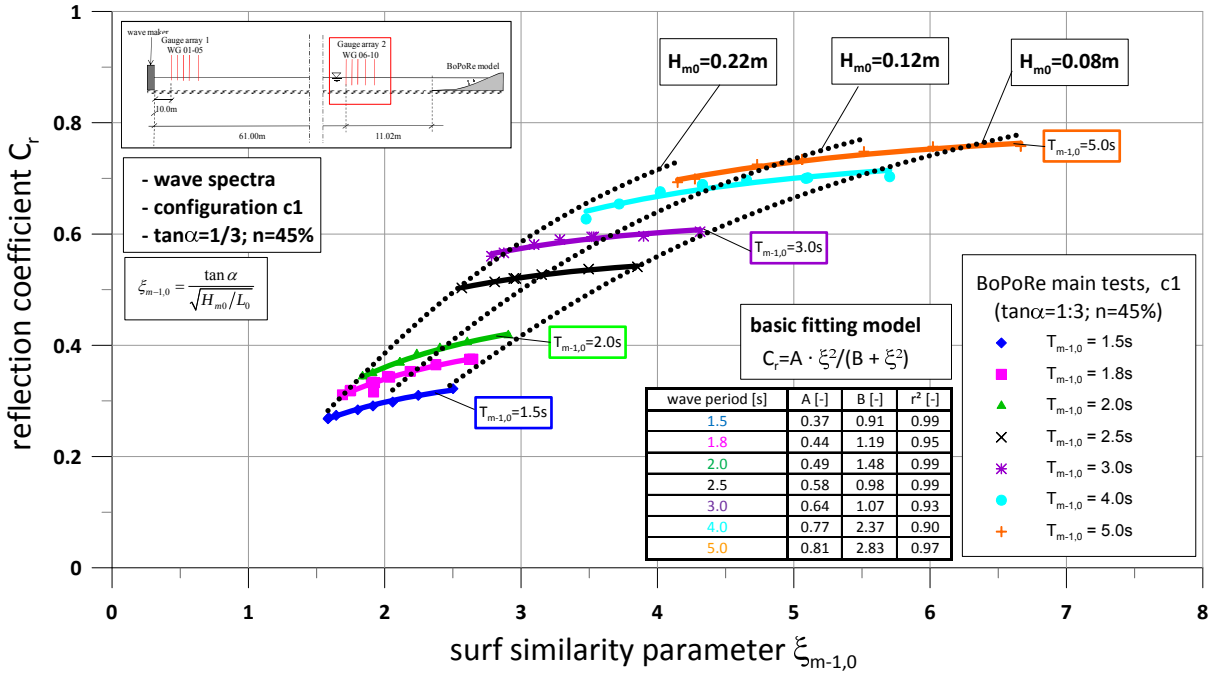

Fig. 5.2: Applied model of Seelig & Ahrens (1981) on the reflection coefficient C_r as a function of surf similarity parameter $\xi_{m-1,0}$ in groups of different wave periods for configuration c1 for wave spectra (slope steepness 1:3)

Fig. 5.2 confirms the findings of Oumeraci et al. (2010b) in the sense that for highly porous revetments the effect of wave period is indeed more important than considered in the surf similarity parameter. This can only be due to the high porosity of the cover layer, because for the configuration c2 with 20% porosity this effect does not occur (also see Fig. 5.1). A larger porosity obviously leads to a decreasing effect of the reflection coefficient especially for small wave periods. For each group of values with the same wave period the reflection coefficient decreases with increasing wave height and decreasing surf similarity parameter, i.e. the dissipation on the revetment is larger for higher waves with the same wave period. For regular waves this clustering is also present but less pronounced than for irregular waves (see Liebisch & Oumeraci (2014)). The same was also found by Oumeraci et al. (2010b). No clustering was

identified by Foyer (2013) and Alcérreca Huerta (2014) in their numerical studies with regular waves.

However, reflection coefficients tending to 1.0 for large surf similarity parameters, are not achieved with the application of the model of Seelig & Ahrens (1981). Consequently another approach is applied for the reflection coefficient which is expected to be physically more appropriate. The obtained results are subdivided into groups of the same wave height H_{m0}, which is directly connected to the incident wave energy and represents thus the basis for the consideration of reflected and dissipated wave energy (see Fig. 5.3)

In the numerical studies of Foyer (2013) and Alcérreca Huerta (2014) two different models were used to fit the data of reflection coefficient C_r. Alcérreca Huerta (2014) applied the tanh-model (see eq. (2.5)) as also proposed by Zanuttigh & Van der Meer (1988) and Foyer (2013) used a modified version of the model of Seelig & Ahrens (1981) (see eq. (5.4)). In this modified model coefficient A is set to 1.0, so that only coefficient B needs to be determined. Thus, C_r tends against 1.0 for large surf similarity parameter, which is physically more appropriate than the original model of Seelig & Ahrens (1981) (see eq. (2.4)):

$$C_r = \frac{\xi_{m-1,0}^2}{B + \xi_{m-1,0}^2} \tag{5.4}$$

In this study both models are applied on the data but only the results of the data fitting with eq. (5.4) are shown, because a better correlation is achieved and the formula is much easier in the application compared to eq. (2.5). The results can be seen in Fig. 5.3 for configuration c1 with different colours and legends for each group of wave heights. For each group the modified model of Seelig & Ahrens (1981) is applied. The different wave periods are indicated with dashed lines.

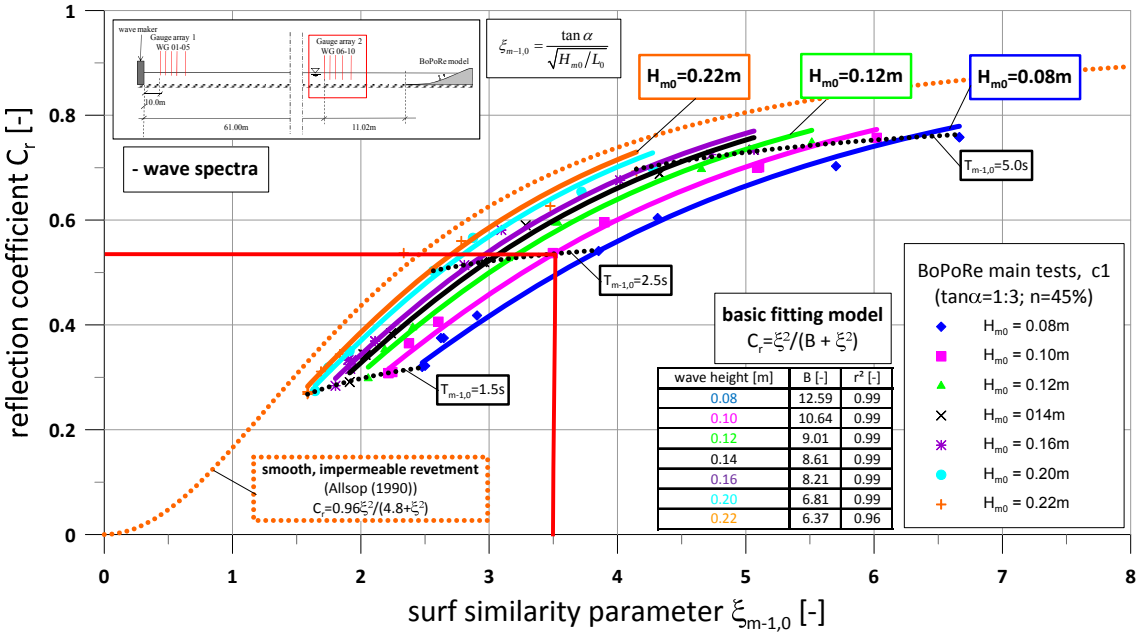

wave height [m]	B [-]	r^2 [-]
0.08	12.59	0.99
0.10	10.64	0.99
0.12	9.01	0.99
0.14	8.61	0.99
0.16	8.21	0.99
0.20	6.81	0.99
0.22	6.37	0.96

Fig. 5.3: Reflection coefficient C_r as a function of surf similarity parameter $\xi_{m-1,0}$ in groups of different wave heights for configuration c1 for wave spectra (slope steepness 1:3)

The approach using the wave height data grouping results in curves which are simply shifted horizontally depending on the wave height. For all curves a very good fitting is obtained using eq. (5.4) and the obtained coefficients B are listed together with the coefficient of determination for the different wave heights. For large wave heights parameter B in eq. (5.4) tends to smaller values which means that the porous structure is less effective in reducing reflection and behaves increasingly like an impermeable revetment with increasing wave heights. For comparison with Fig. 5.3 the GWK-data of Oumeraci et al. (2010b) are downscaled to 1:5 and plotted in Fig. 5.4 using the same approach for data grouping.

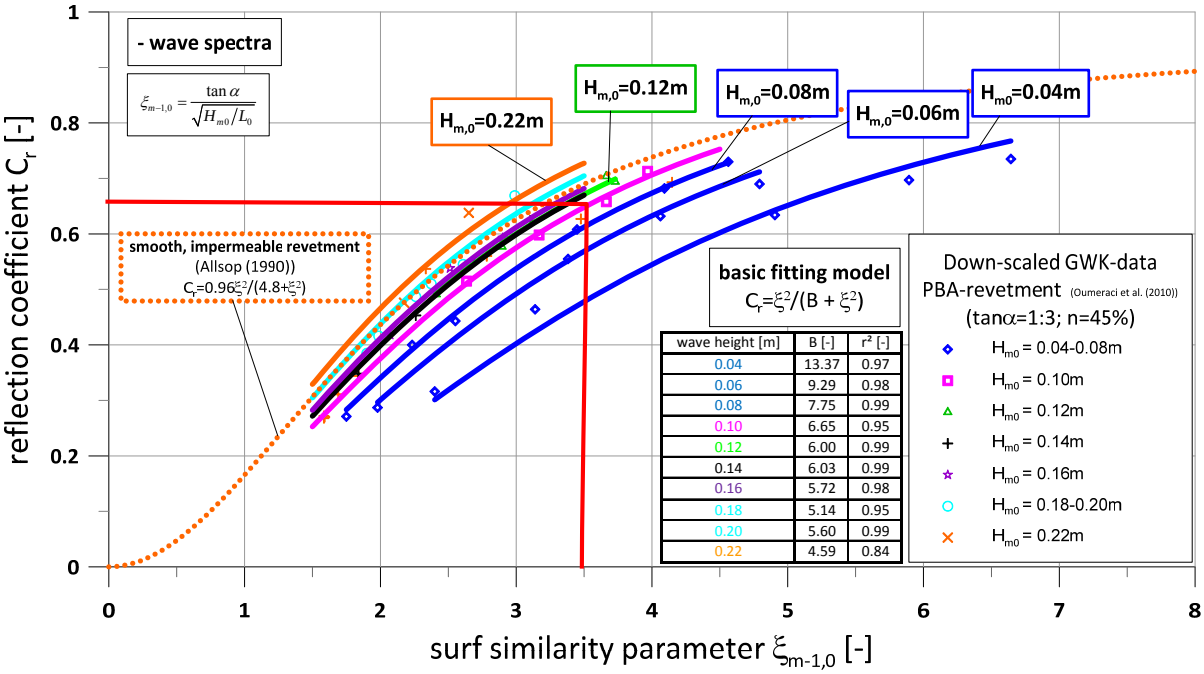

Fig. 5.4: Reflection coefficient C_r as a function of surf similarity parameter $\xi_{m-1,0}$ in groups of different wave heights for down-scaled GWK-data tested for wave spectra (slope steepness 1:3)

A similar shifting of the fitting curves as in Fig. 5.3 (LWI-flume tests) is also observed for the GWK-tests in Fig. 5.4. Also in the GWK-tests parameter B in eq. (5.4) tends to smaller values for larger wave heights indicating that the porous structure is less effective in reducing reflection (larger reflection coefficient C_r). This means that the PBA-revetment in the GWK-tests also behaves increasingly like an impermeable revetment with increasing wave heights. However, for the same wave conditions, indicated with the red line in Fig. 5.3 and Fig. 5.4, the small-scale model provides a smaller reflection coefficient and thus a larger energy dissipation. This also results in larger values of coefficient B for configuration c1 compared to GWK-data for the same wave height. This might be explained by scale effects due to the used distortion factor of 2 for the scaling of the revetment material (see section 4.2). This results in a different ratio between pore size and/or grain size and the incident waves leading to a higher energy dissipation for configuration c1 for almost the same porosity. Obviously the used distortion factor, which was applied to prevent exaggerated viscous effects in the small scale model (Jensen et al. (1983)), cannot prevent all scale effects. It is assumed, the reason can be found in the simplified assumption of a constant hydraulic gradient in Jensen et al. (1983) (also see section 4.1).

In the following the parameter B in eq. (5.4) is examined more closely. In this context the model of Allsop (1990) who applied the model of Seelig & Ahrens (1981) to define a model for an impermeable, smooth revetment is used limit state line for the reflection coefficient, which means that it is assumed that the equation of Allsop (1990) describes the maximum reflection on revetments. Using eq. (5.4) to fit the data produced by the model of Allsop (1990) the following model for impermeable and smooth revetments is obtained:

$$C_r = \frac{\xi_{m-1,0}^2}{5.56 + \xi_{m-1,0}^2} \tag{5.5}$$

Based on the findings for configuration c1 in Fig. 5.3, Fig. 5.5 shows that parameter B tends to a value of 5.56 for very large wave heights which corresponds indeed to the B value in eq. (5.5) for smooth and impermeable revetments.

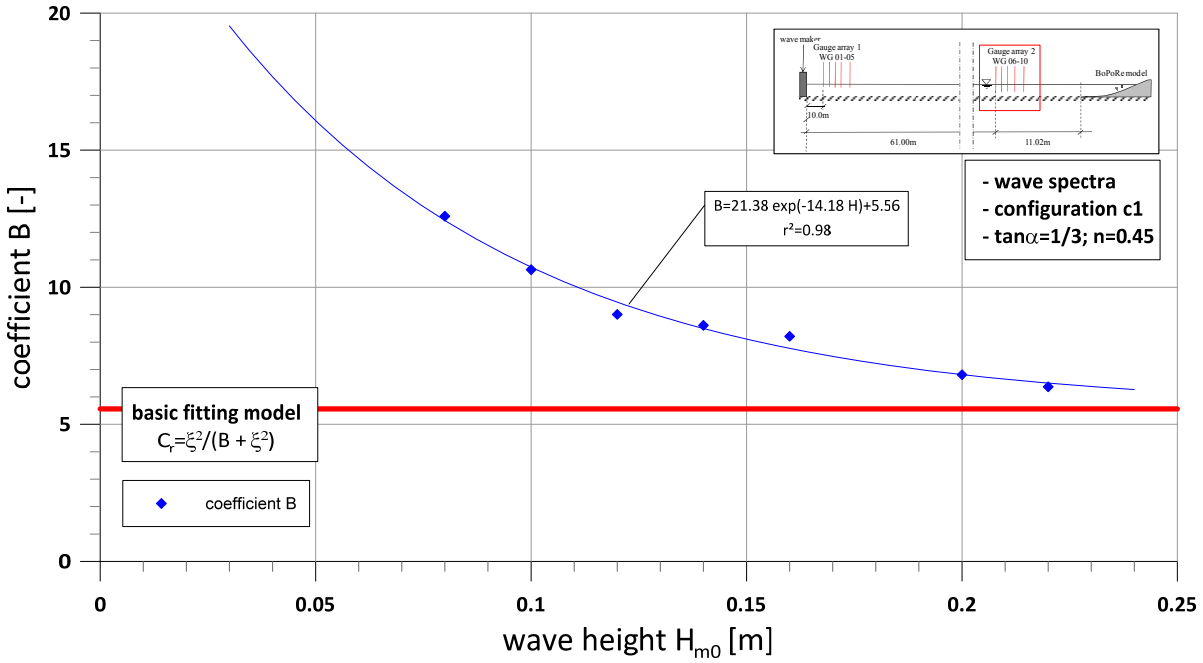

Fig. 5.5: Coefficient B as a function of wave height H_{m0} for configuration c1 for wave spectra (slope steepness 1:3)

The following equation was found for configuration c1 with a slope steepness of 1:3 and a porosity of 45% providing a very good fitting to the obtained data:

$$B = 21.38 \cdot \exp\left(-14.18 \cdot H_{m0}\right) + 5.56 \tag{5.6}$$

$$r^2 = 0.98$$

As afore mentioned, it has to be underlined that scale effects lead to a larger energy dissipation and less wave reflection for configuration c1 compared to the GWK-tests (also see section 4.1). Consequently, particular caution is recommended when using eq. (5.6) which, together with eq. (5.4), describes the additional effect of the wave height on the reflection coefficient.

5.1.2 Effect of the revetment slope steepness

After the analysis of the effect of porosity on wave reflection by considering configuration c1 with n = 45 % and configuration c2 with n = 20 %, both with a slope steepness of 1:3, the effect of slope steepness tanα is analysed in this section. This is done by considering configuration c1 with tanα = 1/3 and configuration c3 with tanα = 1/6, both with a porosity of n = 45%. Fig. 5.6 shows the results for the reflection coefficient for different surf similarity parameters for configuration c1 and c3 tested with wave spectra.

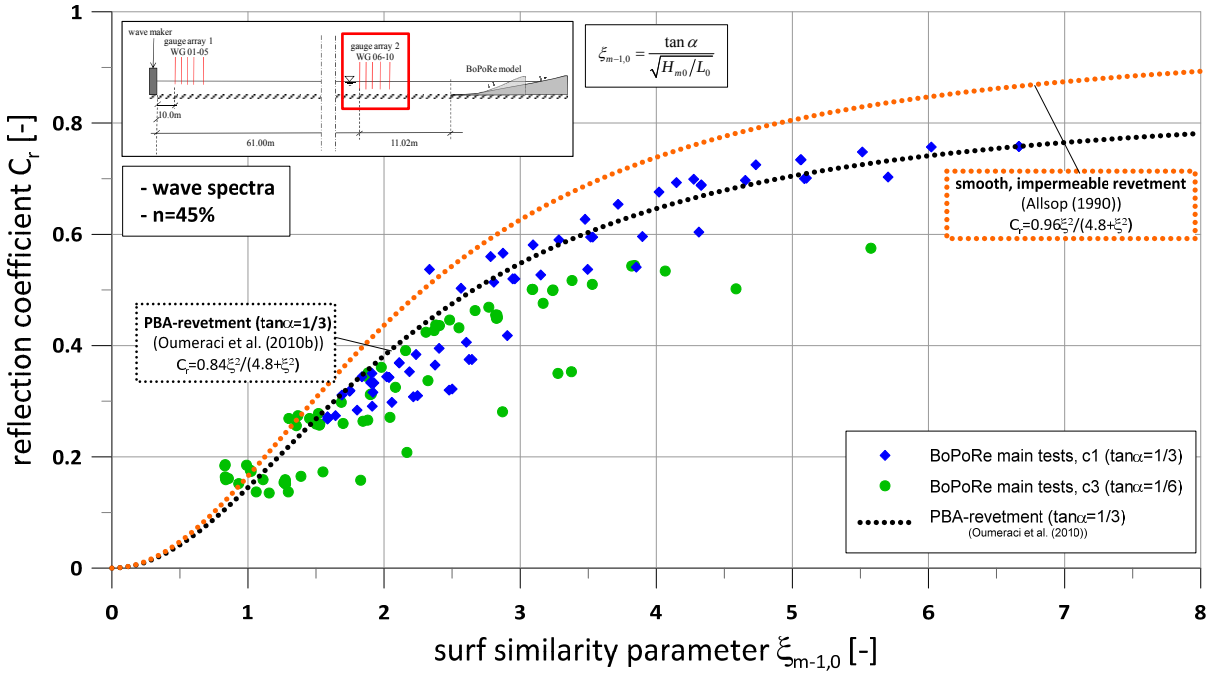

Fig. 5.6: Effect of the revetment porosity on reflection coefficient C_r as a function of surf similarity parameter $\xi_{m-1,0}$ for wave spectra (porosity n = 45%)

In Fig. 5.6 it seems that the values of the reflection coefficient in case of the 1:6 revetment are smaller compared to those of the 1:3 revetment especially for larger surf similarity parameter. This would be in contrast to the findings of the numerical study with regular waves by Foyer (2013), where it was stated that the effect of slope steepness on the reflection coefficient is adequatly considered in the surf similarity parameter. However, for the flatter configuration c3 tests with a very small wave height (H_{m0} = 0.04 m) were conducted (see Tab. 4.6), which might have led to the smaller reflection coefficients.

Consequently, like for the 1:3 revetment in Fig. 5.3, the same grouping approach of the wave height data with is also applied for the 1:6 slope in Fig. 5.7. The results show a similar shifting of the fitting curves depending on the wave height. For large wave heights, when the parameter B reaches values tending to 5.56 (impermeable and smooth revetment) in eq. (5.5), the data scattering gets larger as also indicated by the coefficients of determination getting lower.

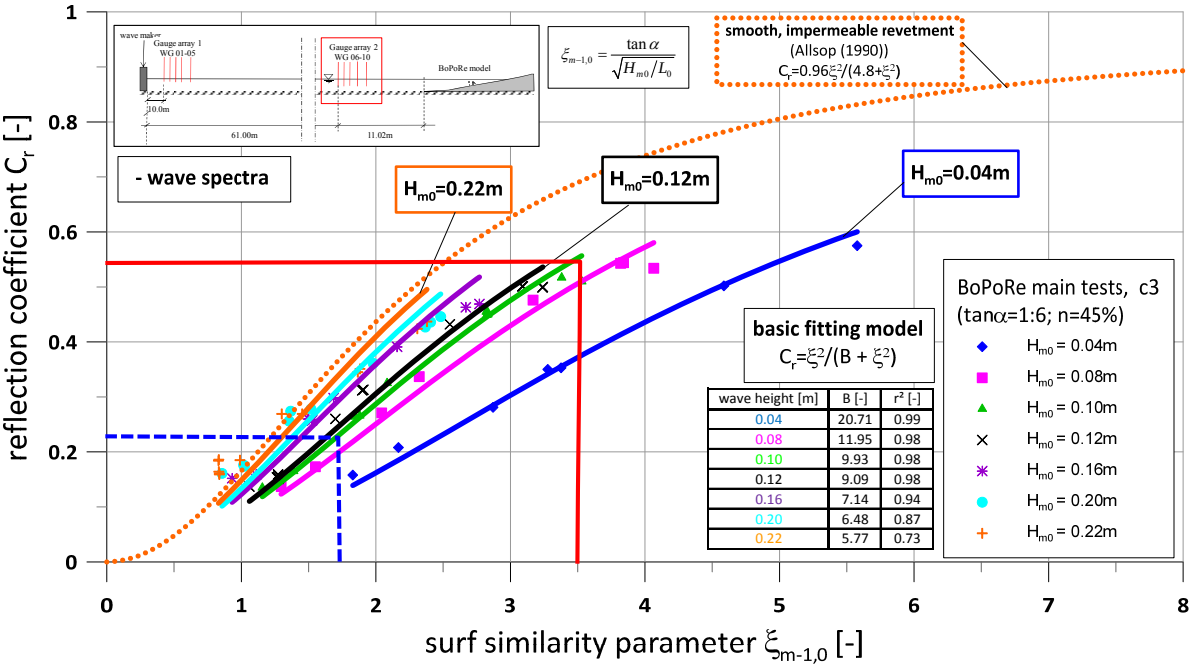

Fig. 5.7: Reflection coefficient C_r as a function of surf similarity parameter $\xi_{m-1,0}$ in groups of different wave heights for configuration c3 for wave spectra (porosity n = 45%)

The results of configuration c3 in Fig. 5.7 also confirm the findings of the previous section that a highly porous revetment behaves increasingly like an impermeable revetment with increasing wave heights. This again supports the assumption that with the smallest wave height (H_{m0} = 0.04 m) the smallest reflection coefficients are provided. For all other wave heights the obtained values for coefficient B for configuration c3 are just slightly smaller than those obtained for configuration c1, which might be caused by a saturation of the porous layers. However, for the same surf similarity parameter, indicated with the red line in Fig. 5.7, almost the same reflection coefficient is obtained as for configuration c1 in Fig. 5.3. This confirms the findings of Foyer (2013) that the effect of slope steepness on the reflection coefficient is adequatly considered in the surf similarity parameter. The same wave conditions like for configuration c1 (red line in Fig. 5.3), indicated with the blue dashed line in Fig. 5.7, would lead to a smaller reflection coefficient. However, as only two different slope steepnesses were considered in Fig. 5.6, its effect on the reflection coefficient has to be verified in further studies with numerical or physical model tests for a wider of the slope steepness values.

The same exponential function like in the previous section was used which tends against a value of 5.56 for large wave heights (see eq. (5.6)). The following equation was found for configuration c3 with a slope steepness of 1:6 and a porosity of 45%:

$$B = 33.29 \cdot \exp\left(-19.88 \cdot H_{m0}\right) + 5.56 \tag{5.7}$$

$$r^2 = 0.99$$

Also for configuration c3 it has to be pointed out that the same scale effects as for configuration c1 with the steeper slope occur and lead to a larger energy dissipation and less reflection for compared to the GWK-tests.

5.1.3 Prediction formula for reflection coefficient C_r

In sections 5.1.1 and 5.1.2 eq. (5.6) and (5.7) were derived for the parameter B based on the modified model of Seelig & Ahrens (1981) (see eq. (5.4)) which provide a very good fitting of the data for both slopes 1:3 and 1:6. Thus, an equation for parameter B can be generally defined as:

$$B = a_{refl} \cdot \exp\left(-b_{refl} \cdot H_{m0}\right) + 5.56 \tag{5.8}$$

For both highly porous revetment configurations c1 and c3 and the GWK-tests, parameter B in eq. (5.8) tends to smaller values for larger wave heights. This leads to a horizontally shifting of the obtained fitting curves based on eq. (5.4) depending on the wave height. This means that the highly porous revetments behave increasingly like an impermeable revetment with increasing wave heights.

For configuration c2 with a porosity of n = 20% no significant differences for parameter B were found depending on the investigated wave heights. It was shown in Fig. 5.1 that configuration c2 almost behaves like an impermeable revetment. Consequently, this means for the prediction model in eq. (5.8) that the parameter a_{refl} is almost zero and the parameter B tends to 5.56.

Coefficients a_{refl} and b_{refl} in eq. (5.8) which are obtained for all tested revetment configurations are given in Tab. 5.1 together with the coefficients of determination. The derived parameter a_{refl} and b_{refl} for configuration c2 and the down-scaled results of Oumeraci et al. (2010b) are also included.

Tab. 5.1: Coefficients a_{refl} and b_{refl} for all revetment configurations

configuration	tanα [-]	porosity [%]	a_{refl} [-]	b_{refl} [1/m]	r^2 [-]
c1	1/3	45	21.38	14.38	0.97
c2	1/3	20	0	-	-
c3	1/6	45	33.29	19.88	0.99
GWK-tests (Oumeraci et al. (2010b))	1/3	40	30.25	34.00	0.98

In the comparison of the small-scale model data (configuration c1) with the GWK-data (also see Fig. 5.3 and Fig. 5.4), larger values for coefficient B in the small-scale model than in the GWK-model are obtained for the same wave height. This results in a larger energy dissipation and less reflected energy for the same wave conditions. This was also seen for configuration c3 with the flatter slope which also provides significantly larger values for parameter B compared to the GWK-tests. The differences for the parameters a_{refl} and b_{refl} in Tab. 5.1 between the down-scaled GWK-tests and the small-scale tests may have the following reasons:

- Scale effects due to the used distortion factor of 2 for the scaling of the revetment material (see section 4.2). This results in a different ratio between pore size and/or grain size and the incident waves leading to a higher dissipation for configurations c1 and c3.
- The slightly smaller values for configuration c3 compared to those of c1 might be explained by the longer residence time of the water on the flatter slope during wave run-up/run-down leading to a "saturation" of the porous structure and less dissipation of the incident waves.

To correct the differences between configuration c1 and the down-scaled GWK-data for the coefficient B, a correction factor $c_{corr,B}$ is introduced in eq. (5.9), which can be determined graphically in Fig. 5.9.

$$c_{corr,B} = \frac{B_{c1}}{B_{GWK}} \tag{5.9}$$

The correction factor $c_{corr,B}$ can be determined for wave heights larger than 0.08 m. For this wave height $c_{corr,B}$ becomes maximum which indicates maximum scale effects. For large wave heights scale effects become negligibly small and $c_{corr,B}$ tends against 1.0. For wave heights $H_{m0} < 0.08$ m further research is necessary.

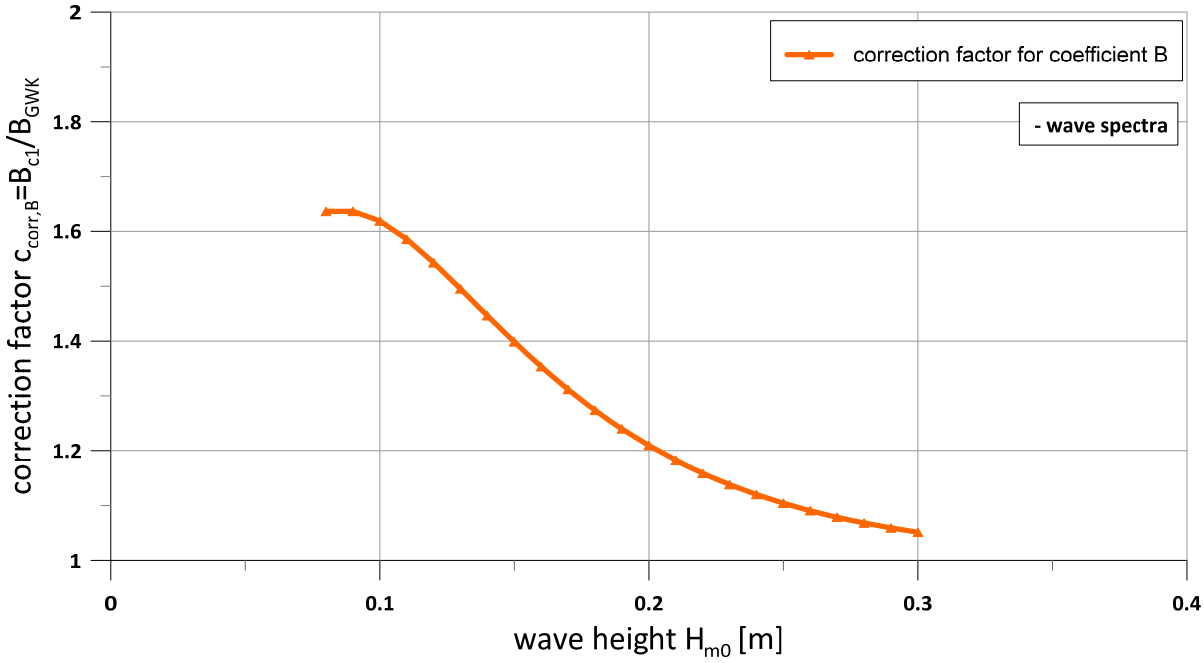

Fig. 5.8: Correction factor for the differences in coefficient B between configuration c1 and the down-scaled GWK data

The calculated values of the reflection coefficient using the modified model of Seelig & Ahrens (1981) in eq. (5.4) with parameter B determined according to eq. (5.8) and Tab. 5.1 are plotted against the experimental data obtained for all configurations c1, c2, c3 and the GWK-data tested with irregular waves, showing a relatively good agreement, particularly for slope for c1 and c2 with slope 1.3.

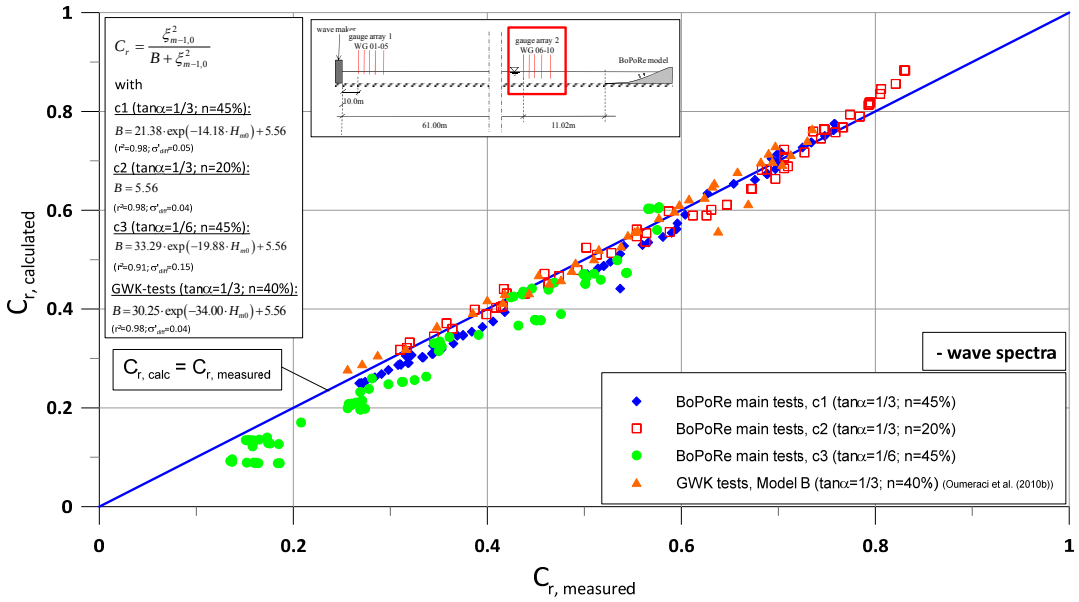

Fig. 5.9: Calculated reflection coefficient $C_{r,calc}$ as a function of measured reflection coefficient $C_{r,measured}$ for wave spectra (all configuration)

An increasing porosity leads to an additional effect of the incident wave height (incident wave energy) on the reflection coefficient. On the highly porous revetment the reflection coefficient tends to smaller values for larger wave heights indicating that the porous structure is less effective in reducing reflection, i.e. with increasing wave heights the revetment behaves increasingly like an impermeable revetment. The low porous configuration does not show this behaviour and behaves almost like an impermeable and smooth revetment for all surf similarity parameters.

The effect of slope steepness on the reflection coefficient C_r is less significant, which confirms the findings of Foyer (2013) that the effect of slope steepness on the reflection coefficient is adequatly considered in the surf similarity parameter. However, this needs to be verified in further studies for a wider variation of the slope steepness by using numerical or physical model tests.

The highly porous small-scale model (configurations c1 and c3) result in smaller reflection coefficients compared to the GWK-data for the same wave conditions (also see Fig. 5.3 and Fig. 5.4). This can be explained by a larger energy dissipation due to scale effects which might be also caused by introducing a distortion factor of 2 for scaling of the revetment material leading to a different relation between pore size and/or grain size and the incident waves. A correction factor was derived for the reflection coefficient obtained in the small-scale model.

5.2 Wave set-up

Wave set-down and wave set-up are induced by the shoaling process (radiation stress increase) and the breaking process (radiation stress decrease), respectively. The former causes the water level to decrease up to incipient breaking from where the water level then increases up to the shoreline. The water level which results from these processes is called mean water level (MWL). Therefore, MWL remains static for regular wave trains and is dynamic for irregular wave trains. Foyer (2013) well demonstrated how wave set-up affects most of the processes on and beneath the revetment and why it is physically more appropriate to define wave run-up and wave run-down with respect to MWL instead of SWL. The definition of wave set-up and set-down can be seen in Fig. 5.10.

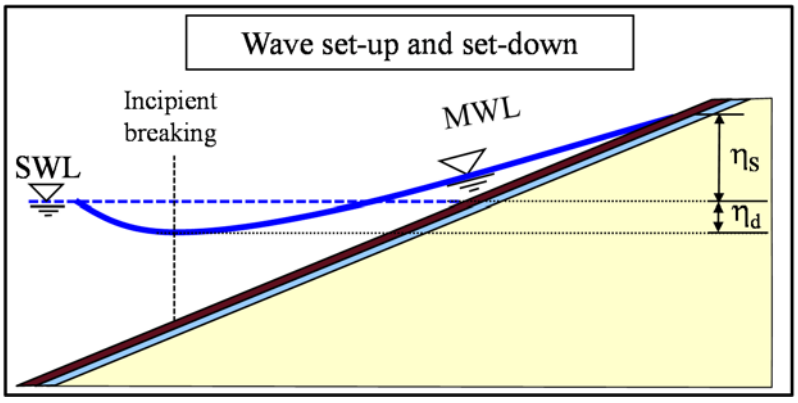

Fig. 5.10: Wave set-up and set-down (definition sketch)

Wave set-down is not regarded in this work, since wave set-up is much more important for the processes on the revetment. Moreover, the linear relation between wave set-up and set-down developed by Foyer (2013) can be used.

As mentioned in section 4.4, the time series of the run-up gauges (RUG) is used to analyse the wave set-up η_S. In the considered time frame of the tests the difference between the SWL and the MWL is determined as the wave set-up η_S. This is shown in Fig. 5.11.

In the preliminary tests of Liebisch et al. (2013b) no change in wave set-up was found for a changing revetment porosity and a significant effect of the slope steepness on the wave run-up was assessed. These statements have to be checked in the main tests. In the following, the relative wave set-up (η_S/L_0) is shown as a function of surf similarity parameters $\xi_{m\text{-}1,0}$ for all tested revetment configurations based on the same model which was successfully used by Alcérreca Huerta (2014) for the numerical data for regular waves. For irregular waves in this study this model is formulated as follows:

$$\frac{\eta_S}{L_0} = a_{su} \cdot \xi_{m-1,0}^{-b_{su}} \tag{5.10}$$

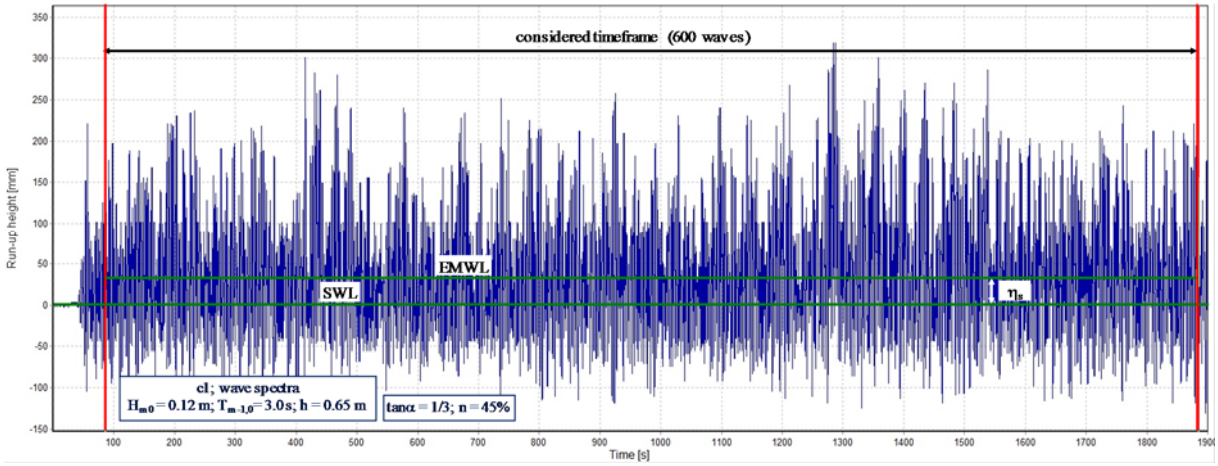

Fig. 5.11: Determination of the wave set-up (test 20130819 01)

5.2.1 Effect of the revetment porosity

Firstly, the relative wave set-up η_S/L_0 is analysed for configuration c1 and c2 both with a slope steepness of 1:3 (see also Tab. 4.2). The porosity changes from n = 45% (configuration c1) to n = 20% (configuration c2). The results for the relative wave set-up η_S/L_0 as a function of surf similarity parameter $\xi_{m-1,0}$ are shown in Fig. 5.12 together with the applied model in eq. (5.10). It is seen that the relative wave set-up is slightly smaller for configuration c1 with a higher porosity which might be explained by the larger energy dissipation compared to configuration c2 with a lower porosity.

The difference between the results of the two tested configurations becomes larger for smaller $\xi_{m-1,0}$ and almost zero for very large $\xi_{m-1,0}$. This might be explained by a smaller dissipation on both revetments for larger surf similarity parameters (also see section 6.2). For smaller $\xi_{m-1,0}$ a larger dissipation on the highly porous configuration c1 occurs which means that the effect of porosity on the wave set-up increases for smaller surf similarity parameters.

The derived fitting functions show a high determination coefficient:

Configuration c1 (n = 45%): $$\eta_S / L_0 = 0.063 \cdot \xi_{m-1,0}^{-2.32} \tag{5.11}$$

Configuration c2 (n = 20%): $$\eta_S / L_0 = 0.071 \cdot \xi_{m-1,0}^{-2.18} \tag{5.12}$$

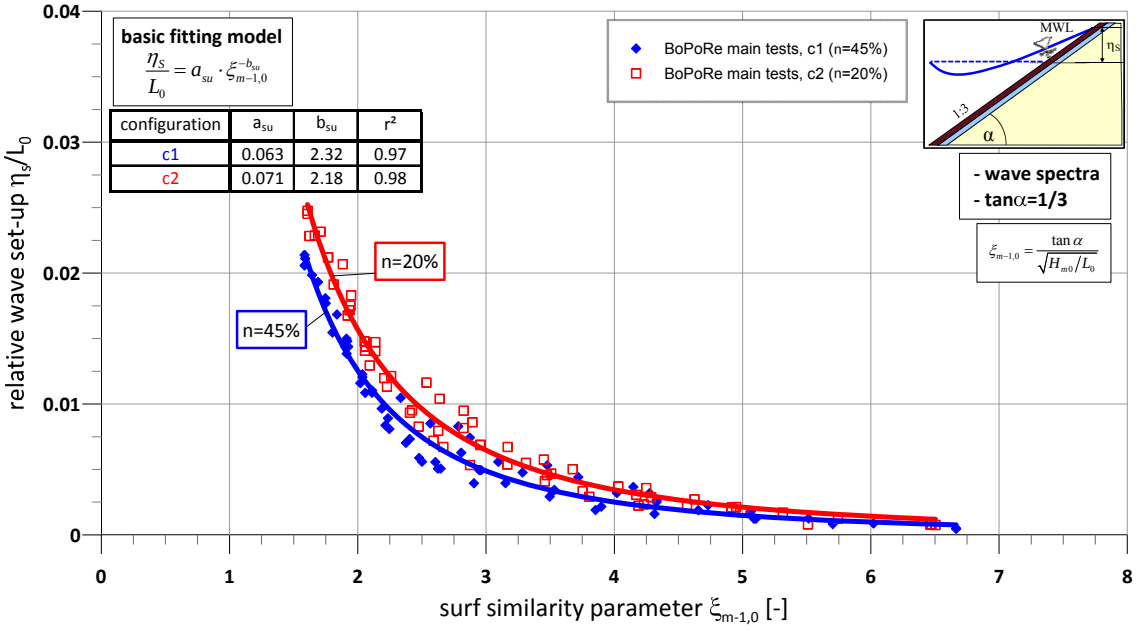

Fig. 5.12: Effect of the revetment porosity on relative wave set-up η_S/L_0 as a function of surf similarity parameter $\xi_{m-1,0}$ for wave spectra (slope steepness 1:3)

5.2.2 Effect of the revetment slope steepness

After the analysis of the effect of the revetment porosity on the relative wave set-up by considering revetments c1 (n = 45%) and c2 (n = 20%) with the same slope 1:3, the effect of the slope steepness is analysed in this section for configurations c1 (tanα = 1/3) and c3 (tanα = 1/6) with the same porosity (n = 45%). Using eq. (5.10) to fit the data of the irregular wave tests, the results are shown in Fig. 5.13.

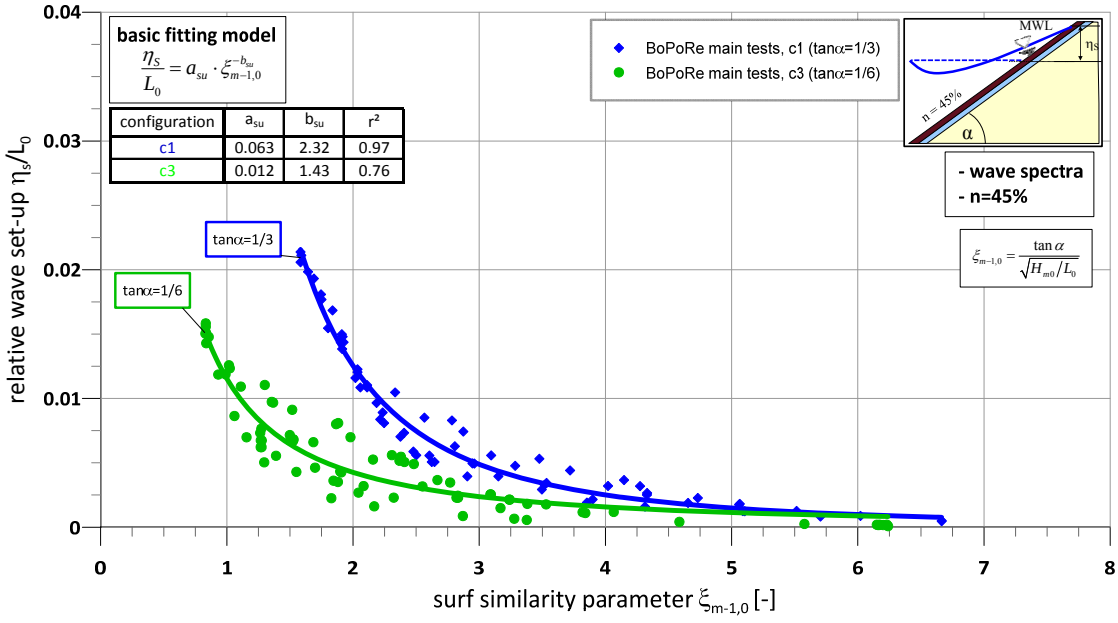

Fig. 5.13: Effect of slope steepness on relative wave set-up η_S/L_0 as a function of surf similarity parameter $\xi_{m-1,0}$ for wave spectra (porosity n = 45%)

As already found by Liebisch et al. (2013b) and Foyer (2013) and shown in Fig. 5.13, the slope steepness of the revetment strongly affects the wave set-up. Configuration c3 with slope 1:6 provides smaller relative wave set-up values compared to configuration c1 with slope 1:3. This may be explained by the shifting of the $\xi_{m\text{-}1,0}$-values which become smaller for flatter slopes for the same incident wave conditions. Consequently, smaller values of the relative wave set-up on flatter slopes are obtained for the same surf similarity parameter. Furthermore, a larger scatter occurs for the flatter revetment which was also observed in Liebisch et al. (2013b). This can be explained by the longer residence time of wave run-up and run-down on the flatter slope. For the fitting function based on eq. (5.10) this means that the coefficient a_{su} becomes significantly smaller for configuration c3 (a_{su} = 0.012) compared to configuration c1 (a_{su} = 0.012), which causes the afore mentioned shifting of the fitting curve in the direction of smaller $\xi_{m\text{-}1,0}$-values.

The following prediction formula was found for configuration c3:

Configuration c3 (tanα = 1/6; n = 45%):

$$\eta_S / L_0 = 0.012 \cdot \xi_{m-1,0}^{-1.43} \tag{5.13}$$

For configuration c1 (tanα = 1/6; n = 45%) see eq. (5.11).

5.2.3 Prediction formula for relative wave set-up η_S/L_0

It was shown in the previous sections, that the effect of the slope steepness on relative wave set-up is much more important than that of the revetment porosity when plotted against surf similarity parameter $\xi_{m\text{-}1,0}$ and that a good fitting was achieved using the model in eq. (5.10), especially for slope 1:3 (see Fig. 5.12).

The coefficients which were determined using eq. (5.10) for all revetment configurations tested with irregular waves are summarized in Tab. 5.2, together with the determination coefficient and the coefficient of variation.

Tab. 5.2: Coefficients a_{su} and b_{su} in eq. (5.10) for all tested revetment configurations

$\frac{\eta_S}{L_0} = a_{su} \cdot \xi_{m-1,0}^{-b_{su}}$	tanα [-]	porosity [%]	a_{su} [-]	b_{su} [-]	r^2 [-]	σ'_{diff} [-]
configuration c1	1/3	45	0.063	2.32	0.97	0.123
configuration c2	1/3	20	0.071	2.18	0.98	0.108
configuration c3	1/6	45	0.012	1.43	0.76	0.302

A smaller coefficient a_{su} in eq. (5.10) results in a shifting of the fitting curve in the direction of smaller $\xi_{m\text{-}1,0}$-values, which was seen for the flatter slope of configuration c3 (see Fig. 5.13). The coefficient b_{su} affects the steepness of the curve.

It is seen that the relative wave set-up is slightly smaller for configuration c1 with a higher porosity which might be explained by the larger energy dissipation compared to configuration c2 with a lower porosity. The difference between the results of the two tested configurations becomes larger for smaller $\xi_{m-1,0}$ and almost zero for very large $\xi_{m-1,0}$. This might be explained by a smaller dissipation on both revetments for larger surf similarity parameters (see also section 6.2). For smaller $\xi_{m-1,0}$ a larger dissipation on the highly porous configuration c1 occurs which means that the effect of porosity on the wave set-up increases for smaller surf similarity parameters.

- a_{su} depends on both revetment slope steepness tanα and revetment porosity n: $a_{su} = a_{su}$ (tanα, n)
- b_{su} depends primarily on revetment slope steepness and only slightly on porosity: $b_{su} = b_{su}$ (tanα)

The effect of the slope steepness on relative wave set-up η_S/L_0 versus surf similarity parameter $\xi_{m-1,0}$ is much more important than the effect of the revetment porosity. This effect becomes larger for smaller $\xi_{m-1,0}$ and almost zero for large $\xi_{m-1,0}$, which might be explained by a larger dissipation in the range of impact loads for the highly porous revetment.

5.3 Wave run-up and run-down

The maximum water elevation above still water level (SWL) to the point where the up rushed water starts to run down the slope again is described by the wave run-up height (see Fig. 5.14), which is a key parameter to determine the crest height of dikes and embankments. The wave run-up height R_u is the highest point of the swash zone, which is bounded at the bottom by the run-down height R_d. The latter is the lowest point under SWL reached by the down rushing water just before the next wave breaks on the slope (see Fig. 5.14). The following incident waves are affected by the wave run-down significantly.

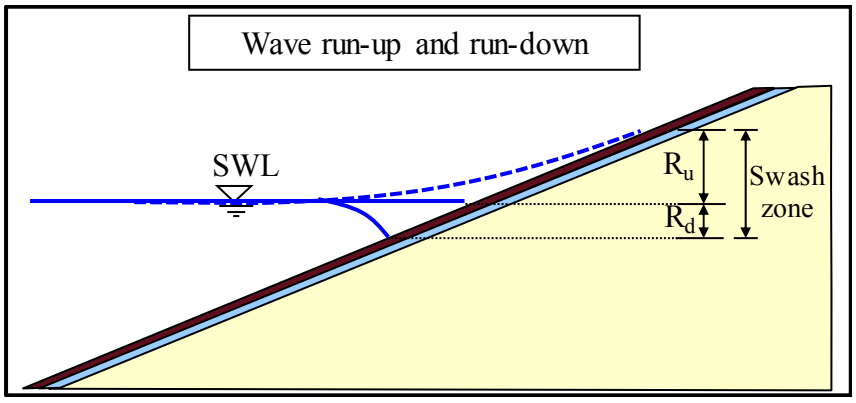

Fig. 5.14: Wave run-up and run-down related to SWL (definition sketch)

The common design formulae (e.g. EurOtop (2007)) for the wave run-up and run-down implicitly include the wave set-up, even though the latter and the former processes are

characterized by significantly different time scales. Consequently, it is more appropriate to consider the wave run-up and run-down and the wave set-up separately, which was also successfully done in the preliminary tests in Liebisch et al. (2013b). However, the wave run-up and the wave run-down related to SWL is first investigated in section 5.3.1 to ensure a direct comparison to the results of previous studies. In section 5.3.2, the wave run-up and run-down is considered again, but related to the external mean water level (EMWL), i.e. without the wave set-up.

In Fig. 5.15 a time series of the wave run-up is shown exemplarily for a regular wave test, which illustrates the run-up height R_u and the run-down height R_d related to SWL as well as both values $R_{u,EMWL}$ and $R_{d,EMWL}$ related to EMWL. For irregular wave tests the wave run-up height $R_{u2\%}$ and the wave run-down height $R_{d2\%}$ which are exceeded by 2% of the respective R_u and R_d-values are determined and analysed.

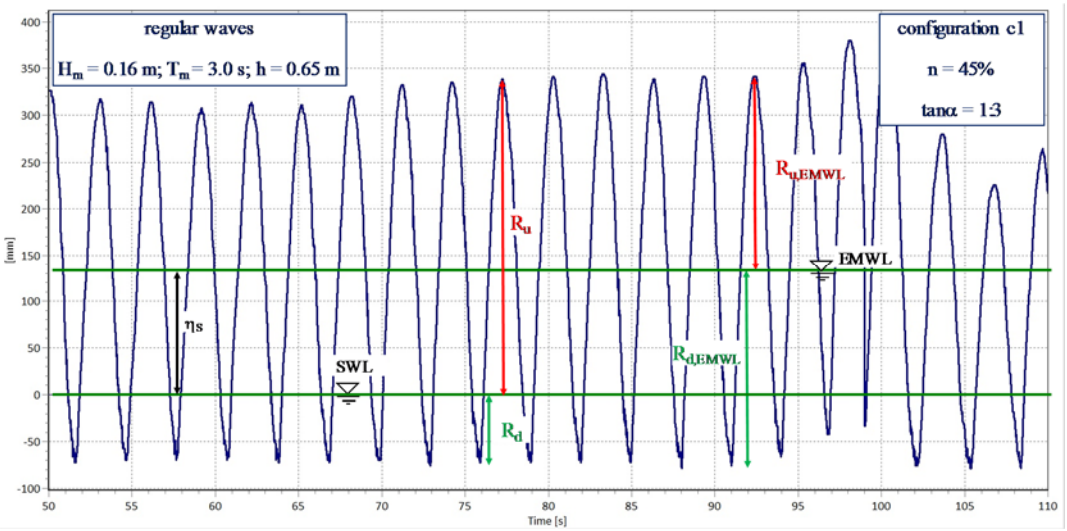

Fig. 5.15: Time series for wave run-up and run-down (configuration c1; test 20130815 08)

For the investigations of the wave run-up and run-down in the preliminary tests (Liebisch et al. (2013b)) the tanh-model proposed by Schüttrumpf (2001) was successfully used in the analysis. For the data fitting in this study this model is applied again, because the generated continuous function was found to be more appropriate compared to current design formulae (e.g. EurOtop (2007)).

Model proposed by Schüttrumpf (2001) for wave run-up:

$$\frac{R_{u2\%}}{H_{m0}} = a_{ru} \cdot \tanh\left(b_{ru} \cdot \xi_{m-1,0}\right) \tag{5.14}$$

For smooth and impermeable revetments Schüttrumpf (2001) obtained the following values for the coefficients a_{ru} and b_{ru} with implicit consideration of the wave set-up:

For wave spectra: $a_{ru} = 3.00$ $b_{ru} = 0.65$

Model proposed by Schüttrumpf (2001) for wave run-down:

$$\frac{R_{d2\%}}{H_{m0}} = a_{rd} \cdot \left(1 + \tanh\left(\xi_{m-1,0} - b_{rd}\right)\right) \tag{5.15}$$

With a_{rd} = -0.7 and b_{rd} = 2.1 for a smooth impermeable revetment and wave spectra (derived in Schüttrumpf (2001) with implicit consideration of the wave set-up).

5.3.1 Wave run-up and run-down related to SWL

5.3.1.1 Wave run-up related to SWL

a) Effect of the revetment porosity

Firstly, the relative wave run-up height $R_{u2\%}/H_{m0}$ is analysed for configurations c1 and c2 with different porosities for the same slope steepness 1:3. The porosity changes from n = 45 % (configuration c1) to n = 20 % (configuration c2). Fig. 5.16 shows the results for the relative wave run-up height as a function of the surf similarity parameters for configurations c1 and c2 tested with wave spectra and the tanh-model (eq. (5.14)) applied for the data. Furthermore, the model proposed by Schüttrumpf (2001) for a smooth and impermeable revetment and the model proposed by Oumeraci et al. (2010b) for a bonded porous revetment are also shown for comparison.

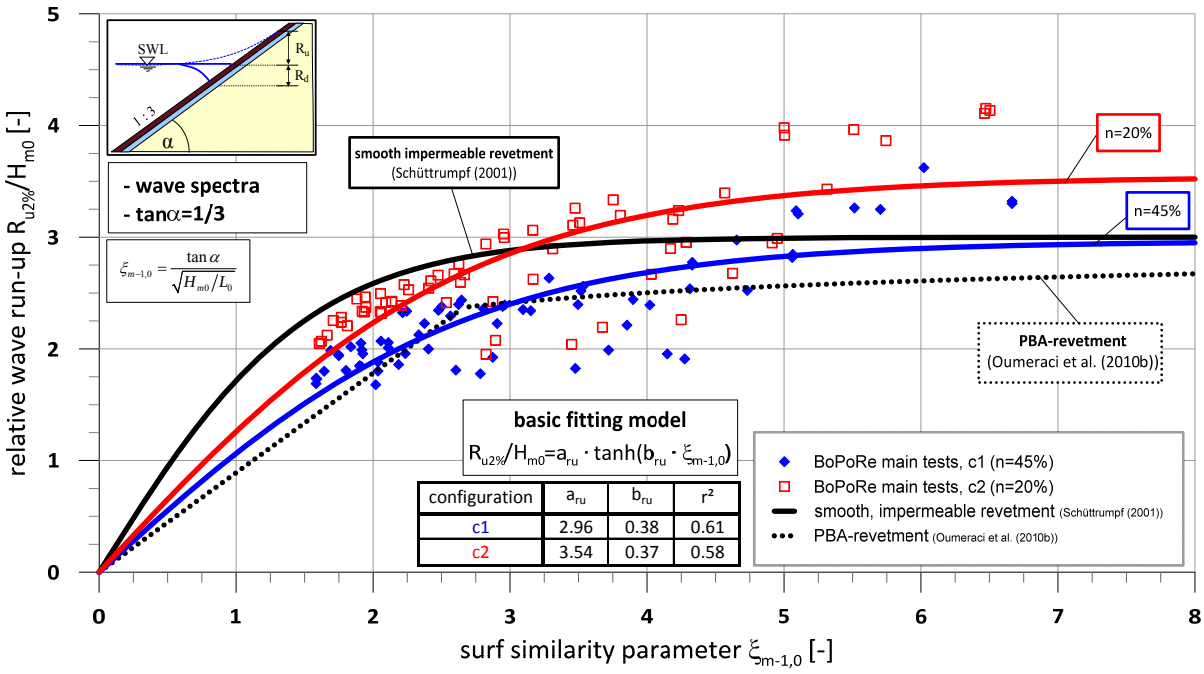

Fig. 5.16: Effect of porosity on the relative wave run-up height $R_{u2\%}/H_{m0}$ for configurations c1 and c2 for wave spectra (slope steepness 1:3)

Fig. 5.16 shows that revetment configuration c1 with the higher porosity (n = 45%) provides as expected smaller relative run-up heights compared to configuration c2 with the smaller porosity (n = 20%). This is expected due to the larger energy dissipation in the highly porous revetment.

Despite the large scatter of the data, the results for configuration c1 show a relatively better agreement with the GWK-tests (dashed curve) of Oumeraci et al. (2010b) for a PBA-revetment than those for the less porous revetment c2. Due to the large scatter of the data for both configurations c1 & c2 and possibly also because the wave run-up height is related to SWL, the comparison with the model by Schüttrumpf (2001) is not satisfactory. Consequently, the wave run-up heights should be analysed like in the preliminary tests, i.e. separated from the wave set-up (see section 5.3.2). The following equations were found for the wave run-up related to SWL:

Configuration c1 (n = 45%):
$$\frac{R_{u2\%}}{H_{m0}} = 2.96 \cdot \tanh\left(0.38 \cdot \xi_{m-1,0}\right) \tag{5.16}$$

Configuration c2 (n = 20%):
$$\frac{R_{u2\%}}{H_{m0}} = 3.54 \cdot \tanh\left(0.37 \cdot \xi_{m-1,0}\right) \tag{5.17}$$

The results of the main tests of configuration c1 (n = 45%) are compared in Fig. 5.17 with the results from GWK-tests (n = 40%) by Oumeraci et al. (2010b) and the data set of the preliminary tests (configuration p2r2: highly porous, very rough cover layer). Since all the test series in Fig. 5.17 are performed for revetments with the same slope 1:3 and nearly the same porosity, the comparative analysis in Fig. 5.17 might possibly allow to identify scale effects.

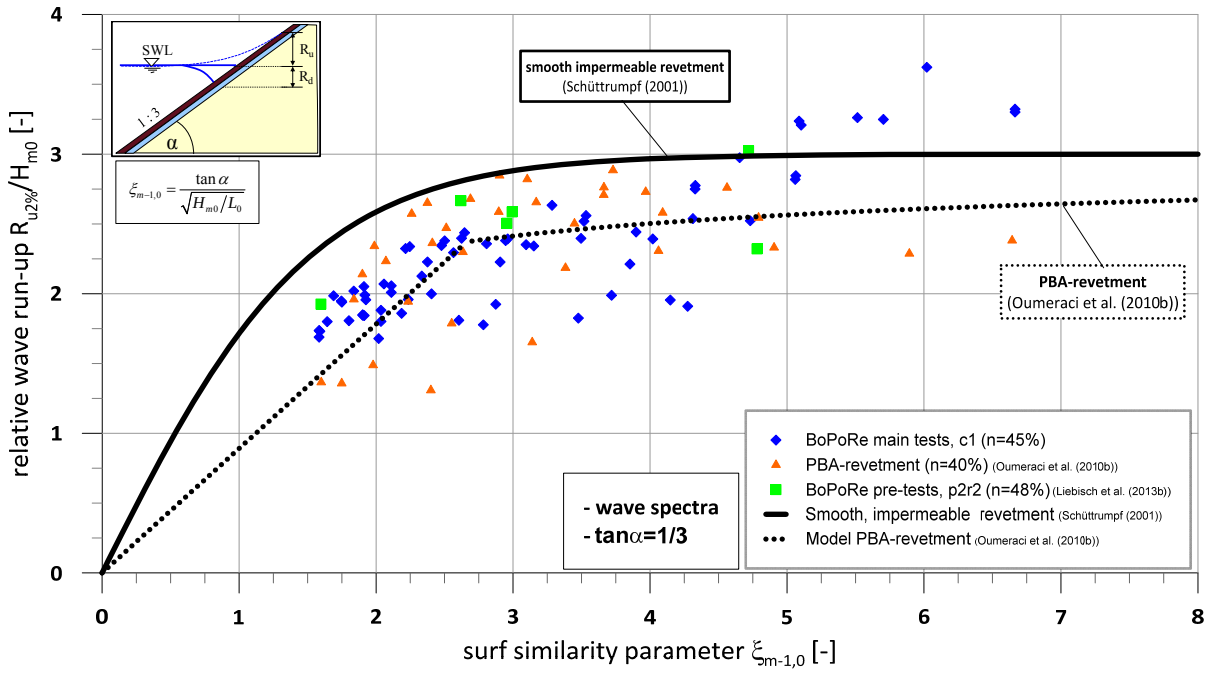

Fig. 5.17: Comparison of different data series of relative wave run-up height $R_{u2\%}/H_{m0}$ as a function of surf similarity parameter $\xi_{m-1,0}$ for wave spectra (slope steepness 1:3)

Fig. 5.17 shows that the data of the GWK-tests are in the same range as those of the BoPoRe main test data, that both depict a similar large scatter and that a comparison of both data sets is hardly possible beyond surf similarity parameters larger than 5, due to the lack of GWK-data for higher $\xi_{m-1,0}$. Nevertheless, for $\xi_{m-1,0} < 5$ the small-scale data set shows a relatively good agreement with those of GWK-tests and indicate that no significant scale effects occur for the

wave run-up related to SWL. The data set of the preliminary tests (Liebisch et al. (2013b)) also shows a relatively good agreement with the two other data sets.

b) Effect of the revetment slope steepness

Fig. 5.18 shows the results for the relative wave run-up related to SWL as a function of surf similarity parameter $\xi_{m-1,0}$ for configurations c1 and c3 tested with the same porosity (n = 45%) and different slopes 1:3 & 1:6 tested with wave spectra. Also shown is a comparison with the model proposed by Schüttrumpf (2001) for a smooth and impermeable revetment and the model proposed by Oumeraci et al. (2010b) for a bonded porous revetment.

The revetment configuration with the flatter slope 1:6 obviously provides higher relative wave run-up than that with the steeper slope 1:3. The following equation was found:

Configuration c3 (tanα = 1/6; n = 45%):

$$\frac{R_{u2\%}}{H_{m0}} = 4.51 \cdot \tanh\left(0.29 \cdot \xi_{m-1,0}\right) \tag{5.18}$$

For surf similarity parameters larger than 5 very high relative wave run-up heights occur similar to the other configurations (see Fig. 5.18).

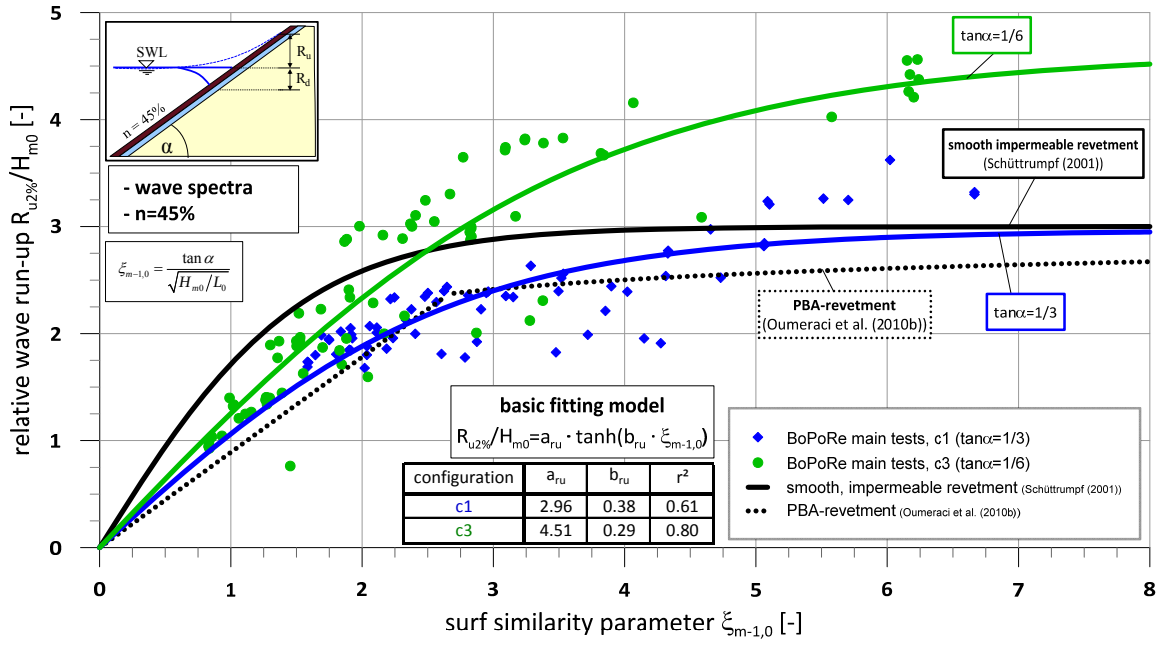

configuration	a_{ru}	b_{ru}	r^2
c1	2.96	0.38	0.61
c3	4.51	0.29	0.80

Fig. 5.18: Effect of slope steepness on the relative wave run-up height $R_{u2\%}/H_{m0}$ for configurations c1 and c3 for wave spectra (porosity n = 45%)

The result can be explained by the shifting of the data points due to the additional effect of the slope steepness already included in the surf similarity parameter. The values for the relative wave run-up heights for configuration c3 are shifted to smaller values of the surf similarity parameter, though a direct comparison of the data for the same revetment porosity with different

slope steepnesses is limited. Therefore, the relative wave run-up is shown as a function of wave steepness H_{m0}/L_0 in Fig. 5.19 for all tested configurations c1, c2 and c3 to enable a direct comparison of the relative effects of porosity and slope steepness on wave run-up.

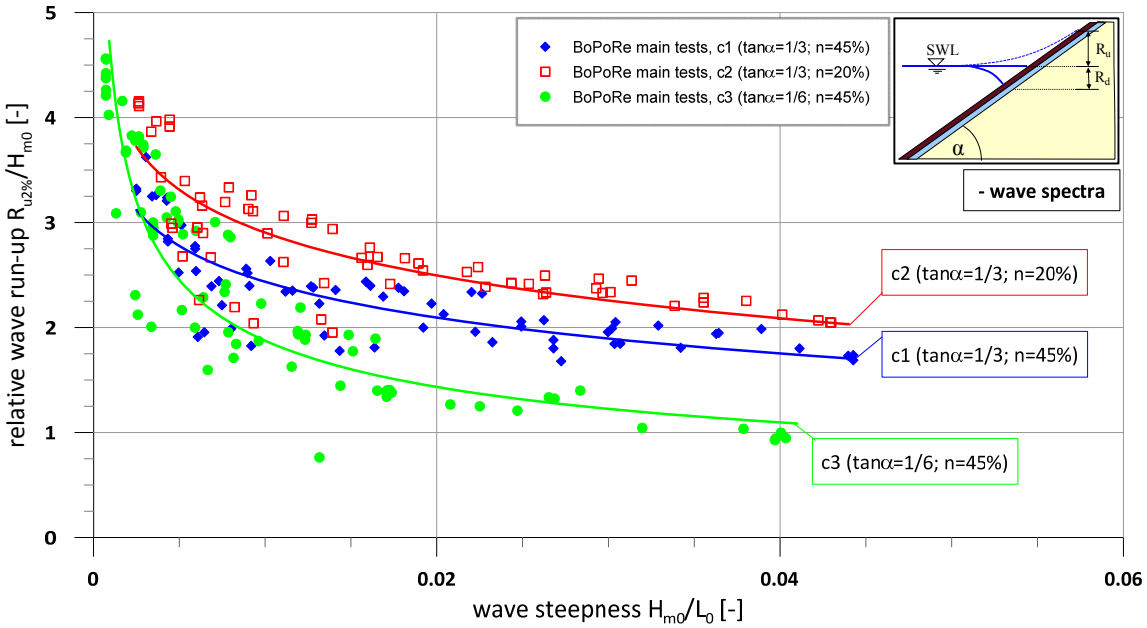

Fig. 5.19: Effect of slope steepness and porosity on relative wave run-up height $R_{u2\%}/H_{m0}$ as a function of wave steepness H_{m0}/L_0 for wave spectra

Fig. 5.19 illustrates the relative importance of the effect of the porosity and that of the slope steepness on the relative wave run-up much more clearly than by comparing Fig. 5.16 and Fig. 5.18. The effect of slope steepness is clearly more important than the effect of porosity, and configuration c3 with the flatter slope of 1:6 and the larger porosity provides the smallest values for the relative run-up heights.

5.3.1.2 Wave run-down related to SWL

a) Effect of the revetment porosity

The relative wave run-down height $R_{d2\%}/H_{m0}$ is first investigated for configurations c1 and c2 with the same slope steepness 1:3, but with different porosities (n = 45% for c1 and n = 20% for c2). Fig. 5.20 shows the results for the relative wave run-down as a function of the surf similarity parameter for configurations c1 and c2 tested with wave spectra, based on the tanh-model described by eq. (5.15).

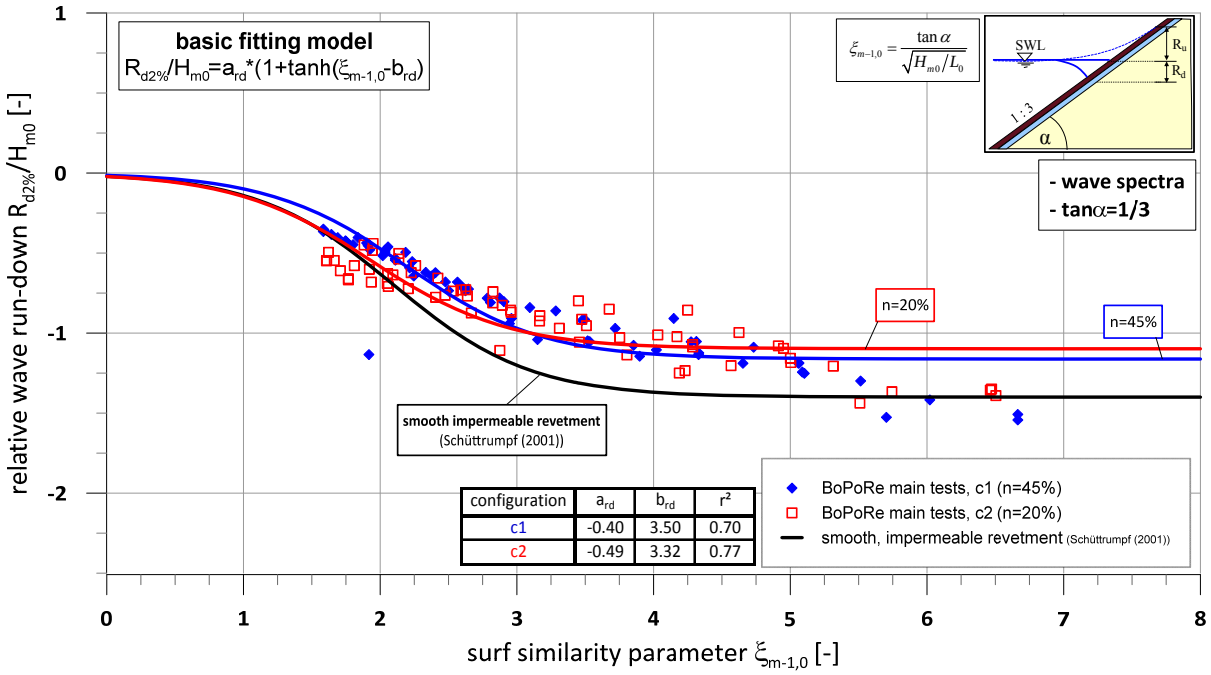

Fig. 5.20: Effect of revetment porosity on relative wave run- down height $R_{d2\%}/H_{m0}$ as a function of surf similarity parameter $\xi_{m-1,0}$ tested for wave spectra (slope steepness 1:3)

Fig. 5.20 shows that both configurations c1 and c2 provide similar values of relative wave run-down heights leading to almost the same fitting functions. The wave run-down is, as expected, smaller compared to the smooth impermeable revetment in Schüttrumpf (2001) for which the water remains on the slope for a longer time before the next incident wave breaks. However, for surf similarity parameters around 2.0 (plunging breakers), configuration c2 obviously provides larger relative run-up heights compared to configuration c1, which might be caused by a higher energy dissipation in the more porous revetment. The values for the wave run-down still continue to increase for $\xi_{m-1,0} > 5.0$ and are thus not properly captured with the applied model.

The following equations are found:

Configuration c1 (n = 45%): $$\frac{R_{d\,2\%}}{H_{m0}} = -0.58 \cdot \left(1 + \tanh\left(\xi_{m-1,0} - 2.19\right)\right) \tag{5.19}$$

Configuration c2 (n = 20%): $$\frac{R_{d\,2\%}}{H_{m0}} = -0.55 \cdot \left(1 + \tanh\left(\xi_{m-1,0} - 1.94\right)\right) \tag{5.20}$$

In Fig. 5.21 the data from the main tests of configuration c1 is compared with the data from GWK-tests (n = 40% and tanα = 1/3) of Oumeraci et al. (2010b) and those of the preliminary tests (configuration p2r2 with n = 48% and tanα = 1/3) of Liebisch et al. (2013b).

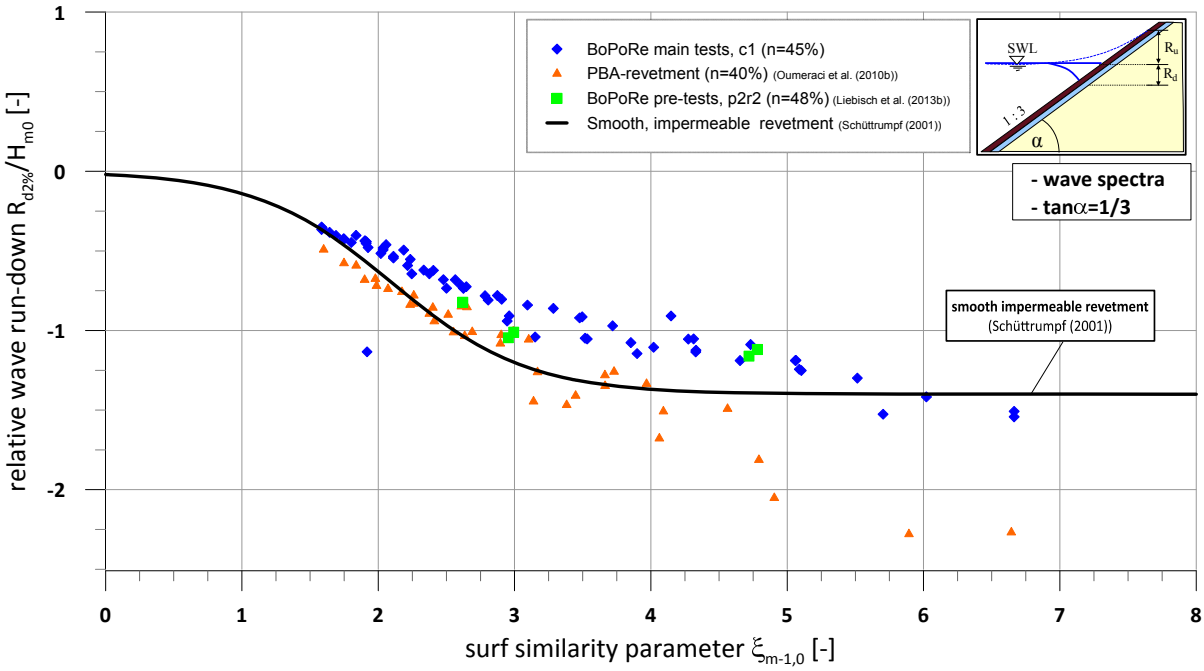

Fig. 5.21: Comparison of different data series of relative wave run-down height $R_{d2\%}/H_{m0}$ as a function of surf similarity parameter $\xi_{m-1,0}$ tested for wave spectra (slope steepness 1:3)

Fig. 5.21 shows that the run-down values of the GWK-tests are larger than those of the BoPoRe main tests. For surf similarity parameters smaller than 4 the fitting function of Schüttrumpf (2001) for smooth and impermeable revetments seems to provide a relatively good fitting also for porous revetments. For larger surf similarity parameters, however, the model proposed by Schüttrumpf (2001) largely underestimates the GWK-data whereas it generally overestimates the BoPoRe-data. The data set of the preliminary tests with wave spectra (Liebisch et al. (2013b)) for the highly porous and very rough revetment configuration are in the range of the main test data. In contrast to the results of the wave run-up in Fig. 5.17, the values from the GWK-tests are larger than those in the smaller scale model tests. This issue will be analysed in more detail in section 5.3.2 where the wave run-down is related to EMWL. It is shown in this section that an analysis of the wave run-down related to SWL is less appropriate than an analysis related to EMWL. Consequently, the effect of slope steepness on relative wave run-down related to SWL is not shown in this study, but can be found in Liebisch & Oumeraci (2014). The effect of slope steepness on wave run-down related to EMWL is shown in section 5.3.2.2.

5.3.2 Wave run-up and run-down related to EMWL

After the analyses of the wave set-up in section 5.2 and the wave run-up and wave run-down related to SWL in section 5.3.1, the wave run-up and run-down is analysed again in this section, but as related to the external mean water level (EMWL). For some tests, especially those with configuration c2 with the lower porosity, wave overtopping occurred. The values for relative wave run-up related to EMWL with significant overtopping are excluded from the analysis.

In contrast to the analysis in Section 5.3.1 using SWL as a reference level, the data for both wave run-up and run-down are analysed in the same graph and the tanh-model proposed by Schüttrumpf (2001) for smooth impermeable slopes is applied to fit the data for both wave run-up (eq. (5.21)) and run-down (eq. (5.22)):

Run-up:
$$\frac{R_{u2\%,EMWL}}{H_{m0}} = a_{ru} \cdot \tanh\left(b_{ru} \cdot \xi_{m-1,0}\right) \tag{5.21}$$

Run-down:
$$\frac{R_{d2\%,EMWL}}{H_{m0}} = a_{rd} \cdot \tanh\left(b_{rd} \cdot \xi_{m-1,0}\right) \tag{5.22}$$

5.3.2.1 Effect of the revetment porosity

The data from the irregular wave tests for relative wave run-up $R_{u2\%,EMWL}/H_{m0}$ and run down $R_{d2\%,EMWL}/H_{m0}$ related to the EMWL of configurations c1 and c2 with the same slope steepness (1:3) and different porosity (c1 with n = 45% and c2 with n = 20%) are plotted against surf similarity parameter $\xi_{m-1,0}$ in Fig. 5.22.

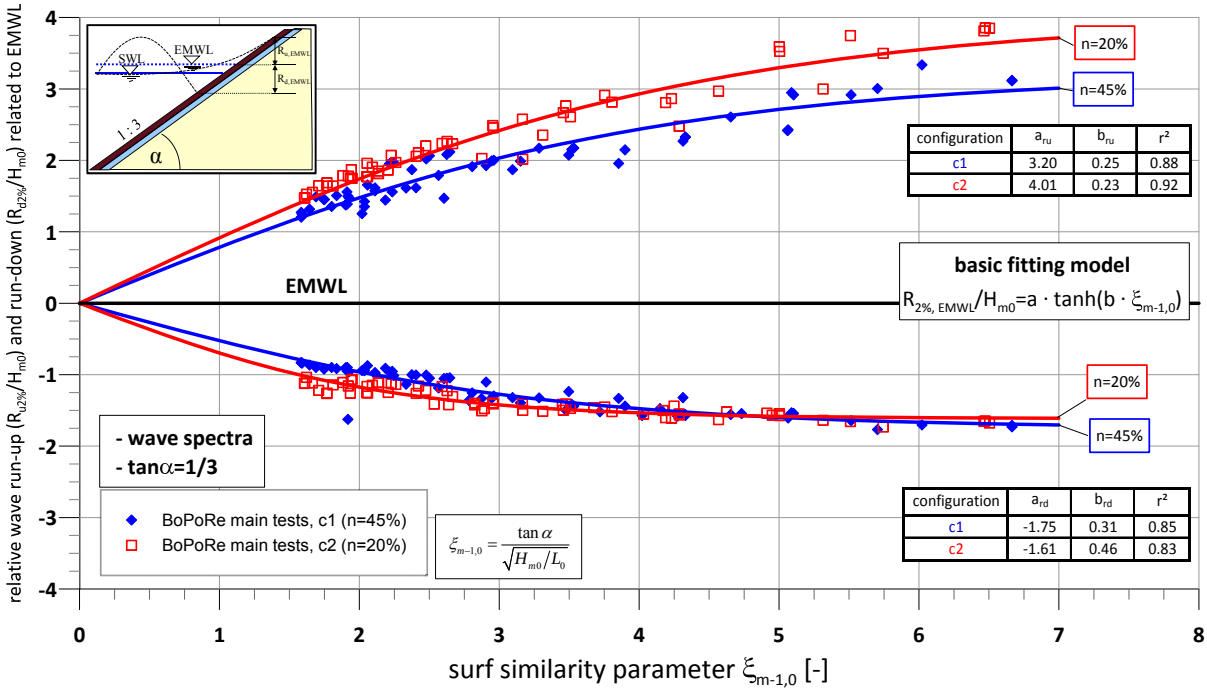

Fig. 5.22: Effect of porosity on relative wave run-up and run-down related to EMWL as a function of surf similarity parameter $\xi_{m-1,0}$ for wave spectra (slope steepness 1:3) using eq. (5.21) and eq. (5.22)

Generally, the more porous revetment provides smaller values for both relative wave run-up and run-down. The effect of the revetment porosity is more pronounced for wave run-up than for run-down, particularly for large $\xi_{m-1,0}$–values where this effect becomes negligible for relative run-down. Furthermore, for both configurations a larger scatter occurs for relative wave run-up than for relative wave run-down. The tanh-model also shows a good correlation for both

porous revetments. For relative run down $R_{d2\%;EMWL}/H_{m0}$ obviously both fitting functions tend against the same maximum value irrespective of the porosity. The following equations are obtained for relative wave run-up related to EMWL:

Configuration c1 (n = 45%): $$\frac{R_{u2\%,EMWL}}{H_{m0}} = 3.20 \cdot \tanh\left(0.25 \cdot \xi_{m-1,0}\right) \quad (5.23)$$

Configuration c2 (n = 20%): $$\frac{R_{u2\%,EMWL}}{H_{m0}} = 4.01 \cdot \tanh\left(0.23 \cdot \xi_{m-1,0}\right) \quad (5.24)$$

For the relative wave run-down related to EMWL the following equations are obtained:

Configuration c1 (n = 45%): $$\frac{R_{d2\%,EMWL}}{H_{m0}} = -1.75 \cdot \tanh\left(0.31 \cdot \xi_{m-1,0}\right) \quad (5.25)$$

Configuration c2 (n = 20%): $$\frac{R_{d2\%,EMWL}}{H_{m0}} = -1.61 \cdot \tanh\left(0.46 \cdot \xi_{m-1,0}\right) \quad (5.26)$$

5.3.2.2 Effect of the revetment slope steepness

In this section the relative wave run-up and run-down related to EMWL of configurations c1 and c3 with the same porosity (n = 45%) and different slope steepnesses 1:3 and 1:6 are analysed. The results are shown in Fig. 5.23.

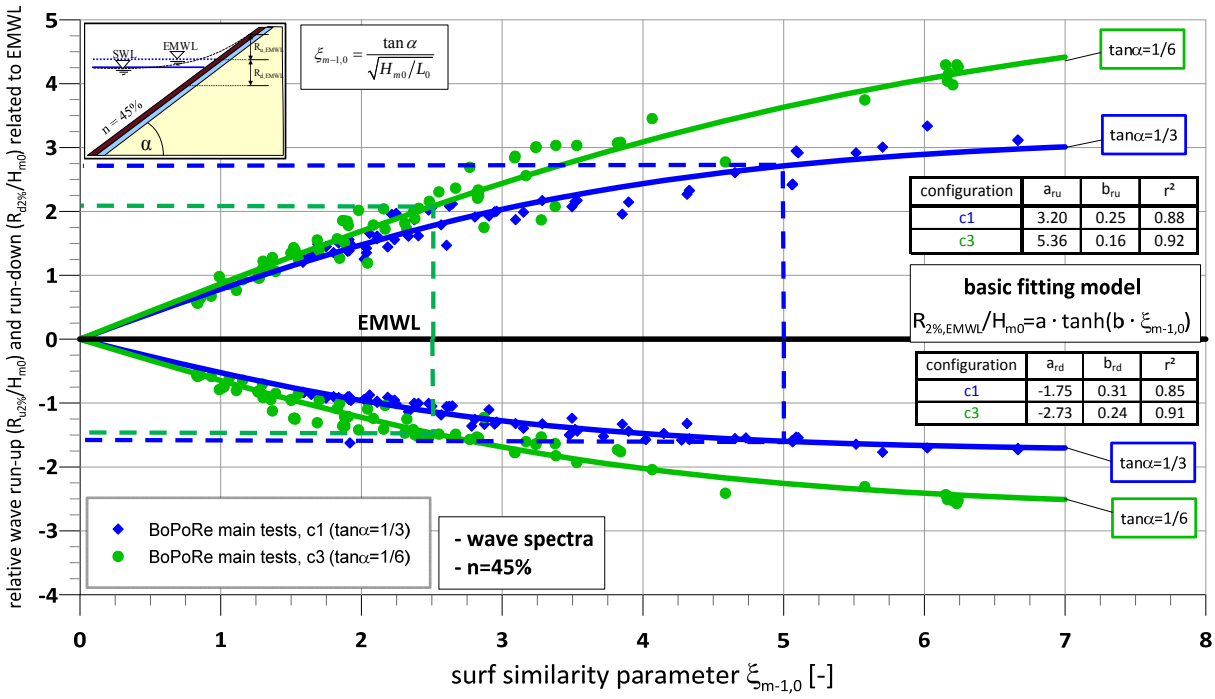

Fig. 5.23: Effect of slope steepness on relative wave run-up and run-down related to EMWL as a function of surf similarity parameter $\xi_{m-1,0}$ for wave spectra (porosity n = 45%) using eq. (5.21) and eq. (5.22)

The results shown in Fig. 5.23 are rather unexpected, because it seems that the flatter slope of configuration c3 provides larger wave run-up and run-down related to EMWL as configuration c1 with a slope 1:3. But this result can be explained by the slope steepness which is directly included in the surf similarity parameter resulting in a shifting of the results in x-direction for the same wave conditions. This is indicated in Fig. 5.23 with the dashed lines in blue for configuration c1 and in green for configuration c3. It is obvious that the flatter configuration c3 provides, as expected, the smaller relative wave run-up and run-down for the same wave conditions due to the resulting smaller surf similarity parameter. The effect of the slope steepness on relative wave run-up is more significant compared to the relative wave run-down. This was already shown in Foyer (2013) for regular waves. However, the two distinct curves for the slopes 1:3 and 1:6, respectively for wave run-up and run-down, rather indicate that the surf similarity parameter does not fully describe the effect of slope steepness on wave run-up und run-down.

The following equations were found for relative wave run-up and run-down related to EMWL for configuration c3:

Configuration c3 ($\tan\alpha = 1/6$; n = 45%):

$$\frac{R_{u\,2\%,EMWL}}{H_{m0}} = 5.36 \cdot \tanh\left(0.16 \cdot \xi_{m-1,0}\right) \tag{5.27}$$

$$\frac{R_{d\,2\%,EMWL}}{H_{m0}} = -2.73 \cdot \tanh\left(0.24 \cdot \xi_{m-1,0}\right) \tag{5.28}$$

The derived formulae for configuration c1 were already shown in eq. (5.23) and eq. (5.25).

5.3.3 Prediction formulae for relative wave run-up and run-down related to EMWL

As already shown in Liebisch et al. (2013b) and Foyer (2013) as well as in sections 5.3.2.1 and 5.3.2.2, the consideration of the wave run-up and run-down related to the EMWL instead of SWL is physically more appropriate. Moreover, for relative wave run-down no positive values are obtained. The tanh-model proposed by Schüttrumpf (2001) for wave run-up on impermeable slopes was used to fit the data of the bonded porous revetments and provided relatively good results.

The values of the coefficients a_{ru} and b_{ru} and a_{rd} and b_{rd} for the different revetment configurations based on eq. (5.21) for relative wave run-up related to EMWL and eq. (5.22) for relative wave run-down related to EMWL are given with the determination coefficient and the coefficient of variation in Tab. 5.3 and Tab. 5.4, respectively.

Tab. 5.3: Coefficients a_{ru} and b_{ru} in eq. (5.21) for all revetment configurations tested with irregular waves

$\frac{R_{u2\%,EMWL}}{H_{m0}} = a_{ru} \cdot \tanh\left(b_{ru} \cdot \xi_{m-1,0}\right)$	tanα [-]	porosity [%]	a_{ru} [-]	b_{ru} [-]	r^2 [-]	σ'_{diff} [-]
configuration c1	1/3	45	3.20	0.25	0.88	0.191
configuration c2	1/3	20	4.01	0.23	0.92	0.190
configuration c3	1/6	45	5.36	0.16	0.92	0.124

Tab. 5.4: Coefficients a_{rd} and b_{rd} in eq. (5.22) for all revetment configurations tested with irregular waves

$\frac{R_{d2\%,EMWL}}{H_{m0}} = a_{rd} \cdot \tanh\left(b_{rd} \cdot \xi_{m-1,0}\right)$	tanα [-]	porosity [%]	a_{rd} [-]	b_{rd} [-]	r^2 [-]	σ'_{diff} [-]
configuration c1	1/3	45	-1.75	0.31	0.85	0.093
configuration c2	1/3	20	-1.61	0.46	0.83	0.058
configuration c3	1/6	45	-2.73	0.24	0.91	0.128

A change of coefficients a_{ru} in eq. (5.21) and a_{rd} in eq. (5.22) would result in a change of the asymptotic value of the tanh-function since $R_{u2\%,EMWL}/H_{m0} = a_{ru}$ and $R_{d2\%,EMWL}/H_{m0} = a_{rd}$ for very large $\xi_{m-1,0}$. Coefficients b_{ru} in eq. (5.21) and b_{rd} in eq. (5.22) affect the steepness of the fitting curves. In Fig. 5.22 it can be seen that the relative wave run-up curves for two different porosities and the same slope steepness are significantly affected in their asymptotic value while the latter is not affected by the porosity for the relative wave run-down. When the slope steepness varies and the porosity remains the same, the asymptotic value and the steepness of both wave run-up and run-down curves change (see Fig. 5.23); i.e. the following implications can be drawn for coefficients a_{ru} and b_{ru} in eq. (5.21) and a_{rd} and b_{rd} in eq. (5.22):

- a_{ru} depends on both revetment slope steepness tanα and revetment porosity n: $a_{ru} = a_{ru}$ (tanα, n)
- b_{ru} depends primarily on revetment slope steepness and only slightly on porosity, so that it can assumed that: $b_{ru} = b_{ru}$ (tanα)
- a_{rd} depends on both slope steepness and porosity, but much more significantly on revetment slope steepness tanα: $a_{rd} = a_{rd}$ (tanα, n)
- b_{rd} depends on both revetment slope steepness tanα and revetment porosity $b_{rd} = b_{rd}$ (tanα, n)

As in Foyer (2013), Alcérreca Huerta (2014) and Liebisch et al. (2013b), the consideration of the wave run-up and run-down related to the EMWL provides physically more appropriate results than the common approach using SWL as a reference level.

A larger porosity leads to lower values of both relative wave run-up and run-down with a more significant effect of the porosity on wave run-up (reduction up to 20%). The tanh-model proposed by Schüttrumpf (2001) for smooth impermeable slope also performs relatively well for porous revetments.

The two distinct curves for the slopes 1:3 and 1:6, respectively for wave run-up and run-down, rather indicate that the surf similarity parameter does not fully describe the effect of slope steepness on wave run-up und run-down.

5.4 Summary and implications of key results

In this chapter the results of the processes taking place in front of and on the revetment were analysed, including wave reflection, wave set-up and wave run-up and run-down. The wave run-up and run-down heights were first analysed according to the common approach using SWL as a reference water level; i.e. both implicitly include the wave set-up. The analysis was then performed without including the wave set-up; i.e. with the EMWL as a reference level.

In section 5.1, it was shown that an increasing porosity leads to a larger effect of the incident wave height on the reflection coefficient. The highly porous revetment behaves increasingly like an impermeable revetment with increasing wave heights. The developed model based on the modified model of Seelig & Ahrens (1981), in which the parameter B depends on the wave height, performed well for all tested configurations. The effect of the slope steepness on the reflection coefficient C_r is less significant.

In section 5.2, the significant effect of the slope steepness on relative wave set up η_S/L_0 was clearly illustrated. The effect of the revetment porosity on relative wave set-up η_S/L_0 is less pronounced than that of the slope steepness. Empirical formulae were successfully developed.

In section 5.3, it was shown that due to the basically different time scales of the wave run-up/run-down and the wave set-up, the analysis of wave run-up/run-down related to EMWL as a reference water level is physically more appropriate than with the commonly used SWL. A larger porosity leads to lower values of both relative wave run-up and run-down with a more significant effect of the porosity on wave run-up (up to 20 % smaller values for revetment c1 with n = 45% compared to revetment c2 with n = 20%, both with the same slope 1:3). The effect of slope steepness, which also reduces wave run-up and run-down, is obviously not fully described by the surf similarity parameter. The tentative prediction models (tanh-models) also provided a much better fitting for the wave run-up/run-down related to EMWL.

Overall, the results of this chapter have contributed to an improved understanding of the processes on the revetments of different porosity and slope steepness. However, these results

have limitations, so that further research will be needed. The results suggest that there is a porosity threshold at which the effect of porosity on the reflection coefficient becomes negligibly small. For this purpose, a systematic parameter study with the validated numerical model available at LWI might be most appropriate to determine further influencing parameters and their relative effect on wave reflection, wave set-up and wave run-up and run-down. The derived model for the wave reflection which accounts for the additional effect of the wave height might also be applied on the extensive existing data sets which were already used in Zanuttigh & Van der Meer (1988) to verify the findings of this study. The effect of the slope steepness by keeping the revetment porosity constant has been investigated numerically by Alcérreca Huerta (2014). Further numerical simulations would be required to investigate the effect of porosity for different slope steepnesses for a wider range of the slope steepness.

6 Wave-induced pressures on the revetment

This chapter addresses the wave-induced pressures on the revetment. This includes the wave load classification, the analysis of the peak pressure, its location on the revetment and the pressure distribution on the revetment. The results of this chapter are based on the measurements of 11 pressure transducers (PT) on the revetment in PT-layer 1 (see Fig. 6.1, and for details Fig. 4.6, Fig. 4.8 and Fig. 4.9). For configurations c2 and c3 only 10 PTs are used to measure the wave-induced pressure on the revetment due to a damage of a PT in the tests with configuration c1.

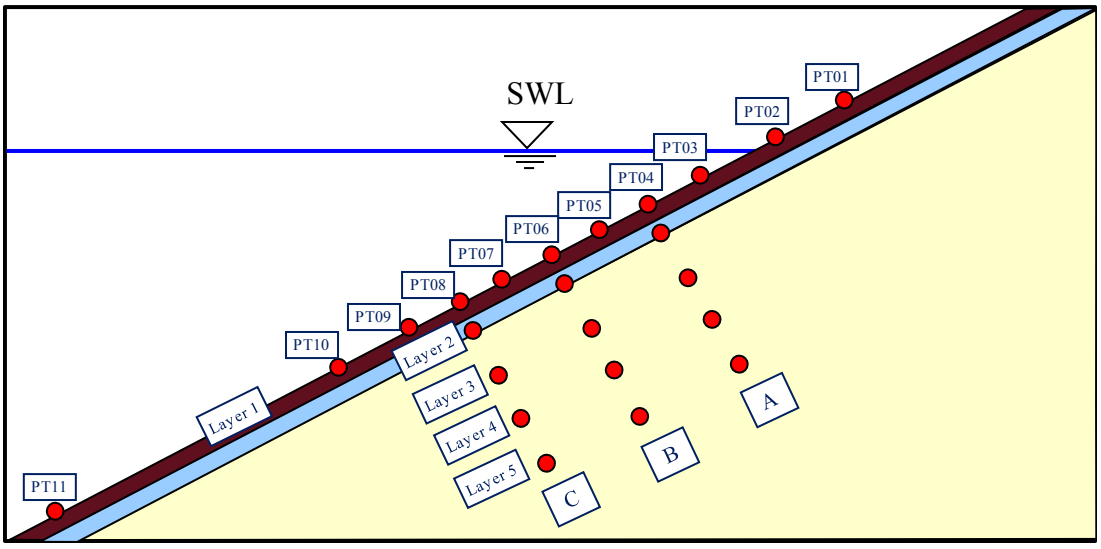

Fig. 6.1: Locations of pressure transducers PT01-11 in layer 1 for the analyses of the wave-induced pressure on the revetment

The wave-induced loads are first classified into impact and non-impact loads in section 6.1. In section 6.2 the peak pressures are analysed. For the development of a prediction model the peak pressures are divided in an impact and quasi-static component. The location of the peak pressure on the revetment is the objective of section 6.3. The spatial pressure distribution on the revetment is analysed in section 6.4.

6.1 Wave load classification and parameterization

All pressure transducers were set to zero at the beginning of all tests which means that the measured pressures were only induced by wave motion. At the pressure transducers under still water level (SWL) the hydrostatic pressure $p_0(x)$ results from the local water depth h(x) at SWL:

$$p_0(x) = \rho \cdot g \cdot h(x) \tag{6.1}$$

This leads to the reference pressure $p_0(x)$ for all PT on and beneath the revetment and in the sand core (Fig. 6.2).

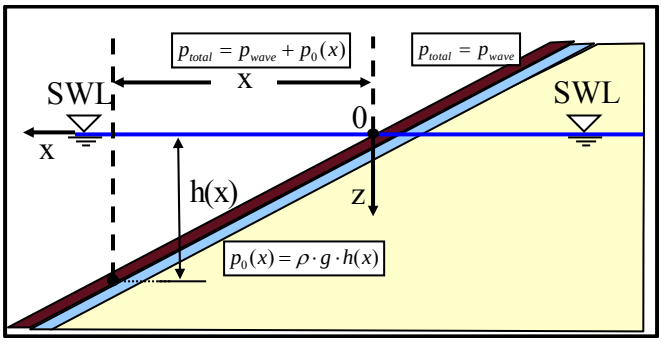

Fig. 6.2: Hydrostatic pressure $p_0(x)$ as a reference for wave-induced pressure p_{wave} (definition sketch)

6.1.1 Wave load classification

The different wave loads on the revetment were also investigated in the preliminary tests by Liebisch et al. (2013b) and compared to those given in Oumeraci et al. (2010b) for a highly porous PBA-revetment and in Alcérreca Huerta & Oumeraci (2012) for an almost impermeable block revetment (IPPB). It was shown that the loading cases slightly differ depending on the revetment roughness and porosity. However, in the preliminary tests by Liebisch et al. (2013b) these loading cases were shown only for regular waves, but not for irregular wave tests. The load classification is conducted in this section for the main tests with a focus on wave spectra tests for a direct comparison with the large-scale tests of Oumeraci et al. (2010b) and Alcérreca Huerta & Oumeraci (2012).

The different loading cases with the limits for regular wave tests in Liebisch et al. (2013b) are sketched in Fig. 6.3 together with the GWK-tests of Oumeraci et al. (2010b) and Alcérreca Huerta & Oumeraci (2012) for irregular waves. Depending on the revetment configuration in Liebisch et al. (2013b) for regular waves, a wider transition zone was obtained compared to Oumeraci et al. (2010b) and Alcérreca Huerta & Oumeraci (2012).

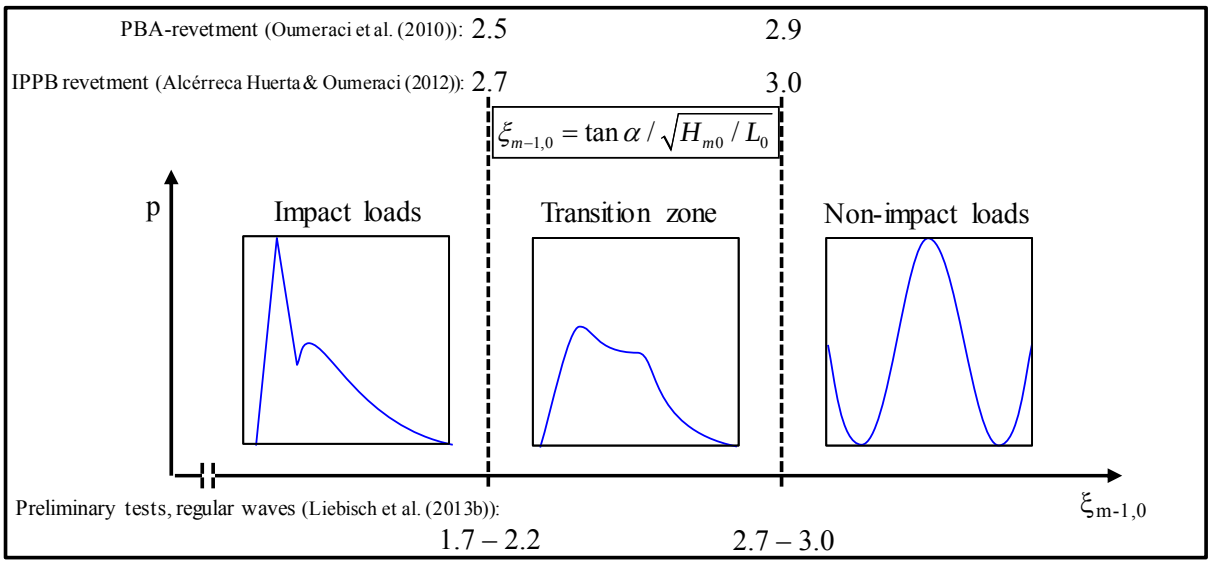

Fig. 6.3: Definition of different loading cases for all configurations in Liebisch et al. (2013b) (regular wave tests)

In the irregular wave tests of this study, a classification of the different breaker types like in Foyer (2013) and Alcérreca Huerta (2014) who used regular wave tests is hardly possible, because the waves strongly differ in irregular wave trains. That is why the classification of Oumeraci et al. (2010b) into impact and non-impact loads is adopted.

The classifications of the loading cases for all tested revetment configurations tested with wave spectra are shown together with the results of Oumeraci et al. (2010b) and Alcérreca Huerta & Oumeraci (2012) in Tab. 6.1.

Tab. 6.1: Classifications of the loading cases for all configurations tested with wave spectra (slope steepness 1:3)

configuration	Impact load	Transition zone	Non-impact load
c1 ($\tan\alpha$ = 1/3; n = 45%)	$\xi_{m-1,0} < 2.35$	$2.35 < \xi_{m-1,0} < 3.10$	$\xi_{m-1,0} > 3.10$
c2 ($\tan\alpha$ = 1/3; n = 20%)	$\xi_{m-1,0} < 2.25$	$2.25 < \xi_{m-1,0} < 3.00$	$\xi_{m-1,0} > 3.00$
c3 ($\tan\alpha$ = 1/6; n = 45%)	$\xi_{m-1,0} < 1.70$	$1.70 < \xi_{m-1,0} < 3.20$	$\xi_{m-1,0} > 3.20$
PBA-revetment ($\tan\alpha$ = 1/3; n = 40%) (Oumeraci et al. (2010b))	$\xi_{m-1,0} < 2.50$	$2.50 < \xi_{m-1,0} < 2.90$	$\xi_{m-1,0} > 2.90$
IPPB-revetment ($\tan\alpha$ = 1/3; n = 3%) (Alcérreca Huerta & Oumeraci (2012)	$\xi_{m-1,0} < 2.70$	$2.70 < \xi_{m-1,0} < 3.00$	$\xi_{m-1,0} > 3.00$

The largest differences in the wave load classification in Tab. 6.1 occur for slope 1:6 (configuration c3), for which the transition zone already begins at a surf similarity parameter of 1.70. This might be explained by the longer residence time of the up- and downrushing water of the flatter 1:6 slope resulting in a damping of the peaks already for smaller surf similarity parameter. But also for the two configurations with the 1:3 slope, the boundary between impact loads and transition zone is shifted to smaller values of surf similarity parameter $\xi_{m-1,0}$ compared to the results of the GWK-tests by Oumeraci et al. (2010b). However, it is assumed that deviations most likely occur in the determination of the boundaries due to the strongly subjective consideration of the different loading cases and breaker types.

For the wave load classification according to surf similarity parameter $\xi_{m-1,0}$, the flatter 1:6 slope provides a larger transition zone than the steeper slopes 1:3 due to the longer residence time of the up- and downrushing water on the flatter slope resulting in a damping of the peaks already for smaller surf similarity parameter ($1.70 < \xi_{m-1,0}$).

6.1.2 Parameterisation of the pressure signals

The different loading classes described in the previous section are characterized by very distinct parameters due to their shape (see Fig. 6.3). The parameterisation of the pressure signals is adopted from Oumeraci et al. (2010b) like in Liebisch et al. (2013b) in order to make the analysis results more easily comparable.

a) Pressure signals of impact wave loads

An impact component of very large pressure and very short duration characterizes impact wave loads which are developed by plunging/collapsing breakers. The pressure peak is superimposed by a cyclic quasi-static component according to the wave motion on the slope. These were idealized by Oumeraci et al. (2010b) with triangles described by three parameters (Fig. 6.4b)

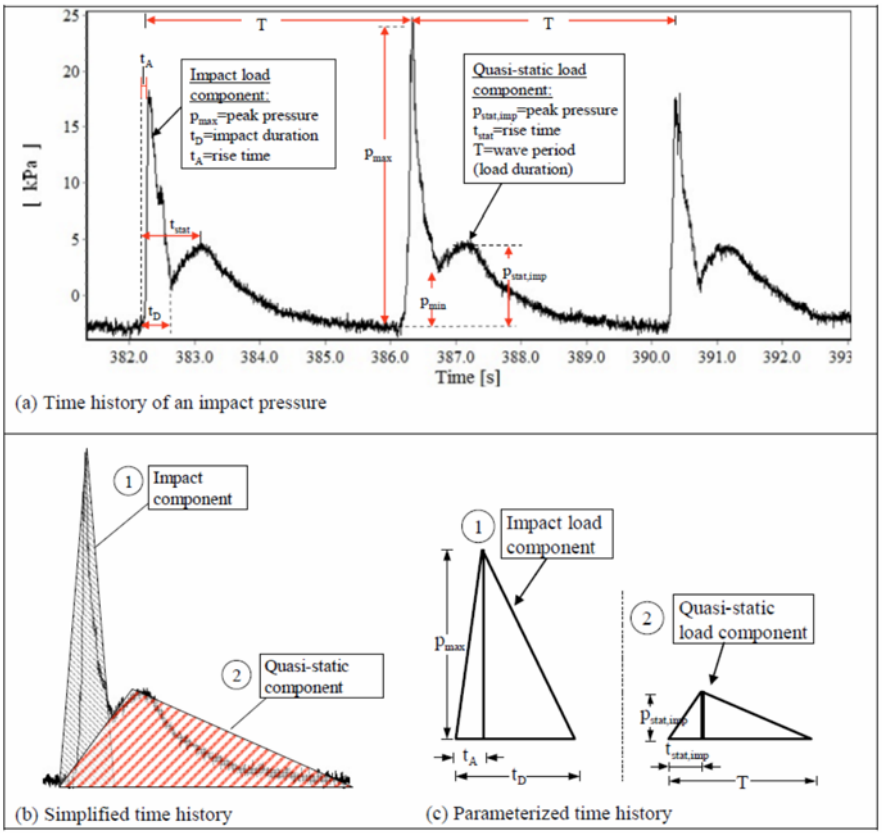

Fig. 6.4: Parameterisation of impact wave loads (Oumeraci et al. (2010b))

b) Pressure signals of non-impact wave loads

Like in Liebisch et al. (2013b) the parameterization of non-impact loads induced by surging breakers with a cyclic variation according to the wave motion on the revetment, was also adopted from the analysis of Oumeraci et al. (2010b). The non-impact loads are similar to the quasi-static component of the impact load and only one pressure peak can be observed in the

time history of the pressure signal ($p_{stat} = p_{max}$). Oumeraci et al. (2010b) idealized the shape of the non-impact pressure with a trapezoid described by four parameters (see Fig. 6.5b).

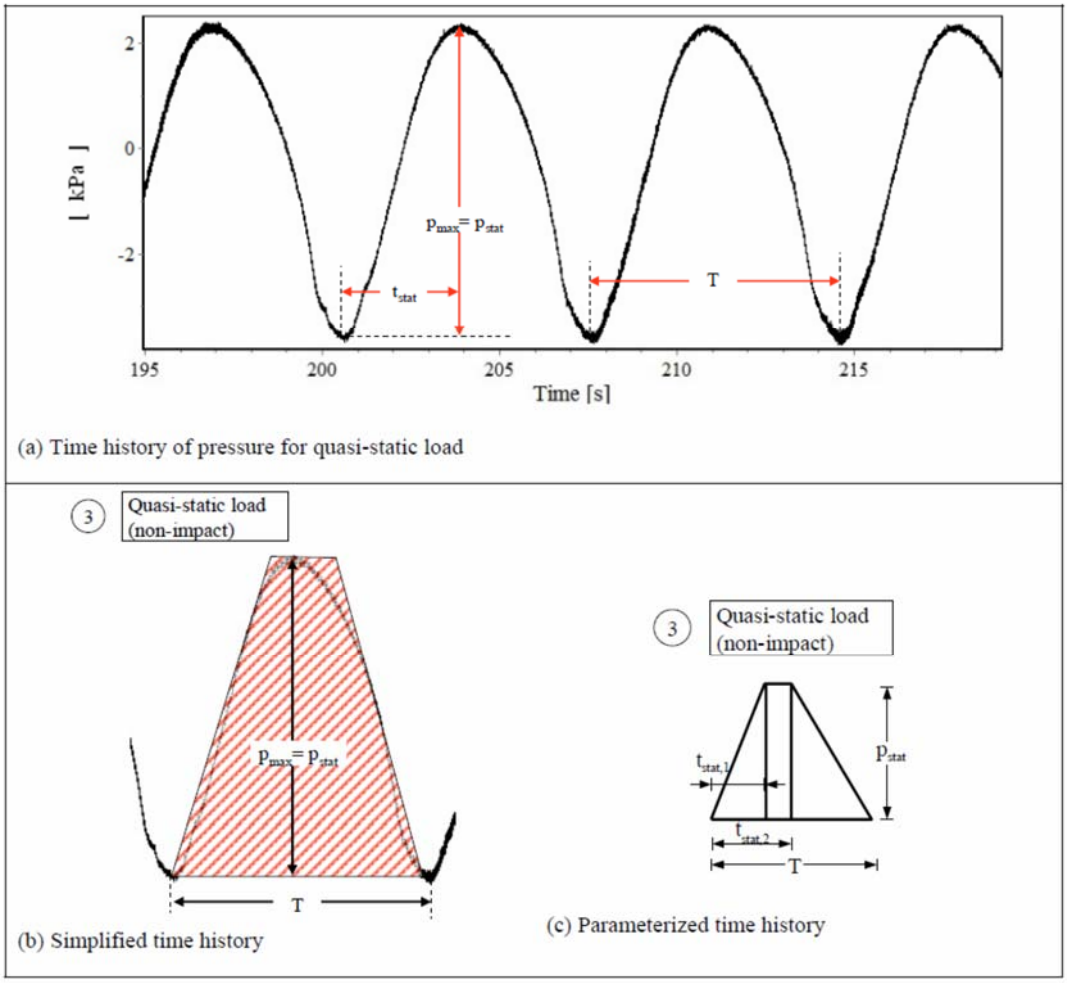

Fig. 6.5: Parameterisation of non-impact wave loads (Oumeraci et al. (2010b))

6.2 Peak pressure on the revetment

The design of a revetment depends on the peak pressure on the revetment and its location which also determine the pressure distribution on and beneath the revetment. Therefore, these two parameters are both used as key parameters for the calculation of all other wave-induced pressure parameters on and beneath the revetment. In doing so, the spatial pressure distribution on and beneath the revetment can be derived.

The peak pressures were used to determine a non-dimensionless parameter in terms of the wave height H_{m0} for wave spectra:

$$\overline{p}_{max} = \frac{p_{max}}{\rho \cdot g \cdot H_{m0}} \tag{6.2}$$

This dimensionless pressure is commonly used for the analysis of wave pressure as a function of the surf similarity parameter or the deep water wave steepness.

Typical signals recorded in PT-layer 1 (see Fig. 6.1) are shown in Fig. 6.6 exemplarily for a selected PT for a) impact loading and b) non-impact loading on configuration c1.

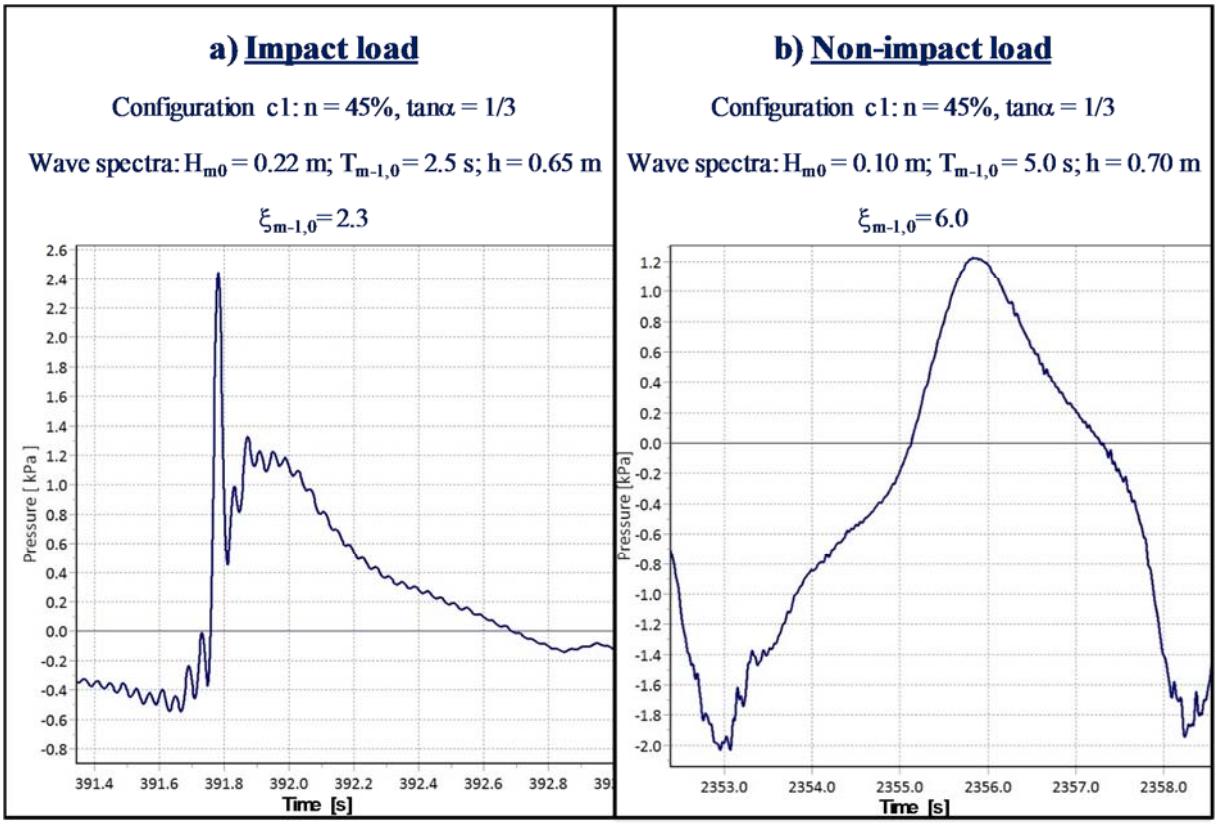

Fig. 6.6: Typical recorded signals of a pressure transducer on the revetment (PT-layer 1) for a) impact loading and b) non-impact loading (configuration c1)

In the following sub-sections the analyses are conducted to determine the effect of the revetment porosity and slope steepness on the relative peak pressure separately.

6.2.1 Effect of revetment porosity

Firstly, the results for the relative peak pressure on the revetments with the same slope steepness (1:3) and different porosity (20% & 45%) are shown in Fig. 6.7 together with the ranges of loading conditions for each revetment (also see Tab. 6.1). Furthermore, the mean behaviour of the relative peak pressure is indicated with a dashed line for each revetment.

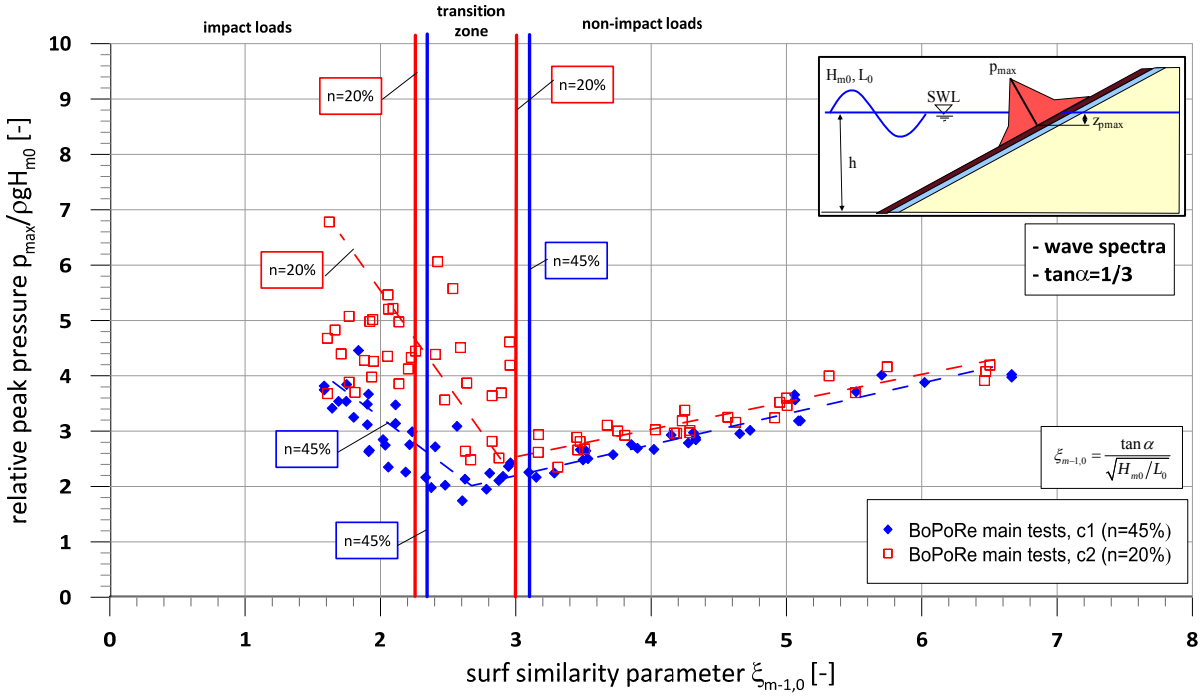

Fig. 6.7: Effect of revetment porosity on the relative peak pressure on the revetment as a function of surf similarity parameter $\xi_{m-1,0}$ for wave spectra (slope steepness 1:3)

For impact loads, much smaller relative peak pressures on the revetment with a larger porosity (c1) are obtained as compared to revetment with the lower porosity (c2), while for non-impact loads, configuration c2 seems to provide only slightly larger values compared to configuration c1 (Fig. 6.7). This confirms the results of the preliminary tests by Liebisch et al. (2013b) for regular waves and wave spectra tests, where it was found that porosity and roughness do not significantly affect the quasi-static loads.

The larger peak pressures induced by collapsing breakers ($2.4 < \xi_{m-1,0} < 4.3$) for larger revetment thickness due to an increasing infiltration and the absence of a water layer on the revetment as reported by Alcérreca Huerta (2014) were not observed in the laboratory tests of this study. They were also not observed in the GWK-tests (Oumeraci et al. (2010b)), so that they are likely numerical artefacts. However, the final answer can only be provided by laboratory tests specifically designed for this purpose. As shown in Fig. 6.7 for the aforementioned range of $\xi_{m-1,0}$-values, configuration c2 with the lower porosity (n = 20%) and the resulting smaller infiltration capacity provides significantly larger peak pressures compared to the highly porous configuration c1 (n = 45%).

For $\xi_{m-1,0} < 3.0$, strong plunging/collapsing breakers occur resulting in large relative peak pressures on the revetment with values up to 4.5 for configuration c1 with the higher porosity and up to ca.7.0 for configuration c2 with the lower porosity. For $\xi_{m-1,0} < 3.0$ (impact loads and transition zone), a larger scatter occurs for the revetment with the lower porosity (c2), which was already observed in the GWK-tests with an almost impermeable IPPB-revetment (Liebisch et al. (2012)). This might be explained by the large variability of wave breaking in this range of surf similarity parameters, which especially occurs on almost impermeable and low porous

revetments. An increasing porosity leads to smaller peak pressures on the revetment for plunging/collapsing breakers and a smaller scatter of the pressure values (see Fig. 6.7). This might be explained by a larger energy dissipation by the highly porous revetment, which was also observed in the comparison of the GWK-tests of Oumeraci et al. (2010b) (see also Fig. 6.8) and Alcérreca Huerta & Oumeraci (2012) in Liebisch et al. (2012). Obviously, the larger energy dissipation by the highly porous revetment also decreases the variability of wave breaking in the transition zone resulting in a smaller scatter.

For both configurations large unexpected non-impact loads occur up to relative peak pressures of 4.0. This was already observed in the GWK-tests on the PBA-revetment for irregular wave tests (see also Fig. 6.8). Furthermore, such a large non-impact pressure event is also shown in Fig. 6.6b) with $p_{max}/(\rho g H_{m0}) = 3.88$ for $\xi_{m-1,0} = 6.0$. Since also the obtained $p_{max}/(\rho g H_{m0})$-values on the smooth, impermeable revetment (p0r0) in the preliminary tests of Liebisch et al. (2013b) are in the same range for $\xi_{m-1,0} > 3.0$, an effect of the revetment porosity is not likely. It is assumed that these large $p_{max}/(\rho g H_{m0})$-values are a result from the analysis of the maximum peak pressure in irregular wave tests. However, this issue needs to be clarified in further studies, because also a comparison with the GWK tests of Gier et al. (2012) with an almost impermeable IPPB-revetment is not possible due to the tested range of $\xi_{m-1,0} < 3.0$.

A comparison of the results for configuration c1 and those of configuration p2r2 and p0r0 from the preliminary tests by Liebisch et al. (2013b), both with a highly porous cover layer (c1: 45%; p2r2: 48%) and a 1:3 slope, with the results from the GWK tests by Oumeraci et al. (2010b) with the same slope steepness and a similar porosity (PBA-revetment: 40%) is performed in Fig. 6.8.

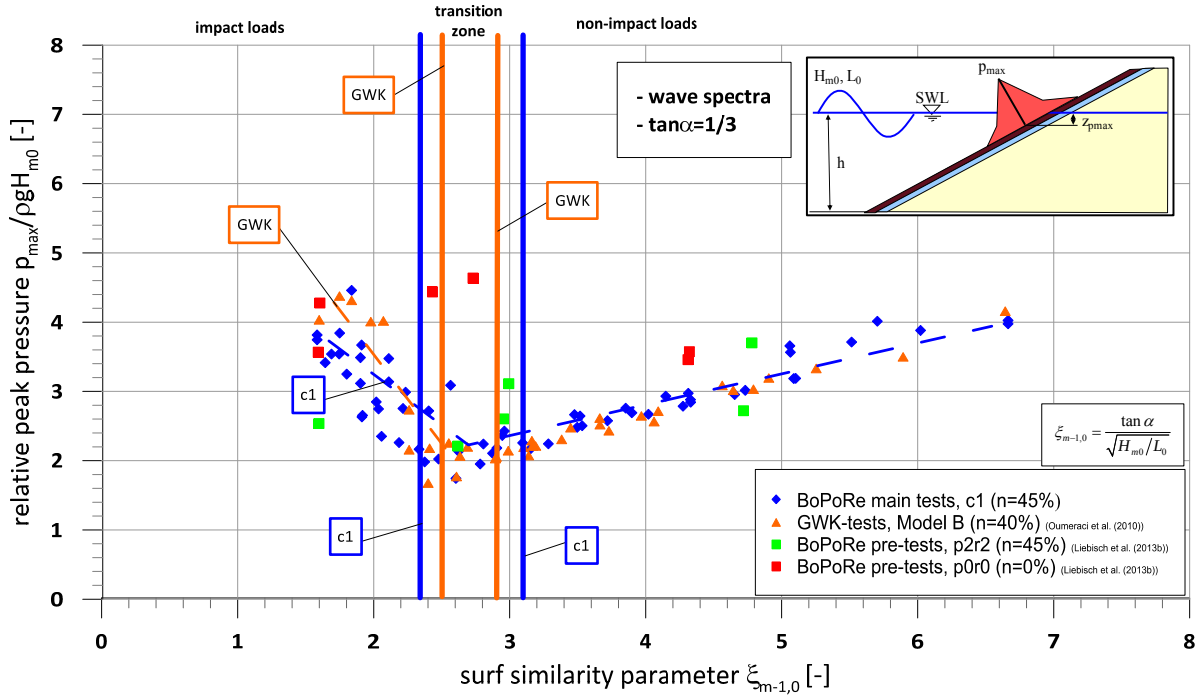

Fig. 6.8: Comparison of relative peak pressure on highly porous revetments as a function of surf similarity parameter $\xi_{m-1,0}$ obtained from different studies for wave spectra (slope steepness 1:3)

The comparison of the (1:5) Froude-scaled data of configuration c1 with the GWK data shows a good agreement for non-impact loads ($\xi_{m-1,0} > 3.1$). In the transition zone ($\xi_{m-1,0} = 2.35\text{-}3.10$), the relative peak pressures are also in the same range for the GWK data and the scaled model results. Only for the strong plunging breakers and the resulting impact loads ($\xi_{m-1,0} < 2.2$), about 10% larger relative peak pressures are obtained in the GWK tests than in the 1:5 scaled model.

These differences between the GWK-tests and the 1:5 scaled BoPoRe-tests for impact loads might be explained by the following possible causes:

- The entrapped and compressed air in plunging breakers cannot be scaled by the Froude-law. The effect of the smaller amoumt of entrapped air is more pronounced in the smaller scale model, thus resulting in a larger damping of the peak pressures for impact loads (Bullock et al. (2001)).
- Since the deep water wave height is used to define the relative peak pressure, smaller wave heights will result in larger relative peak pressures. Differences in the determination of the deep water wave height in the two flumes would result in differences in the relative peak pressure.
- Only the largest pressure event is chosen for the analysis of the peak pressure. The manually selected peak can be different depending on the analyst. The performance of the analysis by different analysts may lead to a different subjective filtering of the measured signals, especially considering possible measuring errors, which leads to deviations in the analysis of maximum peak pressures.
- Different wave generation and wave transformation in the two flumes.

It is assumed that the differences between the two models are not only due to one of the aforementioned causes, but by several of them. The second and the third causes are assumed to be the most relevant. Nevertheless, the data from both models can be used for a qualitative comparison of the revetment configurations and the effect of porosity and slope steepness on the peak pressure.

The following issues which might induce differences in the results of the two model studies can be excluded:

- *Measuring frequency of the PTs:* it is usually not scaled. In the small-scaled tests a large frequency was chosen to measure the very short pressure peaks in the time history. A cutting of the signal resulting in smaller pressure peaks is thus unlikely.
- *Duration of the tests:* generally 600 waves/tests were used in LWI model. However, selected tests for comparison were also conducted with 1000 waves like in the GWK without a significant difference.
- *Data filtering:* The same data filter was used to pre-process the data before the analysis.

6.2.2 Effect of the revetment slope steepness

The analysis of the effect of the slope steepness on the relative peak pressures on the revetment is performed by considering configurations c1 and c3 with the same porosity (n = 45%), but different slope steepnesses (1:3 for c1 and 1:6 for c3). The results are shown in Fig. 6.9.

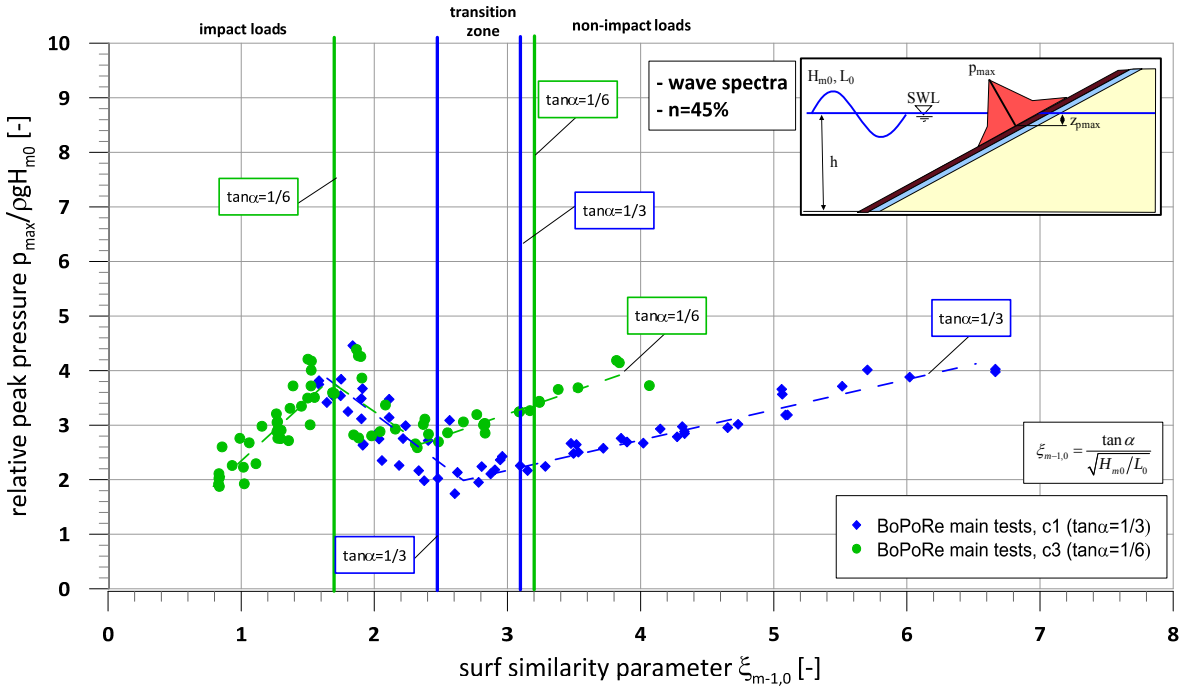

Fig. 6.9: Effect of slope steepness on relative maximum pressure on the revetment as a function of surf similarity parameter $\xi_{m-1,0}$ for wave spectra (porosity n = 45%)

The revetment with the flatter slope c3 provides similar values for the relative peak pressure for surf similarity parameters between 1.5 and 2.5. The highest relative peak pressure values on the revetment for configuration c3 are obtained for plunging breakers at $\xi_{m-1,0}$ = 1.5 which decrease again for $\xi_{m-1,0}$ < 1.5. Surprisingly, for large surf similarity parameters $\xi_{m-1,0}$ > 2.5 larger values compared to configuration c1 are obtained which might be explained by larger water layers on the flatter slope or due to a shifting of the peak pressure values to smaller $\xi_{m-1,0}$-values for configuration c3: the slope steepness included in the surf similarity parameter shifts the peak pressure values for the same wave conditions to smaller $\xi_{m-1,0}$-values. Consequently, a direct comparison of the data for the same revetment porosity with different slope steepnesses is limited. The wider transition zone for the flatter slope (c3) compared to the steeper slope (c1) might be explained by the longer residence time of the up- and downrushing water which affects the incident waves in their breaking behaviour.

Before deriving prediction formulae for the peak pressure p_{max}, the quasi-static component p_{stat} is analysed separately in the next section. This procedure was already successfully conducted by Alcérreca Huerta (2014).

6.2.3 Quasi-static pressure component on the revetment

In Liebisch et al. (2013b), the quasi-static pressure induced by the cyclic wave motion on the revetment was found to be only affected by the slope steepness. Neither the roughness nor the porosity of the revetment had any noticeable effect. Since for surging breakers no impact component occurs, the entire wave load consists only of the quasi-static pressure. For plunging/collapsing breakers, the quasi-static component of impact loads is simply superimposed by the impact component to provide the entire impact load (see Fig. 6.4).

The following model was chosen in Liebisch et al. (2013b), because it provides the best fitting for the range of the surf similarity parameters tested, especially on the 1:3 revetment:

$$\frac{p_{stat}}{\rho g H_{m0}} = a_{stat} \cdot \tanh\left(b_{stat} \cdot \xi_{m-1,0}^{c_{stat}}\right) \tag{6.3}$$

with: a_{stat}, b_{stat}, c_{stat} = empirical coefficients

Alcérreca Huerta (2014) numerically investigated the wave-induced loading of porous, bonded revetments for regular waves. As a result, a prediction model for the entire impact load induced by regular waves was developed which consists of an impact component (see eq. (6.9)) and the quasi-static component which is described by eq. (6.4):

$$\frac{p_{stat}}{\rho g H_m} = 2 \cdot \frac{\xi_m^2 + 5 \cdot \xi_m}{\xi_m^2 + 25.4} \tag{6.4}$$

In fact, no differences in the quasi-static component could be identified for different revetment thicknesses.

In this study the model proposed in eq. (6.3) is used instead of eq. (6.4) proposed by Alcérreca Huerta (2014) to fit the data of the quasi-static loads, because eq. (6.3) does not tend against 2.0 for large surf similarity parameters and eq. (6.4) can thus not describe the large peak pressure values found for non-impact loads on the porous revetments tested in irregular wave tests (Fig. 6.7, Fig. 6.8 and Fig. 6.9). However, due to the large obtained scatter like in Alcérreca Huerta (2014), a conservative approach using upper envelopes for the data is also considered instead of a common approach based on a fitting function with a standard deviation. The aim of this approach is to possibly enclose the analysed data as completely as possible by an upper envelope representing the maximum possible value for any given surf similarity parameter. For design purpose these maximum peak pressures might be considered as more relevant for the stability of the entire structure than the mean values obtained by a common fitting approach. Fig. 6.10 shows a comparison of the quasi-static load components for the revetment configurations c1 and c2 with different porosities and the same slope steepness 1:3. For the impact loads the maximum peak pressures p_{max} is excluded and only the quasi-static load components p_{stat} are considered in the analysis. Upper envelopes for the values are derived applying eq. (6.3).

The quasi-static load components of the two configurations with different porosities in Fig. 6.10 show as expected only slight differences. For configuration c2 with the lower porosity, slightly

larger values are provided, which might be explained by less infiltration into the revetment with the smaller porosity resulting in a larger water layer on the revetment. Furthermore, a larger scatter occurs, which was already observed for the maximum peak pressures in Fig. 6.7. However, also for configuration c1 a larger scattering is observed for $\xi_{m-1,0} < 3.0$ in the range (plunging and collapsing breakers); i.e. only for the quasi-static component of the impact load. It is assumed that this scatter results from the analyses the quasi-static load component associated to the maximum peak pressure of the impact loads on the revetment, which is related to high variability.

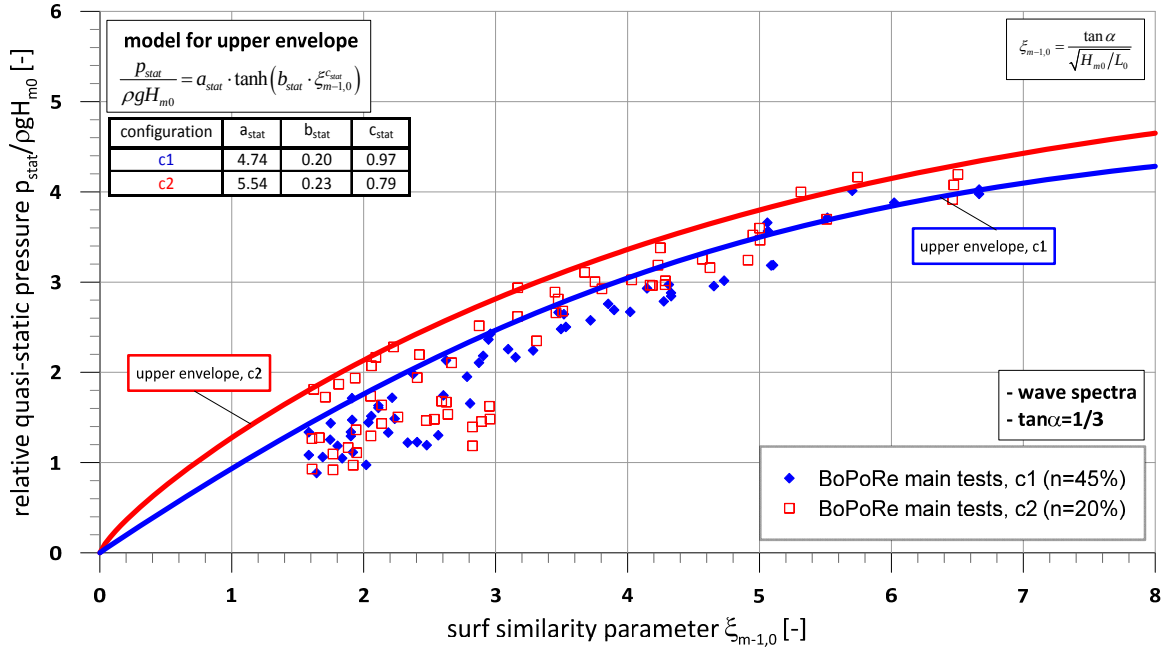

Fig. 6.10: Effect of revetment porosity on the relative quasi-static pressure for wave spectra (slope steepness 1:3) and applied eq. (6.3) by Liebisch et al. (2013b) for upper envelopes

Using eq. (6.3) the following formulae were found for configurations c1 and c2 with the same slope steepness 1:3:

Configuration c1 (n = 45%):
$$\frac{p_{stat}}{\rho g H_{m0}} = 4.74 \cdot \tanh\left(0.20 \cdot \xi_{m-1,0}^{0.97}\right) \tag{6.5}$$

Configuration c2 (n = 20%):
$$\frac{p_{stat}}{\rho g H_{m0}} = 5.54 \cdot \tanh\left(0.23 \cdot \xi_{m-1,0}^{0.79}\right) \tag{6.6}$$

Fig. 6.11 compares the results of small-scale BoPoRe-tests (configurations c1 and c2 with slope steepness 1:3) with the values of quasi-static load component of the large scale tests in GWK of Oumeraci et al. (2010b) and Alcérreca Huerta & Oumeraci (2012) for irregular waves.

The four datasets provide comparable results in Fig. 6.11 for all revetment configurations independently on the scale and the porosity of the cover layer. Also the large-scale tests in GWK confirm the large quasi-static loads up to $p_{stat}/(\rho g H_{m0}) = 4.0$ for large surf similarity parameters. The large scattering for surf similarity parameters smaller than 3 is also observed

for the large scale experiments. Thus, there are no significant model or scale effects for the quasi-static component on the revetment.

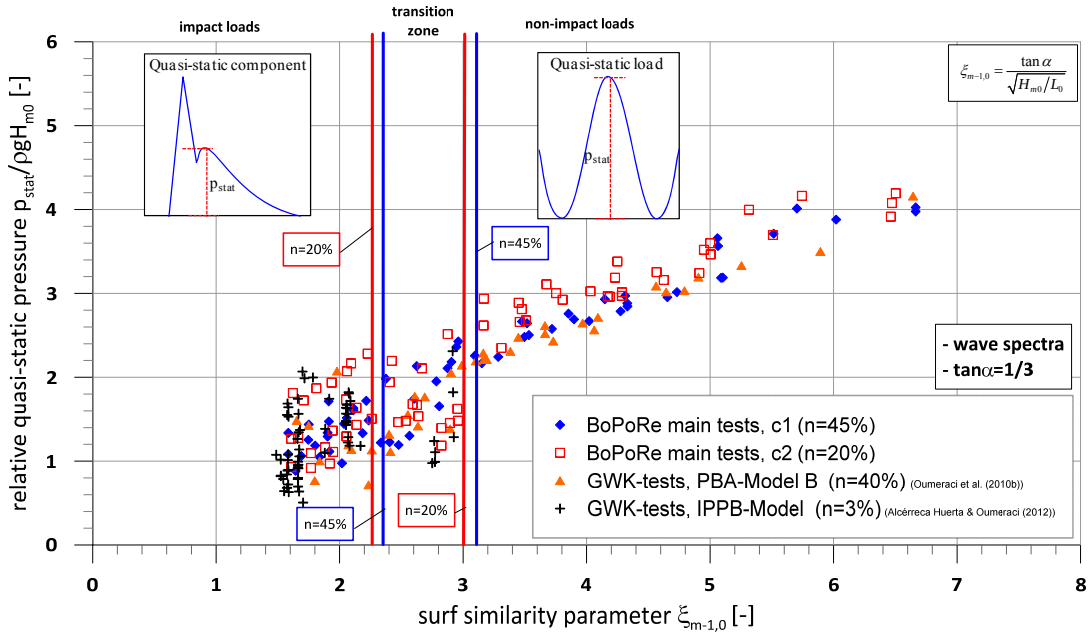

Fig. 6.11: Comparison of different data series of relative quasi-static pressure as a function of surf similarity parameter $\xi_{m-1,0}$ for wave spectra (slope steepness 1:3)

In Liebisch et al. (2013b) it was reported that the quasi-static pressure component was only affected by the slope steepness for regular waves. In Fig. 6.12 the effect of slope steepness on the quasi-static pressure component is shown for wave spectra. The relative quasi-static pressures for $\xi_{m-1,0} < 2.0$ show a good agreement for both revetment configurations c1 and c3 in Fig. 6.12.

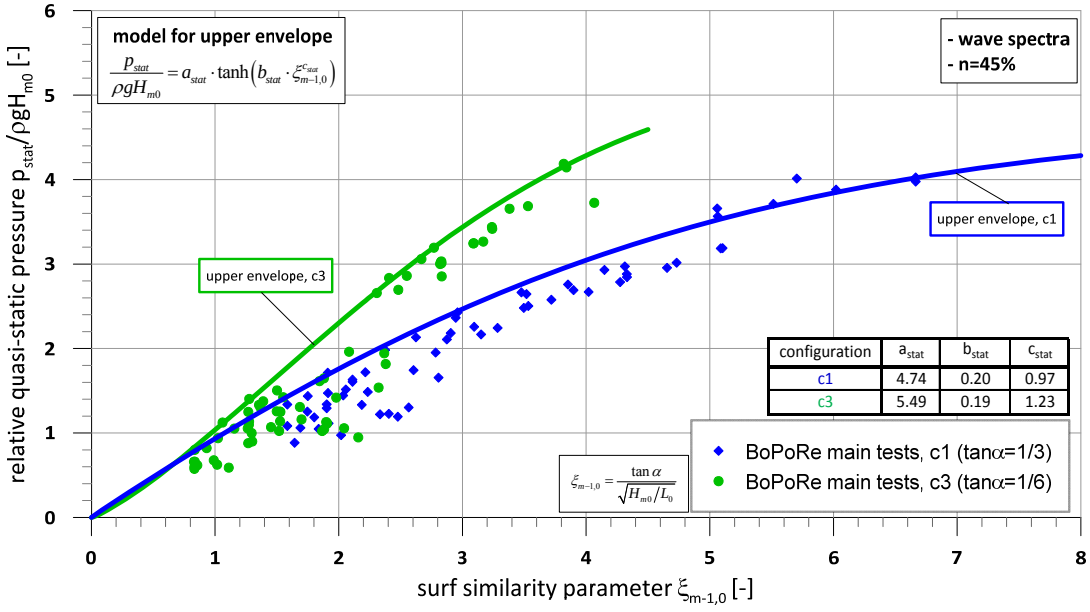

Fig. 6.12: Effect of slope steepness on relative quasi-static pressure on the revetment as a function of surf similarity parameter $\xi_{m-1,0}$ for wave spectra (porosity n = 45%)

Unexpectedly, for surf similarity parameters larger than 2.0 the quasi-static pressure for flatter slopes (c3) is decisively larger than that for the steeper slope (c1). Like in the previous section the chosen fitting model was applied for the upper envelope:

Configuration c3 (tanα = 1/3): $$\frac{p_{stat}}{\rho g H_{m0}} = 5.49 \cdot \tanh\left(0.19 \cdot \xi_{m-1,0}^{1.23}\right) \quad (6.7)$$

Considering the decisively larger relative quasi-static pressure on revetment c3 with a flatter slope 1:6 for surf similarity parameters larger than 2.0 in Fig. 6.12, the results for both configurations c1 and c3 are comparatively shown only against deep water wave steepness H_{m0}/L_0 i.e. without consideration of the slope steepness in Fig. 6.13. The red ellipsis in Fig. 6.13 highlights the peak values of the relative quasi-static component which are shifted to the left on the x-axis in Fig. 6.12. It is obvious that all values with small wave steepness (i.e. with small wave heights and especially large wave periods) cause unexpected large values of quasi-static pressure which can also be seen in Fig. 6.12. This means that for decreasing wave steepness (quasi-static loads) the effect of slope steepness on the pressure on the revetment also decreases and becomes negligibly small. This phenomenon has to be further examined in future laboratory tests or numerical studies for a wider variation range of the slope steepness. Also in Alcérreca Huerta (2014) this was not seen, because the wave pressure analysis was only conducted depending on layer thickness without a variation of slope steepness.

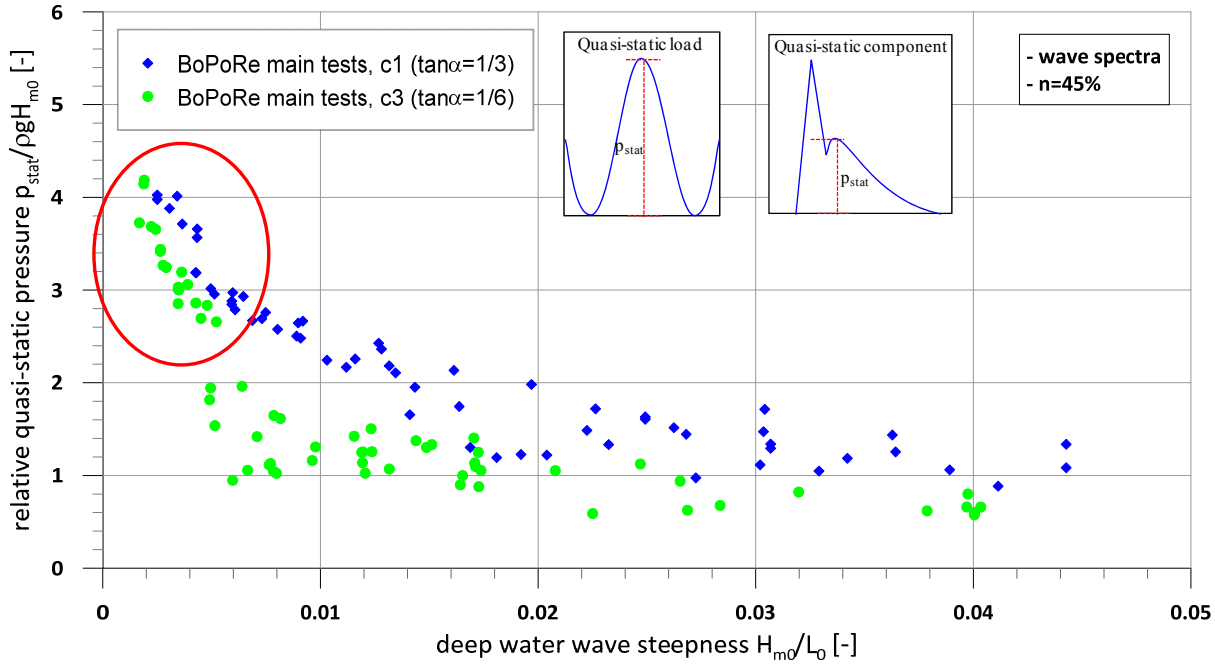

Fig. 6.13: Effect of slope steepness on relative quasi-static pressure on the revetment as a function of deep water wave steepness for wave spectra (porosity n = 45%)

6.2.4 Prediction formulae for wave-induced peak pressure on the revetment

In the previous section the relative quasi-static pressure component was investigated and upper envelopes were determined for the values of the different configurations based on Liebisch et al. (2013b) in eq. (6.3). The coefficients for the upper envelopes of the configurations are summarized in Tab. 6.2.

Tab. 6.2: Coefficients a_{stat}, b_{stat} and c_{stat} in eq. (6.3) for all tested configurations c1, c2 and c3

$\frac{p_{stat}}{\rho g H_{m0}} = a_{stat} \cdot \tanh\left(b_{stat} \cdot \xi_{m-1,0}^{c_{stat}}\right)$	tanα [-]	porosity [%]	a_{stat} [-]	b_{stat} [-]	c_{stat} [-]
configuration c1	1/3	45	4.74	0.20	0.97
configuration c2	1/3	20	5.54	0.23	0.79
configuration c3	1/6	45	5.49	0.19	1.23

For the model development in the next step, the impact pressure component has to be analysed. This component only occurs for breaking waves with surf similarity parameters smaller than 3 corresponding to plunging and collapsing breaker types. The impact component is determined as a difference between the total peak pressure and the quasi-static peak pressure (see Fig. 6.4):

$$p_{imp} = p_{\max} - p_{stat} \tag{6.8}$$

Alcérreca Huerta (2014) also proposed an upper envelope described by the following equation for the impact component:

$$\frac{p_{imp}}{\rho g H_0} = A \cdot \xi_0 \cdot \exp\left(-\frac{\xi_0^2}{B}\right) \tag{6.9}$$

Eq. (6.9) has the advantage that the relative impact pressure is tending against zero again for large surf similarity parameters, which is important because for surging breakers no impact occurs. This model is adopted in this study to get a smoother fitting for the upper envelopes. Therefore, the coefficient c is introduced instead of the exponent. This leads to the following equation:

$$\frac{p_{imp}}{\rho g H_{m0}} = a_{imp} \cdot \xi_{m-1,0} \cdot \exp\left(-\frac{\xi_{m-1,0}^{c_{imp}}}{b_{imp}}\right) \tag{6.10}$$

The coefficients in eq. (6.10) for the relative impact pressure component determined for the tested configurations are summarized in Tab. 6.3. For the impact pressure component no difference between configurations c1 and c3 with the same porosity (n = 45%) and different slope steepnesses was found. Consequently, the same coefficients are used for the upper envelope in eq. (6.10).

Tab. 6.3: Coefficients a_{imp}, b_{imp} and c_{imp} in eq. (6.10) for all tested configurations c1, c2 and c3

$\frac{p_{imp}}{\rho g H_{m0}} = a_{imp} \cdot \xi_{m-1,0} \cdot \exp\left(-\frac{\xi_{m-1,0}^{c_{imp}}}{b_{imp}}\right)$	tanα [-]	porosity [%]	a_{imp} [-]	b_{imp} [-]	c_{imp} [-]
configurations c1 and c3	1/3 and 1/6	45	1.75	304.38	6.59
configuration c2	1/3	20	2.55	50.61	3.60

The derived prediction model for the peak pressure is very similar to the model proposed by Alcérreca Huerta (2014), which consists of an impact and a quasi-static-component described in eq. (6.3) and eq. (6.10) leading to eq. (6.11):

$$\frac{p_{\max}}{\rho g H_{m0}} = \frac{p_{imp} + p_{stat}}{\rho g H_{m0}} = a_{imp} \cdot \xi_{m-1,0} \cdot \exp\left(-\frac{\xi_{m-1,0}^{c_{imp}}}{b_{imp}}\right) + a_{stat} \cdot \tanh\left(b_{stat} \cdot \xi_{m-1,0}^{c_{stat}}\right) \quad (6.11)$$

Based on this model, the following specific formulae are obtained for the upper envelopes of the relative maximum peak pressure on the three revetment configurations tested with wave spectra (Fig. 6.14):

Configuration c1 (n = 45%; tanα = 1/3):

$$\frac{p_{\max}}{\rho g H_{m0}} = 1.75 \cdot \xi_{m-1,0} \cdot \exp\left(-\frac{\xi_{m-1,0}^{6.59}}{304.38}\right) + 4.74 \cdot \tanh\left(0.20 \cdot \xi_{m-1,0}^{0.97}\right) \quad (6.12)$$

$$\text{for } \xi_{m-1,0} < 6.8$$

Configuration c2 (n = 20%; tanα = 1/3):

$$\frac{p_{\max}}{\rho g H_{m0}} = 2.55 \cdot \xi_{m-1,0} \cdot \exp\left(-\frac{\xi_{m-1,0}^{3.60}}{50.61}\right) + 5.54 \cdot \tanh\left(0.23 \cdot \xi_{m-1,0}^{0.79}\right) \quad (6.13)$$

$$\text{for } \xi_{m-1,0} < 6.8$$

Configuration c3 (n = 45%; tanα = 1/6):

$$\frac{p_{\max}}{\rho g H_{m0}} = 1.75 \cdot \xi_{m-1,0} \cdot \exp\left(-\frac{\xi_{m-1,0}^{6.59}}{304.38}\right) + 5.49 \cdot \tanh\left(0.19 \cdot \xi_{m-1,0}^{1.23}\right) \quad (6.14)$$

$$\text{for } \xi_{m-1,0} < 4.2$$

Combining the equations for the upper envelopes of both pressure components, the derived envelopes in Fig. 6.14 enclose almost all obtained data points. Like for the results of the numerical simulations with regular waves by Alcérreca Huerta (2014), this approach using an upper envelope provides relatively good results also for the results of physical model tests

performed in this study with irregular waves. However, for some surf similarity parameters the application of upper envelopes lead to an overestimation up to 50% for the maximum peak pressures, which would result in an overdesigned revetment. Consequently, even though the approach to enclose the data with upper envelopes instead of the application of common fitting functions represents a good alternative to handle the large variability of peak pressure values especially for impact loads and in the transition zone and the included safety for design purposes, more research is necessary to com up with a larger data base for a higher accuracy of this conservative approach.

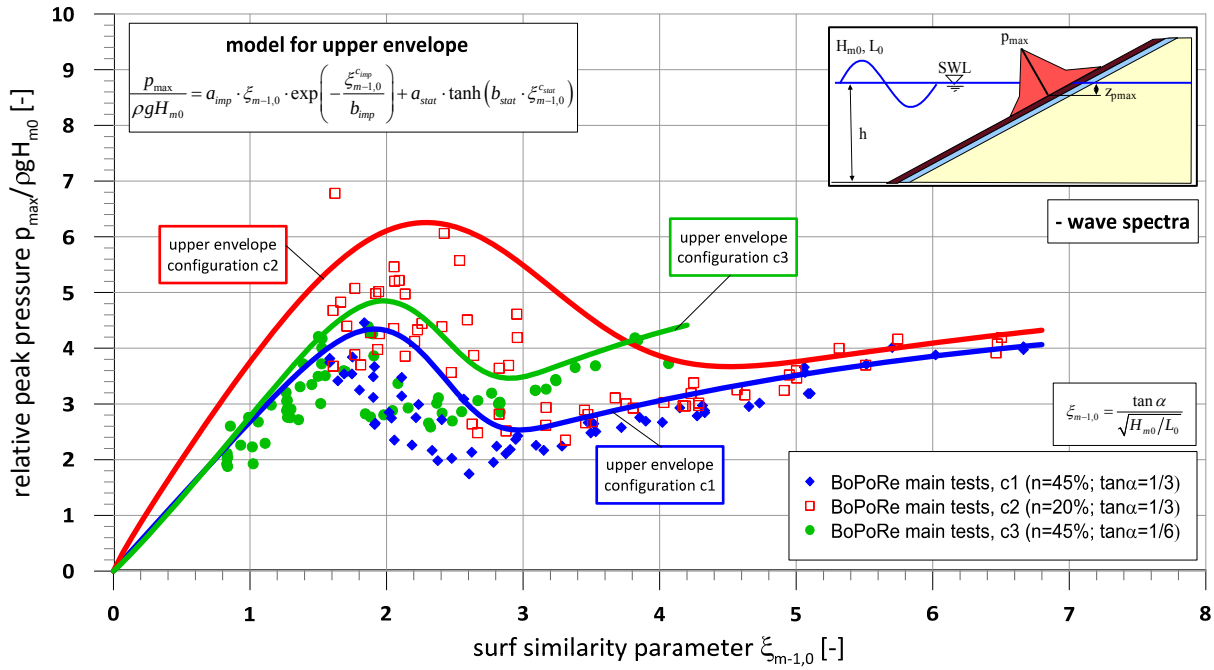

Fig. 6.14: Upper envelopes for relative maximum peak pressure on the revetment as a function of surf similarity parameter $\xi_{m-1,0}$ for wave spectra (all tested configurations)

An increasing porosity increases the damping of impact loads leading to significantly smaller (up to 70%) peak pressures on the revetment, whereas non-impact loads are just slightly affected by a changing porosity. This might be explained by a smaller infiltration into the revetment and subsequent larger water layers on the revetment. Furthermore, an increasing porosity leads to a smaller scatter of the pressure values for $\xi_{m-1,0} < 3.0$ (impact loads and transition zone). Obviously, the larger dissipation on the highly porous revetment also decreases the variability of wave breaking in the transition zone resulting in a smaller scatter. This effect was also observed in the GWK-tests.

The flatter slope1:6 results in a broader transition zone between impact and non-impact loads (c3: $1.70 < \xi_{m-1,0} < 3.20$; c1: $2.35 < \xi_{m-1,0} < 3.10$). The slope steepness also affects the relative peak pressure ($p_{stat}/(\rho g H_{m0})$) of the quasi-static load. In contrast, no noticeable effect of the slope steepness on the impact peak pressure could be identified. The effect of the slope steepness on the $p_{stat}/(\rho g H_{m0})$-values is not well described by surf similarity parameter $\xi_{m-1,0}$, this is shown more explicitly for $p_{stat}/(\rho g H_{m0})$ as a function of the deep water wave steepness.

Therefore, using $\xi_{m-1,0}$ to describe $p_{stat}/(\rho g H_{m0})$ makes the comparability of revetments with different slopes and the same porosity difficult. Further research is needed in order to come up with conclusive results.

For all tested configurations, unexpectedly large non-impact loads up to relative peak pressures of 4.0 occur. This was already observed in the GWK-tests and in the preliminary tests on the smooth, impermeable revetment for irregular wave tests. It is still unclear, if these large peak pressure values for non-impact loads are due the analysis of the maximum peak pressure in irregular wave tests.

A model similar to the one proposed by Alcérreca Huerta (2014) which includes the upper envelope of both peak components of the quasi-static and impact pressure is successfully used to develop a (conservative) prediction model, showing that the effect of the revetment porosity is dominant as compared to the effect of the slope steepness.

For the transition zone and non-impact loads the 1:5 scaled model tests provide a good agreement to the large-scale GWK-tests, but for impact loads ($\xi_{m-1,0} < 2.2$) the GWK-tests provide values for the relative peak pressure which are up about 10% larger than the results of the 1:5 scaled tests. This might be explained by the combination of several effects as outlined in section 6.2.1.

6.3 Location of peak pressure on the revetment

The magnitude of the peak pressure on the revetment was analysed in the previous section 6.2. However, not only the peak pressure is important for design purposes, but also the entire pressure distribution on the revetment. Besides the magnitude of the peak pressure, its location on the revetment is also a key parameter for the parameterization of the pressure distribution. The relative location of peak pressure is described by the vertical distance beneath SWL z_{pmax} divided by the wave height H_{m0} for wave spectra tests:

$$\bar{z}_{p\max} = \frac{z_{p\max}}{H_{m0}} \tag{6.15}$$

The sketch in Fig. 6.15 shows the definition of the location of the peak pressure.

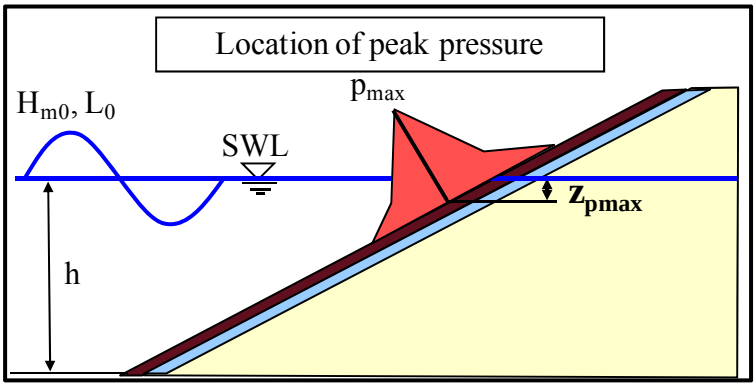

Fig. 6.15: Location of peak pressure p_{max} on the revetment (definition sketch)

The approach of Schüttrumpf (2001) using a tanh-function was adopted in Liebisch et al. (2013b) to fit the obtained data. After slight modifications to make the function tend to zero for small surf similarity parameter (Liebisch et al. (2013b)), the following equation providing a better fitting and including only two empirical coefficients is obtained:

$$\frac{z_{p\max}}{H_{m0}} = a_{loc} \cdot \left(1 + \tanh\left(\xi_{m-1,0} - b_{loc}\right)\right) \tag{6.16}$$

with: a_{loc}, b_{loc} = empirical coefficients

The effect of the revetment porosity and slope steepness on the location of the peak pressure on the revetment are analysed in the following sections 6.3.1 and 6.3.2. Prediction formulae are then proposed which account for both revetment porosity and slope steepness.

6.3.1 Effect of the revetment porosity

The location of the peak pressure on the revetment is first investigated for configurations c1 and c2 with the same slope steepness (1:3) but with different porosities (45% & 20%, respectively). The results are shown in Fig. 6.16 together with the model proposed by Oumeraci et al. (2010b) for a PBA revetment and Schüttrumpf (2001) for a smooth, impermeable revetment.

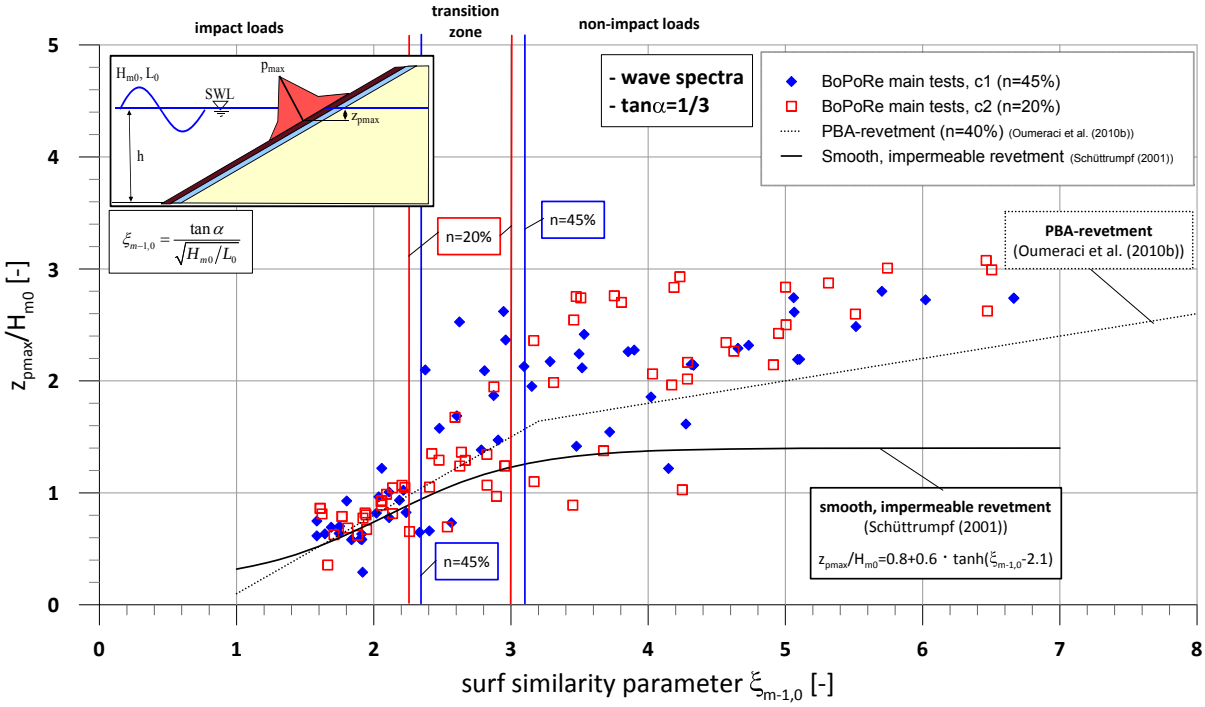

Fig. 6.16: Effect of revetment porosity on the relative location of the peak pressure on the revetment as a function of surf similarity parameter $\xi_{m-1,0}$ for wave spectra (slope steepness 1:3)

No noticeable effect of the revetment porosity on the relative location of the peak pressure can be identified for the two revetment configurations in Fig. 6.16. The close relation between wave run-down and the location of peak pressure was already discussed in Liebisch et al. (2013b) for regular wave tests. It was shown that an increasing roughness shifts the location of the peak pressure upwards the slope. This was also observed for an increasing porosity but less distinctive compared to the effect of roughness. However, the results for wave spectra tests in Fig. 6.16 for both configurations c1 and c2 also show larger values for the relative location of the peak pressure for surf similarity parameters larger than 2.4 compared to the model for a smooth and impermeable revetment by Schüttrumpf (2001). For impact loads the obtained values for all considered models are similar leading to the assumption that porosity does not affect the location of the peak pressure for plunging breakers ($\xi_{m-1,0} < 2.4$). For both configurations, the scatter of the data is particularly significant for the range of surf similarity parameters covering the transition zone between collapsing breakers and surging breakers ($\xi_{m-1,0} = 2.4\text{-}4.0$). A similar scatter was observed in the numerical results by Alcérreca Huerta (2014) for regular waves.

In Fig. 6.17, the results of wave spectra tests are compared, including those with configuration c1 in this study, those with PBA-revetment in GWK by Oumeraci et al. (2010b) and those from the preliminary tests by Liebisch et al. (2013b). The scatter of the results of the GWK-tests are much less pronounced in the transition zone than those of configuration c1 which is obviously caused by a more pronounced effect of the porous structure on the breaking behaviour in this range for the 1:5 scaled model. However, as this larger scatter was also obtained in the numerical results of Alcérreca Huerta (2014) more systematic research is necessary to clarify the underlying processes.

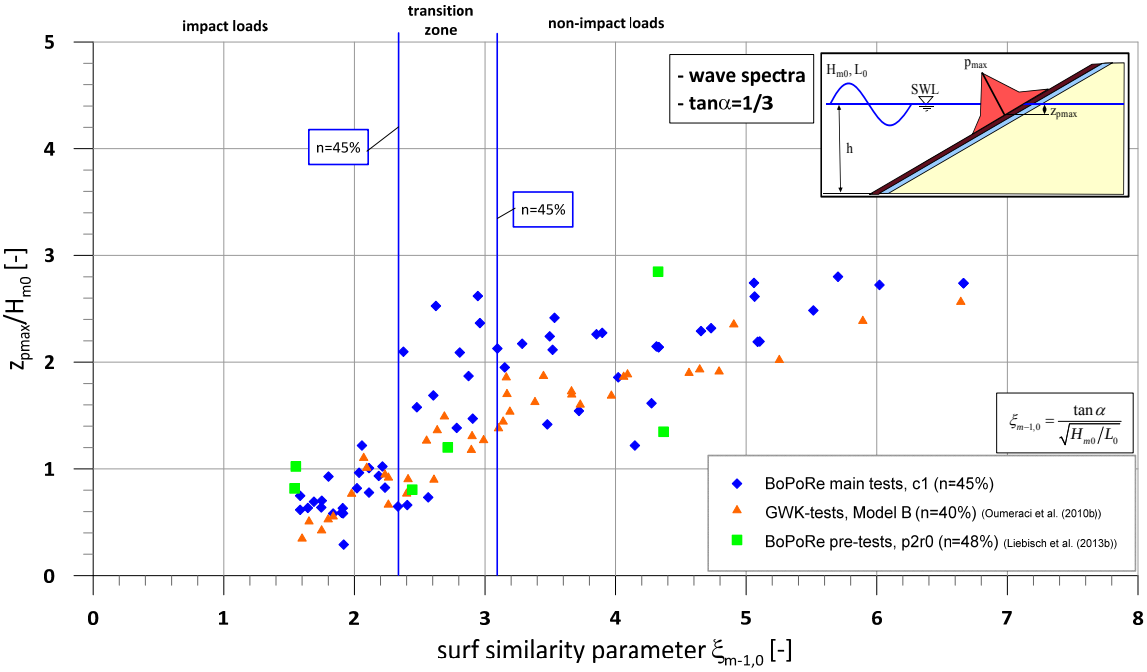

Fig. 6.17: Comparison of different data sets for the relative location of peak pressure on highly porous revetments as a function of surf similarity parameter $\xi_{m-1,0}$ for wave spectra (slope steepness 1:3)

Due to the large scatter obtained in his numerical data for the location of the peak pressure Alcérreca Huerta (2014) successfully used upper and lower envelopes to fit the numerical data for regular wave tests. The application of upper and lower envelopes is also conducted in this study, but based on eq. (6.16). The upper and lower envelopes for configuration c1 and c2 are considered together in Fig. 6.18, because no significant difference occurred in the results for different porosities in Fig. 6.16.

The upper and lower envelopes enclosing the large scatter of the obtained z_{pmax}/H_{m0}-values for surf similarity parameters $\xi_{m-1,0}$ = 2.5-4.0. The scattering decreases for both larger and smaller surf similarity parameters, are described by the following equations:

Upper envelope:
$$\frac{z_{p\max}}{H_{m0}} = 1.51 \cdot \left(1 + \tanh\left(\xi_{m-1,0} - 2.03\right)\right) \tag{6.17}$$

Lower envelope:
$$\frac{z_{p\max}}{H_{m0}} = 1.33 \cdot \left(1 + \tanh\left(\xi_{m-1,0} - 4.28\right)\right) \tag{6.18}$$

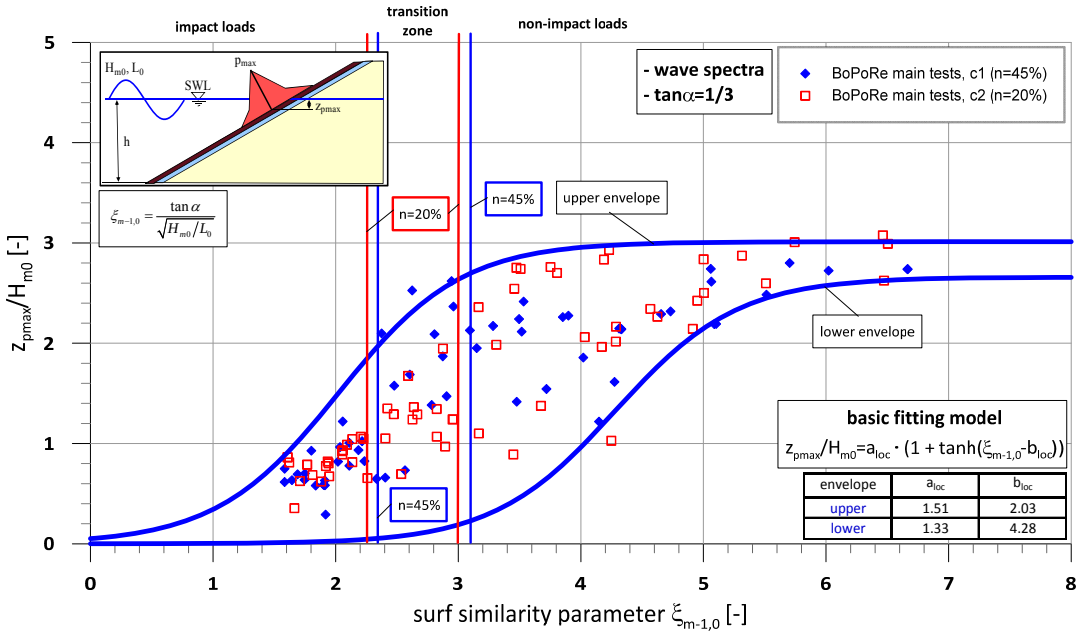

Fig. 6.18: Upper and lower envelopes of relative location of the peak pressure on the revetment based on eq. (6.16) as a function of surf similarity parameter $\xi_{m-1,0}$ for wave spectra (slope steepness 1:3)

6.3.2 Effect of the revetment slope steepness

The effect of the slope steepness on the location of the peak pressure on the revetment is analysed in Fig. 6.19 by considering revetment configurations c1 and c3 with different slope steepnesses but the same porosity (n = 45%). The results are shown with the fitting approach of the previous section using upper and lower envelopes based on eq. (6.16). The upper and lower envelopes for configuration c1 and c2 are also shown in Fig. 6.19 for comparison.

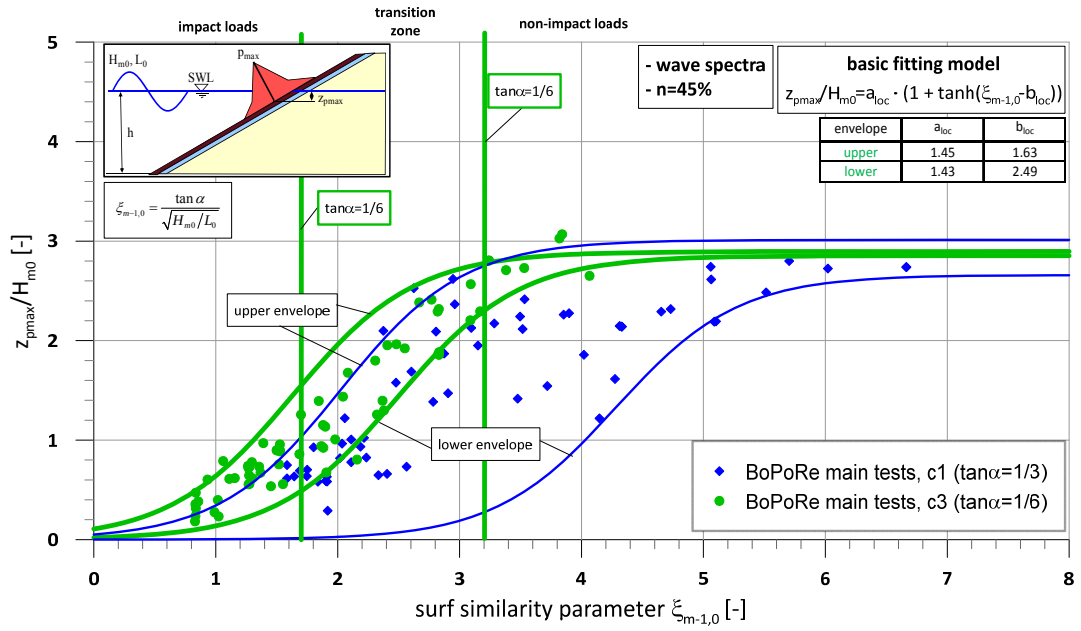

Fig. 6.19: Upper and lower envelopes of relative location of peak pressure on the revetment based on eq. (6.16) as a function of surf similarity parameter $\xi_{m-1,0}$ tested with wave spectra (porosity n = 45%)

The results for the location of the maximum peak pressure for the flatter slope 1:6 of configuration c3 in Fig. 6.19 show significantly less scatter compared to those of configuration c1 and c2 with the steeper slope. This leads to a decisively smaller range which has to be enclosed by the upper and lower envelopes. This might be explained by the smaller vertical distances of the pressure transducers in the model set-up and the resulting smaller measuring range on the flatter slope (also see Fig. 4.9). The effect of slope steepness has to be further examined in future laboratory tests or numerical simulations for a wider variation range of the slope steepness.

The following equations of the upper and lower envelopes for configuration c3 are determined:

Upper envelope:
$$\frac{z_{p\max}}{H_{m0}} = 1.45 \cdot \left(1 + \tanh\left(\xi_{m-1,0} - 1.63\right)\right) \tag{6.19}$$

Lower envelope:
$$\frac{z_{p\max}}{H_{m0}} = 1.43 \cdot \left(1 + \tanh\left(\xi_{m-1,0} - 2.49\right)\right) \tag{6.20}$$

The coefficients for the upper and lower envelopes of all configurations are summarized in Tab. 6.4. The index “up” of the coefficients stands for the upper envelope and “low” for the lower envelope.

Tab. 6.4: Coefficients a_{loc} and b_{loc} in eq. (6.16) for all tested configurations c1, c2 and c3

$\frac{z_{p\max}}{H_{m0}} = a_{loc} \cdot \left(1 + \tanh\left(\xi_{m-1,0} - b_{loc}\right)\right)$	tanα [-]	porosity [%]	$a_{loc,\,up}$ [-]	$b_{loc,\,up}$ [-]	$a_{loc,\,low}$ [-]	$b_{loc,\,low}$ [-]
configuration c1 and c2	1/3	45 and 20	1.51	2.03	1.33	4.28
configuration c3	1/6	20	1.45	1.63	1.43	2.49

The revetment porosity does not affect the location of the peak pressure for impact loads ($\xi_{m-1,0} < 2.4$). In contrast, the effect of the porosity is significant for $\xi_{m-1,0} > 2.4$ leading to larger values compared to the model for a smooth and impermeable revetment by Schüttrumpf (2001). In the transition zone between collapsing and surging breakers ($\xi_{m-1,0} = 2.4\text{-}4.0$) a large data scatter is observed. No significant difference is found for the location of the peak pressure between configurations c1 and c2 with different porosities (45% and 20 %). For all tested configurations upper and lower envelopes enclosing the data scatter are derived.

A much smaller scatter of the data is obtained for the flatter slope 1:6 of configuration c3 compared to that of the steeper slope 1:3 of revetments c1 and c2. However, the effect of the slope steepness is not fully clear and needs further investigations for a wider variation range of the slope steepness using numerical simulations or physical model tests.

6.4 Pressure distribution on the revetment

Together with the peak pressure on the revetment (sections 6.2) and its location (section 6.3), the spatial pressure distribution on the revetment is also crucial for an appropriate design. For the analysis of the wave spectra tests in this section, like in the preliminary tests with regular waves in Liebisch et al. (2013b), the prediction model proposed by Alcérreca Huerta & Oumeraci (2012) is applied to describe the pressure distribution separately for impact loads and non-impact loads:

$$\frac{p}{p_{max}} = \frac{A + B \cdot \left(-z / z_{p\max}\right)}{1 + C \cdot \left(-z / z_{p\max}\right) + D \cdot \left(-z / z_{p\max}\right)^2} \tag{6.21}$$

with: A, B, C, D = empirical coefficients [-]

z = vertical distance between SWL and PT [m]

z_{pmax} = vertical distance between SWL and location of p_{max} [m]

In this section the procedure of analysing the pressure distribution on the revetment is introduced in section 6.4.1. The effect of porosity on the pressure distribution is then analysed in section 6.4.2 separately for impact and non-impact loads. This separation is also applied for the analysis of the slope steepness effect on the pressure distribution in section 6.4.3.

6.4.1 Analysis procedure for the pressure distribution on the revetment

Based on the preliminary results of Liebisch et al. (2013b) the analysis of the spatial pressure distribution on the revetment is conducted separately for impact loads, including the transition zone, and non-impact loads. These results have also shown that the pressure distribution of the quasi-static loads, in contrast to the impact loads, is not affected by the revetment roughness and porosity. A close link between wave run-down and the pressure distribution due to a potential water layer on the slope was also identified. The lowest location of the pressure distribution is indicated by PT11 at the toe of the slope and the highest location is determined by the maximum run-up height (see Fig. 6.1).

Typical pressure signals recorded in the main tests with irregular wave tests are shown in Fig. 6.20 for an impact load and in Fig. 6.21 for a non-impact load on the highly porous revetment (configuration c1). For impact loads (Fig. 6.20), both magnitude and shape of the pressure on the revetment significantly differ from location to location. Comparatively, the shapes of the quasi-static pressure signals do not differ significantly at the different locations on the revetment (Fig. 6.21).

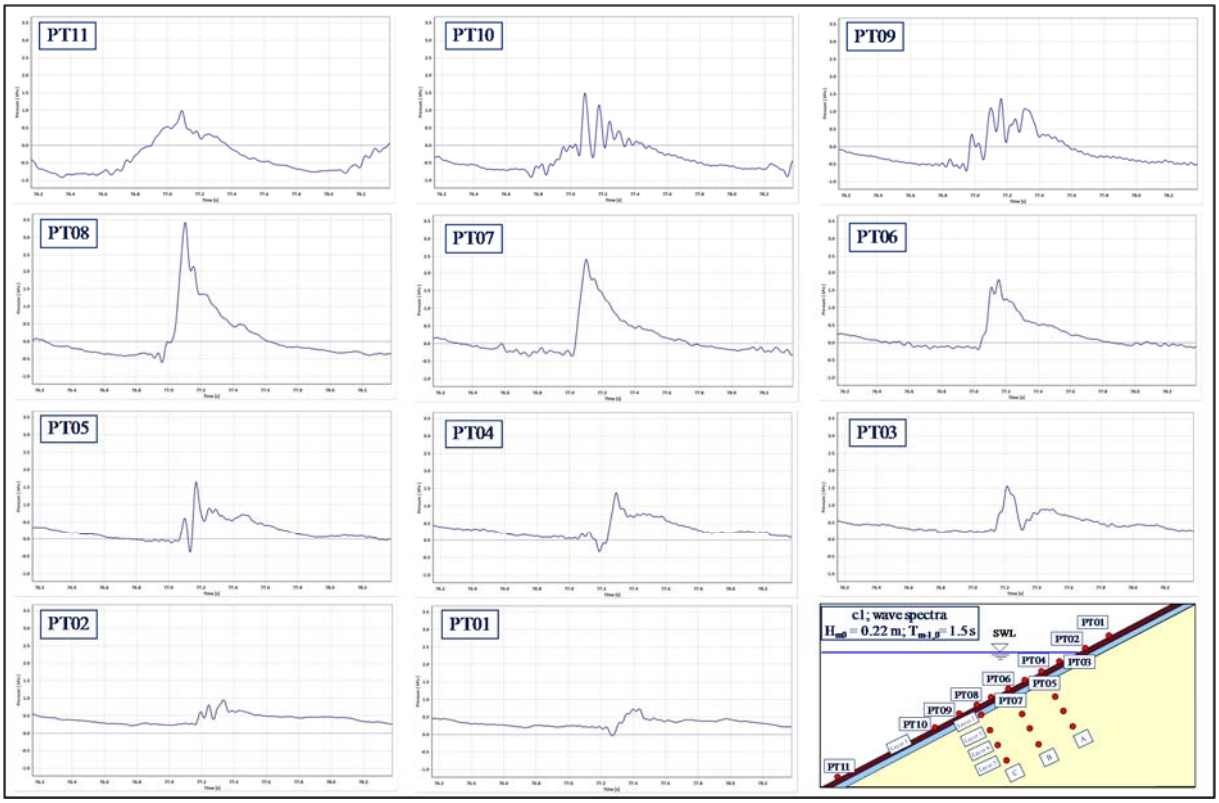

Fig. 6.20: Typical pressure signals recorded for impact load on the highly porous revetment (configuration c1)

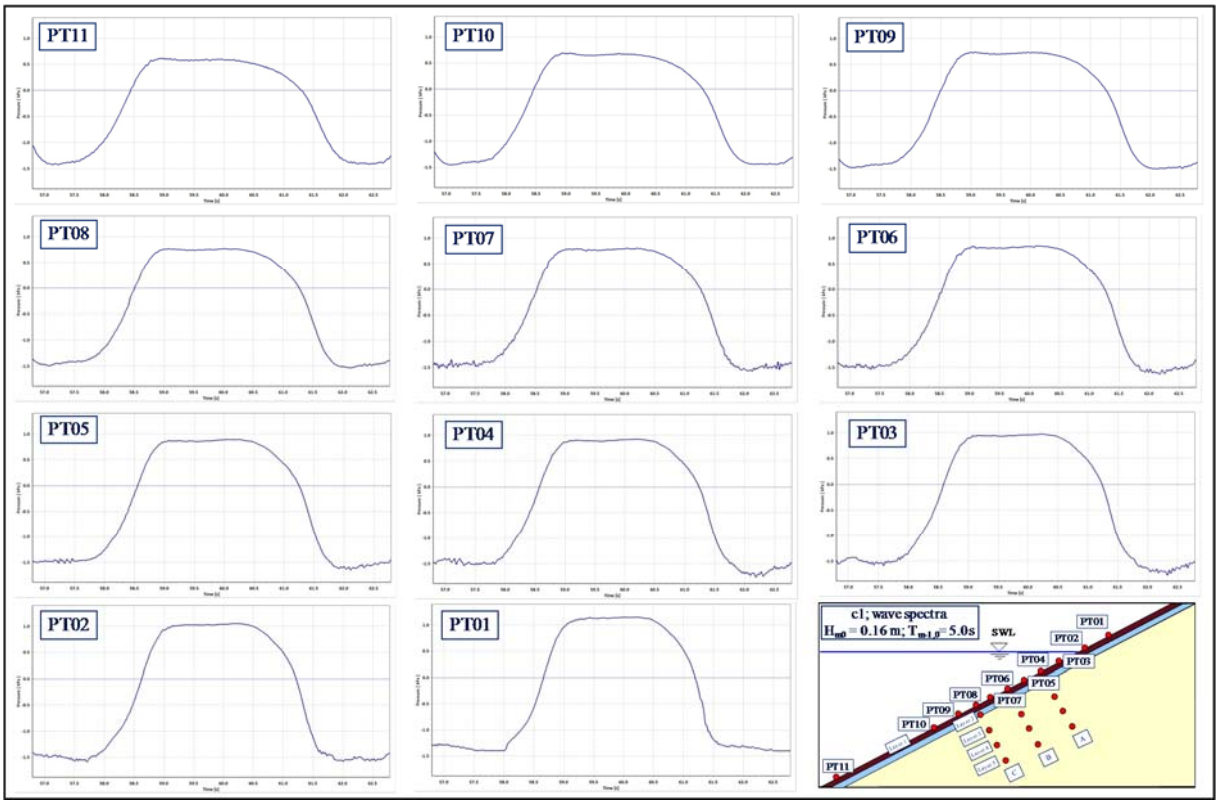

Fig. 6.21: Typical pressure signals recorded for non-impact load on the highly porous revetment (configuration c1)

For the analyses of the pressure distribution the recorded pressures were normalized by the value of the peak pressure measured during the test (p/p_{max}), thus resulting in a maximum value of 1.0 for the peak pressure. The location z of the pressure on the revetment relative to SWL is normalized by the location of the peak pressure z_{pmax} (see Fig. 6.15). For every pressure transducer on the revetment a pair of normalized pressure (p/p_{max}) and distance ($-z/z_{pmax}$) is determined, thus providing a non-dimensional pressure distribution.

The analysis of the pressure distribution is performed separately for the impact loads, including the transition zone, and the non-impact loads. For every test, the obtained values p/p_{max} are plotted against $-z/z_{pmax}$. The fitting model in eq. (6.21) is then applied to the data points of each tested revetment configuration. In contrast to the preliminary tests in Liebisch et al. (2013b), the approach using an upper envelope is applied due to the large scatter observed in all tests and all configurations, especially for impact loads. This procedure was already successfully applied on the data of the relative peak pressures in section 6.2 and also in the numerical study of Alcérreca Huerta (2014) for regular waves.

The empirical parameters A, B, C and D in eq. (6.21) must fulfil the condition $p/p_{max} = 1.0$ for $-z/z_{pmax} = -1.0$ which results from the normalized peak pressure and its normalized location.

6.4.2 Effect of revetment porosity

The pressure distribution on the revetment is analysed for the configurations with different revetment porosities and the same slope steepness (1:3), starting first with the impact loads, including the transition zone, followed by the non-impact loads (see load classification in Tab. 6.1).

6.4.2.1 Impact loads

For impact loads, the pressure distributions on the revetment are comparatively shown in Fig. 6.22a) for configuration c1 (n = 45%) and in Fig. 6.22b) for configuration c2 (n = 20%), both with the same slope 1:3. The pressure distribution for each test is indicated by a thin line connecting the pressure measured at each PT in layer 1 on the revetment. Then eq. (6.21) is applied to derive an upper envelope which encloses most of the data points. Furthermore, the developed model by Oumeraci et al. (2010b) for the PBA-revetment is comparatively shown in Fig. 6.22 a).

For both configurations straight lines leading from the maximum at $p/p_{max}=1$ to the run-up point with $p/p_{max}=0$ were found in some tests. In these tests the peak pressure was measured by PT01 at the highest PT-location. Above this location no pressure measurements were made and due to the straight line between the two data points, the derived upper envelope seems to underestimate the obtained values. Consequently, in the range above $p/p_{max}=0$ the upper envlope is indicated by a dashed line. However, despite the lack of measurement it can be

assumed that the shape of the pressure distribution is as steep as for all other tests in which measurements above the location of peak pressure were possible.

The model of Oumeraci et al. (2010b) in Fig. 6.22 developed in the GWK-tests for a PBA-revetment is hardly comparable with the derived upper envelopes, because it was developed based on the mean values in the GWK-tests. The derived upper envelopes enclose most of the obtained scatter leading to a slight overestimation of the obtained values. As already observed in the numerical investigations of Alcérreca Huerta (2014) for regular waves a larger scatter is obtained beneath the location of peak pressure independent of the revetment porosity which can be explained by the variability of wave breaking also resulting in a variability of pressure distribution. Above the location of peak pressure the trend is much clearer with less scatter up to the wave run-up height.

The second peak further upwards the slope which was observed in the numerical investigations of Alcérreca Huerta (2014) for regular waves was not detected in the physical model tests for both wave spectra and regular waves, probably due to the coarser resolution of the pressure measurement in the physical experiments and to the non-deployment of pressure transducers above PT01. As this occurred only in the numerical simulations in order to exclude the possibility of being only a numerical artefact, it is recommended to conduct more systematic physical model tests with a finer resolution of PTs between SWL and run-up height.

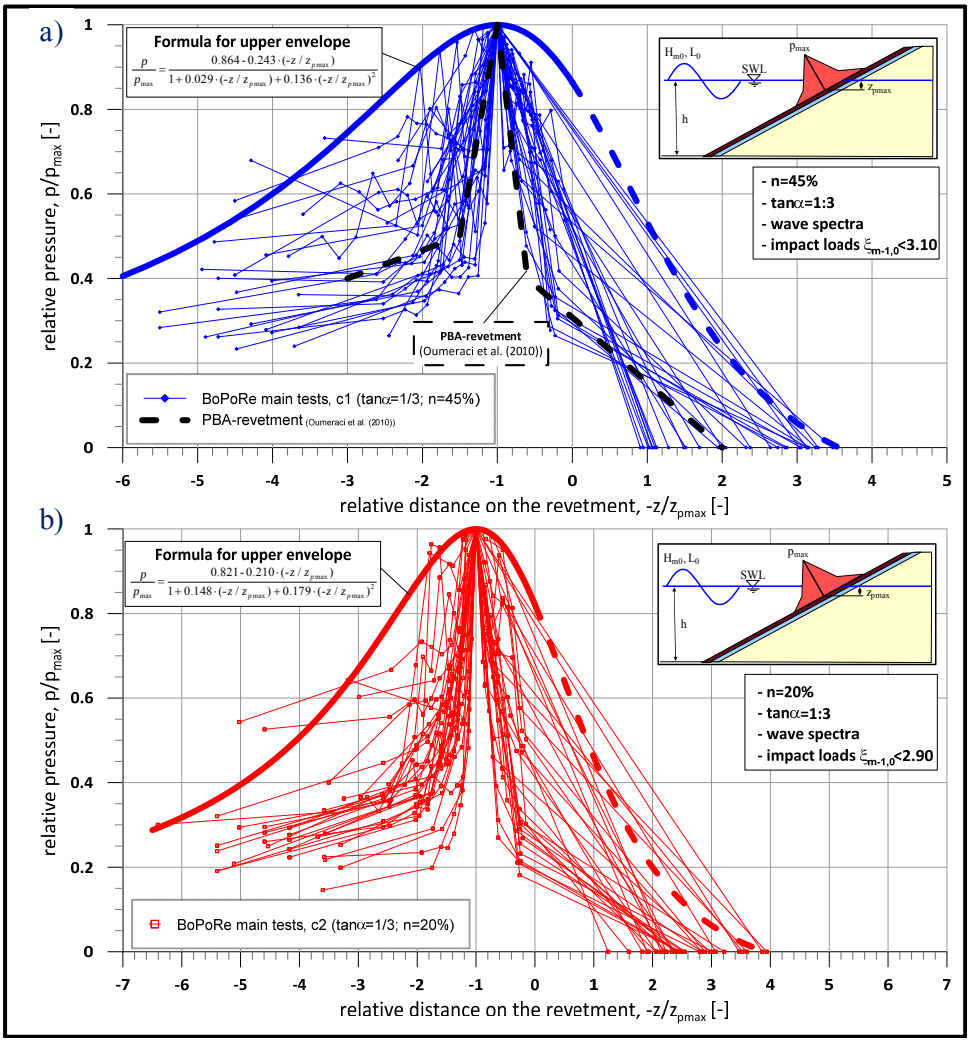

Fig. 6.22: Pressure distribution on the revetment for a) configuration c1 (tanα = 1/3; n = 45%) and b) configuration c2 (tanα = 1/3; n = 20%) for *impact loads* tested with wave spectra (see definition sketch in Fig. 6.1)

The following equations based on eq. (6.21) were found for the upper envelopes:

configuration c1:
$$\frac{p}{p_{max}} = \frac{0.864 - 0.243 \cdot \left(-z / z_{p\max}\right)}{1 + 0.029 \cdot \left(-z / z_{p\max}\right) + 0.136 \cdot \left(-z / z_{p\max}\right)^2} \tag{6.22}$$

configuration c2:
$$\frac{p}{p_{max}} = \frac{0.821 - 0.210 \cdot \left(-z / z_{p\max}\right)}{1 + 0.148 \cdot \left(-z / z_{p\max}\right) + 0.179 \cdot \left(-z / z_{p\max}\right)^2} \tag{6.23}$$

To better illustrate the effect of the porosity on the shape of the pressure distribution only the upper envelopes of the results in Fig. 6.22a) and Fig. 6.22b) are shown together in Fig. 6.23.

The upper envelopes obtained from both Fig. 6.22a) and Fig. 6.22b) differ slightly. As also observed for regular waves in Liebisch et al. (2013b), the upper envelope of the less porous revetment has a slightly steeper shape below the location of peak pressure than that of the more porous revetment. The differences above the location are significantly smaller due to the smaller

scatter of the data. Larger relative distances are obtained for the less porous revetment caused by larger wave run-up heights. However, independently of the porosity, the highest impact pressures are focussed on a relatively small area on the revetment.

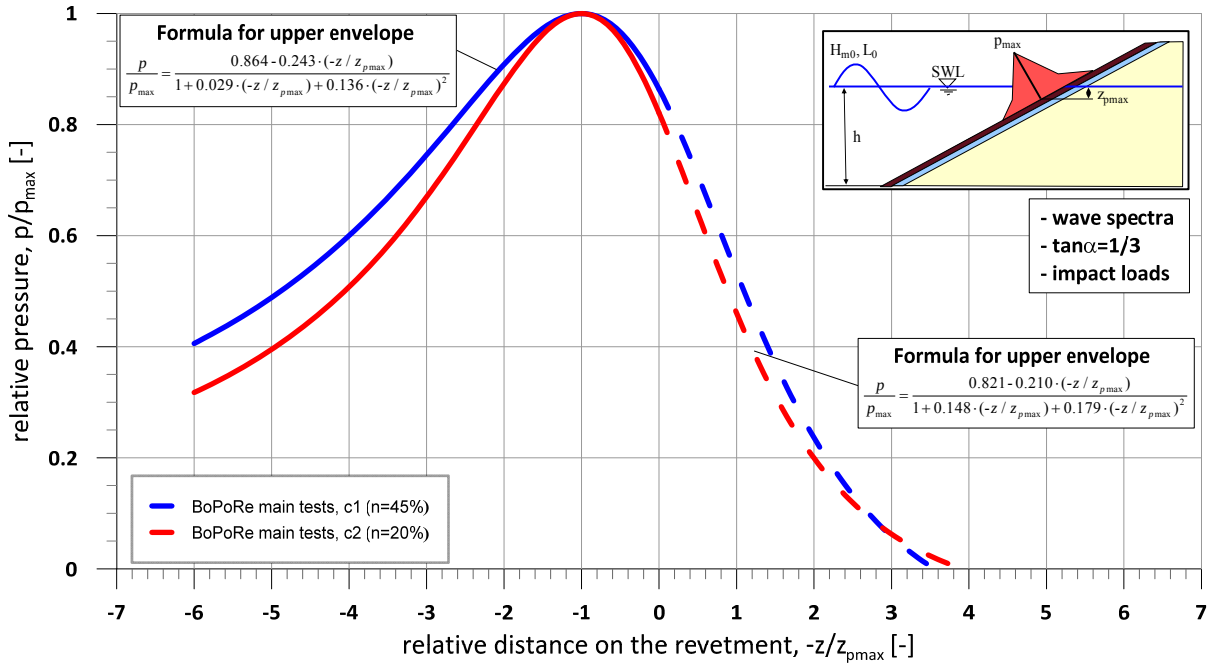

Fig. 6.23: Effect of revetment porosity on pressure distribution on the revetment for *impact loads* tested with wave spectra (slope steepness 1:3)

6.4.2.2 Non-impact loads

The effect of the revetment porosity on the pressure distribution is analysed for non-impact loads by considering the same revetment configurations as for impact loads, namely c1 with porosity 45% and c2 with porosity 20%. The pressure distributions for non-impact loads are comparatively shown in Fig. 6.24a) for configuration c1 and in Fig. 6.24b) for configuration c2 together with upper envelopes obtained by applying eq. (6.21) to the data.

Both Fig. 6.24 a) and b) show significantly less scatter in the pressure distribution compared to the impact loads. Below the location of the peak pressure the scatter slightly increases. This might be due to a larger amount of reflected energy in the lower locations. The model of Oumeraci et al. (2010b) in Fig. 6.24a) developed for non-impact loads in the GWK-tests for a PBA-revetment is in relatively good agreement with the obtained results of configuration c1, showing that the pressure distribution on the revetment for non-impact loads can also be correctly reproduced in the small-scale tests.

Also for non-impact loads the second pressure peak which was detected by Alcérreca Huerta (2014) above the maximum pressure on the slope was not found in the physical model tests due to the non-deployment of pressure transducers in the upper part of the swash zone.

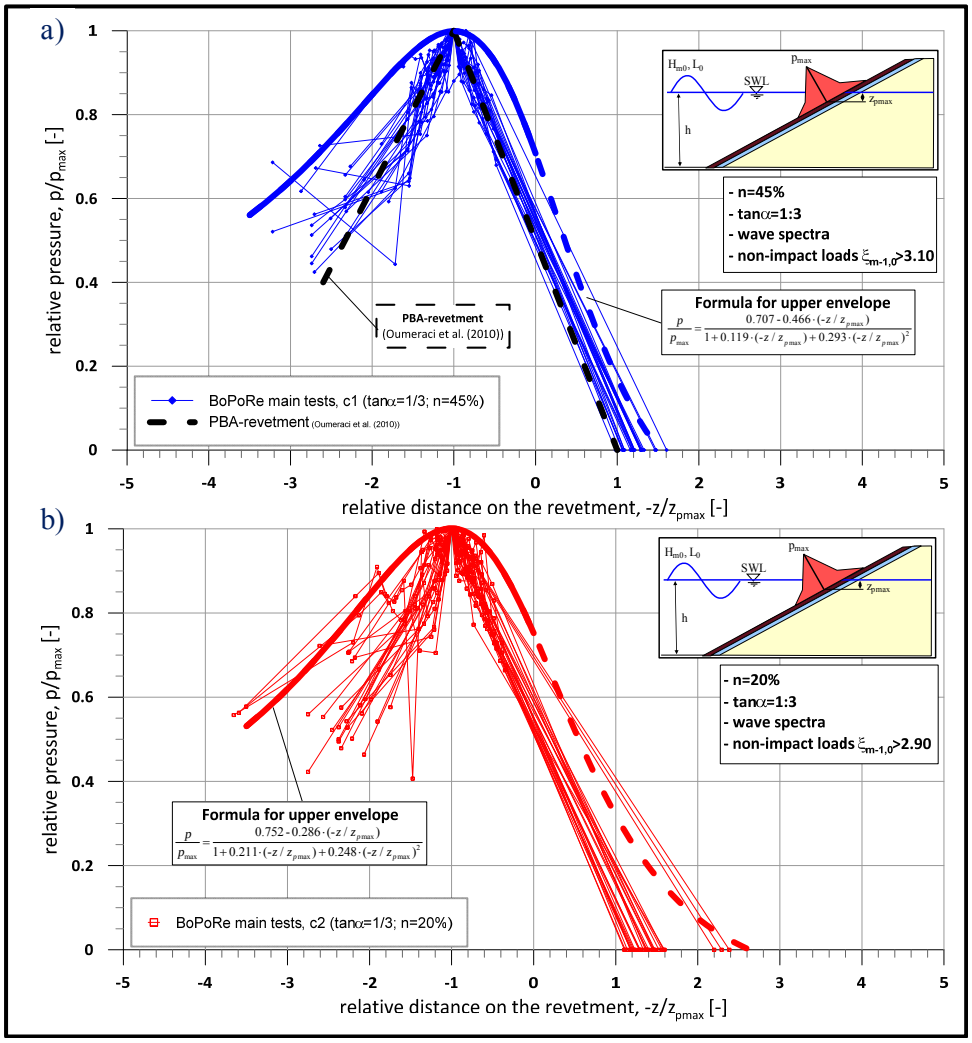

Fig. 6.24: Pressure distribution on the revetment for a) configuration c1 (tanα = 1/3; n = 45%) and b) configuration c2 (tanα = 1/3; n = 20%) for *non-impact loads* tested with wave spectra

Like in the previous section only the upper envelopes of the results for non-impact loads are shown together in Fig. 6.25 to better illustrate the effect of porosity on the pressure distribution.

As already obtained in Liebisch et al. (2013b), the porosity has no significant effect on the pressure distribution on the revetment. As shown in Fig. 6.25, larger differences mainly occur above the location of the peak pressure ($-z/z_{pmax} > -1$), which are caused by larger relative run-up heights on the less porous revetment configuration c2 (see section 5.3). This also confirms the findings of section 5.1 that for larger $\xi_{m-1,0}$ (non-impact loads) less energy is dissipated in the breaking process, so more energy remains for wave run-up. Compared to the pressure distribution for impact loads in Fig. 6.23 the result seems to be vice versa for non-impcact loads for $-z/z_{pmax} > -1$. It is assumed that this is caused by the lack of measurements between the location of peak pressure and the wave run-up height. This has to be proofed in further studies with a finer resolution of measuring points on the slope. Below the location of the peak pressure ($-z/z_{pmax} < -1$), both configurations provide an almost similar pressure distribution for non-impact loads.

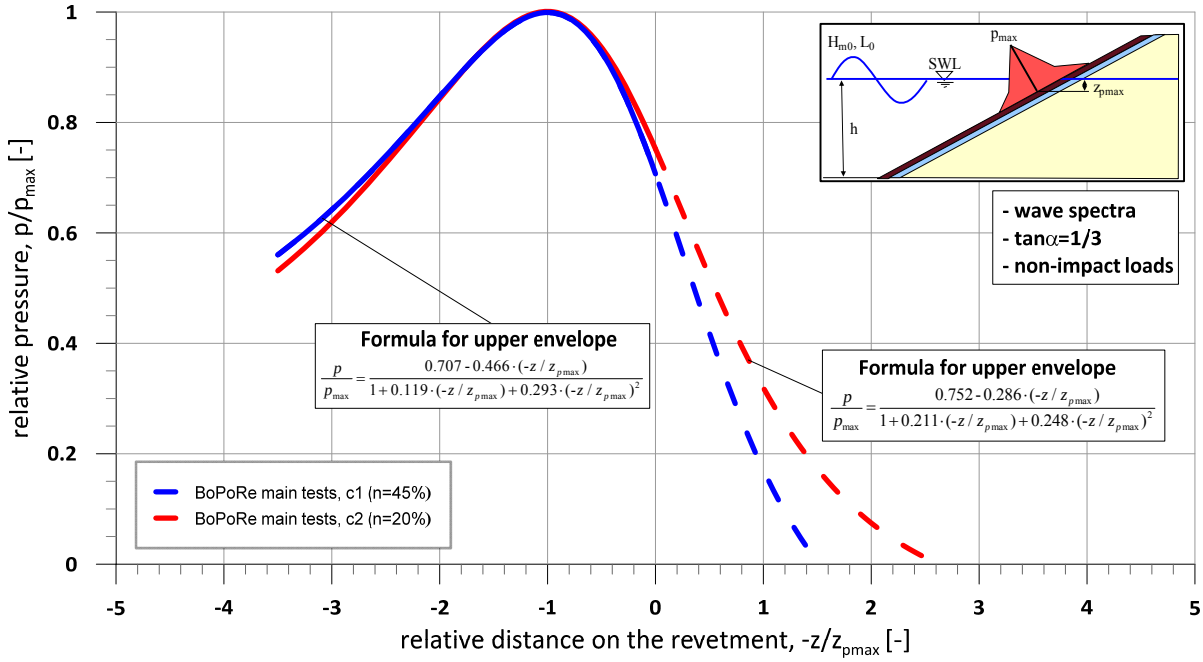

Fig. 6.25: Effect of revetment porosity on pressure distribution on the revetment for non-impact loads tested with wave spectra (slope steepness 1:3)

The following equations based on eq. (6.21) were obtained for the upper envelopes for non-impact loads:

configuration c1:
$$\frac{p}{p_{max}} = \frac{0.707 - 0.466 \cdot \left(-z / z_{p\max}\right)}{1 + 0.119 \cdot \left(-z / z_{p\max}\right) + 0.293 \cdot \left(-z / z_{p\max}\right)^2} \tag{6.24}$$

configuration c2:
$$\frac{p}{p_{max}} = \frac{0.752 - 0.286 \cdot \left(-z / z_{p\max}\right)}{1 + 0.211 \cdot \left(-z / z_{p\max}\right) + 0.248 \cdot \left(-z / z_{p\max}\right)^2} \tag{6.25}$$

6.4.3 Effect of the revetment slope steepness

Like in the previous section for the effect of the porosity, in this section the effect of the slope steepness on the pressure distribution on the revetment is analysed separately for impact loads (and transition zone) and non-impact loads. For this purpose, the tests with configurations c1 with a steeper slope 1:3 and c3 with a slope 1:6, both with the same revetment porosity n = 45%, are comparatively considered.

6.4.3.1 Impact loads

The pressure distributions for all tests with impact loads and the resulting upper envelope based on eq. (6.21) is depicted in Fig. 6.26 for configuration c3 with the flatter slope 1:6, showing a larger scatter of the results of the different tests compared to the results of configurations c1 with the steeper slope 1:3 and the same porosity in Fig. 6.22a).

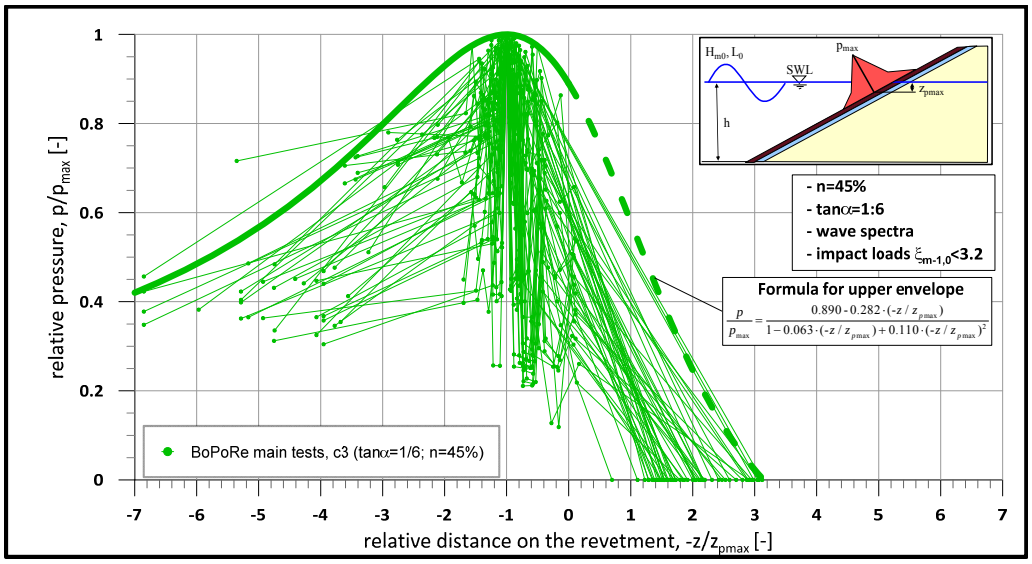

Fig. 6.26: Pressure distribution on the revetment for configuration c3 (tanα = 1/6; n = 45%) for *impact loads* tested with wave spectra

This larger scatter as compared to the steeper slope was also observed for regular waves in Liebisch et al. (2013b). Due to the remaining water layer on the flatter slope during wave run-down, the breaking process of the incident waves is significantly affected, leading to higher turbulence and more complex flow, and thus to more spatial variability of the pressure. To better illustrate the effect of the slope steepness on the shape of the pressure distribution only the upper envelopes of the results in Fig. 6.22a) and Fig. 6.26 are drawn together in Fig. 6.27, clearly showing that the flatter slope 1:6 results in a wider pressure distribution on the revetment than that of the steeper slope 1:3.

The slightly smoother pressure distribution for the flatter slope was also observed in the preliminary tests with regular waves of Liebisch et al. (2013b) for the revetment configurations with the roughness elements on the slope. In both cases the residence time of the water layer on the slope during wave run-dow is longer. This does not only lead to a larger data scatter due to higher turbulence on the slope, but also to a distribution of the energy dissipation over a larger area and accordingly to a wider shape of the pressure distribution. Above the location of peak pressure only slight differences occur for the two revetments with different slope steepnesses with smaller wave run-up heights for the flatter slope 1:6, which was expected.

The following equation based on eq. (6.21) was found for the upper envelope for impact loads on revetment c3 with slope 1:6 and porosity n = 45%:

$$\frac{p}{p_{max}} = \frac{0.890 - 0.282 \cdot \left(-z / z_{p\max}\right)}{1 - 0.063 \cdot \left(-z / z_{p\max}\right) + 0.110 \cdot \left(-z / z_{p\max}\right)^2} \tag{6.26}$$

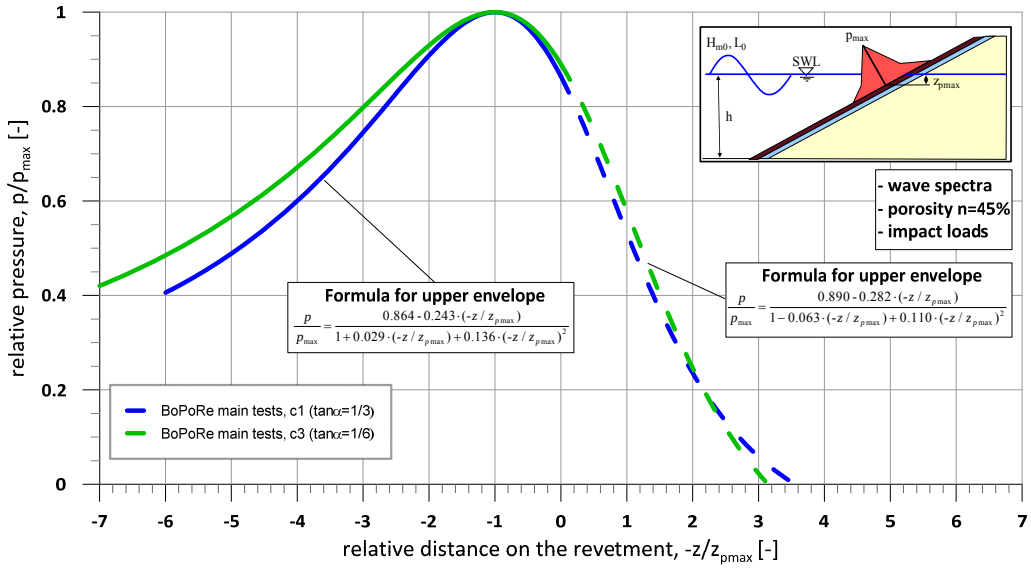

Fig. 6.27: Effect of the slope steepness on pressure distribution on the revetment for *impact loads* tested with wave spectra (porosity n = 45%)

6.4.3.2 Non-impact loads

The effect of the slope steepness on the pressure distribution is analysed for non-impact loads by considering the same revetment configurations as for non-impact loads, namely c1 with the slope 1:6 and c3 with the slope 1:6, both with the same revetment porosity n = 45%. The pressure distribution for non-impact load is shown in Fig. 6.28 for the slope 1:6, which should be compared with Fig. 6.24a) for revetment c1 with the steeper slope 1:3 and the same porosity. This comparison shows a larger data scatter for the 1:6 slope than for the 1:3 slope. This is due to the remaining water layer on the flatter slope during wave run-down. The breaking process of the incident waves is significantly affected, leading to higher turbulence and more complex flow, and thus to more spatial variability (also see section 6.4.2.2).

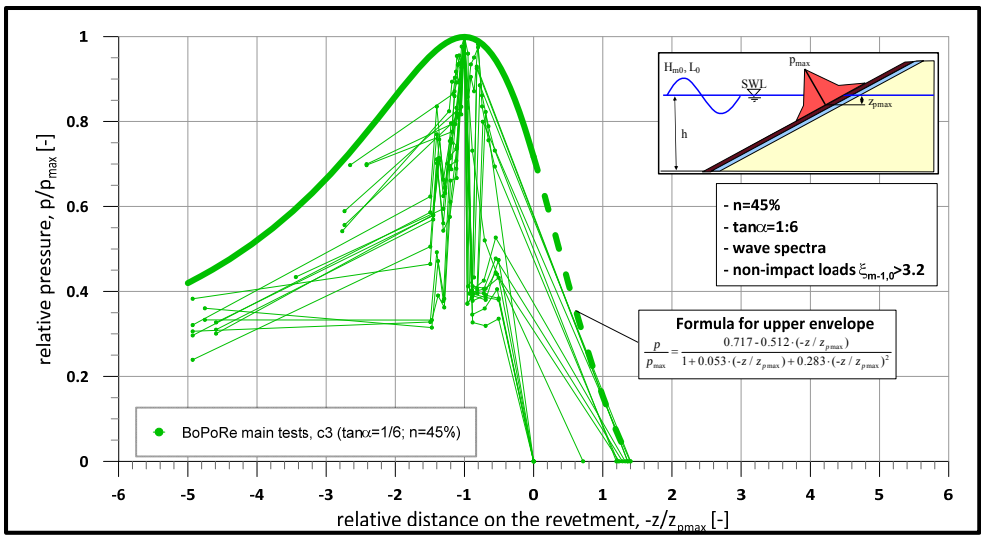

Fig. 6.28: Pressure distribution on the revetment for configuration c3 (tanα = 1/6; n = 45%) for *non-impact loads* tested with wave spectra

To better illustrate the effect of the slope steepness on the shape of the pressure distribution only the upper envelopes of the results in Fig. 6.24a) and Fig. 6.28 are drawn together in Fig. 6.29, clearly showing that, despite the considered scatter of the data in Fig. 6.28, the effect of the slope steepness on the upper envelope of the pressure distribution is neglegibly small, surprinsingly also above SWL ($-z/z_{pmax} > 0$) where the relative wave run-up on the flatter slope 1:6 is only slightly smaller.

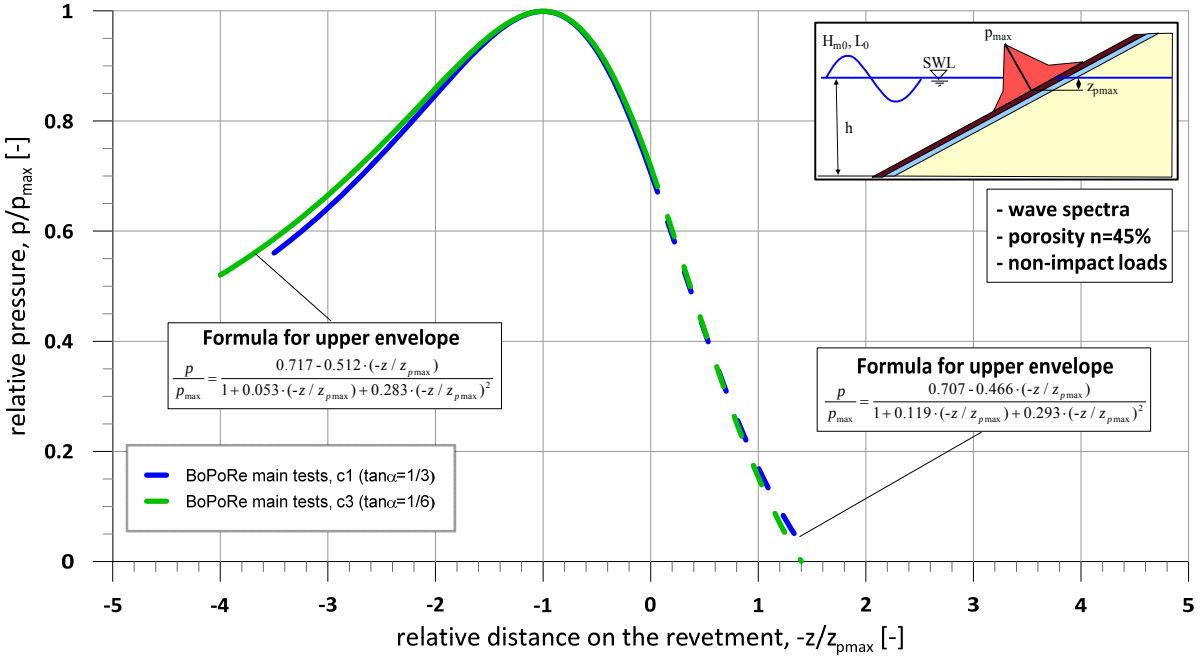

Fig. 6.29: Effect of the slope steepness on the pressure distribution on the revetment for *non-impact loads* tested with wave spectra (porosity n = 45%)

The following equation based on eq. (6.21) was found for the upper envelope for non-impact loads on revetment c3 with slope 1:6 and porosity n = 45%:

$$\frac{p}{p_{max}} = \frac{0.717 - 0.512 \cdot \left(-z / z_{p\max}\right)}{1 + 0.053 \cdot \left(-z / z_{p\max}\right) + 0.283 \cdot \left(-z / z_{p\max}\right)^2} \tag{6.27}$$

The observed difference between the pressure envelopes for the non-impact loads on the three revetment configurations c1, c2 and c3 in Fig. 6.25 and Fig. 6.29 is not significant and the envelopes only differ for the relative wave run-up height.

The values of the coefficients for the upper envelopes based on eq. (6.21) for all tested revetment configurations c1, c2 and c3 are summarized in Tab. 6.5 for both impact and non-impact loads.

Tab. 6.5: Determined coefficients A, B, C and D in eq. (6.21) for all tested configurations for impact loads and non- impact loads

$\frac{p}{p_{max}} = \frac{A + B \cdot \left(-z / z_{p\max}\right)}{1 + C \cdot \left(-z / z_{p\max}\right) + D \cdot \left(-z / z_{p\max}\right)^2}$	impact loads				non-impact loads			
	A	B	C	D	A	B	C	D
c1 (n=45%; tanα=1/3)	0.864	-0.243	0.029	0.136	0.707	-0.466	0.119	0.293
c2 (n=20%; tanα=1/3)	0.821	-0.210	0.148	0.179	0.752	-0.286	0.211	0.248
c3 (n=45%; tanα=1/6)	0.890	-0.282	-0.063	0.110	0.717	-0.512	0.053	0.283

For impact loads, both porosity and slope steepness affect the pressure distribution. With increasing porosity and a flatter slope, the pressure distribution becomes slightly wider over the slope.

For non-impact loads, the effect of the porosity and the slope steepness is noticeable only far above SWL, where the pressure distribution is expectedly wider for steeper slopes and smaller porosity associated with larger wave run-up.

The model proposed by Alcérreca Huerta & Oumeraci (2012) was successfully applied for the upper envelopes of the data. A relatively good agreement is found between the experimental results of configuration c1 and those of the GWK-tests of Oumeraci et al. (2010b) (both with the same slope steepness and a similar porosity).

6.5 Summary and Conclusions

In this chapter, the wave-induced pressure on the revetment were addressed by analysing the effect of the revetment porosity and slope steepness on the peak pressure, its location and the pressure distribution on the revetment for both impact load and non-impact load.

In section 6.1, a wave load classification according to surf similarity parameter $\xi_{m-1,0}$, was conducted. The flatter 1:6 slope provides a larger transition zone than the steeper slopes 1:3.

In section 6.2, it was shown that the effect of the revetment porosity on the damping of impact loads is dominant as compared to the effect of the slope steepness. Non-impact loads are just slightly affected by a changing porosity. The effect of the slope steepness on the peak pressure is generally less clear than that of the porosity. Slope steepness affects the peak pressures for quasi-static loads, but no noticeable effect on the impact pressure peak could be observed. The effect of the slope steepness on the quasi-static pressure on the revetment was found to decrease with smaller deep water wave steepness H_{m0}/L_0. Tentative formulae are provided for all tested configurations considering only the upper envelopes of the total peak pressure values.

In Section 6.3, the results of the analysis of the location of the peak pressure on the revetment show that the effect of the revetment porosity is only significant for $\xi_{m-1,0} > 2.4$ in comparison

with a smooth impermeable revetment. In contrast, no significant difference is found for the results of the tested revetments with porosity 45% and 20 %. The effect of the slope steepness on the location of the peak pressure is more noticeable than that of the porosity particularly shown by the much smaller scatter for the flatter slope 1:6. Due to the obtained scatter upper and lower envelopes are considered for the data.

In section 6.4, the pressure distribution on the revetment was analysed separately for impact and non-impact loads. For impact loads the pressure distribution on the revetment is affected by both revetment porosity and slope steepness. The pressure distribution becomes wider with increasing porosity and a flatter slope of the revetment. For non-impact loads, the effect of the slope steepness is noticeable only far above SWL, where the pressure distribution is expectedly wider for steeper slopes and smaller porosity associated with larger wave run-up. Tentative formulae for the upper envelopes are proposed for all tested revetment configurations, showing the effect of the revetment porosity and slope steepness.

Overall, the results of this chapter have contributed to an improved understanding of the processes on the revetments of different porosity and slope steepness. However, these results have limitations, so that further research will be needed. Unexpectedly large non-impact loads with relative peak pressure values up to 4.0 on the porous revetments tested with different porosities (n = 20% and n = 45%) occurred in the small scale und in the 1:5 up-scaled GWK tests with irregular waves on PBA-revetments (n=40%). Whether and how this is related to the porosity of the revetments can only be answered by further studies. Though the quasi-static component of the peak pressure in the prediction formulae is generally more reliable, further research might be required for the 1:6 slope and surf similarity parameters $\xi_{m-1,0} > 4.5$, since tests for the 1:6 slope were performed only for $\xi_{m-1,0} < 4.5$. The effect of the revetment porosity and slope steepness on the peak pressure, its location and the pressure distribution on the revetment was determined in the main tests of this study by considering only two well-selected values for each of these two parameters. Though these two values were carefully selected based on the results of preliminary tests (Liebisch et al. (2013a)), more systematic physical model tests or numerical studies for a wider range of values of the slope steepness and revetment porosity are still needed. The second pressure peak which was identified within the upper part of the swash zone in the numerical study with regular waves by Alcérreca Huerta (2014) was not be observed in the laboratory tests of this study and of the previous studies. As this occurred only in the numerical simulations in order to exclude the possibility of being only a numerical artefact, it is recommended to conduct more systematic physical model tests with a finer resolution of PTs between SWL and run-up height.

7 Processes in the sand core beneath the revetment and stability analysis

In this chapter the data from the pressure transducers (PTs) in the sand core beneath the revetment (Fig. 7.1 and for more details also Fig. 4.6, Fig. 4.8 and Fig. 4.9) are analysed. The PTs were placed in three columns A, B and C perpendicular to the slope. Each column includes five PTs thus resulting in PT-layers 1 to 5 parallel to the slope.

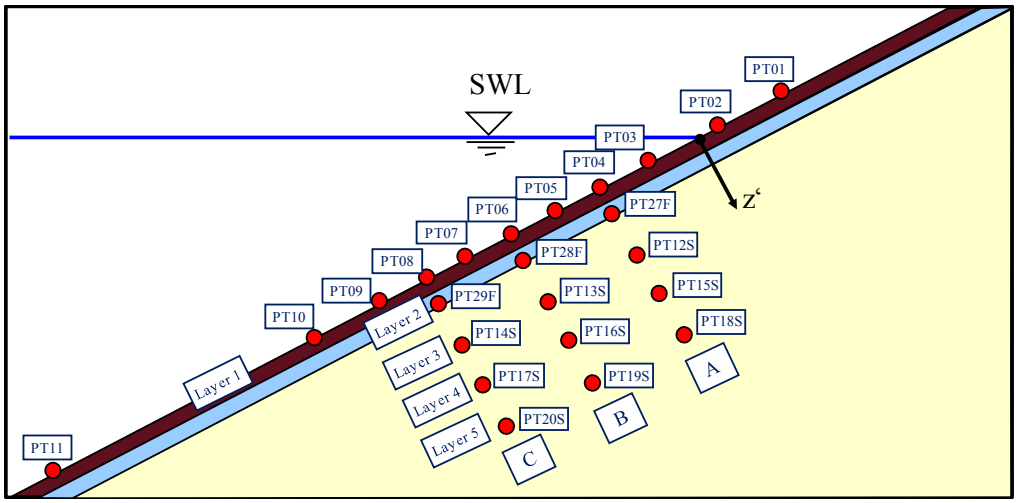

Fig. 7.1: Columns and layers of pressure transducers beneath the revetment

As already shown in section 4.4, the initial pressure p_0 is measured on top of the sand layer in the filter layer (layer 2) while the records obtained in the other three PT-layers at depths of 5 cm (layer 3), 10 cm (layer 4) and 20 cm (layer 5) are used to analyse the damping process of the pore pressures. The locations of the additional pressure transducers in the sand as shown in Fig. 7.2, are at a larger depth in the sand core where the transient pore pressure is fully damped, so that only the residual pore pressure induced by the changes in the internal mean water level (IMWL) is recorded.

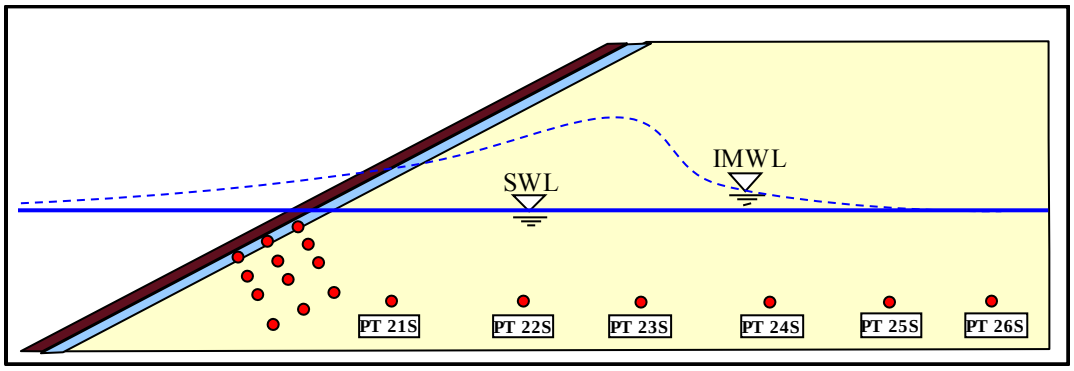

Fig. 7.2: Pressure transducers for the measurement of IMWL

In section 7.1 the wave damping performance of the porous revetments is analysed. The damping of the wave-induced pressure on the revetment, which is transferred through the

revetment in the sand core is addressed in section 7.2. The analysis of the development of the IMWL is performed in section 7.3. Based on the pressure differences between the locations of the PTs in the sand core, a stability analysis of the sand foundation is conducted in section 7.4.

7.1 Wave damping performance of porous revetments

The effect of the structure porosity on the damping of the peak pressure on bonded porous revetment depending on the porosity was already discussed in section 6.2. The effect of the porosity on wave-induced pressure propagating through the porous cover and filter layer was already addressed in the preliminary tests in Liebisch et al. (2013b) for the different cover layers (made of metal sheets) and in the large-scale tests in the GWK-tests with two revetments with significantly different porosities (n = 3% and n = 40%). A comparative analysis of the latter was conducted in Liebisch et al. (2012). For the determination of the wave damping performance, the three pressure transducers on the top of the sand layer PT 27F, 28F and 29F (see Fig. 7.1) are analysed. The pressures in layer 2 for all tests and configurations are determined as related to the maximum pressures p_{max} on the revetment recorded by the PTs in layer 1.

Typical signals recorded in PT-layer 1 and the associated signal in the PT-layer 2 beneath are exemplarily shown in Fig. 7.3 for selected PTs for a) impact load and b) non-impact load on and just beneath revetment configuration c1.

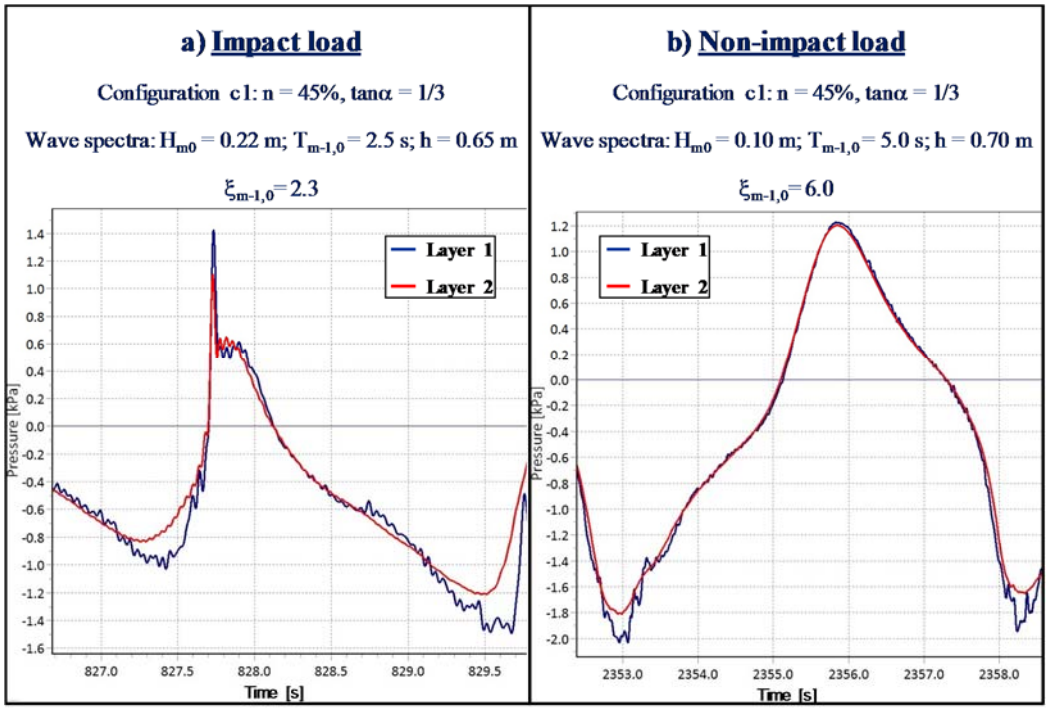

Fig. 7.3: Typical recorded signals of pressure transducers in PT-layer 1 and PT-layer 2 for a) impact load and b) non-impact load on and just beneath revetment configuration c1 (see definition sketch in Fig. 7.1)

Like in the previous chapters, the effect of the revetment porosity and that of slope steepness are analysed separately.

7.1.1 Effect of the revetment porosity

The damping effect of the revetment porosity on the pressure in layer 2 is first investigated for the configurations with the same slope steepness (1:3) and two different porosities (c1: n = 45%; c2: n = 20%). The results are drawn in Fig. 7.4 and in Fig. 7.5 for configuration c1 and c2, respectively.

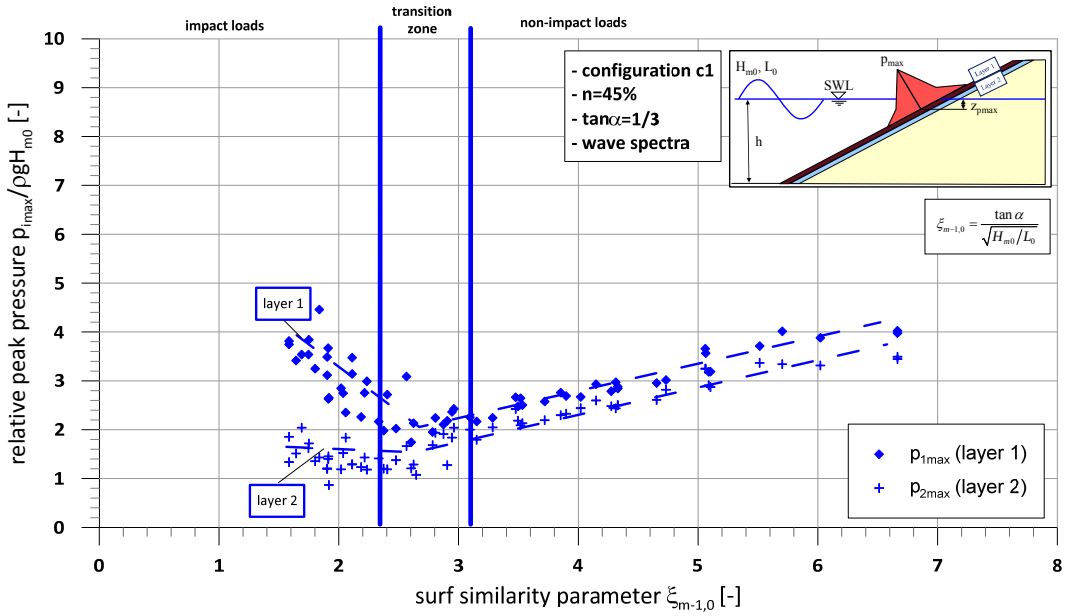

Fig. 7.4: Relative peak pressure on and just beneath configuration c1 tested with wave spectra (porosity n = 45%; tanα = 1/3)

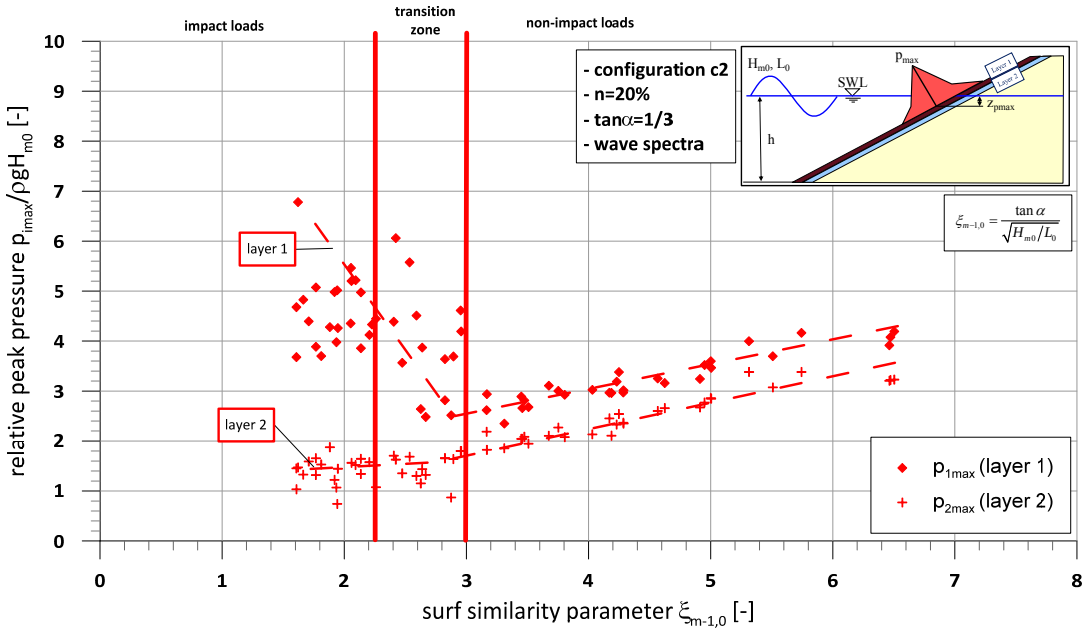

Fig. 7.5: Relative peak pressure on and just beneath configuration c2 tested with wave spectra (porosity n = 20%; tanα = 1/3)

In both figures Fig. 7.4 and Fig. 7.5 the largest damping effect occurs for impact pressures and in the transition zone ($\xi_{m-1,0} < 3.0$), i.e. a large amount of the impact pressure component is damped by the cover layer and is not transferred to layer 2. For comparison, the damping effect for the low-porous revetment is much larger than expected (Fig. 7.5). For the highly porous revetment the impact pressure is strongly damped while the quasi-static pressure is almost not affected by the revetment (Fig. 7.4).

The results in Fig. 7.4 and Fig. 7.5 are brought together in Fig. 7.6 by plotting the damping performance D_p of the wave-induced pressure through the porous revetment (D_p defined in eq. (7.1)) against surf similarity parameter $\xi_{m-1,0}$.

$$D_p = 1 - \left(p_{2max} / p_{1max} \right) \tag{7.1}$$

In fact, Fig. 7.6 better highlights the effect of the porosity on the pressure damping performance D_p through the direct comparison of D_p for a highly porous revetment (c1: n = 45%) with D_p for a less porous revetment (c2: n = 20%). Overall, the latter has a larger damping performance than the highly porous revetment. However, for both porosities, the damping performance varies almost similarly over the entire range of tested surf similarity parameters: D_p increases with decreasing surf similarity parameter in the range of impact loads and the transition zone ($\xi_{m-1,0} < 3.0$) while it is almost not affected for non-impact loads ($\xi_{m-1,0} > 3.0$). Fig. 7.6 also clearly shows that impact loads are hardly transferred through the cover layer while non-impact loads are only slightly damped.

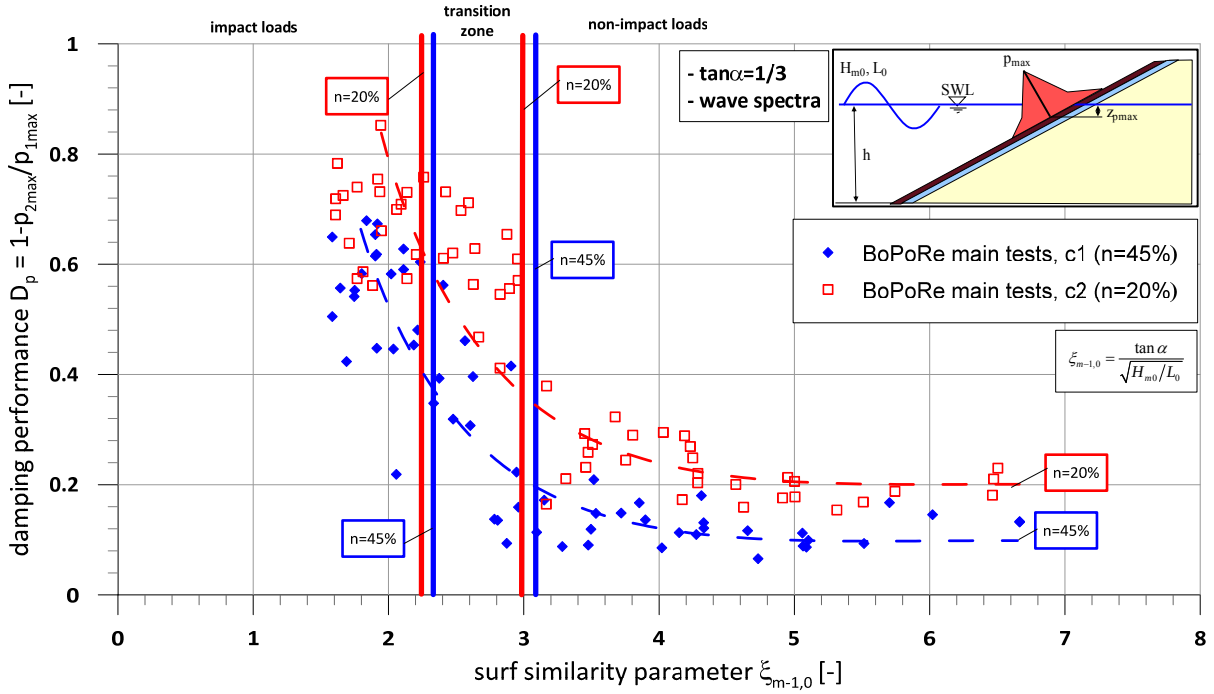

Fig. 7.6: Effect of the revetment porosity on pressure damping performance D_p of the revetment vs. surf similarity parameter $\xi_{m-1,0}$ for wave spectra (slope steepness 1:3)

To get a first rough idea of potential scale effects associated with the pressure damping process, the results of maximum pressure p_{2max} just beneath the revetment of configuration c1 (n = 45%)

are shown in Fig. 7.7 together with the results of the large-scale tests of Oumeraci et al. (2010b) and the preliminary tests of Liebisch et al. (2013b).

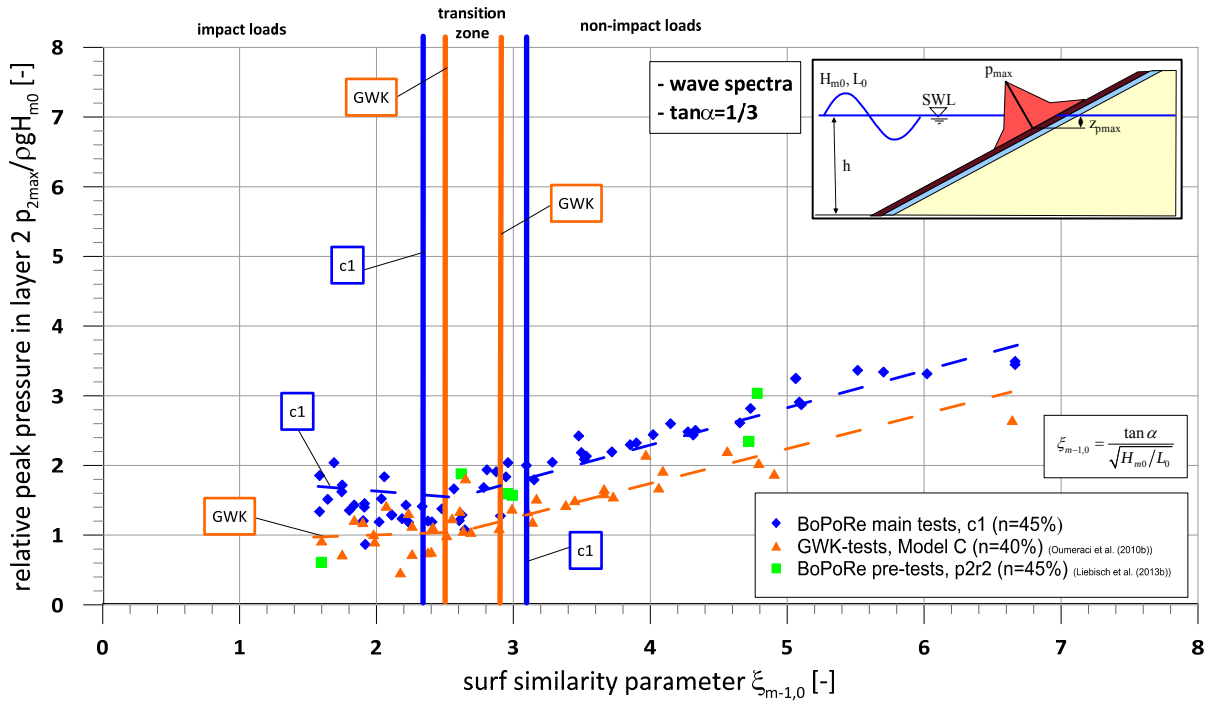

Fig. 7.7: Comparison of different data series of relative peak pressure just beneath the revetment as a function of surf similarity parameter $\xi_{m-1,0}$ for wave spectra (slope steepness 1:3)

Despite the scatter of the data, the GWK-tests in Fig. 7.7 surprisingly provide relative peak pressures beneath the revetment which are up to 40% smaller than the obtained values in the small-scale tests. Even for non-impact loads ($\xi_{m-1,0} > 3.0$) no agreement like in Fig. 6.8 is achieved for configuration c1 and the GWK-tests. This might be explained by the larger revetment thickness for model C of the GWK-tests. The peak pressures on the revetment are transferred and damped accordingly through the revetment and a larger revetment thickness results in a larger damping. For configuration c1 in the BoPoRe-main tests the revetment material was scaled 1:2.5 (GWK: 20/40 mm; BoPoRe: 8/16 mm; see section 4.2) leading to a distortion factor of 2. In Fig. 7.7 this distortion factor is even 2.5, because GWK-model C was made of 16/36 mm crushed granite. For the scaling of the revetment thickness a smaller distortion factor results, which is 1.42 for the revetment thickness of configuration c1 (d_{rev} = 10 cm) in relation to that of GWK-model C (d_{rev} = 35 cm). A direct comparison of the two revetments is therefore hardly possible.

As for the pressure (p_1) recorded in layer 1 on the revetment (see section 6.2.3), a distinction between impact and quasi-static loads is also required in the analysis of the pressure (p_2) recorded in layer 2 just beneath the revetment for the development of a prediction formula, which can be found in section 7.1.3.

7.1.2 Effect of the revetment slope steepness

The damping performance of the cover layer on the wave-induced pressures is investigated in this section with a focus on the effect of slope steepness. For revetment configuration c3 with the same porosity 45% as configuration c1, but with a flatter slope (tanα = 1/6), the results of the relative maximum pressure on the revetment (layer 1) together with the relative pressure just beneath the revetment in layer 2 are shown in Fig. 7.8 as compared to Fig. 7.4 for configuration c1 with tanα = 1/3 and n = 45%.

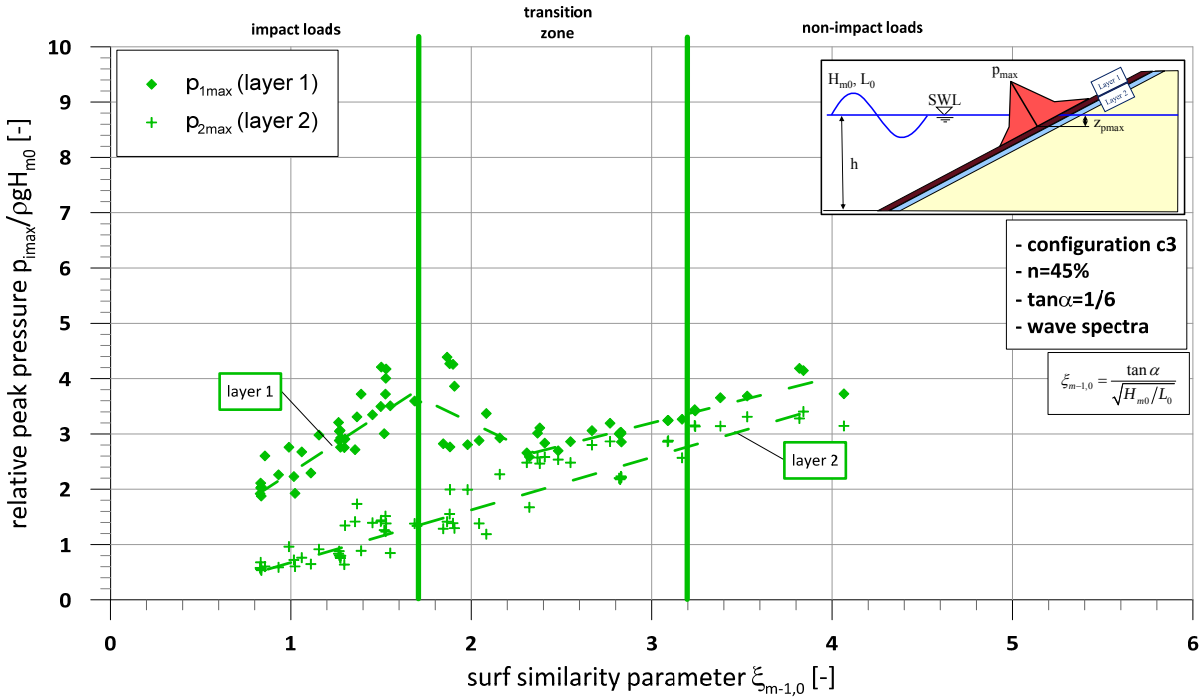

Fig. 7.8: Relative peak pressures on and just beneath configuration c3 tested with wave spectra (porosity n = 45%; tanα = 1/6)

Also for the flater slope 1:6, the damping behaviour of the highly porous revetment becomes obvious in Fig. 7.8. The maximum damping rate is achieved for $\xi_{m-1,0}$-values in the range of impact pressures (see also Fig. 7.9). Compared to configuration 1 with slope 1:3 and the same porosity in Fig. 7.4, the transfer of the impact component seems to be smaller for configuration c3 due to the water layer which remains on the revetment for a longer time, thus leading to an additional damping of the wave-induced pressures. Like for the other two configurations c1 and c2 on the same slope 1:3, the quasi-static component is almost not affected. The damping performance D_p is plotted in Fig. 7.9 comparatively for the two highly porous revetment configurations c1 and c3 with different slopes (1:3 and 1:6 respectively) against surf similarity parameter $\xi_{m-1,0}$ showing that the effect of slope steepness is less significant than that of the porosity and almost negligible for non-impact loads (see Fig. 7.9). For impact loads and the transition zone ($\xi_{m-1,0} < 3.0$) the pressure damping is less pronounced for the flatter slope 1:6. This might be due to the high variability associated with wave breaking in that range and due to the longer residence time of the water layer on the 1:6 slope. A final answer can be obtained only through further studies.

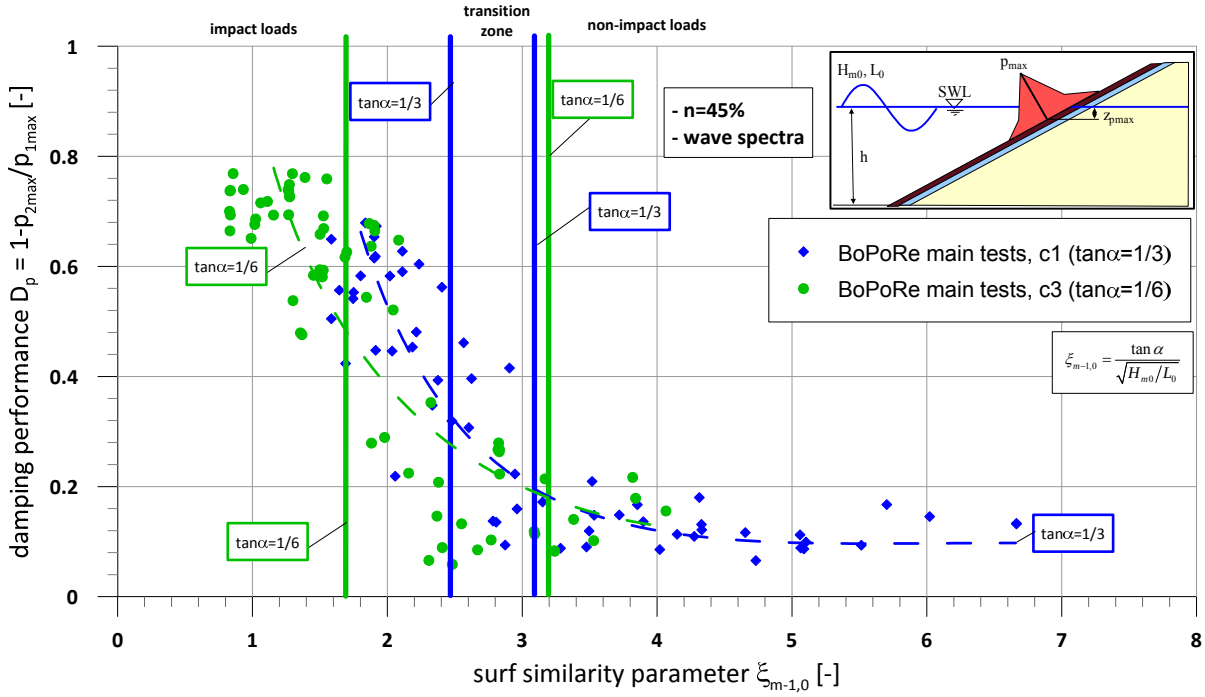

Fig. 7.9: Effect of the slope steepness on pressure damping performance D_p of the revetment vs. surf similarity parameter $\xi_{m-1,0}$ for wave spectra (porosity n = 45%)

7.1.3 Prediction formula for relative wave-induced pressure just beneath the revetment

Like in section 6.2.4 the development of the model to describe the maximum pressures just beneath the revetment is conducted in two steps. The development of empirical formulae for quasi-static pressure p_{2stat} is conducted like in section 6.2.3 (see Fig. 6.10) by deriving upper envelopes for the two data sets based on the model proposed by Liebisch et al. (2013b).

The quasi-static component in layer 2 (p_{2stat}) is considered as a function of surf similarity parameter $\xi_{m-1,0}$ for the two configurations c1 and c2 with a slope steepness of 1:3 and different porosities (c1: n = 45%; c2: n = 20%) in Fig. 7.10. For both porosities, the data scatter increases for $\xi_{m-1,0} < 3.0$. As already discussed for the pressures on the revetment, this scatter is generated by the relatively higher variability of the quasi-static component of the impact loads as compared to the quasi-static load. It can be seen that the quasi-static pressures p_{2stat} of the two revetment configurations with different porosity in Fig. 7.10 show less differences than for p_{1stat} on the revetment (see Fig. 6.10). Due to the lower porosity the relative quasi-static pressure seems to be slightly smaller just beneath the revetment in layer 2. As also indicated in Fig. 7.6, the pressure damping for configuration c2 with the lower porosity is slightly larger for non-impact loads This leads to slightly smaller values for relative quasi-static pressure compared to Fig. 6.10 where they were slightly larger than those for configuration c1 on the revetment. It is expected that this difference becomes larger for larger differences in porosity, but this might need further investigations.

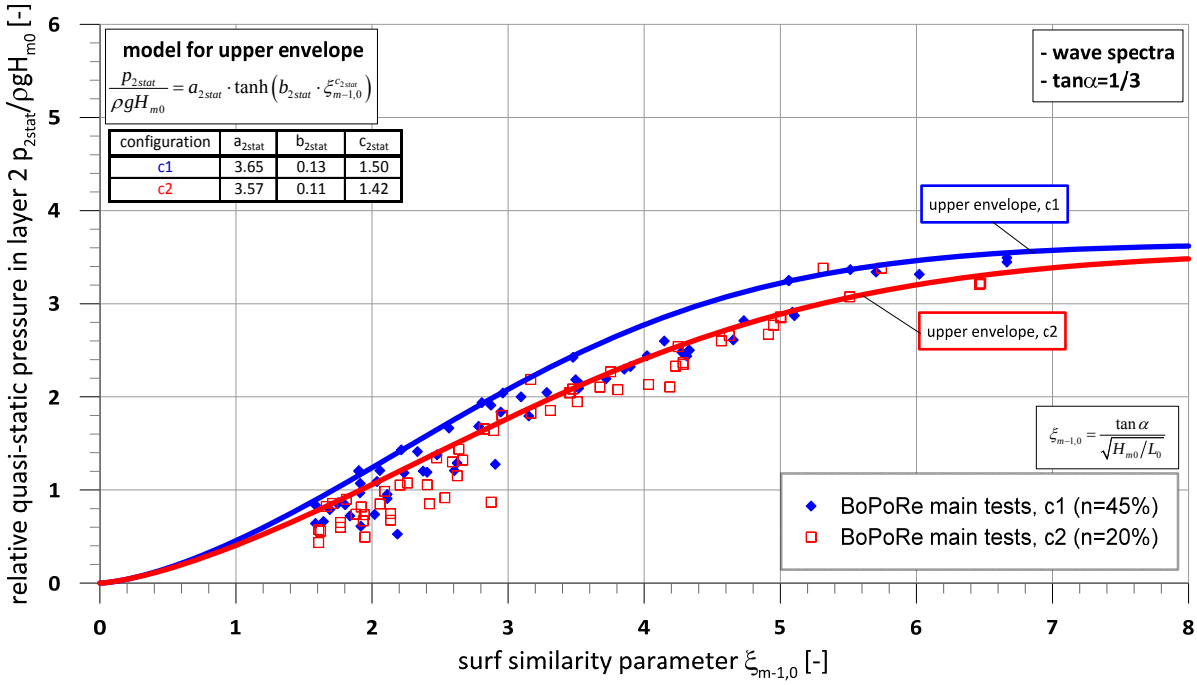

Fig. 7.10: Model of Liebisch et al. (2013b) applied to fit the data of relative quasi-static pressure in layer 2 just beneath the revetment for wave spectra (slope steepness 1:3)

Using eq. (6.3) the following equations describing the relative quasi-static pressure in layer 2 for wave spectra were found for the two configurations c1 and c2 with the same slope steepness of 1:3:

Configuration c1 (n = 45%):
$$\frac{p_{2stat}}{\rho g H_{m0}} = 3.65 \cdot \tanh\left(0.13 \cdot \xi_{m-1,0}^{1.50}\right) \tag{7.2}$$

Configuration c2 (n = 20%):
$$\frac{p_{2stat}}{\rho g H_{m0}} = 3.57 \cdot \tanh\left(0.11 \cdot \xi_{m-1,0}^{1.42}\right) \tag{7.3}$$

The relative quasi-static pressure in layer 2 $p_{2stat}/\rho g H_{m0}$ for configuration c3 is shown in Fig. 7.11 together with the results of configuration c1. Furthermore, the model of Liebisch et al. (2013b) is applied to develop an upper envelope of the data of the more porous and flatter 1:6 revetment.

The values of the relative quasi-static pressure component in Fig. 7.11 show a good agreement for both revetment configurations c1 and c3 for $\xi_{m-1,0} < 2.5$. Like in Fig. 6.12 the quasi-static pressure on the flatter slope 1:6 is decisively larger compared to those of configuration c1 for $\xi_{m-1,0} > 2.5$. This was explained in section 6.2.3 by a shifting of the $p_{2stat}/\rho g H_{m0}$-values to smaller $\xi_{m-1,0}$–values for the tests with smaller wave steepness (small wave heights and especially large wave periods). For decreasing wave steepness (quasi-static loads), the effect of slope steepness on the pressure on the revetment also decreases and becomes negligibly small. This behaviour was already observed for the quasi-static pressures on the revetment which is transferred through the revetment in layer 2. However, this phenomenon has to be more closely examined

in further studies based on numerical or physical model tests for a wider range of different slope steepness.

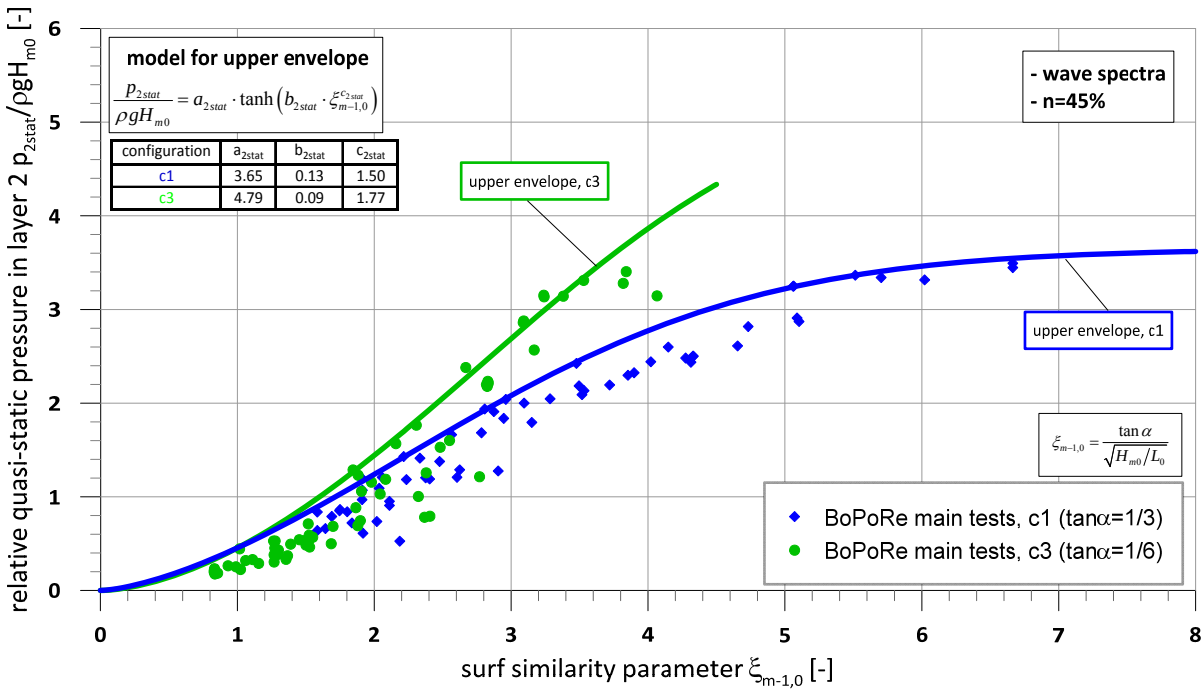

Fig. 7.11: Equation of Liebisch et al. (2013b) applied to fit the data of relative quasi-static pressure in layer 2 just beneath the revetment for wave spectra (porosity n = 45%)

Using eq. (6.3) the following equation was obtained for wave spectra and a slope steepness of 1:6:

Configuration c3 (tanα = 1/6): $$\frac{p_{2stat}}{\rho g H_{m0}} = 4.79 \cdot \tanh\left(0.09 \cdot \xi_{m-1,0}^{1.77}\right) \quad (7.4)$$

The equation for configuration c1 with a slope 1:3 was already shown with eq. (7.2)

The coefficients required to apply eq. (6.3) for the relative peak pressures in layer 2 of all tested configurations are summarized in Tab. 7.1.

Tab. 7.1: Coefficients a_{2stat}, b_{2stat} and c_{2stat} in eq. (6.3) for all tested configurations

$\frac{p_{2stat}}{\rho g H_{m0}} a_{2stat} \cdot \tanh\left(b_{2stat} \cdot \xi_{m-1,0}^{c_{2stat}}\right)$	tanα [-]	porosity [%]	a_{2stat} [-]	b_{2stat} [-]	c_{2stat} [-]
configuration c1	1/3	45	3.65	0.13	1.50
configuration c2	1/3	20	3.57	0.11	1.42
configuration c3	1/6	45	4.79	0.09	1.77

According to eq. (6.8) the next step in the model development is the analysis of the extracted dynamic impact pressure component p_{2imp}, which occurs for $\xi_{m-1,0} < 3.0$ corresponding to

collapsing and plunging breakers. The impact pressure component p_{2imp} just beneath the revetment is significantly smaller than p_{1imp} on the revetment due to the very high damping of the impact loads through the cover layer.

Like for the relative impact pressure component on the revetment, eq. (6.10) is used again to derive upper envelopes for $p_{2imp}/\rho g H_{m0}$. The coefficients in eq. (6.10) found for the relative impact pressure component of all configurations are summarized in Tab. 7.2.

Tab. 7.2: Coefficients a_{2imp}, b_{2imp} and c_{2imp} in eq. (6.10) for all tested configurations

$\frac{p_{2imp}}{\rho g H_{m0}} = a_{2imp} \cdot \xi_{m-1,0} \cdot \exp\left(\frac{-\xi_{m-1,0}^{c_{2imp}}}{b_{2imp}}\right)$	tanα [-]	porosity [%]	a_{2imp} [-]	b_{2imp} [-]	c_{2imp} [-]
configuration c1	1/3	45	0.91	182.54	6.65
configuration c2	1/3	20	0.65	1827.9	9.13
configuration c3	1/6	45	0.84	153.97	5.97

The wave load prediction model which consists of an impact and a quasi-static component was already derived as eq. (6.11). Based on this model and the related coefficients in Tab. 7.1 and Tab. 7.2, the following prediction equations for the wave-induced peak pressure just beneath the revetment for wave spectra tests are proposed:

Configuration c1 (n = 45%; tanα = 1/3):

$$\frac{p_{2\max}}{\rho g H_{m0}} = 0.91 \cdot \xi_{m-1,0} \cdot \exp\left(-\frac{\xi_{m-1,0}^{6.65}}{182.54}\right) + 3.65 \cdot \tanh\left(0.13 \cdot \xi_{m-1,0}^{1.50}\right) \qquad (7.5)$$

$$\text{for } \xi_{m-1,0} < 6.8$$

Configuration c2 (n = 20%; tanα = 1/3):

$$\frac{p_{2\max}}{\rho g H_{m0}} = 0.65 \cdot \xi_{m-1,0} \cdot \exp\left(-\frac{\xi_{m-1,0}^{9.13}}{1827.9}\right) + 3.57 \cdot \tanh\left(0.11 \cdot \xi_{m-1,0}^{1.42}\right) \qquad (7.6)$$

$$\text{for } \xi_{m-1,0} < 6.8$$

Configuration c3 (n = 45%; tanα = 1/6):

$$\frac{p_{2\max}}{\rho g H_{m0}} = 0.84 \cdot \xi_{m-1,0} \cdot \exp\left(-\frac{\xi_{m-1,0}^{5.97}}{153.97}\right) + 4.79 \cdot \tanh\left(0.09 \cdot \xi_{m-1,0}^{1.77}\right) \qquad (7.7)$$

$$\text{for } \xi_{m-1,0} < 4.2$$

The equations for the upper envelopes based on eq. (6.11) are shown together with the related data of the relative peak pressure just beneath the revetment in Fig. 7.12.

Like for the peak pressure on the revetment, the relative peak pressure in layer 2 is slightly overestimated. To which extent this overestimation is compensated by the scale and model effects in Fig. 7.7 is still unknown und can be answered only through further studies.

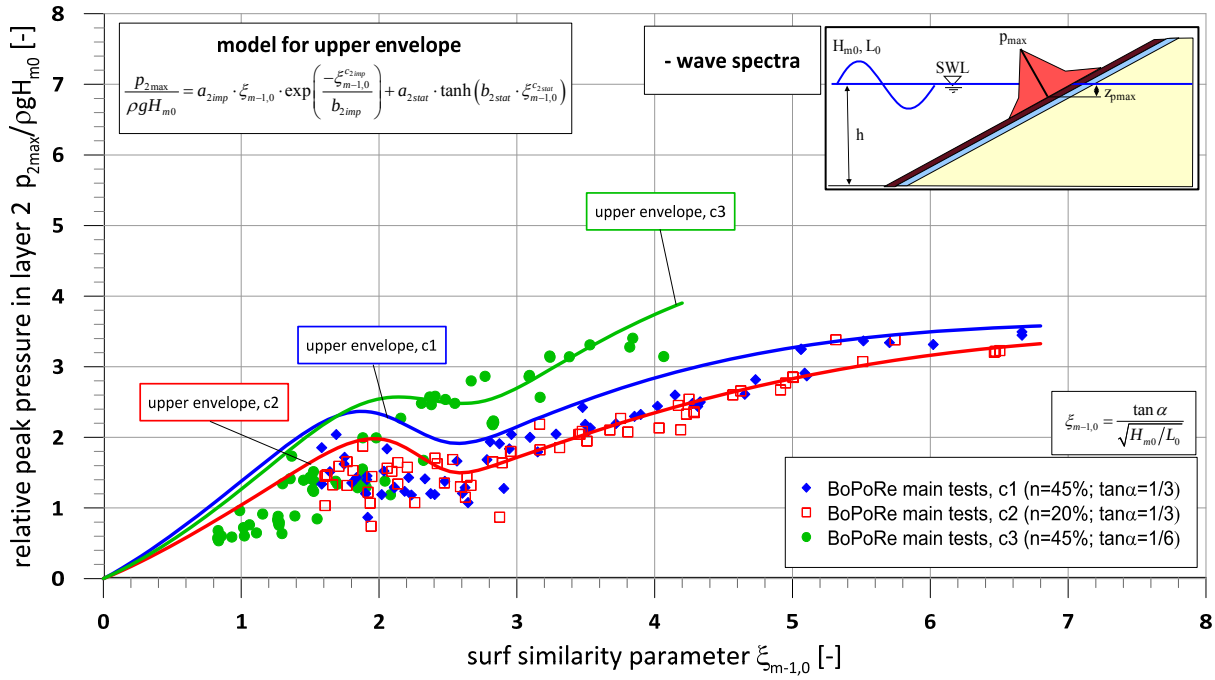

Fig. 7.12: Illustration of upper envelopes for relative peak pressure just beneath the revetment as a function of surf similarity parameter $\xi_{m-1,0}$ for wave spectra (all configurations)

The quasi-static component p_{1stat} of the impact load induced by plunging breakers and collapsing breakers ($\xi_{m-1,0} < 3.0$) is transferred from layer 1 on the revetment to layer 2 with the same data scatter for all tested configurations.

The pressure damping performance D_p of the revetment, defined in eq. (7.1), is generally affected by both slope steepness and revetment porosity, the effect of the latter being more significant. Despite the large scatter of the data, the effect of the porosity and the slope steepness may be summarised as follows:

For the *effect of the revetment porosity*, damping performance D_p is larger for less porous revetments over the entire range of tested surf similarity parameters. However, the impact load component are more strongly damped than the quasi-static component and non-impact loads through the porous revetment.

For the *effect of the slope steepness*, damping performance D_p is generally larger for steeper slopes, but this seems to significantly depend on surf similarity parameter $\xi_{m-1,0}$. The effect of the slope steepness on D_p is negligibly small for $\xi_{m-1,0} > 3.0$ and increases with decreasing surf similarity parameter for $\xi_{m-1,0} < 3.0$.

Tentative formulae to predict the upper envelopes of relative peak pressure $p_{2max}/\rho g H_{m0}$ in layer 2 just beneath the revetment are proposed as a function of $\xi_{m-1,0}$ for all tested revetment configurations.

7.2 Damping of pore pressure in the sand core

As already shown in Fig. 7.1, the wave-induced-pressures beneath the revetment were measured by nine pressure transducers in the sand and three layers parallel to the slope located at different depths in the sand core to describe the pore pressure damping beneath the revetment. The pre-processing of the obtained data was already reported in section 4.4.

Typical pressure signals recorded on the revetment (layer 1) and in layers 2-5 of the sand core beneath the revetment of PT-column A (see definition sketch in Fig. 7.1) are shown in Fig. 7.13 exemplarily for configuration c1.

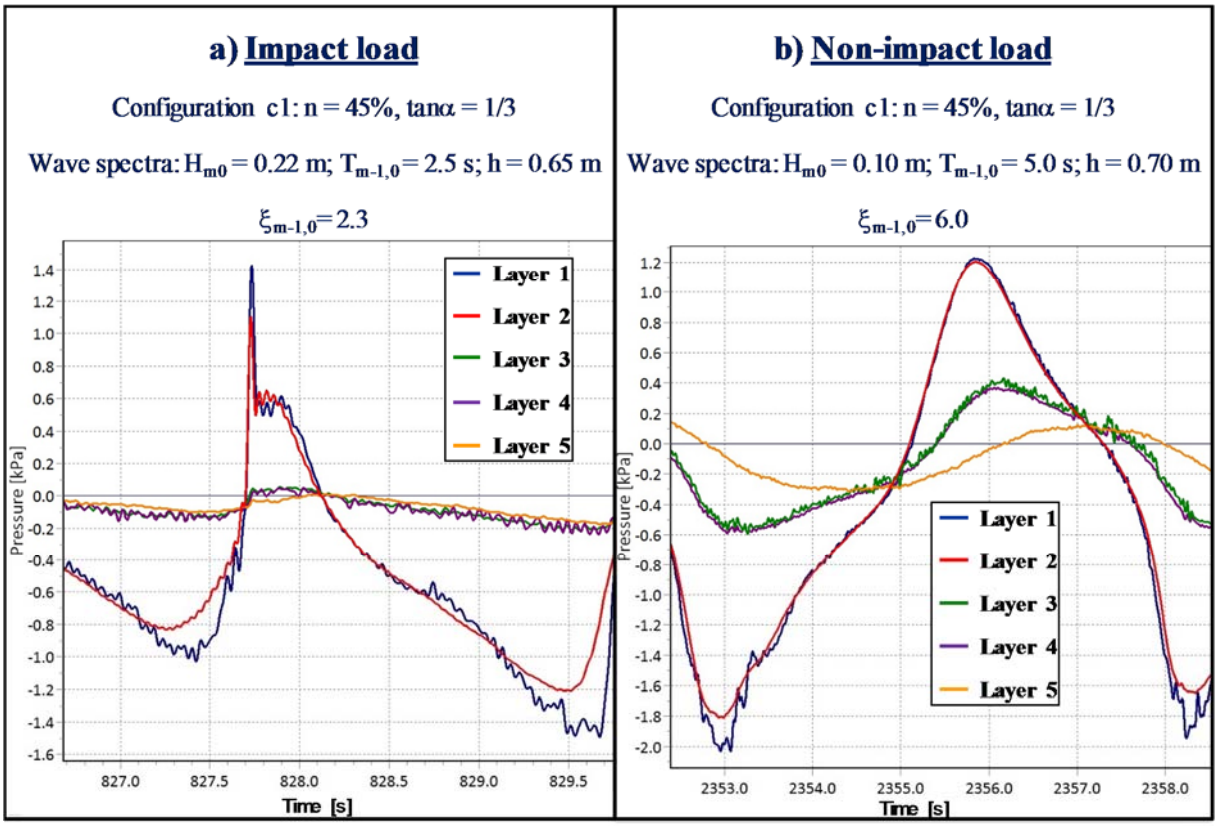

Fig. 7.13: Typical recorded signals of pressure transducers in PT-layer 1 to PT-layer 5 for a) impact load and b) non-impact load (configuration c1) (see definition sketch in Fig. 7.1)

The typical pressure signals for both impact and non-impact load in Fig. 7.13 show that the wave-induced pressures are strongly damped by the first layers of the sand core and that the damping rate rapidly decreases for deeper locations. Furthermore, the waves with larger surf similarity parameter $\xi_{m-1,0}$ and the associated non-impact loads are more easily transferred in deeper layers. Impact loads ($\xi_{m-1,0} < 2.5$) are almost completely damped in the sand core, which is representative for all tests with irregular and regular waves, irrespective of the revetment porosity.

The damping of the pressure through the revetment was already addressed in section 7.1. For the pressure damping through the sand layers no significant differences are expected for the different revetment configurations, since the sand core was the same for all tested

configurations. This assumption is supported by the results of the preliminary tests in Liebisch et al. (2013b) and confirmed by the numerical results of Alcérreca Huerta (2014) for porous revetments with different filter layer thicknesses.

In this section a detailed analysis of the normalized pore pressures (p_i/p_0) is considered in terms of a normalized depth, which is described by the depth in the sand z' normal to the revetment divided by the deep water wave length L_0. The depth z' is measured from the top of the sand core (see Fig. 7.14).

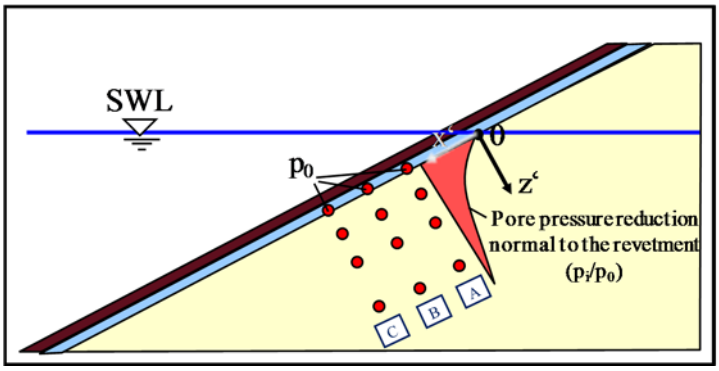

Fig. 7.14: Definition sketch for the pore pressure damping analysis in the sand core

For every revetment configuration, the pressure recorded at the three PT-columns A, B and C are put together in one graph which is justified by the results of previous studies (e.g. Alcérreca Huerta (2014)), which have shown that no significant differences in the pore pressure damping behaviour in the sand core is expected at the different locations along the slope. Fig. 7.15 to Fig. 7.17 describe the normalized pore pressures p_i/p_0 vs. relative depths z'/L_0 for each of the three tested revetment configurations c1, c2 and c3, respectively.

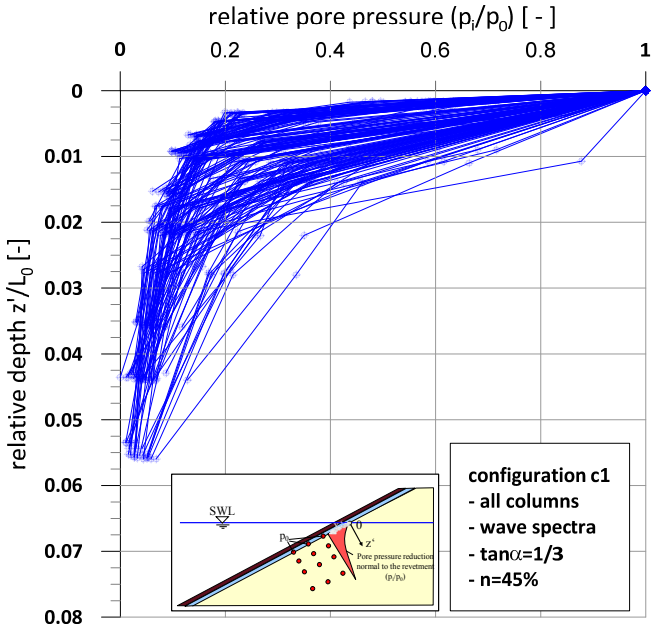

Fig. 7.15: Relative pore pressure vs. relative depth in the sand core beneath revetment configuration c1 for wave spectra

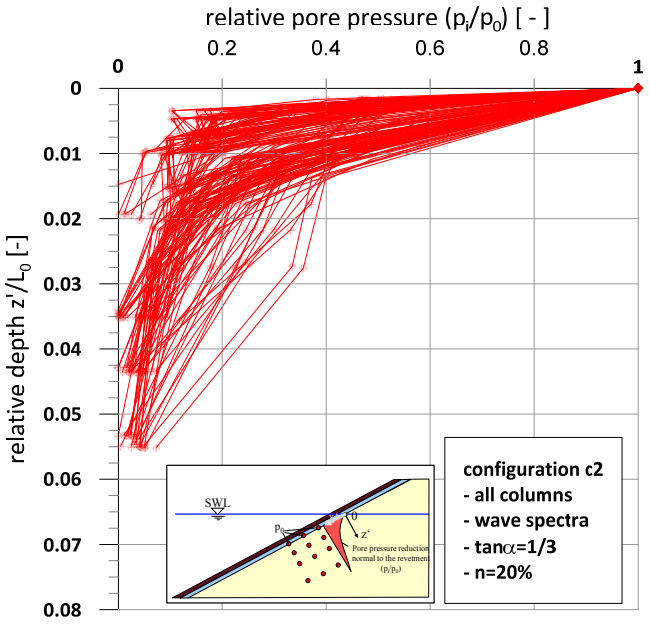

Fig. 7.16: Relative pore pressure vs. relative depth in the sand core beneath revetment configuration c2 for wave spectra

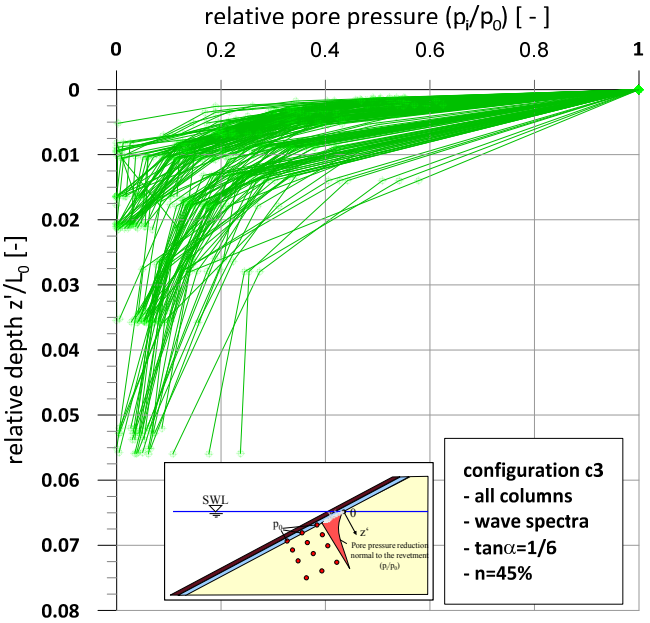

Fig. 7.17: Relative pore pressure vs. relative depth in the sand core beneath revetment configuration c3 for wave spectra

For all revetment configurations, the embankment beneath the revetment is made of the same sand material applying the same compaction procedure during the construction phases, so that it can be assumed that the key properties (e.g. porosity, permeability) of the sand core as a porous medium are similar for the three tested revetment configurations. The latter is important when comparing Fig. 7.15 to Fig. 7.17, showing an exponential damping of the initial pressure on the revetment. Accordingly, the highest damping rates of the relative pore pressure are obtained in the upper layer of the sand core. The exponential damping of wave-induced pore

pressures in the seabed and in further porous structures was already described in several studies (e.g. de Groot et al. (2006), see also section 2.3). In this respect, no fundamental differences (with only stochastic variability) in the pore pressure damping behaviour between the three configurations with different porosities or slope steepnesses can be identified in Fig. 7.15 to Fig. 7.17. Thus, for simplification, all data from the three configurations are put together for further analysis, i.e. without consideration of slope steepness and porosity effects.

The key wave parameter affecting the pressure damping in the sand core, even not explicitly indicated in Fig. 7.15 to Fig. 7.17, is the period of the incident wave. This was already outlined in Fig. 7.13 where the wave-induced pressure of longer waves is transferred in deeper layers (non-impact loads), whereas it is almost completely damped in the deepest layer 5 for shorter waves (impact loads). The significant effect of the wave period on the pressure damping rate was also demonstrated by the results of Alcérreca Huerta (2014). The latter also successfully used the following model for the description of the exponential damping of the pore pressure in the sand core.

$$\frac{p_i}{p_0} = \exp\left(-A_{Sand} \cdot \frac{z'}{L_0}\right) \tag{7.8}$$

Coefficient A was redefined as A_{Sand} to distinguish it from other coefficients. This equation fulfils the requirements that relative pore pressure p_i/p_0 tends against zero for large relative depths z'/L_0 while for $z'/L_0 = 0$ the initial pressure (p_i/p_0=1.0) has to be obtained. The model in eq. (7.8) is used to fit the data of all three revetment configurations grouped according to the wave period. As a result, coefficient A_{Sand} is determined. This is shown exemplarily for configuration c1 and a wave period of 2.5 s in Fig. 7.18.

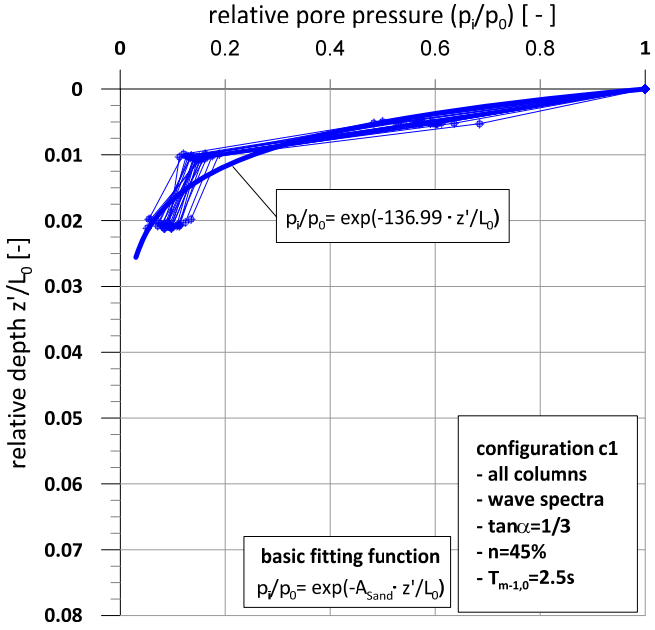

Fig. 7.18: Relative pore pressure vs. relative depths in the sand core based on eq. (7.8), exemplarily for configuration c1 and wave period $T_{m-1,0}$ = 2.5 s

Coefficients A_{Sand} with the related determination coefficient r^2 are given in Tab. 7.3 for the three tested revetment configurations and all tested wave periods.

Tab. 7.3: Coefficients A_{Sand} in eq (7.8) with related determination coefficient r^2 for all tested revetment configurations and wave periods

wave period $T_{m-1,0}$ [s]	c1		c2		c3	
	A_{Sand}	r^2	A_{Sand}	r^2	A_{Sand}	r^2
1.5	72.46	0.88	72.99	0.87	74.63	0.74
1.8	84.75	0.88	88.50	0.91	-	-
2.0	92.59	0.89	123.46	0.72	94.34	0.88
2.5	136.99	0.88	181.82	0.59	185.19	0.88
3.0	169.49	0.91	172.41	0.81	200.00	0.82
4.0	238.10	0.91	250.00	0.82	250.00	0.76
5.0	294.12	0.91	303.03	0.83	333.33	0.62
5.5	-	-	-	-	285.71	0.91

For most of the cases in Tab. 7.3, a high determination is obtained by applying eq. (7.8). A large scatter was obtained with smaller determination when applying eq. (7.8) only for some wave periods leading to the deviations that can be found in Fig. 7.19, e.g. for tested wave periods $T_{m-1,0}$ = 2.5 s and $T_{m-1,0}$ = 5.0 s . However, almost similar values of coefficient A_{Sand} are obtained for the same wave period by considering all three configurations together. The result is shown in Fig. 7.19.

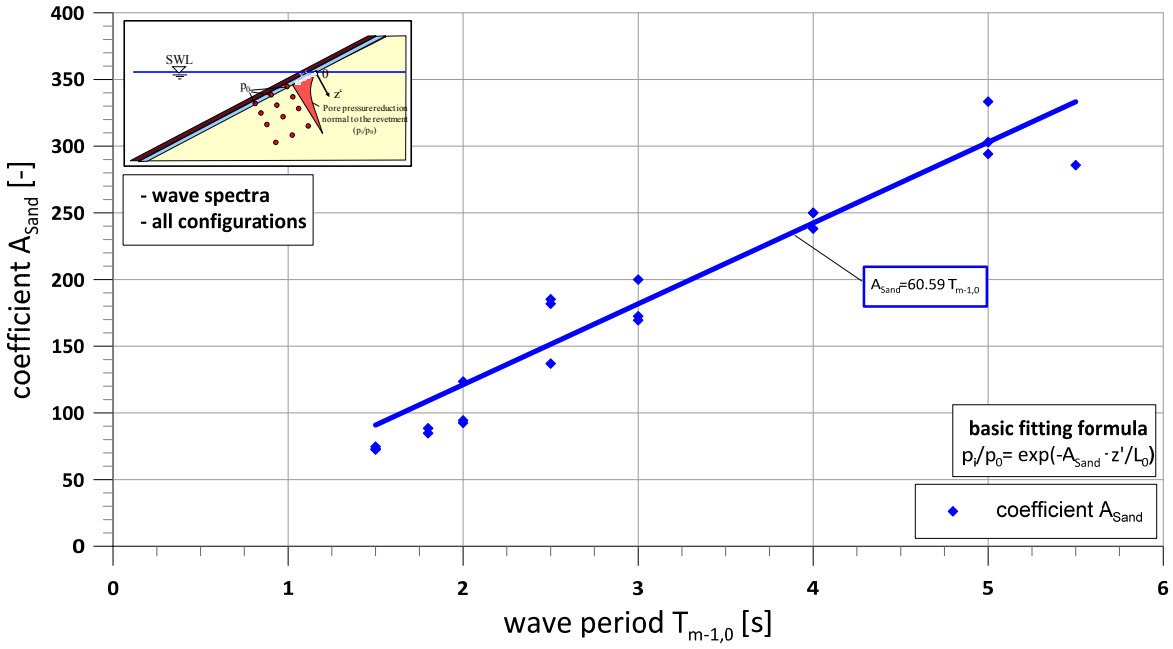

Fig. 7.19: Coefficient A_{Sand} for different wave periods for all configurations

For the pressure reduction a relation for the coefficient A_{Sand} was found in Fig. 7.19 with a determination coefficient $r^2 = 0.98$ and the :

$$A_{Sand} = 60.59 \frac{1}{s} \cdot T_{m-1,0} \tag{7.9}$$

with $T_{m-1,0}$ in seconds

Substituting A_{Sand} from eq. (7.9) in eq. (7.8) the following equation is obtained:

$$\frac{p_i}{p_0} = \exp\left(-60.59 \frac{1}{s} \cdot T_{m-1,0} \cdot \frac{z'}{L_0} \right) \tag{7.10}$$

The following Fig. 7.20 shows the applied model in eq. (7.10) separated by the tested wave periods $T_{m-1,0}$.

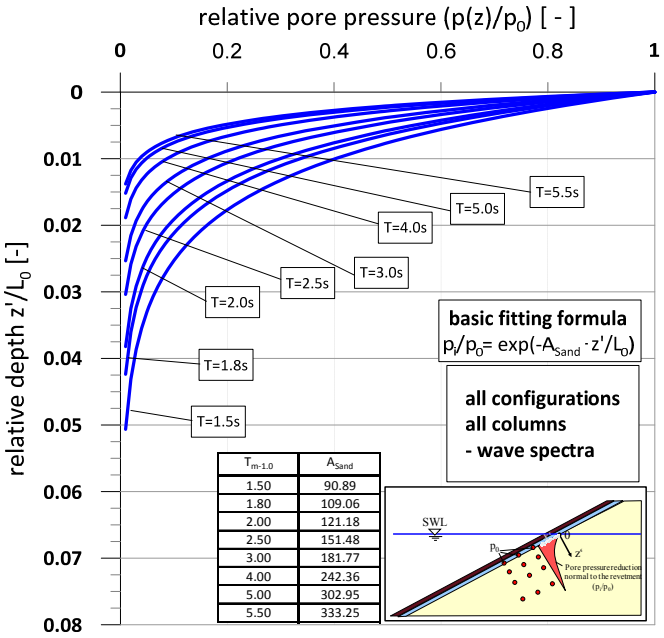

Fig. 7.20: Applied model in eq. (7.10) for the tested wave periods $T_{m-1,0}$ for wave spectra

It is shown that the developed equation adequately describes the behaviour of pressure damping in Fig. 7.20. However, although a quite good result is obtained applying eq. (7.10) to the data of the main model tests in the BoPoRe-project, the problem is that the constant in eq. (7.9) is not dimensionless. Alcérreca Huerta (2014) used the equation of de Groot et al. (2006) to explain the exponential reduction of the pore pressure in the seabed assuming that the pore water compressibility is much larger than the skeleton compressibility due to air content in the pore fluid. According to de Groot et al. (2006), the pore pressure damping in a linear elastic, homogeneous soil can be described by the following equation:

$$\left(\frac{p}{p_0} \right) = \exp\left(\frac{z'}{z_2} \right) \tag{7.11}$$

Parameter z_2 describes the characteristic length for pore pressure amplitude damping due to elastic storage. de Groot et al. (2006) states that in a depth of $3z_2$, the initial pore pressure is completely damped and hardly any pore pressure fluctuation occurs. The parameter z_2 is described by:

$$z_2 = \sqrt{c_{ve} \frac{T}{\pi}} \tag{7.12}$$

with:
$$c_{ve} = \frac{k_f}{\gamma_w (\alpha + n\beta)} \approx \frac{k_f}{\gamma_w n \beta}$$

c_{ve}	=	consolidation coefficient	[m²/s]
k_f	=	hydraulic permeability of the sand	[m/s]
γ_w	=	unit weight of water	[N/m³]
n	=	porosity	[-]
β	=	elastic compressibility of pore water	[m²/N]

A simplification of c_{ve} can be made for elastic, horizontally constrained decompression. For the soil used in the main experiments, the mean permeability is set to $k_f = 1.2 \cdot 10^{-4} m/s$ and the mean porosity to n = 0.47, determined from three undisturbed soil samples. The elastic compressibility β results under the assumption of no significant water column loading the pores in the sand ($p_a = 1.013 \cdot 10^5 Pa$) and an air content in the pores of 1 % (S = 0.99):

$$\beta = \frac{1}{K_w} = \frac{S}{K_{ow}} + \frac{1-S}{p_a} = \frac{0.99}{2.3 \cdot 10^9 Pa} + \frac{1-0.99}{1.013 \cdot 10^5 Pa} = 9{,}915 \cdot 10^{-8} \frac{1}{Pa} \tag{7.13}$$

The consolidation coefficient would be determined to the following value:

$$c_{ve} = \frac{1.2 \cdot 10^{-4}}{9810 \cdot 0.47 \cdot 9{,}915 \cdot 10^{-8}} = 0.262 m^2/s \tag{7.14}$$

$$z_2 = \sqrt{c_{ve} \frac{T}{\pi}} = \sqrt{0.262 \frac{T}{\pi}} = 0.289 \cdot \sqrt{T} \tag{7.15}$$

This leads to the following equation for the exponential pore pressure damping:

$$\left(\frac{p}{p_0} \right) = \exp\left(\frac{z'}{0.289 \cdot \sqrt{T}} \right) \tag{7.16}$$

To compare eq. (7.16) with eq. (7.10), the latter has to be transformed:

$$\left(\frac{p_i}{p_0}\right) = \exp\left(\frac{z'}{0.0165 \cdot T_{m-1,0}^{-1.0} \cdot L_0}\right) \tag{7.17}$$

For a direct comparison, it is convenient for the wave period to have an exponent of -1.5. Therefore, another fitting with this constraint is performed for parameter A_{Sand}:

$$A_{Sand} = 0.0325 \cdot T_{m-1,0}^{-1.5} \tag{7.18}$$

With this fitting a similar function to eq. (7.17) is obtained in (7.19) with a determination coefficient which is only slightly smaller ($r^2 = 0.88$) and which can now be applied for a direct comparison with eq. (7.16):

$$\left(\frac{p_i}{p_0}\right) = \exp\left(\frac{z'}{0.0263 \cdot T_{m-1,0}^{-1.5} \cdot \left(\frac{gT_{m-1,0}^2}{2\pi}\right)}\right) = \exp\left(\frac{z'}{0.0507 \cdot \sqrt{T_{m-1,0}}}\right) \tag{7.19}$$

The derived equation deviates from the theoretical calculated equation of de Groot et al. (2006) by a factor of 6. This does not confirm the findings of the numerical investigations of Alcérreca Huerta (2014) in which a good agreement to the equation of de Groot et al. (2006) was found. This might be explained by the possible direct definition of soil characteristics in the numerical investigations and the assumption that the soil is homogeneous and isotropic. In the model of de Groot et al. (2006) two parameters are contained, which are highly variable in a physical model and can hardly be set as a constant like in the numerical model. These parameters are the hydraulic permeability k and the elastic compressibility of pore water β. The permeability k of the sand was determined in three laboratory measurements on undisturbed soil samples in a permeameter. Deviations in such tests are very common. Thus, a mean value of $k_f = 1.2 \cdot 10^{-4} m/s$ was used for the calculation. To achieve a similar value for the pore pressure reduction in the equation of de Groot et al. (2006) a permeability of approximately $k_f = 4 \cdot 10^{-6} m/s$ is non-realistic. However, a permeability of the used fine sand, which was strongly compacted in the model of $k_f = 1.0 \cdot 10^{-5} m/s$ is definitely in a meaningful range. Much more realistic are deviations in the elastic compressibility of pore water, which is strongly dependent on the air content in the pore fluid. In the calculations of Alcérreca Huerta & Oumeraci (2014) and also here in eq. (7.14), a constant air content of 1 % was assumed in the sand core beneath the revetment. This value was set for a porous seabed for which the equation was developed. For sloped revetment structures, Schulze & Köhler (2004) underline that air contents between 1-15 % are possible. Consequently, it can be expected that the air content in the sand pores during the experiments was much larger than 1 % leading to deviations from the numerical investigations. Assuming an adjusted permeability of $k_f = 1.0 \cdot 10^{-5} m/s$, an air content of 3 % would lead to the derived equation, which is in a realistic range. Consequently, it can be stated that eq. (7.11) with eq. (7.12) by de Groot et al. (2006) can correctly estimate

the pore pressure damping in the sand core, but the parameters used in this equation have to be determined carefully to obtain reasonable results. Small deviations in the determination of these parameters may lead to large deviations in the calculated pore pressures.

Wave-induced pressures are strongly damped by the first layers of the sand core and the damping rate rapidly decreases for deeper locations. Furthermore, the waves with a larger surf similarity parameter are more easily transferred in deeper layers, whereas almost the entire wave-induced pressure is damped in layer 5 for surf similarity parameters smaller than 2.5. Impact pressures ($\xi_{m-1,0} < 2.5$) are almost completely damped in the sand core. No fundamental differences in the exponential pore pressure damping behaviour was identified between the three configurations with different porosities or slope steepnesses. The model by de Groot et al. (2006) to describe the pore pressure damping in the sand can correctly estimate the pore pressure damping in the sand core when the input parameters such as the compressibility of pore water β and the hydraulic permeability k are well selected.

7.3 Development of the internal mean water level (IMWL)

Due to the direct connection of the EMWL with the IMWL through the porous layers placed on the sand core, both water levels are in interaction. As mentioned in section 5.2 the external wave set-up processes results in an uplift of the EMWL in front of and at the structure. The development of the EMWL also strongly affects the internal mean water level (IMWL) in the sand core. A proper investigation of the long-term development of the internal mean water level was conducted in the small-scale model tests in the flume with pressure transducers in the rear sand core (see Fig. 7.2, and for details Fig. 4.6, Fig. 4.8 and Fig. 4.9). The change of the EMWL and IMWL does not change the stability conditions directly, but it shifts the swash zone and the connected area in which uplift forces (directed out of the sand core) occur during run-down (see Fig. 7.21).

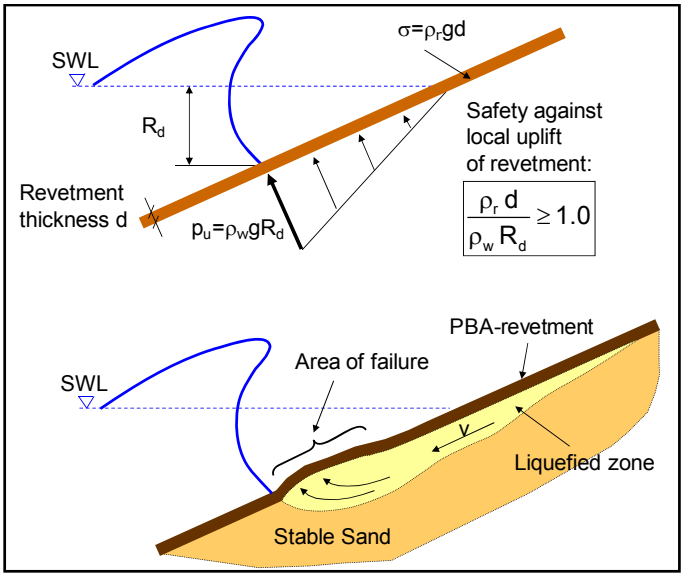

Fig. 7.21: Schematic Illustration of prevailing forces during wave run-down and area of failure in large-scale tests (Oumeraci et al. (2010b))

The uplift forces induce a draining flow out of the sand core which can wash the sand particles out of the upper layers of the revetment and transport them down the slope. This can lead to a partial soil liquefaction and local failures in the sand core. This process is illustrated schematically in Fig. 7.21, showing the failure mechanism during the large-scale experiments of Oumeraci et al. (2010b). For very long waves, e.g. ship waves, the change of IMWL and the associated draining effects and uplift forces are much more important than in the case of a revetment under wave loads, because the duration of the run-down process is significantly larger. The stability of the sand core in the swash zone is addressed in section 7.4. In this section, the interaction of EMWL and IMWL and the development of the IMWL are analysed as a function of the wave conditions and revetment characteristics.

For irregular tests the EMWL is superimposed by fluctuations over the entire tests duration. Depending on the sequence of the different incident waves in the spectra, the EMWL develops over time. Consequently, the IMWL is also affected by this development and rises up to a certain level and with similar fluctuations to those in the EMWL. This is shown exemplarily in Fig. 7.22 for PT21S in a wave spectra test with a surf similarity parameter $\xi_{m-1,0}$ = 1.11 for configuration c3 in which the parameters for the analysis are also shown.

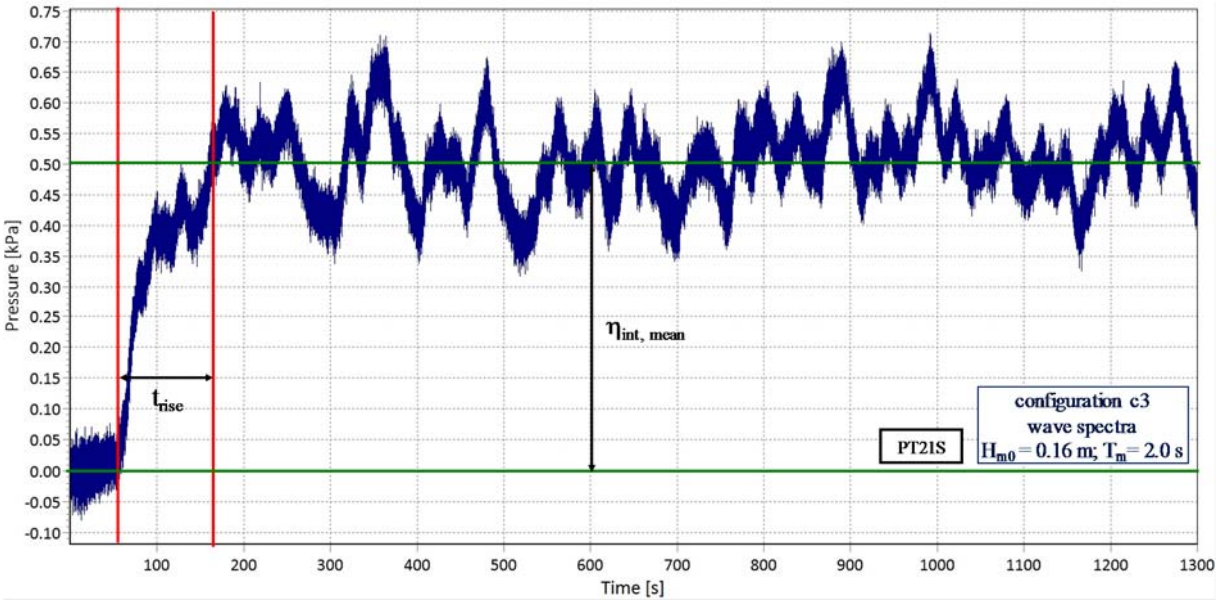

Fig. 7.22: Time series of IMWL with definition of the parameters required for the analysis (wave spectra)

For wave spectra rise time t_{rise} is defined as the time between the point where the IMWL starts to rise up to the time when mean value $\eta_{int,mean}$ is reached, which is analysed as the internal wave set-up η_{int} in this section.

In the current study the location of the pore pressure measurement is defined by the parameter x_{local}, which describes the horizontal distance between the location at the intersection of the external still water level with the surface of the sand core and the location of the considered pressure transducer (Fig. 7.23). For the cases with a negative parameter x_{local}, the measurements of the regarded pressure transducer are not considered for the analysis, because the pore pressure signals also include wave signals.

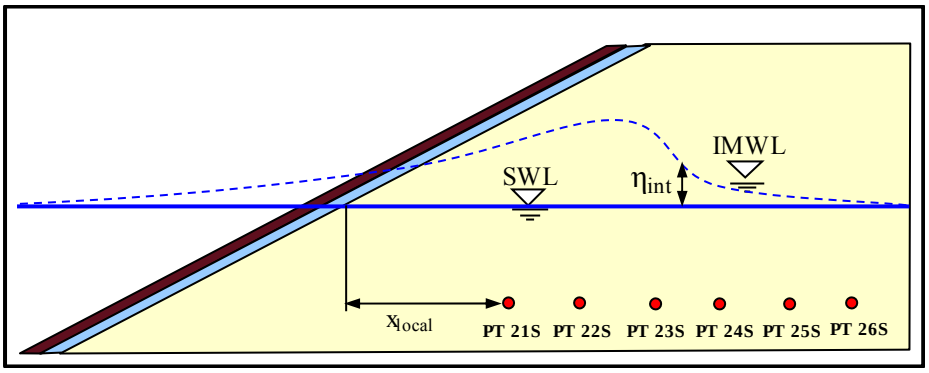

Fig. 7.23: Definition sketch for the parameter x_{local} for the location of pressure transducers to measure the IMWL

7.3.1 Effect of the revetment porosity

The development of the IMWL in the sand core is first analysed for the configurations with the same slope steepness (1:3) and different porosity. In section 5.2 it was shown that the analysis of the external wave set-up η_S resulted in very good results when η_S is normalized by deep water wave length L_0. In Liebisch & Oumeraci (2014) the analysis of the internal wave set-up η_{int} normalized by deep water wave length L_0 as a function of surf similarity parameters $\xi_{m-1,0}$ for the six PT-locations together (as defined in Fig. 7.23) can be found. However, due to six different measuring locations of the IMWL considered in this analysis, it is less meaningful, especially with respect to the spatial distribution of the IMWL. Consequently, due to the direct connection of EMWL and IMWL, it is meaningful to analyse the relation between EMWL and IMWL using the dimensionless parameter η_{int}/η_S. To consider separately the location of the measurement in the sand core and thus the spatial distribution of the IMWL, relative internal wave set-up η_{int}/η_S is plotted against relative distance x_{local}/L_0. This is shown in Fig. 7.24 and Fig. 7.25 for configurations c1 with n = 45% and c2 with n = 20%, respectively.

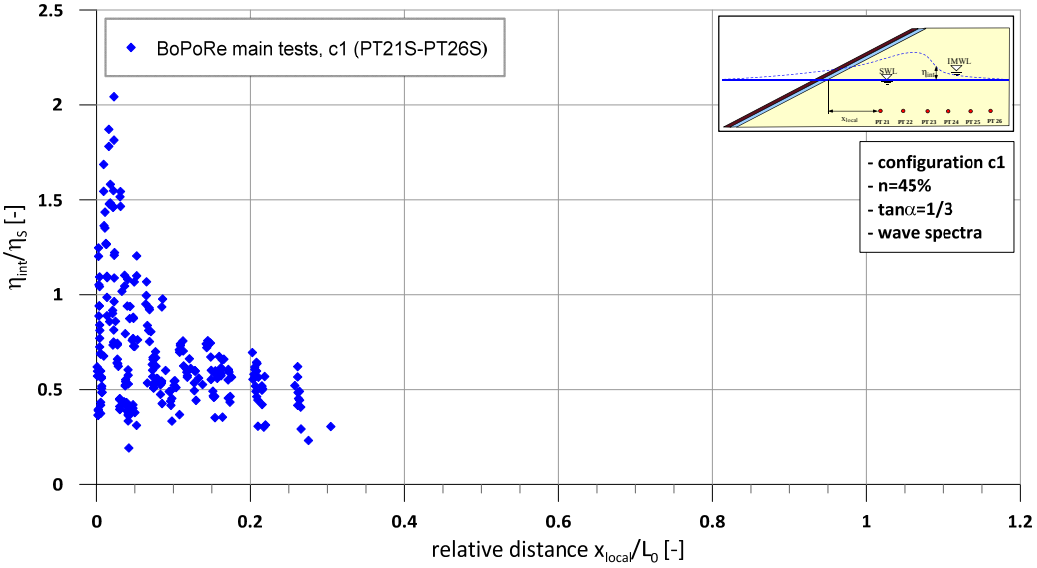

Fig. 7.24: Relation of IMWL to EMWL η_{int}/η_S as a function of relative distance x_{local}/L_0 for wave spectra (configuration c1)

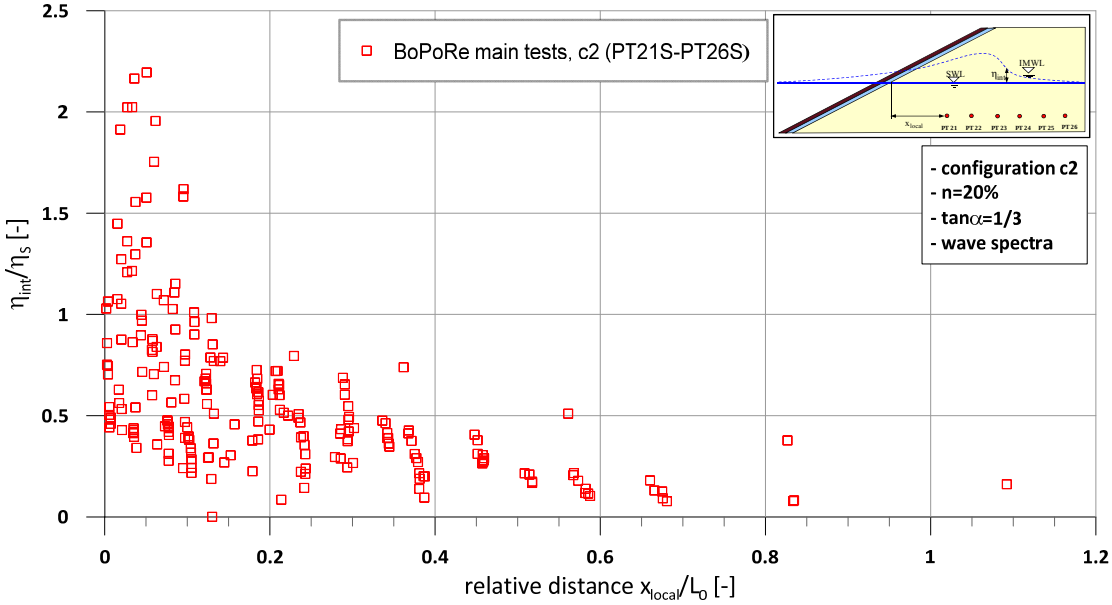

Fig. 7.25: Relation of IMWL to EMWL η_{int}/η_S as a function of relative distance x_{local}/L_0 for wave spectra (configuration c2)

From Fig. 7.24 and Fig. 7.25 the spatial distribution of the IMWL in the sand core for two different revetment porosities and the same slope steepness becomes obvious. In both figures, i.e. irrespective of the revetment porosity, the largest η_{int}/η_S-values are obtained for smaller relative distances x_{local}/L_0 in the sand, i.e. near the intersection of SWL with the sand core and/or for larger deep water wave lengths). Due to the draining processes in the upper sand layers caused by the swash processes on the revetment (wave run-up/down), the IMWL is directly affected by these processes. It is assumed that for smaller x_{local}/L_0-values the internal wave set-up η_{int}/η_S is characterized by a significantly different time scale which corresponds to that of wave run-up/run-down. With increasing relative distance x_{local}/L_0, the internal wave set-up increases up to a maximum. For these larger x_{local}/L_0-values the internal wave set-up has the same time scale as the external wave set-up and is not affected by the swash processes. For smaller wave lengths L_o and larger relative distances x_{local}/L_0, the effect of the swash processes on the development of the IMWL is much smaller and tends against zero. This confirms the findings of section 7.2 that the pressures induced by waves with larger periods have a larger penetration depth in the sand core.

In Fig. 7.24 it is obvious that the selected distances of the pressure transducers in the rear sand core are too small to capture the complete spatial distribution of the IMWL in the sand core. For larger relative distances x_{local}/L_0 the values of relative internal wave set-up η_{int}/η_S should also tend against zero like in Fig. 7.25. However, both configurations (with different porosities) provide similar results, which can be explained by similar values for the external wave set-up (see Fig. 5.12). For configuration c2 with the lower porosity (n = 20%), slightly larger values for the IMWL are obtained with a larger scattering for relative distances $x_{local}/L_0 < 0.1$ which means that the maximum for η_{int}/η_S is more distinctive. This might be explained by the smaller porosity of configuration c2 which admittedly did not lead to larger differences in the external wave set-up (see Fig. 5.12), but to larger wave run-up heights (see section 5.3.2) and the

downrushing water during wave run-down remains on the sloped sand core beneath the revetment for a longer time because the flow discharge is significantly smaller in the less porous revetment. This leads to a larger MWL directly at the sand surface, which results in a larger infiltration into and a reduced exfiltration of the water out of the sand core. Over time larger internal wave set-up heights can develop, which results in the significantly larger η_{int}/η_S-values. Consequently, the conclusion might be drawn that a decreasing porosity leads to larger maximum η_{int}/η_S-values.

As the MWL directly at the sand surface could not be measured in the experiments, this statement should be verified by numerical simulations. In fact, a measurement of the MWL on the sand core just beneath the revetment is hardly feasible in physical model tests.

A prediction model for η_{int}/η_S is developed in section 7.3.3 after the analysis of the effect of slope steepness in the next section 7.3.2.

7.3.2 Effect of the revetment slope steepness

It was already shown in the previous section that the development of the IMWL in the sand core is dependent on the EMWL. The latter was found to be also strongly dependent on the slope steepness (see section 5.2.2). Therefore, for the development of the IMWL, different results are expected for configuration c3 with a slope 1:6 as compared to the two configurations c1 and c2 with the steeper slope 1:3.

Consequently, the approach used in the previous section to analyse the relation between EMWL and IMWL described by η_{int}/η_S against relative distance x_{local}/L_0 is also applied on configuration c3 (Fig. 7.26).

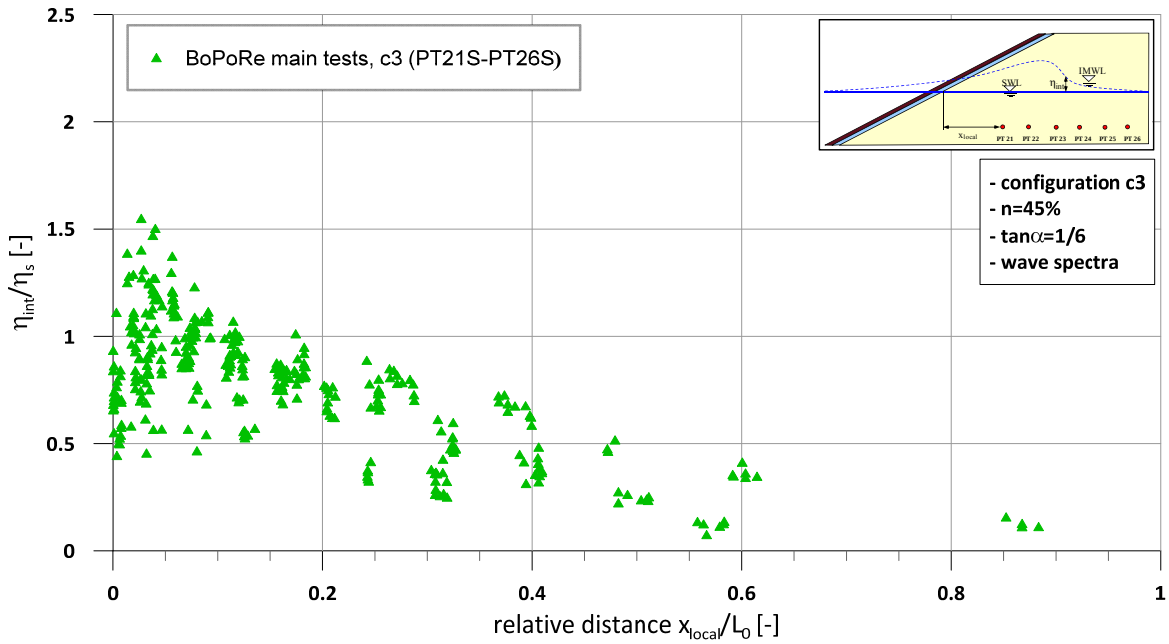

Fig. 7.26: Relation of IMWL to EMWL η_{int}/η_S as a function of relative distance x_{local}/L_0 for wave spectra with upper envelope based on eq.(7.20) (configuration c3)

The results of the relation between internal and external wave set-up for configuration c3 in Fig. 7.26 show a similar behaviour compared to the two steeper revetments c1 and c2 in the previous section. The largest by η_{int}/η_S-values are obtained for smaller x_{local}/L_0, i.e. for larger deep water wave lengths L_0. It is thus confirmed that long waves have a larger infiltration depth. For smaller wave lengths L_0 and thus for larger relative distances x_{local}/L_0, the relative internal wave set-up η_{int}/η_S decreases and tends against zero. Compared to configuration c1 with the same porosity (see also Fig. 7.24), configuration c3 with the flatter slope1:6 provides smaller η_{int}/η_S-values. This can be explained by the larger η_S-values which are obtained for the tests with small wave steepness $H_{m0}/L_0 < 0.01$ (small wave height and especially long waves) on the flatter slope 1:6. In fact, for these tests also the largest internal wave set-up η_{int}-values for all revetment configurations are obtained with η_{int} =0.1-0.2 m, but divided by the large η_S-values, maximum η_{int}/η_S is smaller compared to configuration c1. For very flat slopes and very long waves the relation between external and internal wave set-up η_{int}/η_S should tend against 1.0. The effect of the swash processes on the IMWL become less important.

Furthermore, the different breaking behaviour of the incident waves with the associated energy dissipation also affects the development of the IMWL. Further research is necessary to analyse more systematically the effect of the slope steepness on the IMWL in physical or numerical model tests with a larger variation of slope steepness.

7.3.3 Prediction formula for IMWL in the sand core

In the previous two sections the development of the IMWL in the sand core beneath the different tested revetments configurations was successfully analysed using the relative internal wave set-up η_{int}/η_S and relative distance x_{local}/L_0. Due to the large scattering of the obtained results, a conservative approach using an upper envelope for the data seems to be more meaningful. This approach was already applied successfully for the wave-induced pressures on and just beneath the revetment in section 6.2.4 and 7.1.3 and the spatial pressure distribution on the revetment in section 6.4. For the IMWL a model based on a Rayleigh-distribution is used which is modified to fulfil the following conditions: η_{int}/η_S tends against zero for large x_{local}/L_0-values, $\eta_{int}/\eta_S > 0$ for $x_{local}/L_0 = 0$ and a maximum η_{int}/η_S for small x_{local}/L_0-values. The following model is applied on the results of all configurations to derive an upper envelope for η_{int}/η_S:

$$\frac{\eta_{int}}{\eta_S} = \frac{d_{IMWL} \cdot \left(\frac{x_{local}}{L_0} + c_{IMWL} \right)}{b_{IMWL}} \cdot \exp\left(- \frac{\left(\frac{x_{local}}{L_0} + c_{IMWL} \right)^{a_{IMWL}}}{2 \cdot b_{IMWL}} \right) \tag{7.20}$$

with: a_{IMWL}, b_{IMWL}, c_{IMWL}, d_{IMWL} = empirical coefficients [-]

The derived upper envelopes for the data of η_{int}/η_S for all revetment configurations are shown in Fig. 7.27 for a direct comparison. The upper envelopes enclose almost all obtained data points

thus providing a conservative approach for the determination of the relative internal wave set-up η_{int}/η_S.

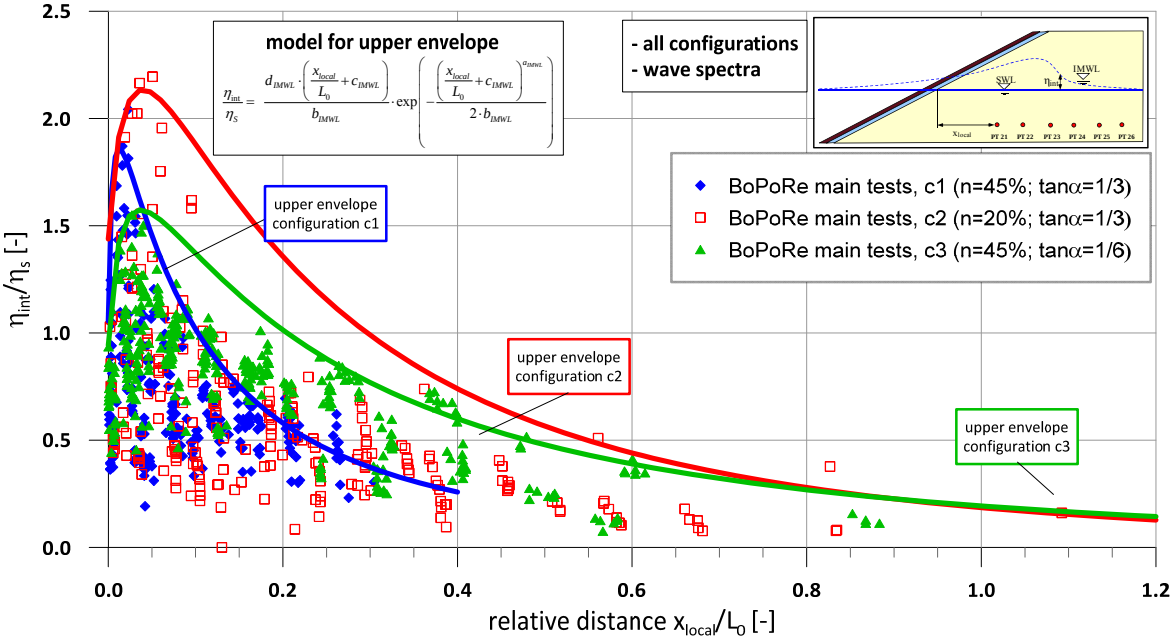

Fig. 7.27: Illustration of upper envelopes for the relation of IMWL to EMWL η_{int}/η_S as a function of relative distance x_{local}/L_0 for wave spectra (all configurations)

For all configurations eq.(7.20) is successfully used to derive an upper envelope, which considers the maximum η_{int}/η_S for small x_{local}/L_0-values and the η_{int}/η_S-values tending against zero for larger relative distances x_{local}/L_0.

The results confirm the findings of Ludwigs & Oumeraci (2011) even though another approach is used to analyse the data and to develop a model:

- The development of IMWL is highly dependent on the development of EMWL
- The relation of IMWL to EMWL is highly affected by the wave period (or wave length): for longer waves, infiltration dominates over exfiltration while exfiltration dominates infiltration for steeper waves.
- Residual pore pressure generation in the sand core depends more on changes in IMWL rather on short drainage times.

The following equations are obtained for the upper envelopes based on eq.(7.20):

Configuration c1 (n = 45%; tanα = 1/3):

$$\frac{\eta_{int}}{\eta_S} = \frac{278.66 \cdot \left(\frac{x_{local}}{L_0} + 0.0014 \right)}{0.043} \cdot \exp\left(- \frac{\left(\frac{x_{local}}{L_0} + 0.0014 \right)^{0.26}}{2 \cdot 0.043} \right) \qquad (7.21)$$

Configuration c2 (n = 20%; tanα = 1/3):

$$\frac{\eta_{\text{int}}}{\eta_S} = \frac{42.43 \cdot \left(\frac{x_{local}}{L_0} + 0.010 \right)}{0.061} \cdot \exp\left(- \frac{\left(\frac{x_{local}}{L_0} + 0.0097 \right)^{0.36}}{2 \cdot 0.061} \right) \tag{7.22}$$

Configuration c3 (n = 45%; tanα = 1/6):

$$\frac{\eta_{\text{int}}}{\eta_S} = \frac{63.66 \cdot \left(\frac{x_{local}}{L_0} + 0.0054 \right)}{0.058} \cdot \exp\left(- \frac{\left(\frac{x_{local}}{L_0} + 0.0054 \right)^{0.30}}{2 \cdot 0.058} \right) \tag{7.23}$$

The coefficients in eq.(7.20) obtained for the upper envelope of the configurations are shown summarized in Tab. 7.4.

Tab. 7.4: Coefficients a_{IMWL}, b_{IMWL}, c_{IMWL} and d_{IMWL} in eq.(7.20) for the upper envelope of the spatial distribution of IMWL in the sand core of all configurations for wave spectra.

$\frac{\eta_{\text{int}}}{\eta_S} = \frac{d_{IMWL} \cdot \left(\frac{x_{local}}{L_0} + c_{IMWL} \right)}{b_{IMWL}} \cdot \exp\left(- \frac{\left(\frac{x_{local}}{L_0} + c_{IMWL} \right)^{a_{IMWL}}}{2 \cdot b_{IMWL}} \right)$	tanα [-]	porosity [%]	a_{IMWL} [-]	b_{IMWL} [-]	c_{IMWL}	d_{IMWL} [-]
configuration c1	1/3	45	0.26	0.043	0.0014	278.66
configuration c2	1/3	20	0.36	0.061	0.0097	42.43
configuration c3	1/6	45	0.30	0.058	0.0054	63.66

Since the IMWL is induced by the EMWL which is superimposed by fluctuations for wave spectra tests and since the EMWL is particularly affected by the slope steepness of the revetment, the associated IMWL is also influenced by this parameter and subject to similar fluctuations. In section 5.2.1 it was shown that the porosity of the cover layer only slightly affects the external wave set-up. This influence seems to be larger for the IMWL, due to the longer residence time of the infiltrated water in the sand core. The latter is more pronounced for the configuration with a smaller porosity. Consequently, the development of the IMWL is directly and much more dependent on the porosity and the associated MWL just beneath the revetment on the sand surface which might be larger than the EMWL. As the measurement of the MWL on top of the sand core is hardly possible in physical model tests, numerical simulations would be required to determine the relation between EMWL and the MWL just beneath the revetment depending on the porosity and the slope steepness.

It was confirmed that a residual pore pressure build-up in the sand core only depends on a change in the IMWL and not on short drainage times. Thus, with a changing IMWL and the

associated infiltration and exfiltration in the sand core, the swash area is just shifted along the slope and no concluding results on the implications for the slope stability can be drawn only from these investigations. For stability analysis, the pressure differences which might also lead to partial or local liquefaction (see Fig. 7.21) have to be taken into account in the next section 7.4.

The development of IMWL is highly dependent on the development of EMWL and the wave period (or wave length). For longer waves, infiltration is larger than exfiltration while the latter dominates for shorter and higher waves. For small relative distance x_{local}/L_0 from the shoreline inside the sand core, the relative internal wave set-up η_{int}/η_S is obviously characterized by a significantly different time scale corresponding to that of wave run-up/run-down. With increasing x_{local}/L_0, η_{int}/η_S also increases up to a maximum. For x_{local}/L_0-value larger than x_{local}/L_0 where η_{int}/η_S becomes maximum, the internal wave set-up has the same time scale like the external wave set-up and is not affected by the swash processes any more.

For the *effect of the revetment porosity*, the conclusion might be drawn that a decreasing porosity leads to larger maximum η_{int}/η_S-values due to a larger MWL directly at the sand surface, which results in a larger infiltration and a reduced exfiltration of the water out of the sand core. As a measurement of the MWL directly at the sand surface is hardly feasible in physical model tests, this conclusion should be verified by numerical simulations.

For the *effect of the slope steepness*, the internal wave set-up η_{int} near the shoreline of the sand core is less affected by the swash processes on the slope for the flatter slope. This leads indeed to larger η_{int}-values for long waves since the EMWL is particularly affected by the slope steepness and the external wave set-up η_S provides larger values on flatter slopes. However, the η_{int}/η_S-values are smaller for long waves compared to steeper slopes.

A residual pore pressure build-up in the sand core only depends on a change in the IMWL and not on short drainage times.

7.4 Stability analysis of the sand core beneath the revetment

The failure of the PBA-revetment observed during the GWK-tests and well-documented by Oumeraci et al. (2010b) highlighted the crucial importance of the stability of the soil beneath the revetment for the stability of the entire structure. Moreover, a first physical interpretation of the failure with a first stability analysis was conducted. This methodology was deepened in the numerical investigations of Alcérreca Huerta (2014) by using the extended results of his parameter study with the developed CFD-CSD model.

No systematic physical investigations of the stability of PBA-revetments and their sandy substructure have yet been conducted. Beside the numerical investigations of Alcérreca Huerta (2014) the systematic model tests performed in this study may also be seen as an attempt to fill the knowledge gap from the physical modelling view point.

The physical background of this stability analysis was already outlined in section 2.3.2 showing that Oumeraci et al. (2010b) identified two processes which may induce soil liquefaction beneath bonded porous revetments:

- Transient or instantaneous liquefaction
- Residual liquefaction

Usually both residual and transient pore pressure occur together during wave attack. The transient pore pressure u_{t*} and the residual pore pressure u_r are superimposed. According to the methodology proposed by Oumeraci et al. (2010b), this superposition is considered in the stability analysis for the identification of liquefaction failures based on eq. (7.24) leading to the following equation:

$$\sigma' = \left(\rho_c g d_c + \rho_f g d_f + \rho'_s g z'\right) - \left[u_{0*} - \left(u_{t*} + u_r\right)\right] \leq 0 \qquad (7.24)$$

This is also illustrated in Fig. 7.28 according to Oumeraci et al. (2010b).

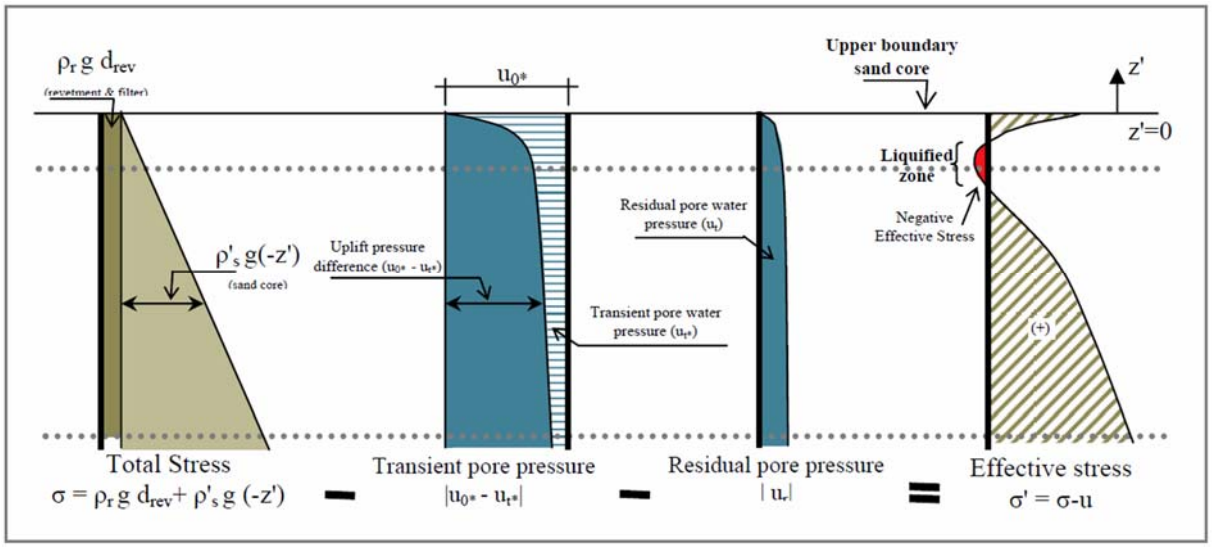

Fig. 7.28: Stability against liquefaction failures in the sand core beneath PBA-revetments (Oumeraci et al. (2010b))

For the stability analysis the characteristics of the revetment configurations are first given in section 7.4.1. Based on the determination of the maximum uplift pressure difference in section 7.4.2, a stability analysis is then conducted based on the present porosity and slope steepness of the revetment configuration in section 7.4.3.

7.4.1 Determination of the total stress of the different revetment configurations

In this section the total stress (resisting force term in eq. (2.46) or eq. (7.24)) due to the weight of the different layers of the revetment configurations and the sand core in depth z' is determined. The results are listed in Tab. 7.5.

Tab. 7.5: Determination of the total stress of the different revetment configurations (resisting force term in eq. (2.46))

description	parameter	unit	configuration c1/c3	configuration c2
density of revetment cover layer	ρ_c	kg/m³	1528	1645
thickness of the cover layer	d_c	m	0.05	0.05
density of revetment filter layer	ρ_f	kg/m³	1528	1528
thickness of the filter layer	d_f	m	0.05	0.05
total stress of revetment	σ_{rev}	kPa	1.499	1.556
bulk density of submerged soil	ρ'_S	kg/m³	0.865	0.865
total stress of sand layer, z‘=5cm	σ_S	kPa	0.424	0.424
total stress of sand layer, z‘=10cm	σ_S	kPa	0.849	0.849
total stress of sand layer, z‘=20cm	σ_S	kPa	1.697	1.697
total stress, z’=5cm	σ	kPa	1.923	1.981
total stress, z’=10cm	σ	kPa	2.348	2.405
total stress, z’=20cm	σ	kPa	3.196	3.253

In the stability analysis using eq. (2.46), the cover and the filter layer are assumed to be completely drained and not submerged. For these layers no reduced weight force due to buoyancy is set. In Liebisch & Oumeraci (2014) the stability analysis for the tested revetment configurations was also conducted under the assumption of complete saturation of the revetment pores. The results clearly showed that the assumption of complete saturation of cover and filter layer is not sustainable, because larger damages would have occurred during the main tests and also in the GWK-tests. Consequently the stability analysis in section 7.4.3 is conducted under the assumption of completely drained cover and filter layer.

7.4.2 Determination of the relative uplift pressure difference

The relative uplift pressure difference is defined in eq. (7.25):

$$\Delta u_{rel} = \frac{|\Delta u|}{\rho g H_{m0}} = \frac{\left|u_{0*} - \left(u_{t*} + u_r\right)\right|}{\rho g H_{m0}} \tag{7.25}$$

To determine the relative uplift pressure difference, the time series recorded by the pressure transducers shown in Fig. 7.1 are used to calculate new time series of the differences between the initial pressure u_{0*} and the pore pressure ($u_{t*}+u_r$) at different depths z’. In doing so, nine new time series of the pressure difference ($u_{0*}-(u_{t*}+u_r)$) at different locations and depths in the sand core are obtained. The determined pressure differences contain both transient and residual components of pore pressure, because in the stability analysis it is not necessary to separate between these two components. The specifications of the time series are summarized in Tab. 7.6.

Tab. 7.6: Specification of new derived time series of pressure difference in the sand core

Specification	Column	PT for initial pressure u_{0*}	PT for pore pressure $u_{t*}+u_r$
Difference A1	A	27F	12S
Difference A2	A	27F	15S
Difference A3	A	27F	18S
Difference B1	B	28F	13S
Difference B2	B	28F	16S
Difference B3	B	28F	19S
Difference C1	C	29F	14S
Difference C2	C	29F	17S
Difference C3	C	29F	20S

The procedure of deriving the time series of the pressure difference out of the initial pressure and the pore pressure in depth z' is illustrated in Fig. 7.29 for a regular wave test.

All time series for pressure differences listed in Tab. 7.6 are analysed event by event. Thus, for every test a maximum and a minimum difference are determined for all nine time series of the pressure difference listed in Tab. 7.6. For the stability of the revetment and its sandy foundation the minimum difference is crucial since it represents the maximum uplift pressure.

In the analysis of the relative uplift pressure difference in the sand core, the worst case of the three columns of pressure transducers for each of the three layers in the sand core was used to calculate the maximum relative uplift pressure difference (eq. (7.25)) as already done in the analysis of the pressures on and just beneath the revetment.

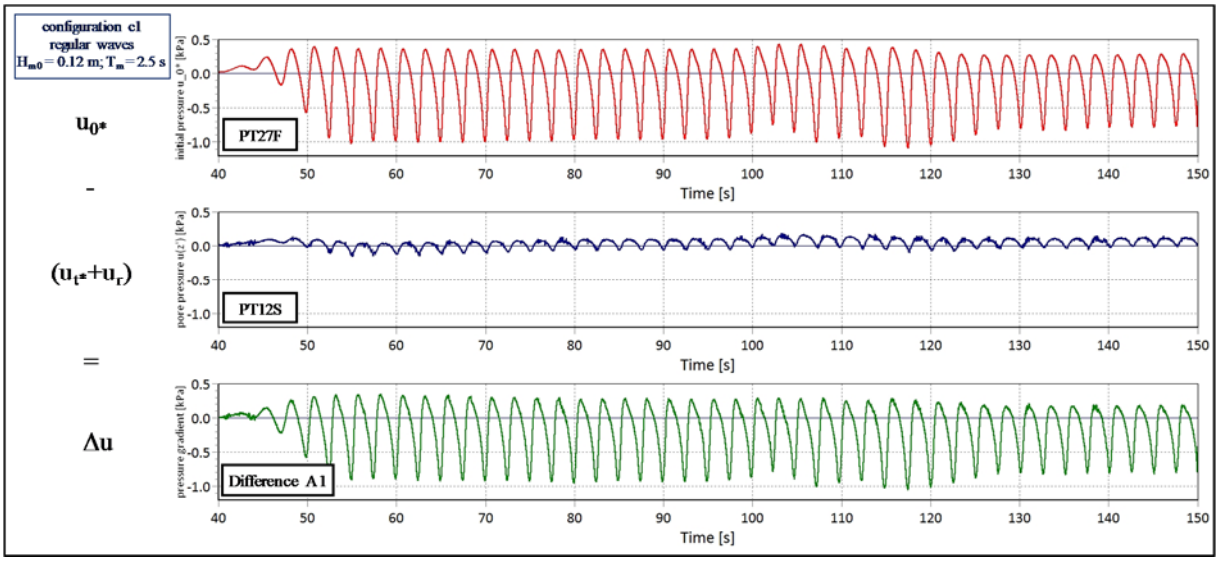

Fig. 7.29: Time series of initial pressure u_{0*} (PT27F) and pore pressure $(u_{t*}+u_r)$ (PT12S) and derived pressure difference (Difference A1) (Test 20130814 09)

In the following, the relative pressure difference Δu_{rel} in the sand core is shown for the three different revetment configurations against different surf similarity parameters $\xi_{m-1,0}$ in different depths z'. This was already done by Alcérreca Huerta (2014) for the numerical results with regular waves. A good correlation of the data in different depths was found with the following equation:

$$\Delta u_{rel} = \frac{A \cdot \xi_0}{1 + B \cdot \xi_0 + C \cdot \xi_0^2} \tag{7.26}$$

This equation provides the advantage that Δu_{rel} becomes zero if ξ_0 is zero. Moreover, Δu_{rel} tends against zero for large surf similarity parameters. This is essential because for very large wave lengths and the associated very slow water level rise, no uplift pressure difference will occur in the sand core. Consequently, the physical limits occurring for the uplift pressure difference are fulfilled. For wave spectra tests eq.(7.26) is re-written as follows:

$$\Delta u_{rel} = \frac{a_{grad} \cdot \xi_{m-1,0}}{1 + b_{grad} \cdot \xi_{m-1,0} + c_{grad} \cdot \xi_{m-1,0}^2} \tag{7.27}$$

with: a_{grad}, b_{grad}, c_{grad} = empirical coefficients [-]

Fig. 7.30 to Fig. 7.32 show the results based on eq. (7.27) for the relative pressure difference Δu_{rel} in different depths z' for the three tested configurations.

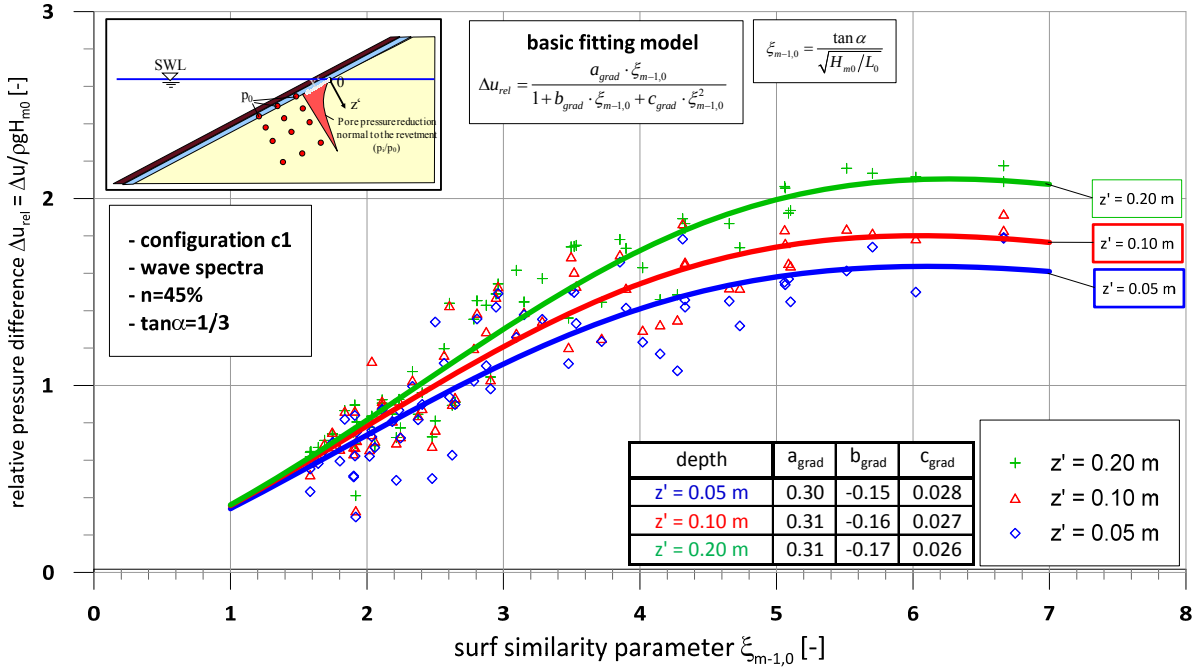

depth	a_{grad}	b_{grad}	c_{grad}
z' = 0.05 m	0.30	-0.15	0.028
z' = 0.10 m	0.31	-0.16	0.027
z' = 0.20 m	0.31	-0.17	0.026

Fig. 7.30: Relative pressure difference Δu_{rel} as a function of surf similarity parameter $\xi_{m-1,0}$ for configuration c1 for wave spectra tests

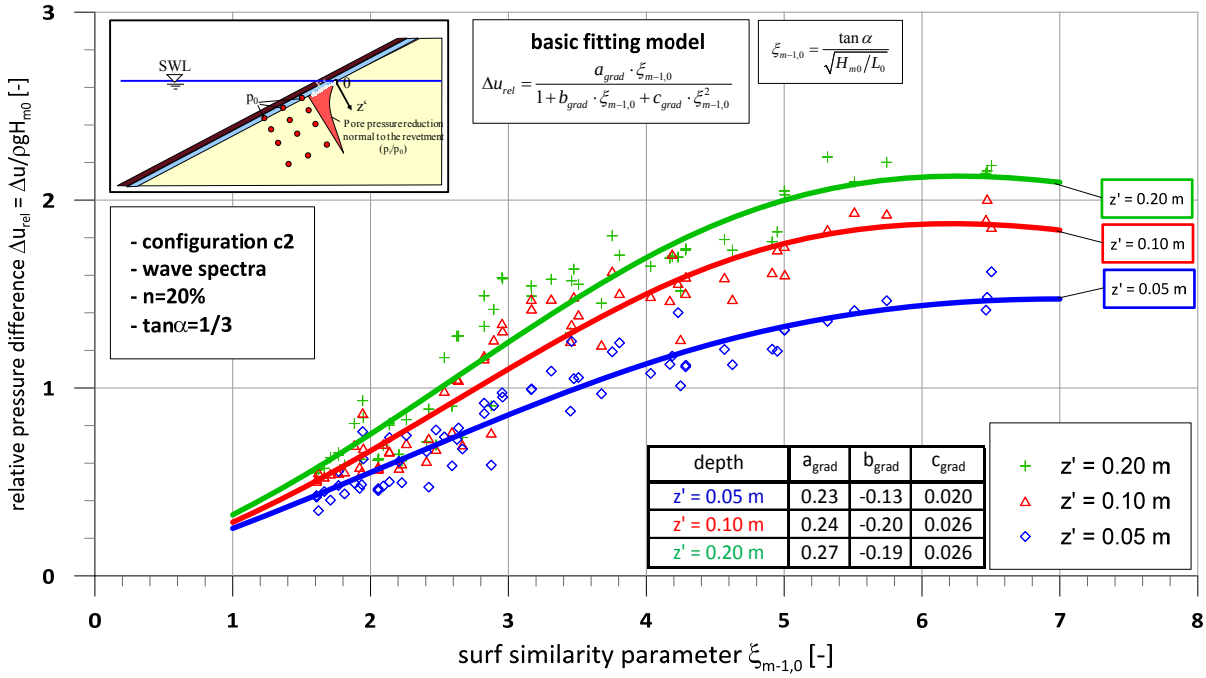

Fig. 7.31: Relative pressure difference Δu_{rel} as a function of surf similarity parameter $\xi_{m-1,0}$ for configuration c2 for wave spectra tests

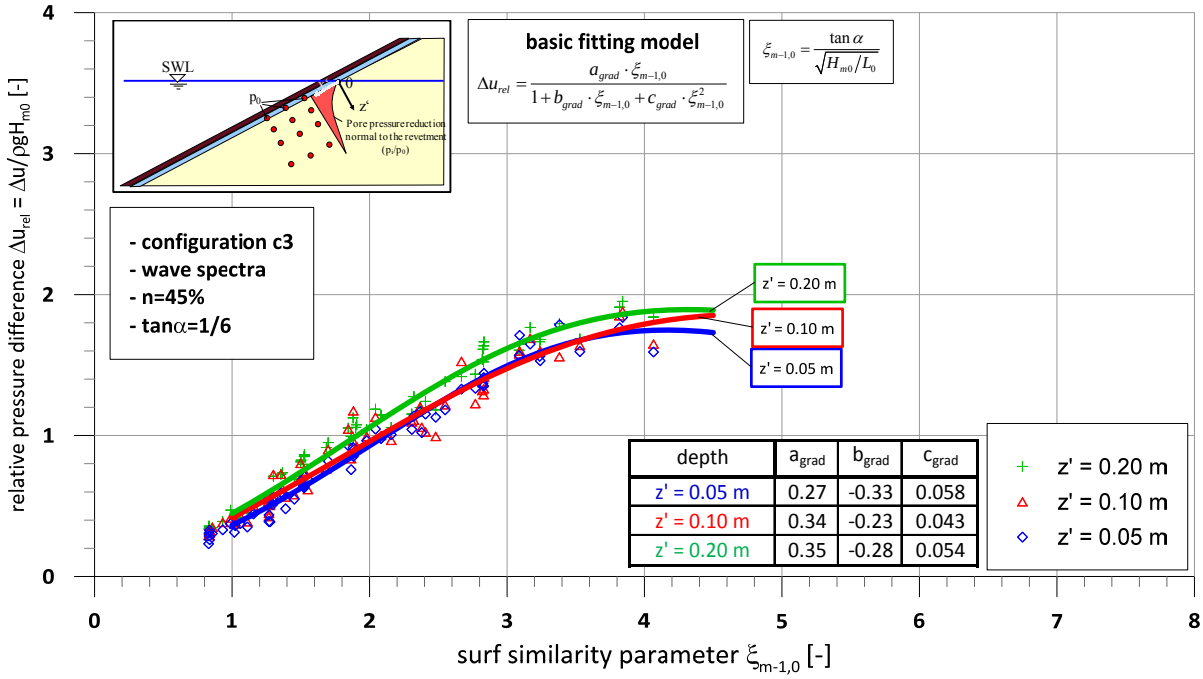

Fig. 7.32: Relative pressure difference Δu_{rel} as a function of surf similarity parameter $\xi_{m-1,0}$ for configuration c3 for wave spectra tests

The coefficients obtained for the different revetment configurations based on eq.(7.27) are listed in Tab. 7.7.

Tab. 7.7: Coefficients a_{grad}, b_{grad} and c_{grad} based on eq. (7.27) for all revetment configurations and wave spectra tests

$\Delta u_{rel} = \frac{a_{grad} \cdot \xi_{m-1,0}}{1 + b_{grad} \cdot \xi_{m-1,0} + c_{grad} \cdot \xi_{m-1,0}^2}$	depth z‘	a_{grad}	b_{grad}	c_{grad}	σ'_{diff}
configuration c1	0.05 m	0.30	-0.15	0.028	0.174
	0.10 m	0.31	-0.16	0.027	0.144
	0.20 m	0.31	-0.17	0.026	0.156
configuration c2	0.05 m	0.23	-0.13	0.020	0.122
	0.10 m	0.24	-0.20	0.026	0.127
	0.20 m	0.27	-0.19	0.026	0.130
configuration c3	0.05 m	0.27	-0.33	0.058	0.069
	0.10 m	0.34	-0.23	0.043	0.100
	0.20 m	0.35	-0.28	0.054	0.074

Compared to the numerical simulations of Alcérreca Huerta (2014) with regular waves, all three figures for the wave spectra tests (Fig. 7.30, Fig. 7.31 and Fig. 7.32) show significantly larger values for the maximum relative pressure difference (up to twice as large). This was expected due to the characteristics of wave spectra tests and the usage of the maximum values in the considered time frame, which might be caused by larger waves in the spectrum. However, the model according to eq. (7.27) shows a good correlation also for wave spectra tests. In the numerical investigations of Alcérreca Huerta (2014), the revetment thickness was varied to achieve a direct comparison to the large scale tests of Oumeraci et al. (2010b). In this study, the revetment thickness is kept constant for all configurations, while the porosity and the slope steepness were varied.

The increase rate of the relative pressure difference Δu_{rel} is much larger in the upper layers of the sand core beneath the revetment than in deeper layers where it is getting much smaller. Considering the linear increase of the resisting force term with increasing depth, liquefaction is more likely to occur in the upper layers. However, Δu_{rel} increases for larger surf similarity parameters (and thus for longer waves). This can be explained by the larger wave run-down heights and the associated larger uplift pressure difference (see also Fig. 7.21). For very large surf similarity parameters, Δu_{rel} should tend against zero, due to the sufficiently long drainage time.

Comparing the results in Fig. 7.30 and Fig. 7.31 for the two revetments with different porosity, it can be seen that no significant difference between the two configurations occurs for the results in a depth z’ = 10 cm and z’ = 20 cm. The scatter for the results in depth z’ = 10 cm is larger for configuration c1 with a larger porosity. However, the applied fitting model shows almost the same equation for both revetment configurations. This is completely different in the upper layer of the sand core. For relative uplift pressure difference Δu_{rel} in a depth z’ = 5 cm, configuration c1 provides significantly larger values compared to the low porous configuration c2. This can be explained by the permeability of the cover layer and the associated exfiltration time. For configuration c2 the water in the revetment needs a longer time to exfiltrate the filter

and cover layer due to the lower permeability of the cover layer. This also leads to smaller relative pressure difference in the sand core underneath. This process is only relevant for the upper layer of the sand core which is thus more likely to be liquefied for configuration c1 (see section 7.4.3).

Comparing the results of the two revetments with different slope steepnesses, configuration c3 with the flatter 1/6 shows a decisively different result compared to the steeper configuration c1 with the same porosity. The uplift pressure differences occurring for the same wave conditions are smaller on the flatter slope and thus liquefaction is less likely. This can be explained by the longer residence time of the water layer on the slope during the swash process and the resulting smaller relative pressure difference during wave-run down. In Fig. 7.32 it is also seen that in deeper layers of the sand core almost no additional relative pressure difference develops under the flatter slope.

The results of this section have shown that the analysis of the different influencing parameters provide a better understanding of the processes beneath the revetment which are crucial for the evaluation of the stability of bonded porous revetments. However, more systematic research would be required to develop general design equations which allow to determine the relative pressure difference in the sand core beneath porous revetments which explicitly consider porosity and slope steepness in the calculation.

7.4.3 Stability analysis

In the previous section the maximum relative pressure difference (driving force) was determined and differences were assessed for the different revetment configurations. From the results of these driving forces, it was shown that liquefaction is more likely to occur in the upper layers of the sand core beneath the revetment. However, to assess whether liquefaction will occur, a stability analysis should be performed by also considering the resisting forces which consist of the weight of the revetment and the submerged soil above the considered location in depth z'. A stability factor S_{up} can be determined for every conducted test by re-writing eq. (2.46) as eq. (7.28). In this limit state equation, the stability against soil liquefaction in depth z' is ensured for $S_{up} < 1.0$:

$$S_{up} = \frac{\left|u_{0*} - \left(u_{t*} + u_r\right)\right|}{\left(\rho_c g d_c + \rho_f g d_f + \rho'_s g z'\right)} = \frac{\left|\Delta u\right|}{\left(\rho_c g d_c + \rho_f g d_f + \rho'_s g z'\right)} \leq 1 \qquad (7.28)$$

Liquefaction occurs, if the stability factor S_{up}, defined as the ratio of driving to resisting forces per unit surface, is larger than 1.0. For the determination of the resisting force term, the values listed in Tab. 7.5 are used. The obtained stability factor S_{up} in a depth z' = 0.05 m is shown in Fig. 7.33 for different wave heights H_{m0} and wave periods $T_{m-1,0}$ for configuration c1. Determined values for $S_{up} > 1.0$ are indicated as red dots to show potential liquefaction. S_{up}-values smaller than 0.85 show no risk of liquefaction and are indicated as green dots. Further intermediate S_{up}-values are indicated as yellow and orange dots to highlight the decreasing safety from the green dots (stable) to the red dots (liquefaction).

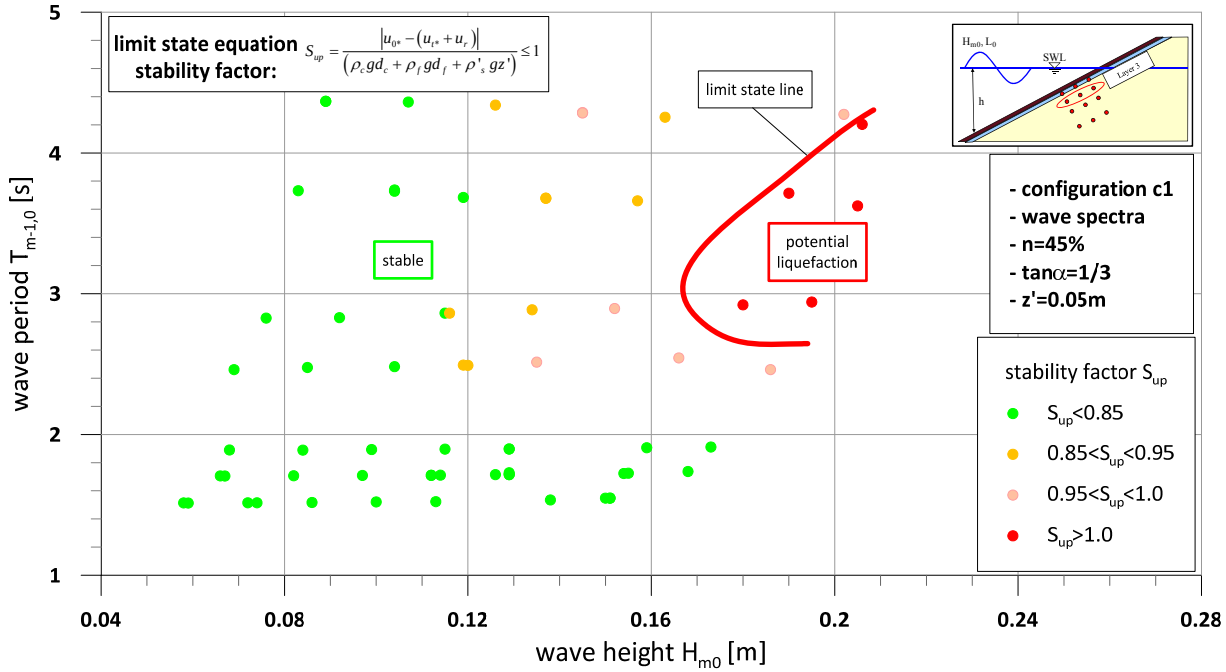

Fig. 7.33: Stability factor S_{up} at depth z' = 0.05 m for different wave conditions for configuration c1 (wave spectra tests)

With the illustration of the stability factor in Fig. 7.33 it is possible to easily identify the range of wave conditions which represent a potential risk of liquefaction at depth z' in the sand core and might result in a failure of the soil at this depth. The latter is illustrated in Fig. 7.33 with the red "limit state line". The red dots (liquefaction) are characterized by wave periods larger than 3.0 s and large wave heights between 0.18 m and 0.21 m. A relation between the stability factor and the wave steepness could not be identified.

The results in Fig. 7.33 are only valid for the investigated model configuration c1 and the tested conditions. These are solely to illustrate the stability analysis and cannot be generalized for other conditions. Moreover, the stability factor in Fig. 7.33 is determined by using the maximum relative uplift pressure difference obtained for the entire test duration, which occurs during the passage of only one wave trough. Nevertheless, this short period can lead to a local liquefaction and a transport of the sand material downwards the slope. This instantaneous local liquefaction may lead to larger damages over time (cyclic wave loading).

For configuration c2 and c3 no values of stability factor S_{up} larger than 0.85 were obtained.

Liquefaction in the sand core beneath porous revetments is more likely for high and especially long waves. Flatter slopes are less vulnerable against soil liquefaction beneath bonded porous revetments than steeper slopes. Furthermore, flatter slopes have the advantage that a transportation of the potential liquefied soil down the slope is much slower and less likely due to the weaker flow in the revetment layers. Revetments with a larger porosity are more vulnerable to liquefaction, which means that a reduction of the pore volume over time (e.g. clogging) has a positive effect in terms of liquefaction risk.

7.5 Summary and conclusions

After the analysis of the wave-induced pressure on the revetment (layer 1) in chapter 6, the hydrodynamic processes just beneath the revetment and in the sand core, including soil liquefaction, were analysed in this chapter.

In section 7.1, it was shown that the pressure damping performance D_p of porous revetments is more significantly affected by the revetment porosity than by the slope steepness. D_p increases with decreasing porosity over the entire range of tested surf similarity parameters $\xi_{m-1,0}$. The impact load component is more strongly damped than the quasi-static component and non-impact loads through the porous revetment. D_p generally increases with steeper slopes only for $\xi_{m-1,0} < 3$ while the effect of the slope steepness becomes negligibly small for larger $\xi_{m-1,0}$-values.

In section 7.2, the results have shown that the wave-induced pressures are strongly damped in the first layers of the sand core and then continue to exponentially decrease at deeper locations. The porosity and slope steepness only affect the initial pressure transmitted through the revetment to the top of the sand core, but not the exponential pore pressure decrease in the sand core. Impact pressures are fully damped in the first sand layers, so that only the non-impact loads and the quasi-static components of the impact loads are transmitted in deeper layers. Moreover, the results confirmed that the model by de Groot et al. (2006) can correctly predict the pore pressure damping in the sand core, if the input parameters such as the compressibility of pore water β and the hydraulic permeability k are properly selected.

In Section 7.3, the analysis of the spatial development of the internal mean water level (IMWL) has shown that the IMWl is directly and closely related to the external water level (EMWL) for all tested revetments with different porosity and slope steepness. Furthermore, the strong dependence of IMWL on the wave period is outlined, showing that for longer waves, infiltration is larger than exfiltration while the latter dominates for shorter and higher waves. A decreasing porosity leads to larger maximum η_{int}/η_S-values due to a larger MWL directly at the sand surface, which results in a larger infiltration and a reduced exfiltration of the water out of the sand core. For the flatter slope 1:6 the internal wave set-up η_{int} near the shoreline of the sand core is less affected by the swash processes on the slope compared to the steeper slope resulting in smaller η_{int}/η_S-values for long waves.

In Section 7.4, the analysis of the relative pressure difference at different depths in the sand core and the related stability analysis against soil liquefaction beneath the all tested revetment configuration have shown that the upper layers in the sand core are mostly affected by soil liquefaction and that this effect rapidly decreases in deeper layers. Moreover, the results also imply that soil liquefaction is more likely beneath steeper than beneath flatter revetments. Revetments with a larger porosity are more vulnerable to liquefaction.

Overall, the results of this chapter have contributed to an improved understanding of the processes in the sand core beneath revetments of different porosity and slope steepness. However, these results have some limitations, so that further research will be needed. As shown for a very limited range of variation of revetment porosity and slope steepness, the damping of

the wave-induced pressure through the revetment is much more affected by both revetment parameters than the damping in the sand core. As the damping performance of the revetment provides the initial pressure at the top of the sand core, more research will be required to extend the obtained results and formulae for a broader range of both revetment porosity and slope steepness. In such further investigations, the internal wave set-up should also be considered, as it affects all processes on and beneath the revetments and particularly the aforementioned initial pressure. Moreover, the validity of the de Groot formulae to predict the exponential damping of the pore pressure in the sand core, which also use the aforementioned initial pressure as a reference value, is confirmed by the results, also showing the crucial need for a more accurate specification of further input parameters such as the compressibility of the pore water β and the hydraulic permeability k of the soil.

8 Summary, Discussion and Outlook

Extensive scale model tests have been successfully conducted to improve the knowledge related to the effect of the revetment porosity for different slope steepnesses on the hydrodynamic processes on and beneath bonded revetments.

In this context, the current knowledge was first reviewed and analysed to identify the knowledge gaps. Preliminary scale model tests with a simplified model set-up were conducted to study the effect of the revetment porosity on the processes and its relative importance as compared to the effect of the slope steepness and roughness. The preliminary tests were primarily used to develop a more realistic model set-up and an optimized programme for the main model tests, which represent the major work phase of this study. A systematic analysis of the following processes involved in the interaction of irregular waves and the porous revetment and its soil foundation was performed with a focus on the effect of the revetment porosity and slope steepness: (a) processes in front of and on the revetment (wave reflection, wave set-up and wave run-up/run-down), (b) wave-induced pressures on the revetment (wave breaking and wave load classification, peak pressure, its location and the spatial pressure distribution on the revetment), (c) processes beneath the revetment (damping of wave-induced pressures in the revetment, pore pressure in the sand core beneath the revetment, internal mean water level, stability of the sand core).

In this concluding chapter, the key findings are summarized, followed by a brief discussion of the results and an outlook.

8.1 Summary of key findings

The key findings as obtained from the analysis of the aforementioned processes in front of and on the revetment, the wave-induced pressure on the revetment, the processes just beneath the revetment and in the sand core, including those obtained from the stability analysis against soil liquefaction of the sand core beneath the sand core may be summarised as follows:

a) Processes in front of and on the revetment

Wave reflection. An increasing porosity leads to a larger effect of the incident wave height on the reflection coefficient. With increasing wave heights, the highly porous revetment behaves increasingly like an impermeable revetment. The less porous revetment (n = 20%) does not show this behaviour and behaves almost like a smooth impermeable revetment for all surf similarity parameters. The effect of the slope steepness on the reflection coefficient C_r is less significant. A new model is proposed which accounts for the effect of the wave height on the reflection coefficient.

Wave set-up. The effect of the revetment porosity on relative wave set-up η_S/L_0 is less pronounced than that of the slope steepness, which is significant. This effect becomes larger for

smaller $\xi_{m-1,0}$ and almost zero for large $\xi_{m-1,0}$, Empirical formulae are provided showing a relatively good agreement with the data.

Wave run-up/run-down. Due to the very different time scales of the wave run-up/run-down and the wave set-up, the analysis based on the EMWL as a reference water level is physically more appropriate than with the commonly used SWL. A larger porosity leads to lower values of both relative wave run-up and run-down with a more significant effect of the porosity on wave run-up. The surf similarity parameter obviously does not fully describe the effect of the slope steepness on the wave run-up and run-down.

b) Wave-induced pressures on the revetment

Wave load classification. The flatter 1:6 slope provides a larger transition zone than the steeper slopes 1:3, whereas porosity does not significantly affect the load classification (see Tab. 6.1).

Peak pressure on the revetment. An increasing porosity increases the damping of impact loads leading to significantly smaller peak pressures on the revetment, whereas non-impact loads are only slightly affected by a changing porosity. The effect of the slope steepness on the peak pressure is generally less clear than that of the porosity. The slope steepness affects the peak pressures for quasi-static loads, but no noticeable effect on the impact pressure peak could be observed. The effect of the slope steepness on the quasi-static pressure on the revetment decreases with smaller deep water wave steepness H_{m0}/L_0. Tentative formulae are provided for all tested configurations by considering only the upper envelopes of the total peak pressure values as a conservative approach.

Location of peak pressure p_{max}. The effect of the porosity on z_{pmax}/H_{m0} is only significant for surf similarity parameter $\xi_{m-1,0} > 2.4$ leading to larger z_{pmax}/H_{m0}-values compared to a smooth and impermeable revetment. The effect of the slope steepness on the location of the peak pressure is more noticeable than that of the porosity particularly shown by the much smaller scatter for the flatter slope 1:6. For all tested configurations upper and lower envelopes enclosing the data scatter are derived.

Pressure distribution on the revetment. For impact loads, the pressure distribution on the revetment is affected by both revetment porosity and slope steepness. The pressure distribution becomes wider with increasing porosity and decreasing slope steepness of the revetment. For non-impact loads, the effect of the slope steepness is noticeable only far above SWL, where the pressure distribution is expectedly wider for steeper slopes commonly associated with larger wave run-up. Tentative formulae for the upper envelopes of the pressure distribution on the revetment are proposed for all tested revetment configurations.

c) Processes in the sand core beneath the revetment

Wave damping performance of porous revetments. The pressure damping performance D_p is more significantly affected by the revetment porosity than by the slope steepness. D_p increases

with decreasing porosity. The impact load component is more significantly damped through the porous revetment than the non-impact loads and the quasi-static component of the impact loads. D_p generally increases with steeper slopes only for $\xi_{m-1,0} < 3$ while the effect of the slope steepness becomes negligibly small for larger $\xi_{m-1,0}$-values.

Damping of pore pressure in the sand core. Wave-induced pressures are considerably damped in the first layers of the sand core and then continue to exponentially decrease at deeper locations. The porosity and slope steepness only affect the initial pressure transmitted through the revetment to the top of the sand core, but not the exponential pore pressure decrease in the sand core. The model by de Groot et al. (2006) can correctly predict the pore pressure damping in the sand core beneath porous revetments, but it is shown that the results are very sensitive to the input parameters of the soil depending on the air content of the pore fluid.

Development of the internal mean water level (IMWL). The spatial development of the IMWL is directly and closely related to the external water level (EMWL) for all tested revetments with different porosity and slope steepness. For longer waves, infiltration is larger than exfiltration while the latter dominates for shorter and higher waves. A lower porosity leads to larger maximum η_{int}/η_S-values. For the flatter slope 1:6, the internal wave set-up η_{int} near the shoreline at the sand slope is less affected by the swash processes on the slope compared to the steeper slope resulting in smaller η_{int}/η_S-values for longer waves.

d) Stability analysis of the sand core beneath the revetment

The upper layers in the sand core are mostly affected by soil liquefaction which is mainly induced by transient pore pressures. As the latter decrease exponentially with depth in the sand core, soil liquefaction potential rapidly decreases in deeper layers. Soil liquefaction is more likely beneath steeper than beneath flatter revetments. Revetments with a higher porosity are more vulnerable to liquefaction than less porous revetments.

8.2 Discussion and Outlook

Overall, the results of this study have revealed for the first time the relative importance of the effect of the revetment porosity and slope steepness on the aforementioned processes involved in the interaction of irregular waves and porous revetments and their soil foundation, thus providing an improved understanding of both effects. More specifically, the most relevant findings of this study may be outlined as follows:

(i) It was shown for the first time that an increasing porosity leads to a larger effect of the incident wave height on the reflection coefficient. A highly porous revetment behaves increasingly like an impermeable revetment with increasing wave heights and the porous structure becomes less effective in reducing wave reflection;

(ii) The effect of the revetment porosity on relative wave set-up η_S/L_0 is less pronounced than that of the slope steepness;

(iii) A larger porosity also results in lower values of both relative wave run-up and run-down with a more significant effect of the porosity on wave run-up;

(iv) Pressure damping performance D_p of porous revetments is more significantly affected by the revetment porosity than by the slope steepness. D_p increases with decreasing porosity over the entire range of tested surf similarity parameters $\xi_{m-1,0}$.

(v) The spatial development of the internal mean water level in the sand core beneath bonded porous revetments, which is crucial for the structure stability, is investigated systematically for the first time considering irregular waves. It is particularly shown that the internal wave set-up η_{int} near the shoreline at the sand core is less affected by the swash processes on a flatter slope (1:6) than on the steeper slope (1:3).

Empirical based equations were derived for all considered processes. As in the main tests only two porosities (n = 20% & n = 45%) and two slope steepnesses (1:3 & 1:6) were considered, the validity of the obtained formulae is cautiously limited to the tested or similar conditions.

Though the results of this study have contributed to an improved understanding of the processes in front of on and beneath bonded porous revetments, they have some limitations, so that further research will necessarily be needed to come up with final conclusions.

Only two well-selected values for the porosity and the slope steepness are considered in this study. Though these two values were carefully selected based on the results of preliminary tests (Liebisch et al. (2013a)), more systematic physical model tests or numerical studies with irregular waves for a wider range of values of the slope steepness and revetment porosity are still needed.

For this purpose, a systematic parameter study with the validated numerical model available at LWI might be most appropriate to determine further influencing parameters and their relative effect on the processes on and beneath bonded porous revetments.

In such further investigations, the internal wave set-up should necessarily be considered, as it affects all processes on and beneath the revetment. The latter particularly applies for the initial pressure on the top of the sand core, which is crucial for the stability of the sand core. Further unsolved issues, which arose in the course of the study can only be answered by further research. An example for such issues is the unexpectedly large non-impact load with relative peak pressure values up to 4.0 on the porous revetments tested with different porosities (n = 20% and n = 45%) which occurred in the small scale and as well in the 1:5 up-scaled GWK-tests with irregular waves on PBA-revetments (n=40%). A further example is the second pressure peak identified within the upper part of the swash zone by the numerical study of Alcérreca Huerta (2014) with regular waves. Further physical model tests specifically designed for this purpose (e.g. with a finer resolution of the pressure transducers between SWL and maximum wave run-up height) will certainly show whether this new phenomenon is the result of real physical processes on the revetment or just a numerical artefact. Moreover, investigations of the importance of the relation between grain/pore size and the incident waves would be required to determine the effect of a changing grain/pore size for the same porosity and thus to extend the applicability of the results to bonded porous revetments with large stone classes (e.g. partly grouted revetments).

9 References

Alcérreca Huerta, J. C. (2014): Process-based modelling of waves interacting with porous bonded revetments and their sand foundation. Ph.D. thesis, Braunschweig, Germany. Leichtweiß-Institute for Hydraulic Engineering and Water Resources, Technische Universität Braunschweig.

Alcérreca Huerta, J. C.; Oumeraci, H. (2012): Wave loading and response of impermeable block revetments and highly porous PBA revetment. Comparative Analysis of large-scale datasets. Braunschweig, Germany (Berichte Leichtweiß-Institut für Wasserbau, Technische Universität Braunschweig).

Alcérreca Huerta, J. C.; Oumeraci, H. (2013): Parametric study of PBA revetments with a CFD-CSD numerical model within the OpenFOAM framework. Progress report 4. Braunschweig, Germany (Leichtweiss-Institute for Hydraulic Engineering and Water Resources,).

Alcérreca Huerta, J. C.; Oumeraci, H. (2014): Process analysis on PBA revetments -A parametric study with a CFD-CSD numerical model within the OpenFOAM® framework-. Progress Report 5. Braunschweig, Germany (Leichtweiss-Institute for Hydraulic Engineering and Water Resources).

Allsop, N. W. (1990): Reflection performance of rock armoured slopes in random waves. In : Proceedings of the 22nd International Conference on Coastal Engineering. ICCE 1990. Delft, The Netherlands, 04.12.2006: American Society of Civil Engineers (ASCE), pp. 1460–1472.

Barends, F. B.J. (1993): Hydromechanics of Porous Media in the Maritime Environment. In M. B. Abbott, W. A. Price (Eds.): Coastal, Estuarial and Harbour Engineer's Reference Book, Chapter 30. London, UK: Chapman & Hall, pp. 425–438.

Battjes, J. A. (1972): Set-up due to irregular waves. In : Proceedings of the 13th International Conference on Coastal Engineering. ICCE 1972. Vancouver, Canada: ASCE, pp. 1993–2004.

Battjes, J. A. (1974): Surf similarity. In : Proceedings of the 14th International Conference on Coastal Engineering. ICCE 1974. Copenhague, Denmark: ASCE, pp. 466–480.

Battjes, J. A.; Janssen, J. P.F.M. (1978): Energy loss and set-up due to breaking of random waves. In : Proceedings of the 16th International Conference on Coastal Engineering. ICCE 1978. Hamburg, Germany: ASCE, pp. 569–587.

Bruun, P.; Günbak, A. R. (1977): Stability of sloping structures in relation to x risk criteria in design. In *Coastal Engineering*, pp. 287–322.

Bullock, G. N.; Crawford, A. R.; Hewson, P. J.; Walkden, M.J.A.; Bird, P.A.D. (2001): The influence of air and scale on wave impact pressures. In *Coastal Engineering* vol. 42, pp. 291–312.

Burcharth, H. F.; Andersen, O. H. (1995): On the one-dimensional steady and unsteady porus flow equations. In *Coastal Engineering* vol. 24, pp. 233–257.

Chanson, H.; Lee, J. F. (1997): Plunging jet characteristics of plunging breakers. In *Coastal Engineering* vol. 31 (no. 1-4), pp. 125–141.

CIRIA/CUR/CETMEF (2007): The Rock Manual. The use of rock in hydraulic engineering. 2nd edition. London (CIRIA / CUR, CIRIA C683).

Dally, W. R.; Dean, R. G.; Dalrymple, R. A.; [Nachname nicht vorhanden] (1985): Wave height variation across beaches of arbitrary profile. In *Journal of Geophysical Research (JGR)* vol. 90 (no. 6), pp. 11917–11927.

Davidse, M. P. (2009): Wave impact on asphaltic concrete revetments - Background and literature review. Master Thesis at Delft University of Technology, Faculty of Civil Engineering, Delft.

de Groot, M. B.; Bolton, M. D.; Foray, P.; Meijers, P.; Palmer, A. C.; Sandven, R. et al. (2006): Physics of liquefaction phenomena around marine structures. In *Journal of Waterway, Port, Coastal and Ocean Engineering* vol. 132 (no. 4), pp. 227–233.

Dean, R.G.; Walton, T.L. (2010): Wave Setup. In Y. C. Kim (Ed.): Handbook of coastal and ocean engineering. Singapore: World Scientific, pp. 1–23.

EAK (2002): Empfehlungen für Küstenschutzwerke. In *Die Küste. Archiv für Forschung und Technik an der Nord- und Ostsee* Heft 65, p. 589.

EurOtop (2007): European Overtopping Manual (Pullen, T.; Allsop, N.W.H.; Bruce, T.; Kortenhaus, A.; Schüttrumpf, H.; Van der Meer, J.W.; Kuratorium für Forschung im Küsteningenieurwesen: Die Küste).

Foyer, G. (2013): Prediction Formulae for Processes on and in Porous Bonded Revetments - An Experimental and Numerical Study -. Ph.D. thesis, Braunschweig, Germany. Leichtweiß-Institute for Hydraulic Engineering and Water Resources, Technische Universität Braunschweig.

Führböter, A. (1991): Wellenbelastung von Deich- und Deckwerksböschungen. In *Jahrbuch der Hafenbautechnischen Gesellschaft* Bd. 46, pp. 225–282.

Führböter, A.; Sparboom, U. (1988): Shock pressure interaction on prototype sea dikes caused by breaking waves. In P. A. Kolkman, J. Lindenberg, K. W. Pilarczyk (Eds.): Modelling soil-water-structure interactions. SOWAS 88. Proceedings of the International Symposium on Modelling Soil- Water- Structure Interactions. Rotterdam, The Netherlands: Balkema, pp. 243–252.

Galvin, C. J. (1968): Breaker type classification on three laboratory beaches. In *Journal of Geophysical Research (JGR)* vol. 73 (no. 12), pp. 3651–3659.

Gier, F.; Schüttrumpf, H.; Mönnich, J.; Van der Meer, J. (2012): Stability of interlocked pattern placed block revetments. In : Proceedings of the 33rd International Conference on Coastal Engineering. ICCE 2012. Santander, Spain.

Goda, Y. (1975): Irregular wave deformation in the surf zone. In *Coastal Engineering in Japan* vol. 18, pp. 13–26.

Goda, Y. (2010): Reanalysis of regular and random breaking wave statistics. In *Coastal Engineering* 52 (1), pp. 71–106.

Hall, K. R.; Foster, D. N. (1990): Internal and external pressure measurements in reshaped breakwaters. In *Coastal Engineering* 14 (3), pp. 215–232.

Hughes, S. A. (2004a): Estimation of wave run-up on smooth, impermeable slopes using the wave momentum flux parameter. In *Coastal Engineering* vol. 51 (no. 11), pp. 1085–1104.

Hughes, S. A. (2004b): Wave momentum flux parameter: a descriptor for nearshore waves. In *Coastal Engineering* vol. 51 (no. 11), pp. 1067–1084.

Hunt, I. A. (1959): Design of seawalls and breakwaters. In *Journal of Waterways and Harbors Division* Vol. 85 (No. WW3), pp. 123–152.

Iversen, H. (1952): Laboratory study of breakers. Washington D.C., USA (National Bureau Standards Circular, Technical Report 52).

Jensen, O. J.; Klinting, P.; [Nachname nicht vorhanden] (1983): Evaluation of scale effects in hydraulic models by analysis of laminar and turbulent flows. In *Coastal Engineering* vol. 7, pp. 319–329.

Kim, Y. C. (Ed.) (2010): Handbook of coastal and ocean engineering. Singapore: World Scientific.

Klein Breteler, M. (2007): Validatie van Golfklap (Report H4134). Delft, The Netherlands.

Klein Breteler, M. K.; Pilarczyk, K. W.; 't Hart, R. (2000): Influence of ageing and wide wave spectra on stability of placed block revetments. In : Proceedings of the 27th International Conference on Coastal Engineering 2000, Volume 3. ICCE 2000. Sydney, Australia: ASCE, pp. 1970–1982.

Kortenhaus, A. (2003): Probabilistische Methoden für Nordseedeiche. Ph.d. thesis, Braunschweig, Germany. Fachbereich Bauingenieurwesen, Leichtweiß-Institut für Wasserbau, Technische Universität Braunschweig.

Kudella, M.; Oumeraci, H. (2006): Development of residual pore pressure in the sandbed beneath a caisson breakwater. In : Proceedings of the 30th International Conference on Coastal Engineering, Vol. 5. ICCE 2006. San Diego, USA, pp. 4554–4566.

Lambe, W. T.; Whitman, R. V. (1969): Soil mechanics. New York, USA: John Wiley & Sons.

Lattermann, E. (2006): Wasserbau-Praxis Band 2 - Binnenwasserstraßen, Seewasserstraßen und Seehäfen, Seebau und Küstenschutz: Bauwerk Verlag.

Liebisch, S.; Alcérreca Huerta, J. C.; Kortenhaus, A.; Oumeraci, H. (2012): Bonded porous revetments - Effect of porosity on wave-induced loads and hydraulic performance. In : Proceedings of the 33rd International Conference on Coastal Engineering, No. 33. ICCE 2012. Santander, Spain, p. 15.

Liebisch, S.; Kortenhaus, A.; Oumeraci, H. (2013a): BoPoRe - Bonded Porous Revetments; General planning of the main model tests; Progress Report 3. Braunschweig, Germany (Leichtweiss-Institute for Hydraulic Engineering and Water Resources).

Liebisch, S.; Kortenhaus, A.; Oumeraci, H. (2013b): BoPoRe - Bonded Porous Revetments; Preliminary model tests to invistigate the effect of porosity on wave-induced loads and hydraulic performance; Progress report 2. Braunschweig, Germany (Leichtweiss-Institute for Hydraulic Engineering and Water Resources).

Liebisch, S.; Oumeraci, H. (2014): BoPoRe - Bonded Porous Revetments; Experimental analysis of the main model tests and model development; Progress Report 4. Braunschweig, Germany (Leichtweiss-Institute for Hydraulic Engineering and Water Resources).

Lo, M. J. (1988): Dynamic wave set-up. In : Proceedings of the 21st International Conference on Coastal Engineering. ICCE 1988. Malaga, Spain. Volume 3: ASCE, pp. 999–1010.

Lock, M. (2008): Early colonization of littoral communities on polyurethane coated substrates: a field and laboratory study. Arcadis Report. Hoofddorp, The Netherlands.

Longuet-Higgins, M. S.; Stewart, R. W. (1964): Radiation stress in water waves; a physical discussion, with applications. In *Deep-Sea Research* 11, pp. 529–562.

Losada, I. J.; Dalrymple, R. A.; Losada, M. A. (1998): Wave-induced mean flows in vertical rubble mound structures. In *Coastal Engineering* 35 (4), pp. 251–281.

Losada, M. A.; Giménez-Curto, L. A.; Gonzalez-Ondina, J. M. (1981): Flow characteristics on rough, permeable slopes under wave action. In *Coastal Engineering* vol. 4, pp. 187–206.

Ludwigs, G.; Oumeraci, H. (2011): Process analysis and model development for wave loading on porous and elastically bonded revetments - Report 2 - Experimental Analysis. Braunschweig, Germany (Technische Universität Braunschweig, Leichtweiß-Institut für Wasserbau).

Ludwigs, Gisa (2009): Wave loads on Elastocoast revetments. Diploma thesis. Leichtweiß-Institut für Wasserbau, Fachbereich Bauingenieurwesen, Technische Universität Braunschweig, Braunschweig, Germany.

Madsen, P. A.; Fuhrman, D. R. (2007): Run-up of tsunamis and long waves in terms of surf-similarity. In *Coastal Engineering* vol. 55, pp. 209–223.

Mansard, E.P.D.; Funke, E. R. (1980): The measurement of incident and reflected spectra using a least square method. In : Proceedings of the 17th International Conference on Coastal Engineering. ICCE 1980. Sydney, Australia: ASCE, pp. 154–172.

McCowan, J. (1894): On the highest wave of permanent type. In *Philosophical Magazine* (38), pp. 351–358.

Miche, M. R. (1944): Mouvements ondulatoires des mers en profondeur constante on decroissante. In *Annales des Ponts et Chaussées*, pp. 131–164.

Miche, M. R. (1951): Le pouvoir réfléchissant des ouvrages maritimes exposés a l'action de la houle. In *Annales des Ponts et Chaussées* vol. 121 (no. 12), pp. 287–319.

Muttray, M.; Oumeraci, H.; ten Oever, E. (2006): Wave reflection and wave run-up at rubble mound breakwaters. In *Abstract for 30th International Conference Coastal Engineering (ICCE)*, pp. 2; Abstract accepted.

Oumeraci, H.; Kudella, M. (2006): Wave-induced pore pressure in the sandy seabed underneath a caisson breakwater. Braunschweig, Germany (Berichte Leichtweiß-Institut für Wasserbau, Technische Universität Braunschweig).

Oumeraci, H.; Muttray, M. (2001): Bemessungswellenparameter vor Strukturen mit verschiedenen Reflexionseigenschaften. Abschlussbericht DFG-Projekt, OU 1/3-3. Braunschweig, Germany (Berichte Leichtweiß-Institut für Wasserbau, Technische Universität Braunschweig).

Oumeraci, H.; Staal, T.; Pfoertner, S.; Kudella, M.; Schimmels, S.; Verhagen, H.-J. (2010a): Hydraulic Performance of bonded permeable elastomeric revetments and sobsoil response to wave loads. In : Proceedings of the 32nd International Conference on Coastal Engineering. ICCE 2010. Shanghai, China.

Oumeraci, H.; Staal, T.; Pfoertner, S.; Ludwigs, G.; Kudella, M. (2010b): Hydraulic performance, wave loading and response of Elastocoast revetments and their foundation- A large scale model study. Braunschweig, Germany (Berichte Leichtweiß-Institut für Wasserbau, Technische Universität Braunschweig).

Popov, L.Ya.; Ryabykh, V. M. (1969): Wave pressure distribution on slopes of hydraulic earth structures. In *Gidrotekhnicheskoe Stroitel'stvo* No.10, pp. 30–33.

Schulze, R.; Köhler, H.-J. (2004): Sicherung einer instabilen Böschung mittels Druckentlastungsbohrungen - Berücksichtigung des Bodens unter Wasser als Dreiphasensystem. In *Mitteilungen des Instituts für Grundbau und Bodenmechanik der Technischen Universität Braunschweig* Heft Nr. 77, Tagungsband zum Seminar „Messen in der Geotechnik 2004“, 09.-10. September 2004, pp. 349–370.

Schüttrumpf, H.; Oumeraci, H. (2005): Scale and model effects in crest level design. In : International Coastal Symposium (ICS). Höfn, Iceland.

Schüttrumpf, Holger (2001): Hydrodynamische Belastung der Binnenböschung von Seedeichen durch Wellenüberlauf. Ph.d. thesis, Braunschweig, Germany. Fachbereich Bauingenieurwesen, Leichtweiß-Institut für Wasserbau, Technische Universität Braunschweig.

Seelig, W. N.; Ahrens, J. P. (1981): Estimation of wave reflection and energy dissipation coefficients for beaches, revetments, and breakwaters. Fort Belvoir, Va., USA (Technical Paper. Coastal Engineering Research Center, 81-1).

Stive, M.J.F.; Wind, H. G. (1982): A study of radiation stress and set-up in the nearshore region. In *Coastal Engineering* Vol. 6, pp. 1–25.

Stive, R.J.H. (1984): Wave Impact on Uniform Steep Slopes at Approximately Prototype Scale. In : IAHR Symposium.

TAW (2004): Wave run-up and overtopping at dikes. Den Haag, The Netherlands (Technische Adviescommissie voor de Waterkeringen (TAW)).

USACE (2002): Coastal Engineering Manual. Engineer Manual 1110-2-1100; US Army Corps of Engineers. Washington D.C., USA.

Van der Meer, J. W. (1993): Conceptual design of rubble mound breakwaters (Publications Delft Hydraulics, no. 483).

Van der Meer, J. W.; Stam, C. J. (1992): Wave run-up on smooth and rock slopes of coastal structures. In *Journal of Waterway, Port, Coastal and Ocean Engineering* vol. 118 (no. 5).

van Gent, M.R.A. (1993): Stationary and oscillatory flow through coarse and porous media. Delft, T. U. Delft, The Netherlands (Faculty of Civil Engineering and Geosciences).

van Vledder, G.Ph. (2001): Literature survey to wave impacts on dike slopes. Report H 976. Delft, The Netherlands (Technische Adviescommissie voor de Waterkeringen (TAW)).

Witte, H.-H. (1988): Druckschlagbelastung durch Wellen in deterministischer und stochastischer Betrachtung. In *Mitteilungen aus dem Leichtweiß-Institut für Wasserbau der Technischen Universität Braunschweig* Heft 102, pp. 1–227.

Zanuttigh, B.; Van der Meer, J. W. (1988): Wave reflection from coastal structures. In : Proceedings of the 21st International Conference on Coastal Engineering. ICCE 1988. Malaga, Spain. Volume 3: ASCE, pp. 4337–4349.

Zhong, H. (1985): Theoretische und experimentelle Untersuchungen über den Druckschlag bei Wellenangriff auf einen 1 zu 4 geneigten Seedeich. In *Mitteilungen aus dem Leichtweiß-Institut für Wasserbau der Technischen Universität Braunschweig* Heft 88, pp. 401–453.

Appendices

A Photo documentation

A.1 Preliminary model tests

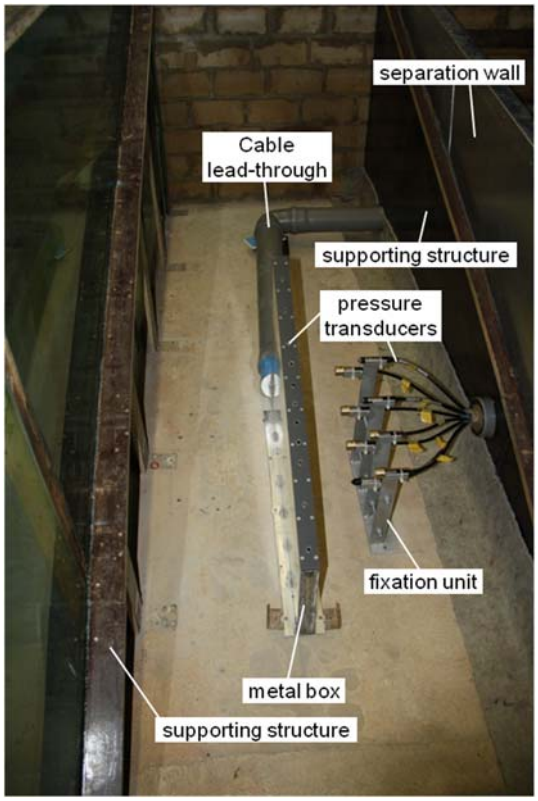

Fig. A1. 1: Metal box and fixation unit with pressure transducers

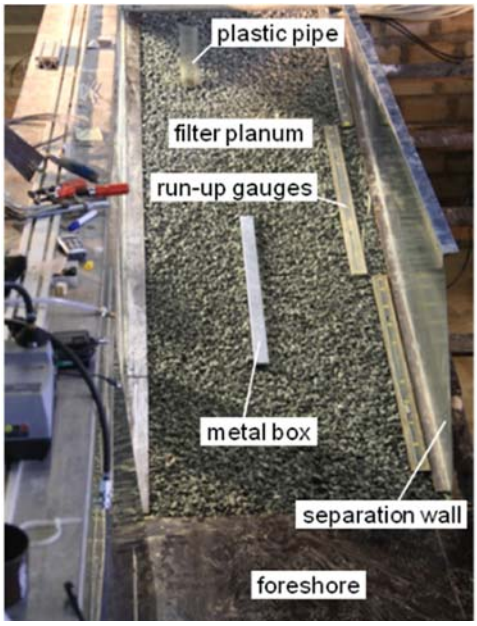

Fig. A1. 2: Filter planum with measuring devices

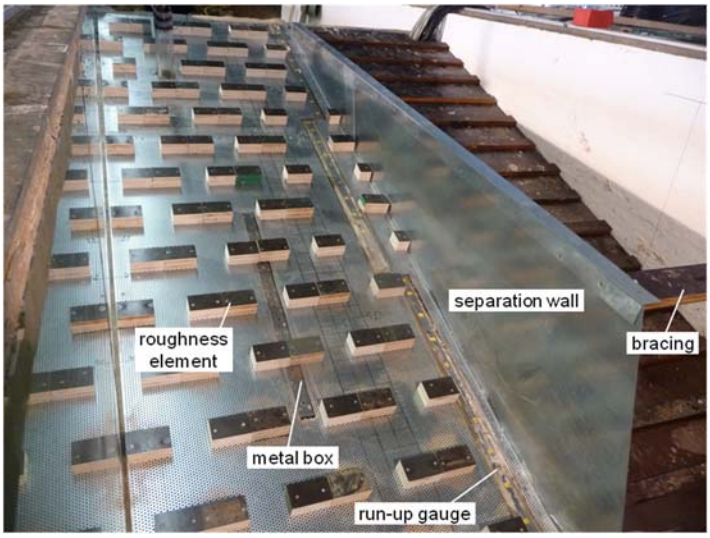

Fig. A1. 3: Roughness elements on configuration p1r2 (slope steepness 1:3)

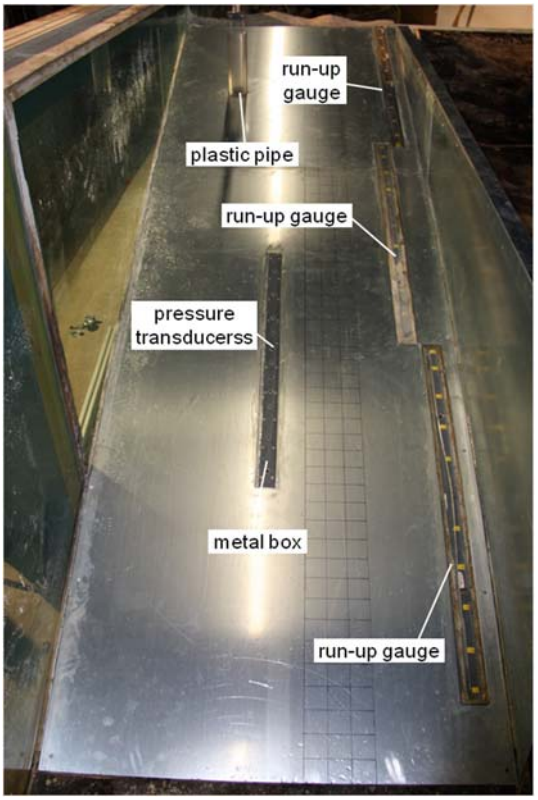

Fig. A1. 4: Measuring devices on configuration p0r0 (slope steepness 1:3)

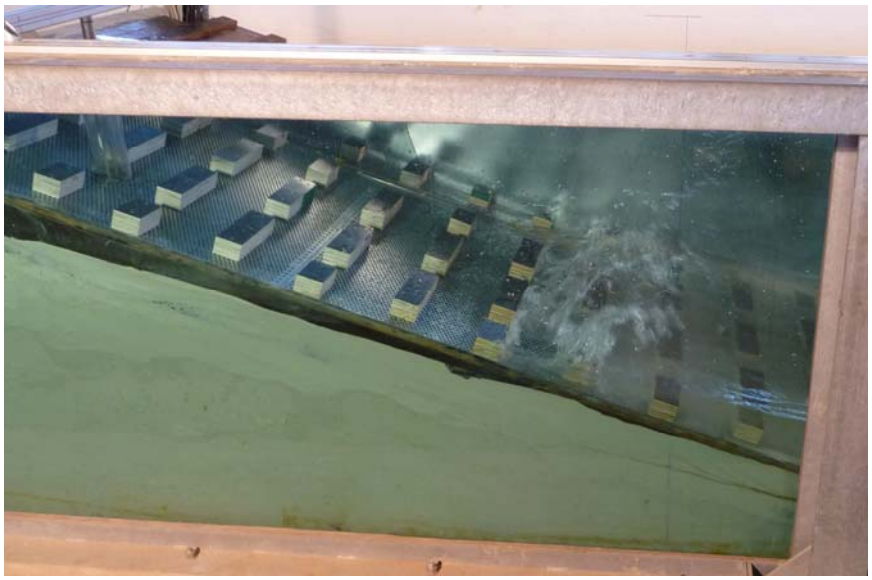

Fig. A1. 5: Configuration p1r2 (slope steepness 1:3) under wave attack

A.2 Main model tests

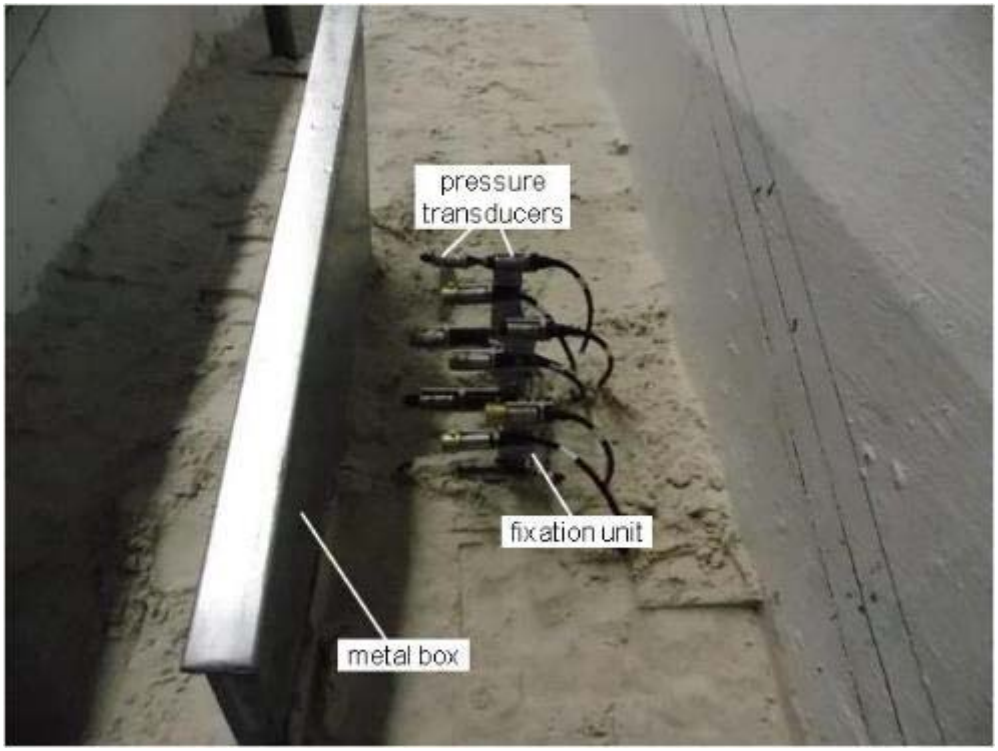

Fig. A2. 1: Metal box and fixation unit with pressure transducers during construction period (slope steepness 1:3)

Fig. A2. 2: Pressure transducers for measurement of the IMWL during construction period

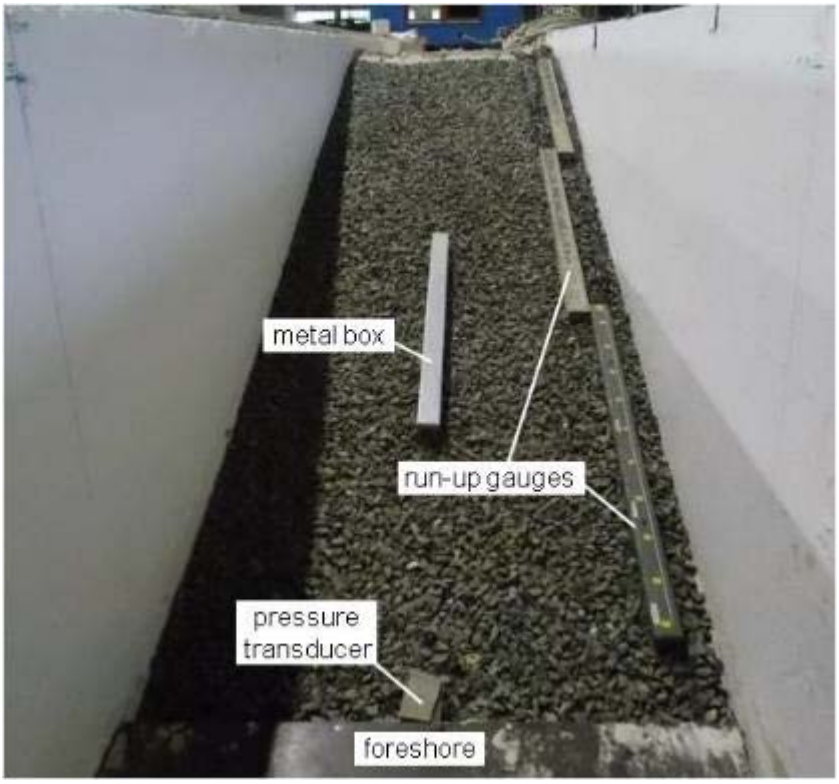

Fig. A2. 3: Filter planum with measuring devices

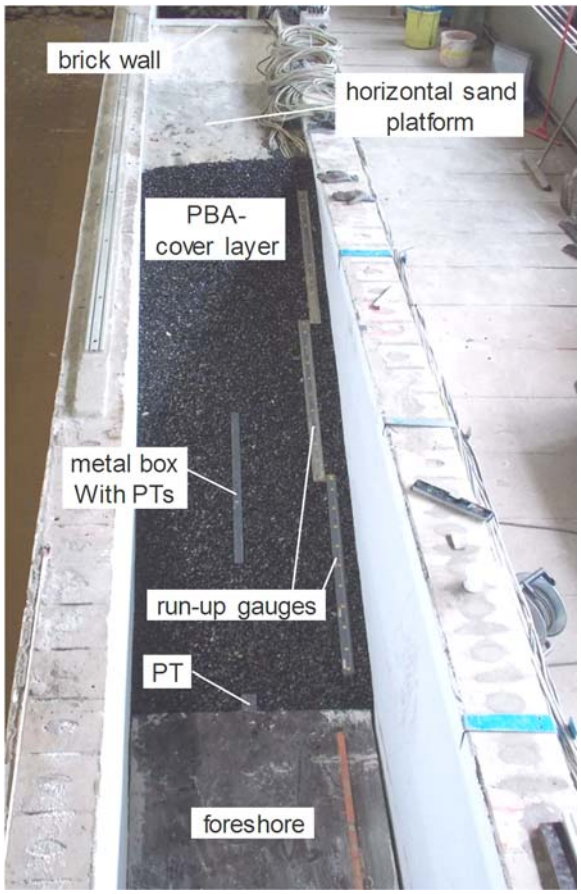

Fig. A2. 4: Configuration c1 (n = 45%; 1:3 slope) in the 1 m-flume

Fig. A2. 5: Configuration c2 (n = 20%; 1:3 slope) in the 1 m-flume

Fig. A2. 6: Configuration c3 (n = 45%; 1:6 slope) under wave attack

B Example application

An existing bonded porous revetment (20/40 mm) (d = 0.25 m) with a slope steepness of 1:3 and a porosity of 45% is affected by clogging effects leading to a reduction of porosity to 20% (see Fig. B. 1). The effect of this porosity reduction on the following parameters needs to be determined: reflection coefficient C_r, wave set-up η_S at the revetment, wave run-up $R_{u2\%}$ and wave run-down $R_{d2\%}$ on the revetment related to EMWL, peak pressure on the revetment p_{max}, uplift pressure difference in the upper sand layer beneath the revetment.

- Given wave parameters: $H_{m0} = 0.50m \left(H_{m0,scaled} = 0.10m \text{ (scale 1:5)}\right)$

$$T_{m-1,0} = 5.0s$$

$$\Rightarrow L_0 = 39.03m$$

$$\Rightarrow L_{0,scaled} = 7.81m$$

$$\Rightarrow \xi_{m-1,0} = 2.95$$

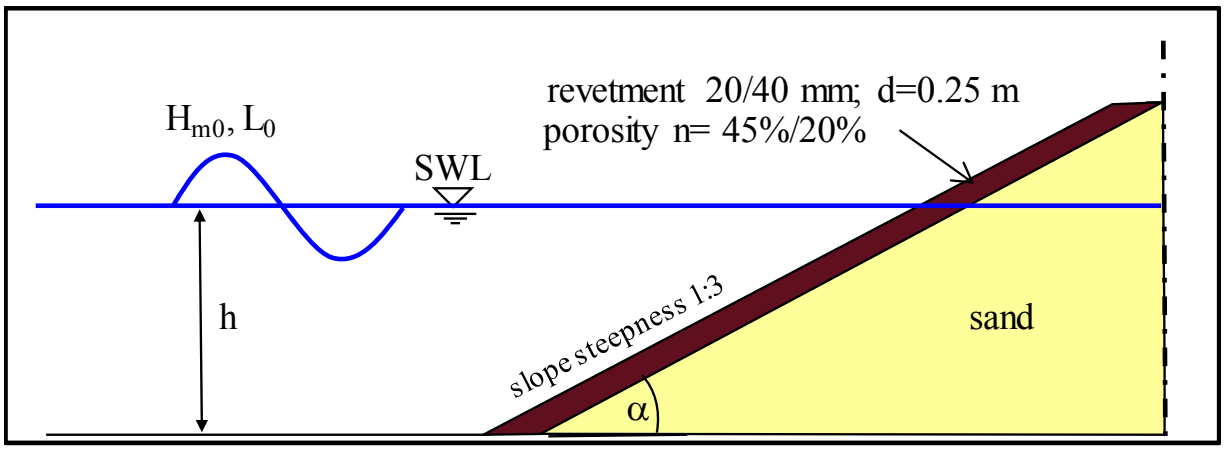

Fig. B. 1: Cross section of the bonded porous revetment considered for the example application

Calculations:

a) Reflection coefficient C_r: eq. (5.4) with eq (5.8) and Tab. 5.1:

$$C_{r,45\%} = \frac{\xi_{m-1,0}^2}{B + \xi_{m-1,0}^2} = \frac{\xi_{m-1,0}^2}{30.25 \cdot \exp\left(-34.00 \cdot H_{m0,scaled}\right) + 5.56 + \xi_{m-1,0}^2}$$

$$C_{r,45\%} = \frac{2.95^2}{30.25 \cdot \exp\left(-34.00 \cdot 0.10\right) + 5.56 + 2.95^2} = 0.57$$

$$C_{r,20\%} = \frac{\xi_{m-1,0}^2}{B + \xi_{m-1,0}^2} = \frac{\xi_{m-1,0}^2}{5.56 + \xi_{m-1,0}^2} = \frac{2.95^2}{5.56 + 2.95^2} = 0.61$$

The reflection coefficient **C_r increases by 4%.**

The equation proposed in Oumeraci et al. (2010b) for a PBA-revetment under irregular wave attack would lead to the following reflection coefficient:

$$C_{r,40\%} = \frac{0.84 \cdot \xi_{m-1,0}^2}{4.8 + \xi_{m-1,0}^2} = \frac{0.84 \cdot 2.95^2}{4.8 + 2.95^2} = 0.54$$

b) Wave set-up η_S: eq. (5.10) with Tab. 5.2

$$\eta_{S,45\%} = a_{su} \cdot \xi_{m-1,0}^{-b_{su}} \cdot L_0 = 0.063 \cdot \xi_{m-1,0}^{-2.32} \cdot L_0 = 0.063 \cdot 2.95^{-2.32} \cdot 39.03m = 0.20m$$

$$\eta_{S,20\%} = a_{su} \cdot \xi_{m-1,0}^{-b_{su}} \cdot L_0 = 0.071 \cdot \xi_{m-1,0}^{-2.18} \cdot L_0 = 0.071 \cdot 2.95^{-2.18} \cdot 39.03m = 0.26m$$

The wave set-up **η_S increases by 0.06 m (30%).**

c) Wave run-up $R_{u2\%}$ related to EMWL: eq. (5.21) with Tab. 5.3

$$R_{u2\%,45\%} = a_{ru} \cdot \tanh\left(b_{ru} \cdot \xi_{m-1,0}\right) \cdot H_{m0}$$

$$R_{u2\%,45\%} = 3.20 \cdot \tanh\left(0.25 \cdot \xi_{m-1,0}\right) \cdot H_{m0} = 3.20 \cdot \tanh\left(0.25 \cdot 2.95\right) \cdot 0.50m = 1.00m \text{ (related to SWL: } 1.20m\text{)}$$

$$R_{u2\%,20\%} = 4.01 \cdot \tanh\left(0.23 \cdot \xi_{m-1,0}\right) \cdot H_{m0} = 4.01 \cdot \tanh\left(0.23 \cdot 2.95\right) \cdot 0.50m = 1.18m \text{ (related to SWL: } 1.44m\text{)}$$

The wave run-up related to EMWL $R_{u2\%}$ **increases by 0.18 m** (18%). Related to SWL $R_{u2\%}$ **increases by 0.24 m** (20%), which is a decisive change for the required crest height of the structure.

The common design equation for wave run-up related to still water level (SWL) in EurOtop (2007) is used to determine a reduction coefficient γ_f based on the results obtained for the wave run-up with eq. (5.21):

$$\gamma_{f,45\%} = \frac{R_{u2\%,45\%}}{\left[4.0 - \frac{1.5}{\sqrt{\xi_{m-1,0}}}\right] \cdot H_{m0}} = \frac{1.20m}{\left[4.0 - \frac{1.5}{\sqrt{2.95}}\right] \cdot 0.50m} = 0.77$$

$$\gamma_{f,20\%} = \frac{R_{u2\%,20\%}}{\left[4.0 - \frac{1.5}{\sqrt{\xi_{m-1,0}}}\right] \cdot H_{m0}} = \frac{1.44m}{\left[4.0 - \frac{1.5}{\sqrt{2.95}}\right] \cdot 0.50m} = 0.92$$

The reduction coefficient γ_f determined for the highly porous revetment confirms the findings of Oumeraci et al. (2010b) in the large-scale tests (γ_f = 0.77). A reduction of the porosity increases the reduction coefficient to a value of 0.92, which is common for almost impermeable and slightly rough (e.g. grass) slopes.

d) Wave run-down R_d related to EMWL: eq. (5.22) with Tab. 5.4

$$R_{d\,2\%,45\%} = a_{rd} \cdot \tanh\left(b_{rd} \cdot \xi_{m-1,0}\right) \cdot H_{m0}$$

$$R_{d\,2\%,45\%} = -1.75 \cdot \tanh\left(0.31 \cdot \xi_{m-1,0}\right) \cdot H_{m0} = -1.75 \cdot \tanh\left(0.31 \cdot 2.95\right) \cdot 0.50m = -0.63m$$ (related to SWL: $-0.43m$)

$$R_{d\,2\%,20\%} = -1.61 \cdot \tanh\left(0.46 \cdot 2.95\right) \cdot 0.50m = -0.70m$$ (related to SWL: -0.44m)

The wave run-down related to EMWL $R_{d2\%}$ **increases by -0.07 m** (11%). Related to SWL $R_{d2\%}$ **increases by -0.01 m** (2%). Consequently, the effect of a reduction of the revetment porosity on possible uplift pressures during wave run-down process is negligibly small.

e) Peak pressure p_{max} on the revetment: eq. (6.11) with Tab. 6.2 and Tab. 6.3

$$\frac{p_{max}}{\rho g H_{m0}} = \frac{p_{imp} + p_{stat}}{\rho g H_{m0}} = a_{imp} \cdot \xi_{m-1,0} \cdot \exp\left(-\frac{\xi_{m-1,0}^{c_{imp}}}{b_{imp}}\right) + a_{stat} \cdot \tanh\left(b_{stat} \cdot \xi_{m-1,0}^{c_{stat}}\right)$$

$$p_{max,45\%} = \left(1.75 \cdot 2.95 \cdot \exp\left(-\frac{2.95^{6.59}}{304.38}\right) + 4.74 \cdot \tanh\left(0.20 \cdot 2.95^{0.97}\right)\right) \cdot 1.0t/m^3 \cdot 9.81m/s^2 \cdot 0.5m = 12.44kPa$$

$$p_{max,20\%} = \left(2.55 \cdot 2.95 \cdot \exp\left(-\frac{2.95^{3.60}}{50.61}\right) + 5.54 \cdot \tanh\left(0.23 \cdot 2.95^{0.79}\right)\right) \cdot 1.0t/m^3 \cdot 9.81m/s^2 \cdot 0.5m = 27.37kPa$$

The peak pressure p_{max} on the revetment **increases by 14.93 kPa** (120%).

The significantly larger peak pressures p_{max} on the revetment for a reduced porosity are decisive for the stability of the entire structure, because the structural integrity of the revetment can be threatened by the larger pressure peaks, possibly resulting in a collapse of the structure.

f) Determination of the uplift pressure difference Δu in the upper sand layer: eq. (7.27) with Tab. 7.7

$$\Delta u_{rel} = \frac{|\Delta u|}{\rho g H_{m0}} = \frac{a_{grad} \cdot \xi_{m-1,0}}{1 + b_{grad} \cdot \xi_{m-1,0} + c_{grad} \cdot \xi_{m-1,0}^2}$$

$$|\Delta u|_{45\%} = \frac{0.30 \cdot 2.95}{1 - 0.15 \cdot 2.95 + 0.028 \cdot 2.95^2} \cdot 1.0 t/m^3 \cdot 9.81 m/s^2 \cdot 0.5 m = 5.42 kPa$$

$$|\Delta u|_{20\%} = \frac{0.23 \cdot 2.95}{1 - 0.13 \cdot 2.95 + 0.020 \cdot 2.95^2} \cdot 1.0 t/m^3 \cdot 9.81 m/s^2 \cdot 0.5 m = 4.21 kPa$$

The uplift pressure difference Δu beneath the revetment **decreases by 1.21 kPa** (22%). Consequently, the upper layers of the sand core beneath the revetment are less vulnerable against soil liquefaction for the revetment with the reduced porosity.

Concluding remarks on the results of the example application:

The example application shows clearly the effects of a reduction of the revetment porosity on the different loading parameters. For the revetment with a lower porosity the reflection coefficient is slightly increased (4%). Significant negative effects are expected for the wave run-up heights and the peak pressures on the revetment. The wave run-up heights related to the SWL are increased by 20%, because the revetment with the lower porosity almost behaves like an impermeable, smooth revetment ($\gamma_f = 0.92$). This is a decisive change for the required crest height of the structure, which has to be considered in the design process of a highly porous bonded revetment. Furthermore, significantly larger peak pressures (+120%) are expected on the structure with the lower porosity, which may result in a significantly larger risk of a collapse of the structure due to the possible loss of structural integrity induced by the larger pressure peaks. However, the uplift pressure difference in the upper layers of the sand core beneath the revetment is smaller for the revetment with the lower porosity leading to a smaller vulnerability against soil liquefaction for the revetment with the reduced porosity.